UNIVERSIDADE DE LISBOA
FACULDADE DE CIÊNCIAS
DEPARTAMENTO DE FÍSICA

Calculation of S-values and their uncertainties for Nuclear Medicine

Ana Margarida Rocha Almeida

Mestrado em Engenharia Biomédica e Biofísica

Dissertação orientada por:
José María Fernández-Varea
Brígida da Costa Ferreira

2024

Acknowledgements

This dissertation is the result not only of the work developed in the last few months, but it also reflects the knowledge and growth acquired in five years of hard work.

Firstly, I would like to thank my external supervisor Professor José Fernández-Varea for all his support and guidance throughout this project. I am deeply grateful for the trust that was placed in me and the continuous encouragement to successfully achieve the objectives. I would like to acknowledge Dr. Mª Amor Duch and Dr. Mª Emilia Seren Takahashi for their contributions and constant availability to help during this whole project, it was essential to a successful conclusion.

I would like to express my profound gratitude to Professor Brígida Ferreira for supporting me along this journey and for the willingness shown.

Não posso deixar de agradecer a todos os meus amigos que a vida académica, e Lisboa em particular, me deram a conhecer. Foram um dos pilares essenciais durante esta etapa. Um grande obrigado também para as amigas de Viseu, que estiveram sempre ao meu lado, mesmo estando longe.

Ao grupo dos M's: o meu eterno obrigado. Vocês fizeram com que Barcelona parecesse "casa" durante estes seis meses e tornaram esta experiência inesquecível. Sei que a amizade que se criou permanecerá.

Um grande obrigado a toda a minha família, por todo o amor e apoio incondicional durante este percurso, em especial à avó Aurora, ao avô Rocha e à avó Nanda que são e sempre serão imprescindíveis. Avô Nando, sei que estará orgulhoso de mim.

O meu maior e mais sentido agradecimento é dirigido aos meus pais. Obrigado por me terem permitido perseguir os meus sonhos sem qualquer entrave no meu caminho, mesmo que isso tenha implicado alguns sacrifícios no vosso.

Abstract

Over the years, there have been notable technological advances in the medical techniques used to diagnose and treat tumour-related pathologies. In nuclear medicine techniques such as PET or SPECT, the use of radiopharmaceuticals that emit ionising radiation is fundamental, both for the acquisition of medical images and for the treatment of tumours. In this field, the distribution of the radiopharmaceuticals in the human body must be evaluated. It is crucial to accurately calculate the absorbed dose in tissues and, to facilitate these calculations, there are tables with S-values that represent the amount of energy absorbed per unit mass per nuclear decay.

The overall aim of this study was to update the available tables with S-values calculated using the most recent version of the PENELOPE Monte Carlo code and updated decay databases.

S-values were calculated for the decay of various radionuclides within voxels of different sizes. These values were computed by applying a simplified methodology based on a referenced bibliography and using two different radioactive decay databases: DECDATA and PenNuc. For voxel level calculations, the tables were extended to include two additional radionuclides and three more voxel size values.

S-values were also calculated at the cellular level using two methodologies: direct Monte Carlo (MC) simulations and Dose Point Kernel (DPK). The values calculated for the two databases were also evaluated. At the cellular level, thirty-nine different combinations of cell and nucleus radii and two different source-target combinations were considered, allowing the calculation of S-values for other combinations due to their additive properties.

The S-values calculated at the voxel level and at the cellular level are tabulated and presented in this dissertation.

Keywords: S-values, Monte Carlo simulation, radionuclide decay, dosimetry

Resume

A medicina nuclear é um campo que engloba técnicas de imagem médica para diagnóstico e terapia de patologias oncológicas, nomeadamente PET e SPECT, nas quais o princípio fundamental se prende com a deteção da distribuição de radiofármacos dentro do corpo humano. Estes são substâncias ativas, geralmente, compostas por dois componentes: um radionuclídeo, que é responsável pela emissão de radiação, e um composto farmacológico não-radioativo, cuja função é direcionar o radionuclídeo até às células-alvo. Os radiofármacos podem ser administrados ao paciente por via intravenosa, via oral, via respiratória ou por injeção direta na área de interesse. O decaimento radioativo do radionuclídeo provoca a emissão de radiações ionizantes (raios γ, partículas α ou β) que pode ser útil para a criação de imagem médica ou para tratamento de tumores por meio de destruição de células tumorais. A escolha do radiofármaco tem em consideração o objetivo (diagnóstico ou tratamento) e depende de diversos fatores, como o tipo de emissão do isótopo, a energia da radiação e o tempo de semi-vida. A dosimetria interna em medicina nuclear tem por objetivo estimar a dose administrada em lesões ou tumores, garantindo que a dose nos órgõas críticos não tenha excedido os limites aceitáveis. Em 1988, o MIRD (Medical Internal Radiation Dose), organizado pela Society of Nuclear Medicine, propôs um método para estimativa da dose absorvida, combinando os dados de distribuição biológica do radiofármaco com as propriedades físicas dos radionuclídeos. De acordo com o formalismo MIRD, os S-values são valores que quantificam a energia absorvida por unidade de massa e por decaimento radioativo. Estes valores são calculados tendo em consideração o esquema de decaimento do radionuclídeo, a distância em relação à fonte radioativa e as dimensões do alvo (neste caso, pode ser um órgão ou tecido).

Esta dissertação visa atualizar as tabelas atualmente disponíveis para *S-values*, recorrendo a bases de dados atualizadas para os esquemas de decaimento dos isótopos, bem como utilizando a versão mais recente do programa PENELOPE para simulações Monte Carlo. Este estudo realiza uma análise detalhada dos *S-values* tanto a nível de vóxeis quanto a nível celular.

No que diz respeito aos *S-values* calculados em voxel (*volume element*), os valores considerados como referência e aceites pela comunidade científica foram publicados pelo MIRD *Committee*, em 1998, tabelando valores para cinco radionuclídeos e para dois valores distintos de dimensão de voxel. Estes valores foram calculados e tabelados com base numa geometria cúbica (11×11×11 vóxeis), subdividida em cubos menores, os vóxeis. Dado que a emissão da fonte radioativa é isotrópica, apenas foi considerado o octante positivo da geometria, visto que os restantes valores podem ser calculados a partir deste, de acordo com a simetria cúbica. Neste estudo, foi aplicada uma metodologia semelhante; contudo, a dose absorvida não foi calculada para cada voxel individualmente do octante, mas sim agrupando os vóxeis segundo as distâncias a que se encontravam do centro da fonte radioativa. Assumindo que os vóxeis que são equidistantes da fonte absorvem a mesma quantidade de energia, os *S-values* foram calculados como a média da dose absorvida em cada grupo de vóxeis. Com a geometria considerada, foram identificadas 45 distâncias distintas ao centro, o que possibilita uma redução das tabelas de 216 para 45 valores de *S-values*. De forma a comparar os valores simulados com os valores de referência, foram realizadas simulações dos mesmos radionuclídeos (^{32}P, ^{89}Sr, ^{90}Y, ^{99m}Tc e ^{131}I), utilizando vóxeis cúbicos com dimensões de 3 mm e 6 mm. Neste estudo, foram utilizadas duas bases de dados para o esquema de decaimento dos isótopos: PenNuc e DECDATA. Os resultados das simulações indicam algumas discrepâncias em relação aos valores publicados pelo MIRD *Committee*, independentemente da base de dados utilizada. Os desvios em relação aos valores de referência são menores para os radionuclídeos ^{99m}Tc e ^{131}I. Em relação aos resultados das simulações em que fonte de radiação continha ^{32}P, ^{89}Sr ou ^{90}Y, são notórias diferenças mais acentuadas, com desvios percentuais na ordem dos 70-90%. Quando a fonte radioativa contém ^{32}P, foi aplicada a metodologia do MIRD *Committee*, de forma a excluir a

possibilidade das diferenças verificadas se deverem à simplificação dos cálculos. Verificou-se que as variações se mantinham e, portanto, são devidas a outras modificações. Em suma, a avaliação de *S-values* a nível de vóxeis sugere que, apesar da aplicação de uma metodologia simplificada, a atualização dos valores tabelados introduziu variações nos *S-values*. Para atingir todos os objetivos desta dissertação, foram disponibilizadas tabelas de *S-values* calculadas aplicando a mesma metodologia para dois novos radionuclídeos com relevância para a Medicina Nuclear, ^{177}Lu e ^{153}Sm. Adicionalmente, foram publicadas tabelas para os setes radionuclídeos em questão, considerando três novas dimensões de voxel que atualmente são utilizadas em equipamentos médicos (2.26 mm, 4.52 mm e 9.04 mm).

Em relação aos *S-values* a nível celular, foram consideradas duas abordagens: simulações diretas de Monte Carlo e *Dose Point Kernel*, utilizando como fontes radioativas quatro radionuclídeos (^{67}Ga, ^{123}I, ^{111}In e ^{201}Tl). Em ambas as abordagens, foi aplicada uma geometria, que consiste em duas esferas concêntricas a representar a estrutura de uma célula, com trinta e nove possíveis combinações de raio da célula e respetivo núcleo. Foram também analisadas duas situações distintas: uma em que o núcleo consistia simultaneamente na fonte e alvo da radiação (N ← N) e outra em que a fonte de radiação se encontrava no citoplasma e o alvo no núcleo da célula (N ← Cy).

No cálculo de *S-values* recorrendo a simulações diretas de Monte Carlo, foram efetuadas simulações para cada combinação de raio da célula e raio do núcleo, bem como uma para cada combinação fonte-alvo, resultando num número total de 936 simulações. Os resultados foram comparados com valores publicados recentemente, cuja metodologia se assemelha bastante à utilizada neste estudo. Verificou-se que, no caso N ← N, os valores calculados com a base de dados DECDATA se aproximavam mais dos valores considerados como referência, com desvios percentuais máximos entre 2-6%. Para a mesma combinação fonte-alvo, os valores calculados com PenNuc eram geralmente inferiores que os considerados como referência, com desvios entre 8-20%. Na situação N ← Cy, os resultados, para ambas as bases de dados, apresentam variações menores que 7%. Os valores apresentados não têm em consideração o caso do radionuclídeo ^{67}Ga. Excecionalmente, em ambas as combinações fonte-alvo, os resultados calculados para ^{67}Ga com a base de dados PenNuc refletem maiores divergências (entre 37% e 42%). De um modo geral, os desvios percentuais são geralmente maiores nos valores calculados para N ← N do que para N ← Cy e os resultados obtidos com a base de dados DECDATA estão em maior conformidade com os valores de referência.

A segunda metodologia para o cálculo de *S-values* a nível celular envolve a utilização de *Dose Point Kernel* que, através de fatores geométricos, calcula a dose absorvida para qualquer combinação de raio da célula e do respetivo núcleo. Ao incorporar expressões analíticas, também é possível, com esta abordagem, obter valores para qualquer combinação fonte-alvo. Com esta metodologia, foi necessário efetuar apenas uma simulação para cada um dos radionuclídeos considerados. Por sua vez, os *S-values* calculados foram comparados com valores publicados pelo MIRD *Committee*, em 1993. Esta comparação permitiu verificar a existência de divergências, uma vez que, apesar dos valores calculados pelo MIRD *Committee* serem obtidos utilizando metodologias analíticas semelhantes, estes assentam em modelos físicos distintos e simplificados.

Os valores encontrados no âmbito desta dissertação foram calculados de modo a seguir aproximadamente as metodologias previamente implementadas que demonstram ser, atualmente, referências em medicina nuclear. As diferenças observadas nos valores prendem-se com a utilização de uma versão mais recente do programa PENELOPE para as simulações Monte Carlo, bem como a utilização de bases de dados que contenham atualizações científicas. Deste modo, conclui-se que os valores previamente publicados se encontravam desatualizados, denotando-se grandes divergências em relação aos valores calculados neste estudo. Por fim, todos os *S-values* calculados foram tabulados e publicados nesta dissertação.

Palavras-chave: *S-values*, simulações Monte Carlo, decaimento radioativo, dosimetria

Table of contents

List of Figures

List of Tables

Acronyms

AE Auger Electrons.

BIGS Box Isotropic Gauss Spectrum.

CK Coster-Kronig Electrons.

CSDA Continuous Slowing Down Approximation.

CT Computed Tomography.

DCS Differential Cross Section.

DNA Deoxyribonucleic Acid.

DPK Dose Point Kernel.

EDTMP Ethylenediaminetetramethylene-phosphonate.

EGS Electron Gamma Shower.

FDA Food and Drug Administration.

FLUKA Fluktuierende Kaskade.

GATE Geant4 Application for Tomographic Emission.

GEANT4 Geometry and Tracking.

GRF Geometric Reduction Factor.

HMPAO Hexamethylpropylene Amine Oxime.

IC Internal Conversion Electrons.

IMP Iodoamphetamine.

ICRP International Commission on Radiological Protection.

ICRU International Commission on Radiation Units & Measurements.

IDAC Internal Dose Assessed by Computer.

LET Linear Energy Transfer.

MAA Albumin Macroaggregate.

MAG3 Mercaptoacetyltriglycine.

MC Monte Carlo.

MCNP Monte Carlo N-Particle.

MDP Methylene Diphosphonate.

MIBG Metaiodobenzylguanidine.

MIRD Medical Internal Radiation Dose.

MRI Magnetic Resonance Imaging.

OLINDA/EXM Organ Level Internal Dose Assessment for Exponential Modelling.

PDF Probability Distribution Function.

PENELOPE Penetration and Energy Loss of Positrons and Electrons.

PET Positron Emission Tomography.

PSMA Prostate-Specific Membrane Antigen.

RADAR Radiation Dose Assessment Resource.

SNM Society of Nuclear Medicine.

SPECT Single Photon Emission Computed Tomography.

TRT Target Radionuclide Therapy.

VSV Voxel S-value.

CHAPTER 1

Introduction

This dissertation project proposes to evaluate and compare the S-values calculated by different methods and assess the impact of the variations in nuclear medicine applications. This work is the result of a Master of Science final project of the University of Lisbon, accomplished at the Universitat de Barcelona (UB, Spain) under the supervision of Dr. José M. Fernández-Varea and in collaboration with Dr. Mª Amor Duch from Universitat Politécnica de Catalunya (UPC, Spain) and Dr. Mª Emilia Seren Takahashi from the Universidade Estadual de Campinas (UNICAMP, Brasil).

The context and motivation, the objectives, and the workflow structure will be presented in this chapter.

1.1. Context and motivation

After the discovery of radioactivity by Henri Becquerel at the end of the 19th century, scientists began to explore biological applications of radioactive isotopes; however, nuclear medicine did not emerge as a prominent field until 1971. Through the years, important developments have been established in the nuclear medicine field, especially due to the scientific advances in chemistry and the development of radionuclides and radiolabelled compounds [1]. Nowadays, it is considered one of the most essential areas in medicine, recognised for its tools in the diagnosis and treatment of diseases, particularly in oncology. According to the Society of Nuclear Medicine (SNM), in the United States, 20 million nuclear medicine procedures are conducted each year [2]. This high number of procedures is reflected in improved healthcare services, aiming to enhance quality of life.

Nuclear medicine comprehends extensive research and the benefits of the use of radioactivity have become essential for medical procedures. Nevertheless, it is important to evaluate the impact of the hazards for the patients' health [3]. Nuclear medicine involves the use of radionuclides, and it requires a precise and accurate preliminary study to carefully determine the radiation dose that will be delivered to the patient. Dosimetry has gained a central role, aiming to deliver precise absorbed doses of radiation to tumour tissues while protecting healthy tissues from side effects. To achieve this level of accuracy, several studies have been published reporting different approaches for dosimetry calculations [4].

Despite time consumption for calculations, dosimetry must not be neglected, and all risks must be considered. Monte Carlo (MC) simulations are an excellent tool for estimating the absorbed dose with outstanding accuracy [5]. There is literature available with calculations for internal dosimetry. The important question: are they updated with the most recent developments? In this dissertation, dosimetry calculations are described and compared with the current references.

1.2. Objectives

The main goal of this dissertation project was to assess the variances in the calculation of S-values, that can be caused by differences in the applied methodology. Secondary goals that also were to be achieved:

- Review of the current literature to identify the existing methods used to calculate voxel S-values and cell-level S-values through Monte Carlo simulations and the decay data used;
- Monte Carlo simulations to determine S-values at the voxel level, using nuclear decay information from different databases for multiple radionuclides and various voxel dimensions;
- Perform data analysis of the results obtained and discuss discrepancies;
- Calculate S-values at the cellular level, applying different nuclear decay information in the input files for multiple radionuclides and various radii of the cell and the cell's nucleus;
- Perform data analysis for the S-values obtained and compare them with the values reported in the literature.

1.3. Structure of this dissertation

The dissertation is composed of six chapters. The first chapter introduces the theme of the study, by presenting the context and motivation for the development of this dissertation, the objectives and the workflow structure. In Chapter 2, the scientific theory and the state-of-the-art of the study topic is presented. Chapter 3 includes a review of the basic concepts of Monte Carlo simulations and a simple description of the PENELOPE code. Materials and methods are described in Chapter 4, including a brief description of all the input files used to run the simulations. Chapter 5 presents the results, data analysis and discussion. Finally, a conclusion of the findings of this work is presented in Chapter 6, as well as suggested future work.

CHAPTER 2

Scientific background

2.1. Fundamentals of PET and SPECT in Nuclear Medicine

Single Photon Emission Computed Tomography (SPECT) and Positron Emission Tomography (PET) are currently used for diagnostic and therapy. Nuclear imaging is highly valuable in providing functional imaging of in vivo metabolism and it is frequently combined with anatomical imaging such as Computed Tomography (CT) or Magnetic Resonance Imaging (MRI) [6]. In this way, patient's diagnosis and treatment planning become more comprehensive, significantly improving the quality of healthcare.

SPECT and PET are characterized by the administration of radiopharmaceuticals to the patients, containing radionuclides. The radionuclides will subsequently decay, emitting ionizing radiations according to its decay scheme. A schematic representation of the fundamentals behind PET and SPECT is presented in Figure 2.1.

PET images are obtained from radionuclides that decay via positron emission [7]. The positron (positively charged) is emitted from the nucleus and, when it interacts with an electron, these annihilate (electron-antimatter interaction) [8] and two gamma rays are emitted in opposite directions, each one with energy of 511 keV due to the conversion of the positron and electron masses. These gamma rays are detected by a pair of detectors in the PET scanner, disposed in opposite positions in a ring geometry. The detectors are generally formed by scintillation crystals connected to photomultiplier tubes [9]. This will enable the acquisition of three-dimensional images of the distribution of the radiotracer in the body [2], [6].

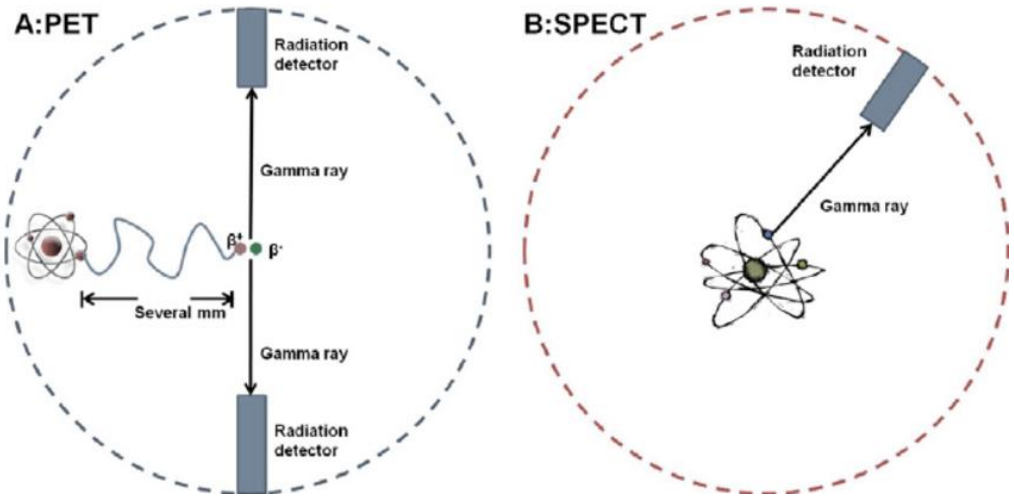

Figure 2.1: Basic concepts of PET and SPECT imaging techniques (from [10]).

SPECT is a non-invasive imaging technique that detects a single gamma ray emission at specific energies, resulting from the disintegration of a radionuclide [7]. This type of tomograph is equipped with gamma cameras, consisting of a lead collimator, a scintillation crystal and electronics [6],[8]. The emitted photon is converted into voltage signal by the gamma camera, which is used to form an image of the biodistribution of the administered radiopharmaceutical [10],[11]. Therefore, a volumetric image is reconstructed, enabling functional imaging.

2.2. Radiopharmaceuticals in Nuclear Medicine

According to Alsharef *et al. 2020* [12], about 95% of radiopharmaceuticals are used for diagnostic purposes and just 5% for therapy. Targeted radionuclide therapy (TRT) is an oncologic therapeutic approach that allows simultaneously scanning and treatment by using selected radiopharmaceuticals. Later in this chapter, some examples of radionuclides used in nuclear medicine with relevance to this report will be described.

Radionuclides can be naturally produced, can be synthetically produced through the utilization of cyclotrons and particle accelerators, or they can be created through the decay of existing radionuclides and acquired from radionuclide generators [13]. The radiopharmaceuticals used in TRT are essentially composed of two elements: a radioactive material, *i.e.*, a selected radionuclide responsible for delivering ionizing radiation to the tumour, and a non-radioactive component (tracer) whose function is to direct the radionuclide to the target, usually cancer cells [12]. These compounds are generally designed as theragnostic agents: the ionizing radiation aids in eradicating the tumour but also enables the acquisition of medical images, *e.g.*, by PET or SPECT, when the cancer-targeting material is paired with an appropriate radionuclide. These radiopharmaceuticals can be administered via oral, intravenous, inhalation or direct injection, and each radiopharmaceutical dosage must be determined prior to the administration and should take into account that the absorbed dose should be within 10% of the prescribed dose or dosage range [14], [15].

Radionuclides are nuclei characterized by a surplus of energy that makes them unstable. These radioactive isotopes exhibit either a very high atomic number, an imbalance in the ratio of protons to neutrons or exist in a metastable energy state, ultimately leading to radioactive decay. This might prompt the emission of particles (α, $\beta^{+/-}$) and/or electromagnetic radiation (gamma ray photons, γ), and as a secondary effect X-rays, conversion electrons and Auger electrons. For each nuclide, the decay scheme includes information regarding nuclear level (energy, total angular momentum, *etc*), decay probabilities and energy of the emitted radiation. The decay schemes for each radionuclide with relevance for this report are presented in Appendix A.

When a radionuclide decays and emits alpha particles, its atomic number decreases by two, along with a reduction in atomic mass by four units. Alpha particles, characterized by their heavy mass and slow velocity, have low penetration power and can travel a distance of 50 to 100 μm within a tissue, releasing energy at a significantly high density over this short range [13], [14]. In medical physics, alpha emitters are commonly inhaled or ingested as radiopharmaceuticals and can damage living tissue. However, as an external emitter, this type of particle cannot penetrate the dead layer of the skin, due to its short range (Figure 2.2) [16].

When beta disintegration occurs, an electron (β^- decay) or a positron (β^+ decay) may be emitted. Beta particles can be either negatively or positively charged. The beta particles exhibit a higher penetration power compared to alpha particles due to their significantly lower mass [17]. With a distance of travel in tissue ranging from 0.8 to 5 mm, beta particles deposit energy at a lower density but over a longer range (Figure 2.2). Due to its electric charge, the beta particles inflict damage on organs, albeit

to a lesser extent than alpha particles, making them a viable option for therapeutic applications, particularly in targeting and eradicating tumour tissue [8], [13]. This has driven increased research into beta decay; and, consequently, simulations are relying on complex analytical expressions of energy spectra.

The initial kinetic energy E of the electron or positron emitted in a beta transition is a random variable that takes values in the interval from zero up to a characteristic maximum energy $E_{\beta max}$ and the total energy of the β particle includes its rest mass $W = 1 + \frac{E}{m_e c^2}$ [18], [19]. The energy distribution of electrons and positrons emitted is represented by the Fermi Spectrum [20], [21], described by the following equation

$$p(W) \propto (W^2 - {m_e}^2 c^4)^{\frac{1}{2}} W\left(W_{\beta max} - W\right)^2 F(Z_f, W) a_n(W), \tag{2.1}$$

where $W_{\beta max} = E_{\beta max} + m_e c^2$ is the total energy, and p is the linear momentum of the emitted particle,

$$p \equiv \sqrt{W^2 - 1}\,. \tag{2.2}$$

In Equation 2.1, $a_n(W)$ represents a factor for a transition of order of forbiddenness n [20]. The Fermi function, introduced by Fermi in 1934, $F(Z_f, W)$, describes the distortion of the wave function of the outgoing electron or positron, where Z_f represents the atomic number of the final nucleus (after the decay). The terms m_e and c, presented in Equation 2.1, represent the mass of an electron and the speed of the light, respectively.

Gamma radiation is emitted from the radioactive nuclide in the guise of photons, signifying their lack of mass or charge, and the decay process does not involve any alteration in the atomic number or mass number. Due to its high energies, γ rays have high penetration power when compared to beta particles and therefore can be used for deep tumour treatment (Figure 2.2). When an isotope emits β particles and γ rays, usually the β-radiation is utilized for therapy while the γ emissions are useful for imaging, allowing the monitoring of the treatment [16], [22].

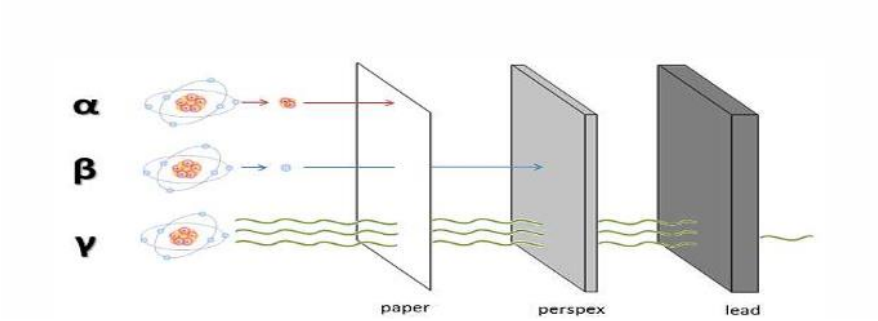

Figure 2.2: Penetration power of α and β particles and γ rays (from [12]).

The selection of an isotope for a therapy or diagnosis depends on numerous factors which, when combined, provide the best outcomes for medical imaging (diagnosis) and for the patient (control and treatment of the tumour). In nuclear medicine, the primary challenge is to determine the radioisotope that is the most suitable for the intended application. Factors that need to be considered are the decay spectrum, the half-life and the energy levels, ease of production and access, cost, tissue targeting and quality control [23]. Characteristics of the radioisotopes selected for this study report will be presented in this chapter. Due to their different purposes, the characteristics of isotopes used for diagnosis will differ from those used in therapy, particularly in the type of particle emission [23].

Radioisotopes with alpha or beta emission have been largely used for therapy; although, β-emitters represent the largest group of radioisotopes employed in TRT mostly due to their large range in the tissue. The mean energy of the released electrons ranges from 0.2 to 1.0 MeV, which results in a low linear energy transfer (LET) in tissues (lower amount of energy released per unit length) [24]. According to Eary *et al.* (2007) [23], their energy is mostly dissipated within an organ (approximately 95%), indicating that β emission is suitable for treating larger tumours (multicellular volumes) [23].

When the study aims to assess the absorbed dose at the cellular level, beta emitters are not appropriate. As mentioned above, the range of this type of emission is significantly larger than the dimensions of a cell. Accordingly, in these circumstances, the absorbed doses are mostly influenced by the interactions of Auger electrons (AE), Coster-Kronig (CK) electrons and internal conversion (IC) electrons. In the context of TRT, some radionuclides have a large yield of AE. These electrons are emitted as a consequence of the generation of a vacancy in an atomic inner shell during the nuclear decay processes (*e.g.*, electron capture and IC). As these vacancies are promptly filled, new ones are continuously produced in higher subshells, resulting in a large cascade of low-energy AEs. These electrons have an extremely short penetration distance in tissue (~ 0.1– 10 μm), leading to high LET due to the large number of AEs emitted in cascade. This means that a large energy deposition is produced in the vicinity of the decay site, providing a precise and localized irradiation for cancer treatment. AEs are considered highly potent for causing clustered damage in macromolecular targets, particularly DNA and cell membrane. Interest in the use of AE emitter radionuclides in TRT is increasing, with numerous preclinical and some clinical studies indicating their significant promise.

Besides the type of particle emitted in the decay scheme of the radioisotope, there are other aspects with significant impact on the choice of radioisotopes such as their physical and effective half-life. Equation 2.3 expresses the activity of the radioactive source, depending on the uptake, the biological decay and the physical decay of the radiopharmaceutical. T_u represents the characteristic time for the uptake of the radiopharmaceutical, T_b refers to the biological time for the excretion from the organ and $T_{\frac{1}{2}}$ is the physical half-time of the isotope. Since the activity can be defined as the number of disintegrations per unit time, in an organ or cell, it will vary due to the three mentioned factors. The physical half-time is a factor that has implications for the availability of the isotope, and it may limit the time available for its use. This means that the radionuclide must have a half-life that enables it to be available for transport (when needed) and to target the tissue/tumour before decay to achieve a maximum tissue-to-background ratio [23]. The time evolution of the activity is given by

$$A(t) = A(0)\underbrace{\left[1 - \exp\left(-\frac{\ln 2}{T_u}t\right)\right]}_{\text{uptake}}\underbrace{\exp\left(-\frac{\ln 2}{T_b}t\right)}_{\text{biological decay}}\overbrace{\exp\left(-\frac{\ln 2}{T_{\frac{1}{2}}}t\right)}^{\text{physical decay}} \tag{2.3}$$

^{32}P is a pure β-emitter and the maximum energy of the β-particles is 1.71 MeV. It has a half-time of 14.28 days and it is produced in a nuclear reactor via the ^{32}S(n,p)^{32}P reaction [25]. This radionuclide is one of the most commonly used radionuclides in TRT and can be administrated as ^{32}P-sodium phosphate or ^{32}P-chromic phosphate (Table 2.1) [26], [27].

Similarly to ^{32}P, the ^{89}Sr isotope is also a pure β^- emitter with a half-life of 50.57 days and a maximum energy for the β-particles of 1.49 MeV [23], [26]. It is produced in a nuclear reactor via ^{89}Y(n,p)^{89}Sr. Due to its similar behaviour to calcium, this radionuclide accumulates in areas of high osteoblastic activity (Table 2.1) [28].

^{90}Y is a pure β^- emitter with a high endpoint energy of 2.28 MeV and a half-life of 2.7 days. This radionuclide is produced by a generator system from ^{90}Sr [26], [27]. It is suitable for three different applications (Table 2.1) [29], [30]. Note that the microspheres, mentioned in Table 2.1, are of single use, which means that they cannot be metabolized or excreted and have a continuous radiotherapeutic effect.

^{99m}Tc has a half-life of 6.01 hours and it is produced via a generator system from ^{99}Mo. It has an $E_{\beta max}$ of 0.44 MeV and emits γ rays of 140 keV [23]. It is the most common radionuclide for SPECT imaging, especially for diagnosis, and has a wide range of ^{99m}Tc-labelled radiopharmaceutical kits available [27], [31]. This dissertation will focus on the most used in nuclear medicine (Table 2.1).

^{131}I is a common radionuclide used in SPECT imaging. It is a β^- emitter with an energy of 0.61 MeV and it has a half-life of 8.1 days. The production of this radionuclide is conducted in a nuclear reactor by irradiating ^{130}Te [23], [26]. ^{131}I emits high-energy γ rays (364 keV) and, consequently, patients treated with ^{131}I must follow a regulatory requirement for safety measures to minimise radiation exposure to others [32]. Table 2.1 summarizes the application of this radionuclide in medicine [27], [32].

^{153}Sm is a low energy β-emitter radionuclide with $E_{\beta max}$ of 0.81 MeV. It is produced by neutron irradiation of ^{152}Sm-oxide and has a half-life of 1.9 days [23], [26]. According to its decay scheme, there is 28% of γ rays emission with energy of 102.3 keV, which allows bone imaging. Table 2.1 resumes the application of this radionuclide in medicine [27], [33].

^{177}Lu is a β^- emitter with a maximum energy of 0.49 MeV and a γ emitter of rays with energy of 208 keV. This radionuclide has a half-life of 6.7 days, and it is produced by irradiating ^{176}Lu in a nuclear reactor [23], [26]. Similar to ^{153}Sm, the γ rays emitted by ^{177}Lu allow imaging and it is widely used in nuclear medicine (Table 2.1) [34], [35], [36].

Table 2.1: Applications of radiopharmaceuticals in medicine [29]-[36].

Isotope	Radiopharmaceutical	Application	Administration	Recommended Activity
^{32}P	^{32}P-sodium phosphate	Palliation of pain from bone metastasis	Intravenous or oral	Hundreds of MBq
		Treatment of myeloproliferative diseases (polycythaemia vera and thrombocythemia)	Intravenous	37 - 740 MBq
	^{32}P-chromic phosphate (normally as a colloid)	Treatment of malignant diseases of the serosal cavities, cystic neoplasms, and radiosynoviorthesis	Via injection directly into the cavity (pleural, pericardial or peritoneal)	Vary according to the cavity being treated
^{89}Sr	^{89}Sr-chloride	Palliation of pain from bone metastasis or mixed osteoblastic lesions	Intravenous	~ 150 MBq
^{90}Y	^{90}Y-microspheres	Treatment of non-resectable hepatomas and liver metastases	Injection via an intra-arterial catheter in the hepatic artery	1.5 - 2.5 GBq
	^{90}Y-ibritumomab tiuxetan	Treatments of patients with relapsed or refractory, low-grade or follicular B-cell non-Hodgkin's lymphoma	Intravenous	Depends on factors such as the patient's weight
	^{90}Y-silicate/citrate (as a colloid)	Treatment of inflammatory joint conditions in the radiosynoviorthesis	Injection into the joint	1.2 – 3.0 GBq
^{99m}Tc	^{99m}Tc-labelled albumin macroaggregate (MAA)	Scintigraphy for assessing lung shunt fraction and scanning lung perfusion	Injection via intra-arterial	75 - 150 MBq
	^{99m}Tc-methylene diphosphonate (MDP)	Bone metastases imaging	Intravenous	370 - 740 MBq
	^{99m}Tc-mercaptoacetyltriglycine (MAG3)	Renal function imaging	Intravenous	>740 MBq
	^{99m}Tc-sulphur (as a colloid)	Liver/spleen scans, gastric emptying scans	Intravenous	Depends on the area being evaluated
		Lymphoscintigraphy	Subcutaneous	

Isotope	Radiopharmaceutical	Application	Administration	Recommended Activity
^{131}I	^{131}I-sodium iodine	Treatment of residual thyroid cancer and metastatic disease; hyperthyroidism and non-toxic multinodular goitre	Oral	1.1 - 11.1 GBq
	^{131}I-labelled metaiodobenzylguanidine (MIBG)	Treatment of stage III or IV neuroblastoma, inoperable phaeochromocytoma, inoperable carcinoid tumour, inoperable paraganglioma, and metastatic or recurrent medullary thyroid cancer	Intravenous	3.7 - 11.2 GBq
	^{131}I-Lipiodol	Treatment of hepatic cancer	Injected into the hepatic artery in the form of fat droplets	0.9 - 2.4 GBq
	^{131}I-tositumomab	Treatment of follicular non-Hodgkin's lymphoma	Intravenous	Depends on the specific treatment protocol
^{153}Sm	^{153}Sm-lexidronam	Palliation of pain from bone metastasis	Intravenous	~ 37 MBq/kg
	^{153}Sm-ethylenediaminetetramethylene-phosphonate (EDTMP)			
^{177}Lu	^{177}Lu-DOTATATE	Treatment of neuroendocrine tumours	Intravenous	7.4 - 29.6 GBq
	^{177}Lu-Prostate-specific membrane antigen (PSMA)	Treatment of prostate cancer and its metastases	Intravenous	6 - 7.4 GBq
	^{177}Lu-DOTMP or ^{177}Lu-EDTMP	Palliation of bone pain	Intravenous	1.0 - 2.5 GBq

AE emitters are being increasingly investigated for theragnostic effects. Besides its applications for diagnosis, typically due to γ emissions, these radionuclides have an Auger spectrum that can be useful for therapy although they are not yet being used clinically. However, there is an increasing number of studies approving the effects of ^{67}Ga in the theragnostic context [37].

^{67}Ga is a radionuclide that disintegrates by 100% electron capture and emits γ rays. It has a half-life of 3.26 days and is produced in a cyclotron by irradiating ^{68}Zn. This radionuclide is considered for Auger therapy due to its spectra with emission of AEs [26]. ^{67}Ga is used for scintigraphy and SPECT imaging to detect inflammation and granulomatous reactions, since this radionuclide accumulates in areas of increased metabolic activity. It is typically administrated intravenously, with activity ranging from 1 to 3 GBq [38].

^{111}In is a radionuclide that decays by electron capture and is produced in a cyclotron; it is a γ emitter with a half-life of 2.8 days. ^{111}In-DPTA and ^{111}In-octreotide are radiopharmaceuticals used for scintigraphic imaging for diagnosis purposes. The recommended activity ranges between 10 and 160 GBq [39].

Also, ^{123}I is a commonly used radionuclide, with a half-life of 13.2 hours. It can be produced in a cyclotron by irradiating ^{124}Te. It emits γ rays with energies of 159 keV, which makes it suitable for SPECT imaging. Currently, it is used labelled with different compounds for thyroid, brain and myocardial imaging, such as ^{123}I-octreotide and ^{123}I-iodoamphetamine (IMP) [39].

^{201}Tl is a radionuclide used for SPECT imaging, agreeing with the previous nuclides; it emits γ rays, has a half-life of 73 hours and it is produced by irradiating ^{203}Tl in a cyclotron. This pharmaceutical is used to image lung, brain, bone and soft tissue tumours [39].

2.3. Dosimetry in Nuclear Medicine

The emission of ionizing radiation by the radionuclides used in nuclear medicine techniques has effects on the organs and tissues exposed to it and makes crucial the assessment and control of the absorbed dose in the target and non-target tissue [40], [41]. Therefore, this field is called internal dosimetry, which refers to the evaluation and assessment of energy deposited in organs or tissues after the administration of radiopharmaceuticals, while cellular dosimetry is referred to the measurement of the absorbed dose on individual cells.

Dosimetry in nuclear medicine can be classified into different techniques:

- Internal dosimetry:
  - voxel-based dosimetry, which evaluates the absorbed dose delivered to each voxel within a three-dimensional image.
  - organ-based dosimetry, where the assessment of the absorbed dose is more complex involving the segmentation of organs.
- Cellular dosimetry:
  - cell-based dosimetry, where the absorbed dose calculation is implemented in individual cells and other cellular components.

In the voxel-based approach, the heterogeneity of the medium tissues is not considered, contrarily to when using an organ-based methodology. Ideally, calculations must take into account the different compositions of the human body and the patient-specific anatomical geometry. This would require a CT scan of the whole body to posterior division into different sections based on the

composition (bone, muscle tissue, fat tissue, etc). After this, all the simulations to assess the absorbed dose may be performed according to the respective composition. This cannot be implemented in nuclear medicine procedures due to its high cost and the extensive time required for each patient. For that reason, the approaches in nuclear medicine must provide a combination of good accuracy and simple implementation.

In organ-based dosimetry, the calculations assume a uniform distribution of activity within the organs, which is a major limitation of this technique [42]. According to Lee *et al.* [42], voxel-based approaches are more suitable for calculations when a nonuniform activity distribution in organs is considered.

2.4. MIRD formalism

There are important absorbed dose calculations that must be accurately evaluated such as the absorbed dose both in the tumour and in the healthy tissue. For each tissue, the absorbed dose is determined as the amount of energy absorbed per unit mass. The Medical Internal Radiation Dose (MIRD), Committee of the Society of Nuclear Medicine (SNM), has an extensive archive of reports regarding radiation dosimetry and its implications when a radiopharmaceutical is administered. Therefore, the concept of S-values was introduced by MIRD to quantify the absorbed dose received by organs and tissues as well as the cellular S-values (dosimetry at the cellular level).

According to the MIRD scheme, the mean absorbed dose $\overline{D}$ is given by the cumulated activity Ã distributed in a source regium S (monoenergetic and containing the radionuclide) to the target volume T:

$$\overline{D} = \tilde{A}S(\mathrm{T} \leftarrow \mathrm{S}) \tag{2.4}$$

$$\tilde{A} = \int_{t_1}^{t_2} A(t)dt \tag{2.5}$$

where S represents the S-value.

In the case of a polyenergetic source, the S-value is calculated through the following equation, involving multiple decay modes:

$$S(\mathrm{T} \leftarrow \mathrm{S}) = \sum_{i=1}^{n} \frac{\Delta_i \phi_i(\mathrm{T} \leftarrow \mathrm{S})}{m_T} \tag{2.6}$$

where Δ_i is the mean energy per nuclear transition of the *i*-th radiation component and $\phi_i(\mathrm{T} \leftarrow \mathrm{S})$ is the corresponding fraction of energy emitted from the source region that is absorbed in the target volume, whose mass is m_T [43].

In 2003, another formalism was established. The RAdiation Dose Assessment Resource (RADAR) instituted a formalism to calculate an internal dose estimation through the following equation:

$$D = N \times \mathrm{DF} \tag{2.7}$$

where N is the number of disintegrations that occur in a source organ and DF is the 'dose factor' [43], given by

$$\mathrm{DF} = \frac{k \sum_i n_i E_i \phi_i}{m} \tag{2.8}$$

where k represents a proportionality constant ($(\mathrm{rad} \cdot \mathrm{g})/(\mu\mathrm{Ci} \cdot \mathrm{hr} \cdot \mathrm{MeV})$ or $(\mathrm{Gy} \cdot \mathrm{kg})/(\mathrm{MBq} \cdot \mathrm{s} \cdot \mathrm{MeV})$), n_i the number of radiations with energy E_i emitted per nuclear transition, ϕ_i the absorbed fraction and m the mass of the target [44]. The 'dose factor' is multiplied by the time-integrated activity to obtain the absorbed dose per disintegration [43]. Mathematically, this method is equivalent to the MIRD formalism.

2.5. S-values in Nuclear Medicine

As described above, S-values might be calculated to evaluate the absorbed dose for tissues or tumours after the emission of radiation due to radionuclide decay. As shown in Equation 2.4, these values are fundamental in those calculations where the aim is to assess the quantity of radiation that reaches the tumour and non-tumour tissues. From a clinical perspective, the calculations with S-values are essential for diagnosis and therapeutic planning, where it is necessary to assess the biodistribution of the radiopharmaceuticals and minimize absorbed dose delivery to healthy tissues while maximizing it to the target to destroy tumour cells. This allows to achieve a positive outcome of the disease diagnosis or therapy, *i.e.*, to increase the efficacy [45]. Internal dosimetry has also a strong influence on calculations for radiation protection, by estimating the total absorbed dose received. On behalf of that, S-values calculations have an important role in safety procedures, allowing the development of protocols for patients and professionals [36]. By providing a better understanding of radiation dosimetry and by improving the accuracy of dosimetry calculations, these values are useful for patients and clinical professionals. Figure 2.3 illustrates the basic steps for the absorbed dose calculations in the clinical workflow [46]. The cumulated activity, Ã, might be assessed after the determination of the radiopharmaceutical activity, which is often measured with activity calibrators (with low uncertainties, ~5%) [47]. Thus, the absorbed dose is calculated by Equation 2.4, where it is essential to have an adequate S-value.

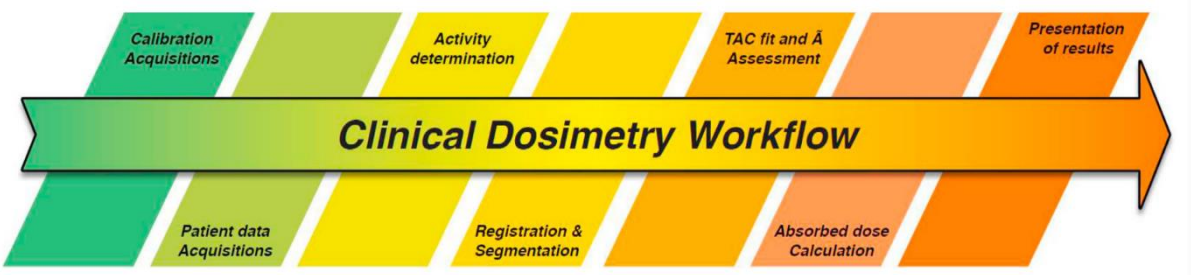

Figure 2.3 Steps for the absorbed dose calculation (from [46]).

Recognizing the extreme importance of internal dosimetry in nuclear medicine therapies, there are several studies for S-values calculations, using different methodologies [48]. For three-dimensional internal dosimetry, there are three approaches with relevance for this dissertation: the convolution of voxel S-values (VSV), the convolution of Dose Point Kernel (DPK) and the direct MC simulation. The methodology related to direct MC simulations is the most accurate approach but the one that requires more computational time and resources, making it only practicable for research or for S-value

generation. The results can also be physically distinct since the approach implemented depends on diverse factors such as:

1. Geometry and organ size: as mentioned in section 2.3, there are two different approaches for internal dosimetry regarding the geometry and, for that reason, the absorbed dose might be calculated by using anthropomorphic models or voxelized targets.
2. Radionuclide database and distributions: currently there are several databases that provide decay data for the radionuclides used in nuclear medicine. Furthermore, the distribution of the radionuclide is also a factor that needs to be considered for these calculations.

In summary, S-values can be calculated by using various methods, which implies an extensive review and comparison to understand their effect on internal dosimetry.

Despite the use of AE in therapeutic practices remains uncommon, there is a continuous increase of research on their applications for nuclear medicine. Similarly to internal dosimetry, S-values have significant importance in cellular dosimetry, as absorbed dose calculation methods are essential [49]. Standard dosimetric approaches provide methods to estimate the mean absorbed dose at the organ level. However, it is relevant to supply methods for determining the absorbed dose in individual cells in TRT [24].

2.6. State-of-the-art

This report aims to calculate S-values at the voxel and cellular levels through Monte Carlo simulations and using the MIRD formalism, developed by the MIRD Committee. This committee has several responsibilities concerning radiation dosimetry, being one of the most prestigious references in this field. They have published numerous pamphlets, reports and books with the developments of methodologies, models, assumptions, and mathematical schemas for radiation dosimetry. In addition to the MIRD Committee, the work of the International Commission on Radiological Protection (ICRP) is also highly regarded by medical physics experts. The ICRP has issued various publications, most of them particularly focused on radiological protection. Hence, ICRP offers recommendations for radiation protection based on the effects of ionizing radiation. The International Commission on Radiation Units & Measurements (ICRU) is also a notable reference due to its publications with recommendations on quantities and units, terminology, measurement procedures and data for applications involving ionizing radiation. These commissions share a common expertise in radiation dosimetry, making their publications essential references for the objectives of this dissertation.

2.6.1. Voxel-level S-values

The use of radiopharmaceuticals has become a regular practice in nuclear medicine; thus, tables of S-values are frequently being published by medical and research organizations, enabling fundamental data to be available for clinical practice.

MIRD Pamphlet 17 [50] serves as a reference for S-values at the voxel level. This pamphlet delineates the fundamental approaches for conducting voxel dosimetry in accordance with the MIRD formalism. It reports tabulations of voxel S-values for five radioisotopes and for two voxel dimensions, calculated with version 4 of the Electron Gamma Shower (EGS4) code, with the PRESTA algorithm, for MC simulations of radiation transport. To model part of the human body, MIRD Pamphlet 17 [50]

developed a cubical phantom divided into 1331 cubical voxels with 3 mm or 6 mm side dimensions, representing an 11×11×11 voxel cube (Figure 2.4). In this geometry, the central voxel contains the radioactive source, where the activity is assumed to be uniformly distributed within that voxel and the radiation passing through adjacent voxels is then calculated. Also, the model is placed in a homogeneous infinite medium composed of soft tissue, with composition according to Eckerman and Christy's, Oak Ridge report [51] for specific absorbed fractions of energy. For nuclear decay data, the Eckerman and Christy, Oak Ridge report [52] database, dated from 1993, was used. The results are presented in different tables according to the radionuclide selected. The absorbed dose is calculated for each voxel, which is represented by a coordinate system where the central voxel is positioned in the origin with the coordinates (0,0,0) and axes x, y, and z are centred on it. Due to the geometry considered, there is a cubical symmetry, and, for that reason, the pamphlet only presents values for positive coordinates, which are symmetrical to those for negative coordinates. Consequently, in the appendices, the tables only display values for one octant of the cubic geometry.

Although MIRD Pamphlet 17 [50] is used for professional and medical intents, it lacks certain details necessary for a comprehensive understanding of the methodology, such as the number of histories simulated, and the uncertainties associated with the tabulated values. Additionally, various platforms provide S-values calculated using different formalisms and MC codes with specific parameters.

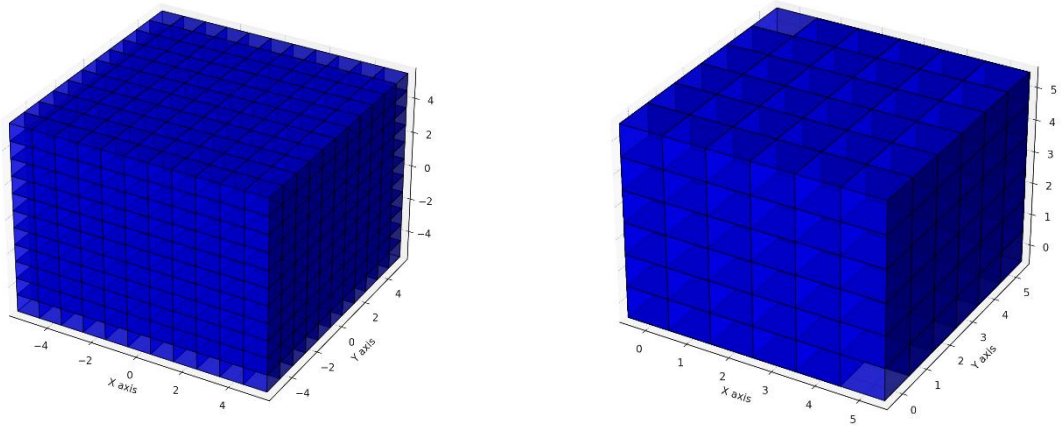

Figure 2.4: The left image represents the whole geometry, a 11×11×11 voxels cube; the right image is a representation of the positive octant (image created with AI).

A free and online available database developed by Bologna University (www.medphys.it, 2011) offers voxel S-values for seven radionuclides with relevance for nuclear medicine (^{177}Lu, ^{131}I, ^{153}Sm, ^{186}Re, ^{89}Sr, ^{188}Re, ^{90}Y) and thirteen different voxel sizes [40]. The MC simulations were carried out using the EGSnrc code, for monoenergetic photon and electron sources. The decay data for the electron and photon spectra of the radionuclides were obtained from the Brookhaven National Laboratory database by Stabin *et al*. (2002) [53]. This study scored the energy deposited in grids of cubic voxels, with the source uniformly distributed in a voxel, irradiating the surrounding voxels isotropically. The geometry defined is a representation of an approximately infinite medium (a homogeneous region that can encompass the entire target region) and can consist of two homogeneous tissues: soft tissue, with composition defined by Cristy and Eckerman [51], or bone tissue, as defined by ICRU Report 10b [54]. Regarding simulation parameters, a cutoff energy of 1 keV was selected for both electrons and photons and 25 million particles were tracked [40]. The energy scored in the simulations was converted into units of

absorbed dose (mGy MBq^{-1} s^{-1}) and the contribution of each monoenergetic source (electron or photon) was applied according to the decay spectra.

In the early 1990s, a software called 'MIRDOSE' was developed to calculate the absorbed dose for nuclear medicine applications. The code was written in the VisualBasic programming language and was based on the MIRD formalism, although it was neither approved nor reviewed by the MIRD Committee. About ten years later, this code was rewritten in the Java programming language and named OLINDA/EXM (Organ Level Internal Dose Assessment for EXponential Modeling). Currently, only version 2.0 is available, and it is part of Hermes Medical Solutions [44], [55]. This approach uses mathematical models for S-values calculations, specifically the RADAR formalism (section 2.4). Version 2.0 includes updated computational phantoms that are voxel-based and anatomically realistic, developed by Segars *et al.* (2001) [56] and aligned with the organ masses in ICRP Publication 89 [57]. Therefore, this database includes male and female phantoms for various ages, namely 1-year-olds, 5-year-olds, 10-year-olds, and 15-year-olds, adults and pregnant women. Absorbed dose estimates are presented for over 1000 radioisotopes, with nuclear decay data based on the Brookhaven National Laboratory database [53]. From a broad perspective, this database aims to calculate absorbed doses in realistic phantoms closely approximating reality, despite the computational time required. Consequently, some data in Table 2.2 are incomplete, such as the distribution of the radioactive source or the uncertainties associated with the calculations.

In addition, the absorbed dose can be calculated by "Internal Dose Assessed by Computer" (IDAC-Dose, 2017), a free software for research purposes. IDAC-Dose 2.1 is an internal dosimetry computer software that employs a MATLAB program for calculations in nuclear medicine, based on the MIRD formalism [58]. A total of 48048 MC simulations were conducted with the MCNP 6.0 code to generate specific absorption fraction (SAF) data for the software. Similar to OLINDA 2.0, this software also uses computational voxel phantoms for adults, as given by the ICRP Publication 89 [57]. In this database, absorbed doses are estimated for up to 1252 radionuclides, with decay information derived from ICRP Publication 107 [60]. Users have the possibility to select the placement of the source and its activity distribution (uniformly or nonuniformly) within the region. However, the number of particles used in the MC simulations was not disclosed.

OpenDose (2020) is the result of a collaboration aimed at freely generating and providing dosimetric data [61]. It comprises 18 research teams from 30 institutes. For that reason, the published data were calculated using a variety of MC codes, including Electron Gamma Shower (EGS), FLUktuierende KAskade (FLUKA), Geant4 Application for Tomographic Emission (GATE), GEometry ANd Tracking (Geant4), Monte Carlo N-Particle (MCNP) and PENELOPE [61]. Despite the large number of teams, a defined framework ensured that all teams followed essentially the same methods, using the same input models and delivering the data in a common output format. OpenDose adopts human voxel-based phantoms to perform simulations, based on the considerations of ICRP Publication 110 [62], which includes segmented regions and different media for various voxel dimensions. These models are representations of the average anatomy of male and female bodies. The radioactive source can be uniformly or pointwise distributed in a voxel, and the nuclear decay data is obtained from ICRP Publication 107 [60], covering 1252 radioisotopes. This database recommended the use of at least 10^8 primary particles and the S-values are presented along with their associated statistical uncertainties.

A graphical user interface, named National Cancer Institute Dosimetry System for Nuclear Medicine (NCINM, 2020) gives values for internal dosimetry [63]. This database offers S-values calculated following the MIRD formalism. It uses computational human phantoms developed in a collaboration between the University of Florida and the National Cancer Institute, with anatomical data from ICRP Publication 89 [57]. Similar to OLINDA, these phantoms include male and female models for various ages- 1-year-olds, 5-year-olds, 10-year-olds, 15-year-olds, and adults. A comprehensive set of photon and electron absorbed fractions were computed using MCNPX version 2.7 and, like IDAC-Dose, a

MATLAB program was used to calculate the S-values. This database includes a set of 300 radionuclides, with decay data from ICRP Publication 107 [60]. For the MC simulations, a total of 100 million particles were simulated, resulting in statistical uncertainties below 1%.

Except for MIRD Pamphlet 17 [50] and the database by Bologna University [40], all the databases use complex geometries, such as human organ phantoms, which compromises high computational times for clinical practices by dosimetry physicists. Pistone *et al.* (2022) [48] validated an analytic model for fast calculations of VSVs for ^{177}Lu and for voxel dimensions between 2 mm and 6 mm. This model surpasses the necessity of implementing numerous MC simulations for specific voxel dimensions not available in the literature, by allowing to deduce VSVs for specific voxel dimensions. However, it is only available for ^{177}Lu, which is not efficient for clinical use.

Table 2.2 summarizes the fundamental characteristics of each database, mentioned in this section. The S-values are extremely useful for oncological therapies in nuclear medicine. This type of medical equipment offers a wide range of voxel sizes, based on factors such as the acquisition field of view, the reconstruction matrix utilized, the zoom factor applied, and the specific manufacturer. As a result, many more calculations are needed to obtain the S-values for all the situations when using different equipment and/or different settings. These calculations must be conducted by physicists in clinical departments and it may not be viable to perform MC simulations for each necessary S-value [40]. Dr. Maria Emilia Seren Takahashi provided insights into current needs, identifying the most significant voxel dimensions for cancer TRT in three PET and SPECT equipments available in the Nuclear Medicine Department of Universidade de Campinas. Table 2.3 summarizes information for one of the equipments, indicating the fact that there are indeed many different settings for operating these devices. The highlighted lines identify the values most commonly used in clinical practice. Figure 2.5 helps the reader to understand the spatial orientation of the voxels within the body.

Table 2.2: Analysis of different databases.

Database	Methodology	Radionuclides	Formalism	MC code	Material composition	Material composition database	Radioactive source distribution	Nuclear decay database	Number of histories
MIRD Pamphlet 17 [50]	Voxel (2 sizes)	5	MIRD	EGS4	Soft tissue	Oak Ridge Report [51]	Uniform in the central voxel	Oak Ridge Report [52]	N/A
Free Database MedPhys [40]	Voxel (13 sizes)	7	MIRD	EGSnrc	Soft tissue	Oak Ridge Report [51]	Uniform in the central voxel	Brookhaven National Laboratory Report [53]	25×10^6 particles
					Bone tissue	ICRU Report 10b [54]			
OLINDA 2.0 [55]	Voxel-based, anatomically realistic phantoms	Over 1000	RADAR	N/A	Various	ICRP 89 [57]	N/A	Brookhaven National Laboratory Report [53]	N/A
IDAC-Dose 2.1 [58]	Voxel-based phantoms	1252	MIRD	MCNP 6.0	Various	ICRP 89 [57]	Uniform or point (defined by the user)	ICRP 107 [60]	N/A
OpenDose [61]	Voxel-based phantoms	1252	MIRD	Variety of codes	Various	ICRP 110 [62]	Uniform or point (defined by the user)	ICRP 107 [60]	At least 10^8 particles
NCINM [63]	Uses phantoms	300	MIRD	MCNPX version 2.7	Various	ICRP 89 [57]	N/A	ICRP 107 [60]	100×10^6 particles

N/A: does not provide information or it is not clear.

Table 2.3: Specific parameters of the medical equipment for SPECT/CT imaging (Manufacturer: GE Healthcare; model: Millennium MG (H3000ZL); manufactured: 30 July 2009).

Matrix	Zoom	Thickness (reconstruction)	Voxel (x) [mm]	Voxel (y) [mm]	Voxel (z) [mm]
64x64	1.0	1	9.04	9.04	9.04
		2	9.04	9.04	18.08
64x64	1.14	1	7.91	7.91	7.91
		2	7.91	7.91	15.82
64x64	1.33	1	6.78	6.78	6.78
		2	6.78	6.78	13.56
64x64	1.60	1	5.65	5.65	5.65
		2	5.65	5.65	11.3
64x64	2.0	1	4.52	4.52	4.52
		2	4.52	4.52	9.04
128x128	1.0	1	4.52	4.52	4.52
		2	4.52	4.52	9.04
128x128	1.14	1	3.95	3.95	3.95
		2	3.95	3.95	7.9
128x128	1.33	1	3.39	3.39	3.39
		2	3.39	3.39	6.78
128x128	1.60	1	2.82	2.82	2.82
		2	2.82	2.82	5.64
128x128	2.0	1	2.26	2.26	2.26
		2	2.26	2.26	4.52

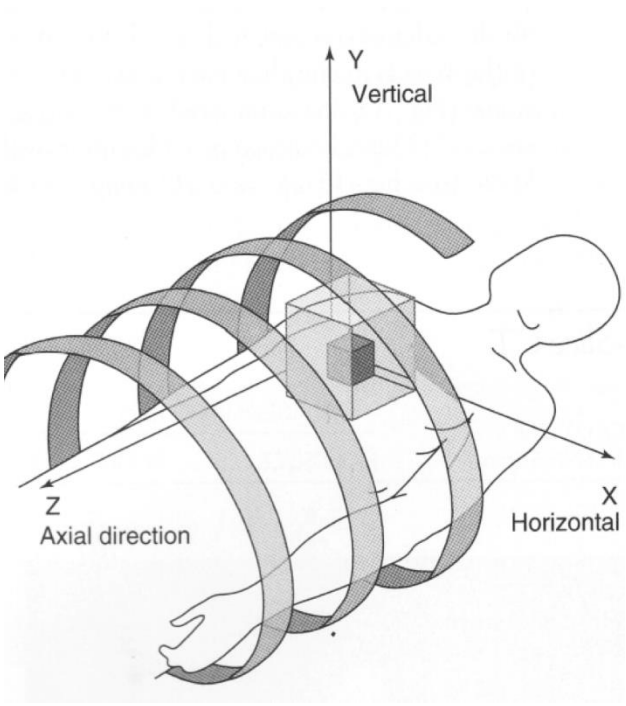

Figure 2.5: Schematic representation of x, y and z axes for SPECT and PET imaging (from [64]).

2.6.2. Cellular-level S-values

At the cellular level, the majority of the absorbed dose within the components of the cell results from the decay of radionuclides that emit AE and CK electrons [65]. Various radionuclides have been suggested for tumour treatments in radiotherapy of small metastases and disseminated cancer cells [39], [66]. These electrons typically have a range approximately equivalent to the dimensions of condensed DNA within the cells, causing biological effects at the cellular level [67], [68]. Since S-values might be described as the absorbed dose to the target volume per unit of cumulated activity in the source region, at the cellular level there can be four source regions (nucleus (N), cytoplasm (Cy), cell (C), and cell surface (CS)) where the radionuclide is emitting radiation and three target volumes (nucleus (N), cytoplasm (Cy) and cell (C)). Hence, there are twelve possible (T ⟵ S) combinations. Due to the additive nature of S-values, only six combinations are required to obtain the values of all of them (Equation 2.9).

$$\mathrm{S(C \longleftarrow N) = S(N \longleftarrow N) + S(N \longleftarrow Cy)} \tag{2.9}$$

Equation 2.9 reflects the additivity of S-values since the absorbed dose in the cell can be distributed into absorbed dose in the nucleus and the cytoplasm when the source region is the same emitting radiation. In this context, the absorbed dose is calculated in individual cells. Figure 2.6 depicts the cellular model, consisting of two concentric spheres of radii R_C and R_N, which correspond to the radii of the cell and its nucleus, respectively.

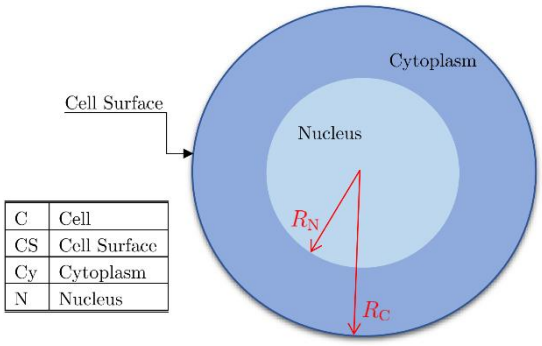

Figure 2.6: MIRD cell model. (from [24]).

Currently, the MIRD Committee [69] has reference values for cellular S-values for spheric cell geometries with concentric nuclei. Several source-target combinations are presented, including C ⟵ C, C ⟵ CS, N ⟵ N, N ⟵ Cy and N ⟵ CS. The concept of S-values follows the MIRD schema, as presented in section 2.4. In Equation 2.6, the S-value depends on $\phi_i(\mathrm{T \longleftarrow S})$, which corresponds to the fraction of energy emitted from the source S to the target T. This factor can be straightforwardly determined with MC simulations or analytically. However, a separate simulation is needed for each cell geometry and composition, making it a time-consuming process [70]. This reference uses analytical and mathematical models to calculate cellular S-values for a comprehensive list of radionuclides (used in diagnostic and therapeutic applications) and for twenty-seven combinations of (R_C, R_N). More specifically, the MIRD Committee published cellular S-values calculated using the DPK method. This method can be more efficient than direct MC simulations [24]. Important to note that the MIRD calculations were performed with simplified physics, where the electrons move in a straight line and the

energy deposition is dictated by the stopping power, *i.e.*, the elastic scattering is neglected and the energy loss is calculated by using the continuous slowing down approximation (CSDA).

The DPK approach models the distribution of absorbed dose due to a radioactive source at a microscopic level. Conceptually, a point and isotropic source immersed in an infinite and homogeneous medium made up of liquid water is defined, emitting monoenergetic electrons or other particles with a given kinetic energy *E*. Considering that this source is located at a certain point $\overrightarrow{r_0}$, the absorbed dose received by a spherical shell of thickness dr at a distance r will be $D(r)$, the radial dose distribution [70]. Knowing that the mass of the spherical shell is $4\pi r^2 dr\,\rho$, where ρ is the mass density of the medium, the fraction of energy deposited in it can be determined as

$$d\phi(r,\overrightarrow{r_0}) = 4\pi r^2 dr \rho \frac{D(r)}{E}\,. \tag{2.10}$$

When a target volume T is placed in the same medium (Figure 2.7), the fraction of that energy deposited in T will be $\phi(\mathrm{T} \leftarrow \overrightarrow{r_0})$. The fraction of the spherical surface lying inside the target region is represented by $\psi_{\mathrm{T}\leftarrow\overrightarrow{r_0}}(r)$ (identified in red in Figure 2.7) and, as a consequence, the fraction of energy deposited is

$$\phi(\mathrm{T} \leftarrow \overrightarrow{r_0}) = \int_{r=0}^{\infty} \psi_{\mathrm{T}\leftarrow\overrightarrow{r_0}}(r)\, d\phi(r,\overrightarrow{r_0}) = \int_{r=0}^{\infty} 4\pi r^2 \rho \frac{D(r)}{E} \psi_{\mathrm{T}\leftarrow\overrightarrow{r_0}}(r)\, dr. \tag{2.11}$$

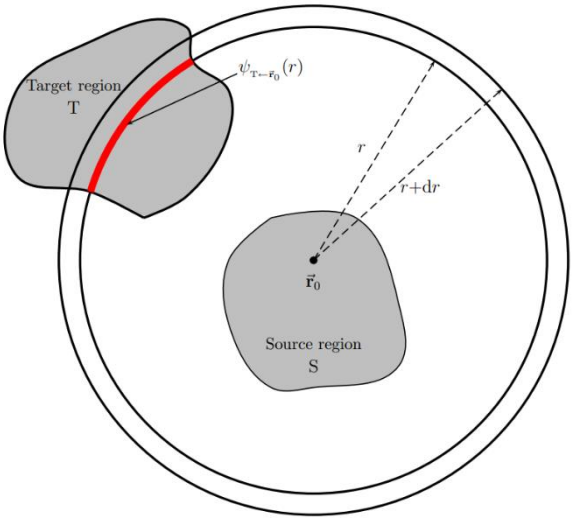

Figure 2.7: Dose Point Kernel approximation. (from [24]).

This equation must only be used when the source is considered to be a point. If the source is extended to a region S, each point within S may be perceived as an independent radiation emitter that contributes with a proportional fraction of energy to the total absorbed dose D to the target volume T.

$$\phi(\mathrm{T} \leftarrow \mathrm{S}) = \int_{r=0}^{\infty} 4\pi r^2 \rho \frac{D(r)}{E} \psi_{\mathrm{T}\leftarrow\mathrm{S}}(r)\, dr. \tag{2.12}$$

After these considerations and taking into consideration Equation 2.6 (section 2.4), the S-values calculated with DPK methods can be expressed as

$$S(\mathrm{T} \leftarrow \mathrm{S}) = \frac{1}{m_T} \int_0^{\infty} 4\pi r^2 \rho \, D(r) \, \psi_{\mathrm{T}\leftarrow\mathrm{S}}(r) \, dr. \tag{2.13}$$

The function $\psi_{\mathrm{T}\leftarrow\mathrm{S}}(r)$, previously defined, is known as geometric reduction factor (GRF), and it can also be defined as the probability that an arbitrarily oriented vector of length r that starts from a random point within the source region S ends within the target volume T. Goddu *et al.* (1997) [69] published the analytical expressions for GRFs, for source-target combinations N ⟵ N, N ⟵ Cy, N ⟵ CS, CS ⟵ CS and C ⟵ C. GRF expressions for only three combinations will be presented in this dissertation (Equation 2.14 - 2.17). Important to consider that these equations only can be applied when the cell is represented by two concentric spheres. When nonconcentric nucleus or ellipsoidal cells are considered, the S-values must be calculated by MC simulations.

$$\psi_{\mathrm{N}\leftarrow\mathrm{N}}(r) = \begin{cases} 1 - \dfrac{3}{4}\dfrac{r}{R_N} + \dfrac{1}{16}\left(\dfrac{r}{R_N}\right)^3 & \text{if } 0 \le r \le 2R_N, \\ 0 & \text{otherwise.} \end{cases} \tag{2.14}$$

$$\psi_{\mathrm{N}\leftarrow\mathrm{CS}}(r) = \begin{cases} \dfrac{2R_C r + {R_N}^2 - {R_C}^2 - r^2}{4R_C r} & \text{if } R_C - R_N \le r \le R_C + R_N, \\ 0 & \text{otherwise.} \end{cases} \tag{2.15}$$

If $R_C \le 3R_N$:

$$\psi_{\mathrm{N}\leftarrow\mathrm{Cy}}(r) = \begin{cases} Qr^2\left({R_N}^2 - \dfrac{r^2}{12}\right) & \text{if } 0 \le r \le R_C - R_N, \\ Q\left[\begin{array}{c} \dfrac{1}{2}\left({R_C}^2 - {R_N}^2\right)\left({R_N}^2 - r^2\right) + \\ +\dfrac{2r}{3}\left({R_C}^3 - {R_N}^3\right) - \dfrac{1}{4}\left({R_C}^4 - {R_N}^4\right) \end{array}\right] & \text{if } R_C - R_N < r \le 2R_N, \\ \dfrac{Q}{12}\left[\begin{array}{c} r^4 + 6\left({R_C}^2{R_N}^2 - r^2{R_C}^2 - r^2{R_N}^2\right) + \\ +8r\left({R_C}^3 + {R_N}^3\right) - 3\left({R_C}^4 + {R_N}^4\right) \end{array}\right] & \text{if } 2R_N < r \le R_C + R_N, \\ 0 & \text{if } r > R_C + R_N. \end{cases} \tag{2.16}$$

If $R_C > 3R_N$:

$$\psi_{\mathrm{N}\leftarrow\mathrm{Cy}}(r) = \begin{cases} Qr^2\left({R_N}^2 - \dfrac{r^2}{12}\right) & \text{if } 0 \le r \le 2R_N, \\ \dfrac{{R_N}^3}{{R_C}^3 - {R_N}^3} & \text{if } 2R_N < r \le R_C - R_N, \\ \dfrac{Q}{12}\left[\begin{array}{l} r^4 + 6\left({R_C}^2{R_N}^2 - r^2{R_C}^2 - r^2{R_N}^2\right) + \\ +8r\left({R_C}^3 + {R_N}^3\right) - 3\left({R_C}^4 + {R_N}^4\right) \end{array}\right] & \text{if } R_C - R_N < r \le R_C + R_N, \\ 0 & \text{if } r > R_C + R_N. \end{cases} \quad (2.17)$$

In these expressions, $Q = \frac{3}{4r({R_C}^3 - {R_N}^3)}$.

MIRD book by Goddu *et al.* (1993) [41] published cellular S-values for various radionuclides (^{32}P, ^{35}S, ^{51}Cr, ^{67}Ga, ^{86}Rb, ^{89}Sr, ^{90}Y, ^{91}Y, ^{99m}Tc, ^{111}In, ^{114m}In, ^{123}I, ^{125}I, ^{131}I, ^{201}Tl, ^{203}Pb, ^{210}Po, ^{212}Pb, ^{212}Bi and ^{212}Po). In that study, the cells were considered spherical with concentric nucleus, submersed in an infinite medium of liquid water. The S-values presented were calculated mathematically by a FORTRAN 77 program code, according with the previously explained DPK methodology and the expressions defined for $\psi_{\mathrm{T}\leftarrow\mathrm{S}}(r)$. The radioactive source was uniformly distributed in various cells compartments, and values were calculated for various source-target combinations: C ← C, C ← CS, N ← N, N ← Cy, N ← CS. The radii of the cell and cell nucleus ranged from 2 to 10 μm, totalling twenty-two combinations. The radionuclides decay data for beta and alpha emitters were taken from Weber *et al.* [71] and for AEs emitters from the American Association of Physicists in Medicine Task Group report [72].

The study conducted by Uusijärvi *et al.* (2006) [73] reported a comparison of cellular S-values calculated with DPKs generated by various MC codes: PENELOPE, MCNPX and GEANT4. The two concentric spheres that formed the model had radii of 6 μm and 4 μm, representing the radii of the cell and the cell nucleus, respectively. The S-values were generated for three source-target combinations, N ← N, N ← Cy and N ← CS, using a monoenergetic electrons source with energies of 10 keV, 100 keV, 500 keV and 1MeV. The activity was assumed to be uniformly distributed within the source region. The results showed good agreement between the three MC codes, except for the cases when the source is located on the cell surface. In 2009, Uusijärvi *et al.* [74] published a similar comparison, adding also ETRAN MC code. The methodology used for the simulation was the same as the previous one. Instead of tables, the results were displayed in graphics to demonstrate the variation in DPK when the target is at different distances from the source. The conclusions corroborated the previous findings, indicating that the choice of MC code does not affect the S-values in a significant way.

Falzone *et al.* (2015) [75], in a more recent approach, calculated S-values at the cellular level, comparing different methodologies: direct MC simulations and DPK. Both approaches were calculated using the PENELOPE MC code with the same parameters: the absorption energy for electrons, photons and positrons was 50 eV, the cutoff energies were set to zero (event-by-event simulation) and the same number of primary particles (2×10^9 histories) was used. The cell model was similar to the one illustrated in Figure 2.6, composed of two concentric and homogeneous spheres of liquid water, immersed in an infinite water medium. The radii of the cell varied from 3 to 12 μm and the radii of the nucleus from 1

to 11 μm. The N ← N, N ← Cy and N ← CS combinations were selected. The nuclear decay data was taken from the RADTABS software, version 2.2. This software is an early version of DECDATA software. The values calculated showed great accordance with those published by the MIRD Committee [69], noticing the largest discrepancies when the source and target volumes were farther apart. This article also furnishes information regarding the influence of the non-concentricity of the nucleus in the cell, but this is not part of the objectives of the present dissertation.

CHAPTER 3

Monte Carlo Simulations

Monte Carlo (MC) simulations are used to solve mathematical and physical problems using non-deterministic (stochastic) algorithms. The name was given after the Monte Carlo Casino in Monaco and was firstly used at Los Alamos by scientists during World War II for a nuclear weapon project. Nowadays, it has become an efficient tool for problems with multiple independent variables [76].

MC simulations are particularly accurate for radiation transport applications describing the penetration and energy loss of electrons and photons [77]. In the medical field, this method has been largely used due to its capability to address situations that are relatively difficult to solve analytically [76]. Those simulations demonstrate to be important for diagnostic medical imaging research. In the previous chapter, S-values, in the context of radiation dosimetry, were defined as the absorbed dose within a designated target volume, resulting from the decay of a radioactive source distributed in a source region. In this chapter, basic concepts of MC simulations are presented to provide a better understanding of this powerful method.

3.1. Basic concepts

The main characteristic to describe MC simulations is the use of non-deterministic algorithms, *i.e.*, involving random numbers and random variables, which are associated with a probability distribution function (PDF). Summarized, the propagation of radiation in matter is defined by numerically sampling, where the history (track) of a particle is perceived as a random series of free flights that culminate in an interaction event where the particle changes direction and/or loses energy and, occasionally, produces secondary particles [70], [78]. Therefore, if we consider I as a random variable and $\bar{I}$, $\sigma^2(I)$ represents the mean and the variance of I, respectively, the relative uncertainty is given by

$$\frac{\sigma(I)}{\bar{I}} = \frac{1}{\sqrt{N}} \tag{3.1}$$

where N is the number of primary histories.

This is an important consideration regarding MC simulations. To decrease the uncertainties related to the simulations, it is mandatory to increase the number of histories. For instance, if we want to reduce the uncertainty to half, the number of histories must be increased in four times. This will affect the computational time and the speed of the simulation. Furthermore, there will be a compromise between the computer time and the uncertainty that we want to achieve.

3.1.1. Elements of probability theory

The PDF describes the probability of each value of the random variable (when the variable is discrete) or the probability of the value being within a particular interval (when the variable is continuous). In the following equation, it is expressed the probability of obtaining x in a differential interval of length dx about x_1,

$$\mathcal{P}\{x|x_1 < x < x_1 + dx\} = p(x_1)dx, \tag{3.2}$$

where $p(x)$ is the PDF of x, that must be positive and normalized,

$$p(x) \geq 0, \qquad \int_{x_{min}}^{x_{max}} p(x)dx = 1\,. \tag{3.3}$$

Hence, the PDF is defined by these conditions. When the random variable takes discrete values, the PDF is defined by

$$p(x) = \sum_i p_i\, \delta(x - x_i)\,. \tag{3.4}$$

For both continuous and discrete variables, the cumulative distribution function can be expressed as

$$\mathcal{P}(x) \equiv \int_{x_{min}}^{x} p(x')dx'\,. \tag{3.5}$$

3.1.2. Random-sampling methods

As mentioned above, MC methods include the generation of random numbers with specified PDFs. Random-sampling algorithms produce a sequence of random numbers ξ uniformly distributed in the interval $(0,1)$ of a variable x distributed in the interval (x_{max}, x_{min}).

3.1.2.1. Inverse-transform method

The cumulative distribution function $\mathcal{P}(x)$, presented in Equation 3.5, can be inverted analytically, having as an inverse function $\mathcal{P}^{-1}(\xi)$. A new random variable is created when the transformation $\xi = \mathcal{P}(x)$ is defined, which values are in the interval $(0,1)$. Due to the correlation between the variable x and ξ values, the PDF of ξ, denoted as $p_\xi(\xi)$, is directly linked to the PDF of x, $p(x)$, through $p_\xi(\xi)d\xi = p(x)dx$. Consequently,

$$p_\xi(\xi)d\xi = p(x)\left(\frac{d\xi}{dx}\right)^{-1} = p(x)\left(\frac{d\mathcal{P}(x)}{dx}\right)^{-1} = 1. \tag{3.6}$$

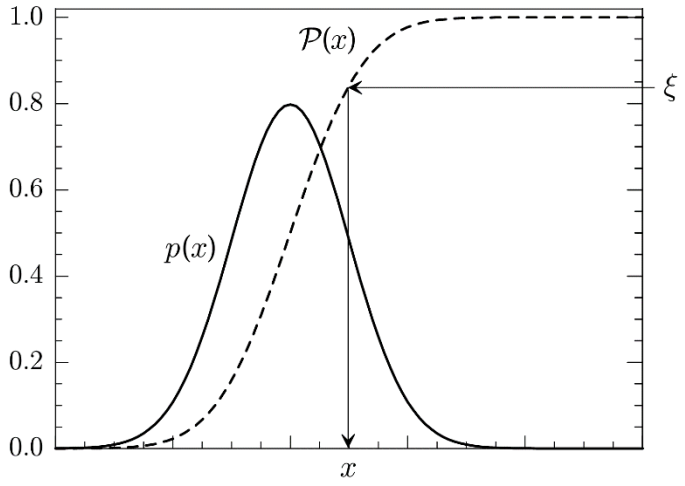

Figure 3.1: Random sampling from a distribution p(x) using the inverse-transform method. (from [76]).

From this, we can conclude that, if ξ is a random number, the variable x defined by $x = \mathcal{P}^{-1}(\xi)$ is randomly distributed in the interval (x_{min}, x_{max}) with the PDF $p(x)$ (Figure 3.1). The randomness of x is guaranteed by that of ξ. These are the main bases of inverse-transform method, where the equation

$$\xi = \int_{x_{min}}^{x} p(x')dx' \tag{3.7}$$

represent the sampling equation of the variable x.

The inverse-transform method can also be used to sample from discrete PDFs, as sketched in Figure 3.2. In this case, i is the integer that fulfils the following conditions,

$$P_i < \xi \leq P_{i+1}\,. \tag{3.8}$$

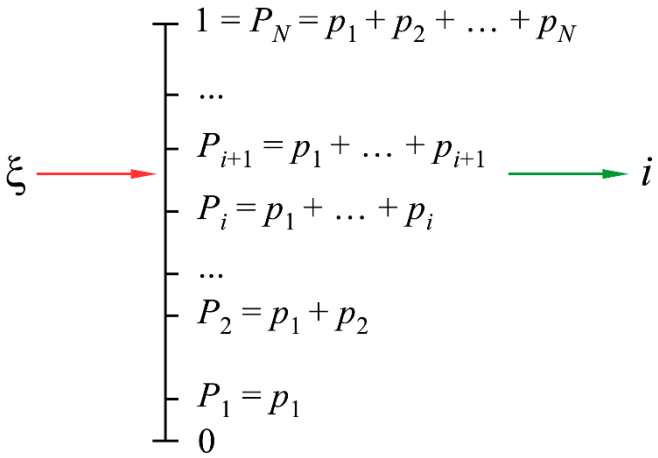

Figure 3.2: Inverse- transform algorithm to sample the integer index *i* from a discrete PDF. (from [79]).

3.1.2.2. Rejection methods

The inverse-transform method for random sampling, previously described, relies on establishing a one-to-one correspondence between x and ξ values, articulated through a single-valued function. The rejection method is another sampling approach that involves selecting a random variable from a distinct distribution (different to $p(x)$) and then subjecting it to a random test to ascertain if it is suitable for acceptance or rejection [76], [79]. Initially, it is sampled two random numbers (x, y) uniformly distributed in the rectangle $(a, b) \times (0, c)$ for posterior analysis. If $y > p(x)$, the point is rejected, as shown in Figure 3.3, where is represented the sampling of random kinetic energies of the electrons emitted in the β^- disintegration of ^{90}Y by using rejection algorithms. The crosses and circles in the figure represent the points rejected and accepted, respectively.

This rejection method can be described by the following sampling algorithm:

[1] Select an arbitrary upper bound c such that $p(x) < c$
[2] Sample a random point (x, y) uniformly distributed in $(a, b) \times (0, c)$ using the inverse transform recipe $x = a + (b - a)\xi_1, y = c\xi_2$
[3] If $y > p(x)$ reject the point; go to [2]. Else, deliver x.

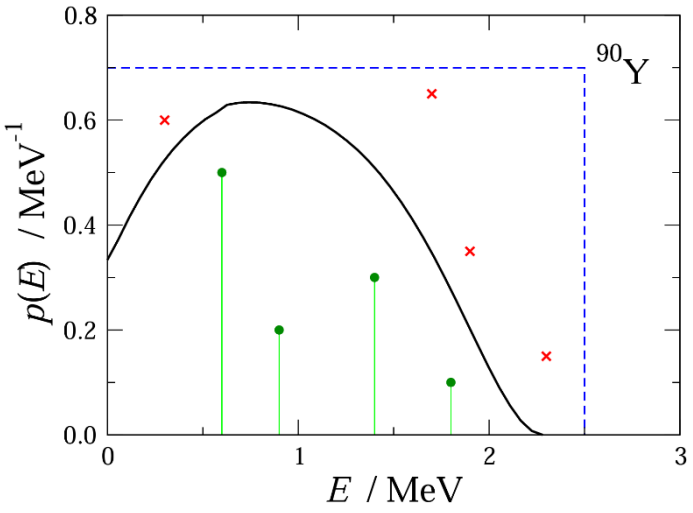

Figure 3.3: Rejection algorithm to sample the kinetic energy of the electron emitted in the β^- decay of 90Y. (from [79]).

3.1.3. Simulation of radiation transport

MC methods of radiation transport simulate the propagation and interaction of radiation in matter, by numerically sampling the distance between physical interactions, the kind of interaction, angular deflection and/or energy loss and generation of secondary radiation, using a detailed simulation method, where all the interactions are simulated event-by-event [70], [80]. When we consider the interactions of photons, the energy is limited within an interval from 50 eV up to 1 GeV. This range predominantly encompasses the photoelectric effect, coherent (Rayleigh) scattering, incoherent (Compton) scattering and electron-positron pair production. Other interactions, such as photonuclear absorption, occur with a much lower probability and are generally negligible for most practical purposes

[81]. Therefore, MC always simulates photon transport by using a detailed method (interaction by interaction). Regarding electrons and positrons, the possible interactions are elastic scattering, inelastic collisions and bremsstrahlung emission (for positrons are also annihilation). Due to the significant number of interactions undergone by an electron or positron prior to reaching a rest state, performing a detailed simulation becomes impractical at high energies. This challenge is surpassed by employing a mixed simulation approach instead of an event-by-event simulation.

In summary, there are two types of algorithms for electron transport simulation. The first one, called condensed simulation or Class I, where interactions are grouped in a few simulation steps, allows to decrease computational time at the expense of introducing acceptable distortion of the values simulated. A mixed simulation, Class II, combines the detailed simulation of hard events (*i.e.*, events with polar angular defection θ or energy loss W larger than previously selected cutoff values θ_C and W_C) with condensed simulation of soft events, in which $\theta < \theta_C$ or $W < W_c$. These are called transport parameters and can be adjusted by the user (section 4.2.2).

3.1.3.1. Scattering model

The interactions between the beam particles and atoms or molecules of the medium occur through various competing mechanisms, which are characterized by the associated differential cross section (DCS). The DCS is a function of the particle state variables, *i.e.*, a function that allows the measurement of the probability of an event occurring, due to the interaction of particles.

Considering a particle with energy E (Figure 3.4), it may lose energy *W* and change its direction of movement in each interaction, where ϕ represents the angle between the particle directions before and after the interaction (azimuthal angle, ϕ). The angular deflection of the particle is represented by the polar scattering angle θ and its PDF after a single elastic collision is proportional to the DCS.

Considering that the atoms or molecules in the medium are randomly oriented, the DCS is independent of the azimuthal scattering angle. The angular distribution of scattered particles is axially symmetrical around the direction of incidence, *i.e.*, the azimuthal scattering angle is uniformly distributed on the interval (0, 2π).

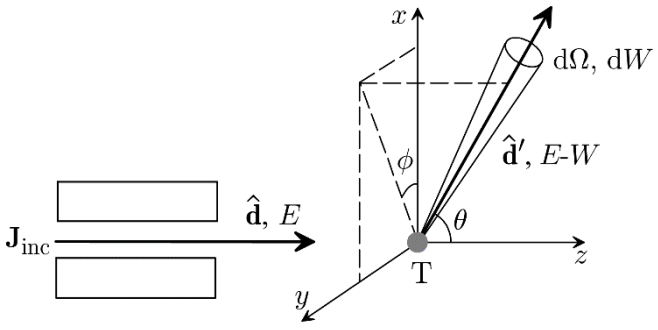

Figure 3.4: Schematic diagram of an experiment to measure the DCS. Incident particles move in the direction of the z axis; and θ and ϕ are the polar and azimuthal scattering angles, respectively. (from [76]).

3.1.3.2. Generation of random tracks

Initially, each particle starts off with a given initial state (with initial position, direction and energy). To simulate histories and generate a random track, it is needed to define the distance between physical interactions (events), the type of interaction, angular deflection and/or energy loss and if there is generation of secondary radiation and its initial state [82]. All these random variables were sampled from the corresponding PDFs. Therefore, a particle track is defined by repeating these steps and randomly sampling the state of the particle immediately after an interaction (Figure 3.5). The trajectory is finished when one of the following conditions is achieved: either when the particle crosses a boundary of the sample or when the energy becomes smaller than a given value E_{abs}, which is the value of energy where electrons are assumed to be stopped and absorbed in the medium.

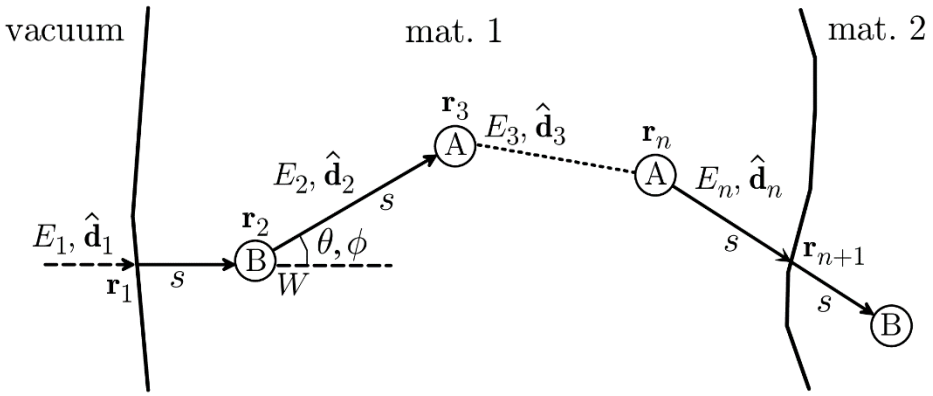

Figure 3.5: Generation of random trajectories using detailed simulation. A particle enters material 1 from the vacuum and, after multiple interactions, crosses the interface between materials 1 and 2. (from [76]).

3.2. PENELOPE: a Monte Carlo code

In the present dissertation, the work developed to simulate the S-values for various radionuclides and for voxel or cell sizes is described. For this purpose, a computer code system PENELOPE was used to perform MC simulations in a wide energy range from a few hundred eV to about 1 GeV [82]. PENELOPE is an acronym for PENetration and Energy LOss of Positrons and Electrons.

Figure 3.6 describes how PENELOPE works, and it is possible to understand which files the user has the responsibility to provide to the program to perform a full simulation [82].

PenEasy (Sempau *et al.* 2011, [82]) is a general-purpose main program for PENELOPE. It is written in Fortran 95 and contains a set of subroutines including source models, tallies and variance-reduction techniques. This program has the capability to minimize the programming effort required for adjusting the current routines and for generating new ones through duplication.

3.2.1. Geometry and materials

PENELOPE includes a geometry package *PENGEOM*, which applies an algorithm to define complex geometries. It consists of homogeneous bodies limited by well-defined quadric surfaces. The user is responsible for the definition of the surfaces and for instructing which surfaces are delimitating each body. Along with that, *GVIEW2D* and *GVIEW3D* programs are available to visualize the geometry and facilitate debugging of the file. Also, each body created for a PENELOPE simulation must be associated to a specific material. PENELOPE code provides a *MATERIAL* program which offers an extensive list of 280 prepared materials that contains the physical properties, interaction cross section, relaxation data, *etc*. Alternatively, this program provides an option to create the material by inserting the chemical composition, mass density, mean excitation energy and energy and oscillator strength of plasmon-like excitations. Therefore, the quadric surfaces defined are projected as boundaries for the particle path in the radiation transport. Summarily, when the particle reaches a boundary, the track is stopped and restarted again when enters a new medium (this also works when both sides of the interface have the same material).

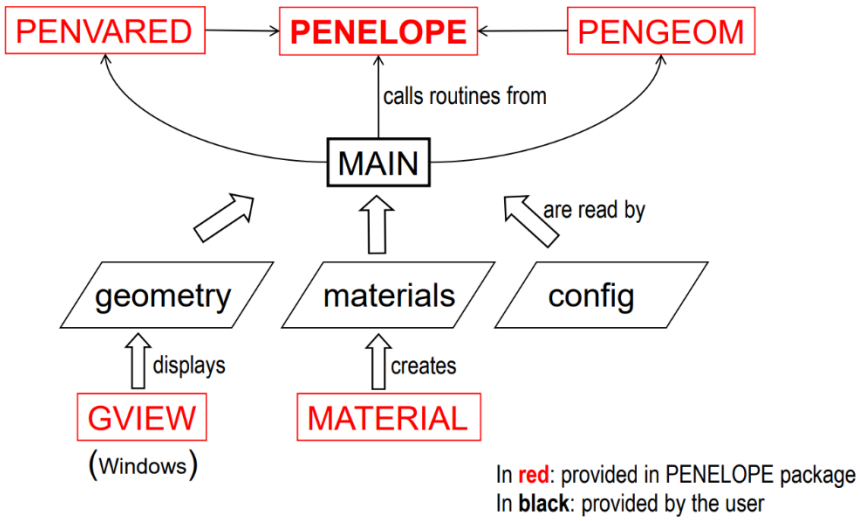

Figure 3.6: Code structure for PENELOPE: packages and inputs. (from [83]).

3.2.2. Source model for PENELOPE simulations

PENELOPE simulations, in particular performed by penEasy, include two source models in the input file: Box Isotropic Gauss Spectrum (BIGS) and Phase-Space File. For this dissertation, all the results were produced by simulations where only the BIGS model was activated and, for that reason, this section will only provide information regarding the BIGS source model.

The input file allows the user to define some configurations regarding the source. For instance, the user is responsible for choosing the particle type (electrons, photons or positrons) and the position, direction and energy of the emission. The particles are generated inside a source box (rectangular parallelepiped), whose sides along the x, y and z directions are defined in the input file, and the user

must identify the coordinates of the box centre. If the box sides were all set to zero, the source is specified as a point. BIGS also allows users to define a source material with arbitrary shape.

In addition, the user must introduce an energy spectrum, where each entry must contain two numbers, one for the energy and the other for the unnormalized probability. Therefore, the input energy distribution is coded as a histogram in the form

$$\begin{array}{ll} E_1 & P_1 \\ \vdots & \vdots \\ E_i & P_i \\ E_{i+1} & \vdots \\ \vdots & \vdots \\ E_N & P_N \\ E_{N+1} & -1 \end{array}$$

where P_i is the relative probability of the interval (E_i, E_{i+1}). Note that the energy spectrum terminates always when a meaningless negative probability (-1) is found.

Often the source spectrum is known in tabular form, say (E_j, f_j) with $j = 1,2,\dots,M$, where $f_j \equiv f(E_j)$ and the previous method may be applied using a linear interpolation scheme (Figure 3.7), by adopting the same energy grid, $\{E_j; j = 1,2,\dots,M\}$ and obtaining the probabilities through the following equation

$$P_j = \int_{E_j}^{E_{j+1}} \frac{1}{2}(f_j + f_{j+1})dE = \frac{1}{2}(f_j + f_{j+1})(E_{j+1} - E_j). \tag{3.9}$$

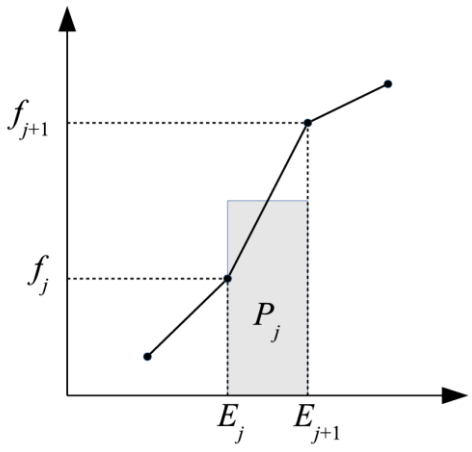

Figure 3.7: Representation of the interpolation scheme (from [82]).

3.2.3. S-value calculations by PENELOPE

As already mentioned in this dissertation, S-values are designated as the mean absorbed dose per unit of cumulative activity [67]. Hence, when performing MC simulations, the aim is to assess the absorbed dose in specific targets. The penEasy main program incorporates various tallies that allow to score a number of quantities [82]. Each tally can be used to evaluate these quantities in different situations and all of them available in PenEasy are detailly explained in Sempau *et al*. [82]. The tallies may be considered as the output of each simulation and the user may specify the relative uncertainty that he/she intends to achieve. This can be a condition to stop the simulation and if the requested uncertainty is set to zero, then the simulation will not stop for this cause. This report will be focused on the Spatial Dose Distribution Tally and Energy Deposition Tally.

The Spatial Dose Distribution Tally provides information regarding the 3D absorbed dose distribution per history. The values are tallied in the x, y and z intervals and respective bins defined by the user, *i.e.*, the energy deposition is collected in spatial bins. Note that these bins do not exist in the geometry definition, thus they do not represent boundaries for the particle transport. Additionally, each bin is considered homogeneous by the program code and, for that reason, the user needs to guarantee that the bins are indeed homogeneous since the code does not confirm that condition. Moreover, this tally should not be used in voxelized regions because of inhomogeneities. The mass density is determined from the value found at the bin centre (reason that justifies the necessity of assuring the homogeneity) and the absorbed dose distribution values are presented in eV/g.

The Energy Deposition Tally is the second tally with relevance for this dissertation. This tally scores the energy deposited per history in each material and it is reported in eV per history. It is scored the energy absorbed in every material present in the geometry input file. Contrarily to the previous tally, the energy values are calculated in each material present on the geometry and not in bins defined by the user. For instance, the user does not need to assure the homogeneity and boundaries can exist when using this tally.

Thus, all simulations conducted using MC codes have a statistical uncertainty for each output value, depending fundamentally on the number of primary histories (particles). The results of MC simulations are typically presented as follows:

$$Q_{MC} = \bar{q} \pm k\sigma(\bar{q}) \tag{3.10}$$

where Q_{MC} represents the output value, $\bar{q}$ is the mean value, $\sigma(\bar{q})$ is the standard deviation of the mean (Equation 3.1) and k is the coverage factor. This factor determines the confidence level of the interval and in general $k = 2$ (95% confidence).

CHAPTER 4

Materials and Methods

4.1. Nuclear Decay Data

In this study, several databases for nuclear decay schemes were considered and thoroughly explained in subsections 4.1.1 - 4.1.3. The decay schemes provided in each database are based on different literature sources, which may lead to potential discrepancies between them.

4.1.1. PenNuc Package

To execute the decay of radionuclides in a simulation, PENELOPE and penEasy work in conjunction with the Fortran subroutine package PenNuc, source files *pennuc.f* and *decays.f*. This package allows the simulation of random nuclear decays of a list of radionuclides. The decay process utilizes random number generators and tools for electromagnetic transitions (γ emission, internal conversion) and beta decay ($\beta^{\pm}$ disintegrations, electron capture) [84]. This package allows to generate a cascade of charged particles and photons that describe a complete decay pathway. The PenNuc subroutines uses data files from the NUCLEIDE Table of Isotopes website [85], which contains energies and probabilities of each transition, as input data. Notice that all energies are given in eV and α particles are not considered by this MC code [84]. The PenNuc files are complemented with PDF files containing detailed information about each transition and the spectrum.

The PenNuc package also includes the files *pdatconf.p14* and *pdrelax.p11* in the same data directory. The first of these files contains information regarding ground-state configuration, (sub)shell ionization energies and atomic level widths, while the second one offers data on the transition probabilities and energies for singly ionized atoms [84].

Hence, PenNuc is the result of an international decay data evaluation project, widely recognized as a reference for nuclear decay. Thus, it allows to obtain the nuclear data in a simple way. In the input file, the PenNuc radioisotope information is placed in the BIGS section (Figure 4.1).

```
[SECTION SOURCE BOX ISOTROPIC GAUSS SPECTRUM v.2014-12-21]
 ON                              STATUS (ON or OFF)
 Co-60.nuc                       PARTICLE TYPE (1=ELECTRON, 2=PHOTON, 3=POSITRON) OR RADIONUCLIDE FILENAME
  SUBSECTION FOR PHOTON POLARIZATION:
 0                               ACTIVATE PHOTON POLARIZATION PHYSICS (0=NO, 1=YES)
 0.0 0.0 0.0                     STOKES PARAMETERS (USED ONLY IF ACTIVATE POLARIZATION=1)
  SUBSECTION FOR PARTICLE POSITION:
 0.0  0.0  0.0                   COORDINATES (cm) OF BOX CENTER
 0.0  0.0  0.0                   BOX SIDES (cm)
 0.0  0.0                        FWHMs (cm) OF GAUSSIAN X,Y DISTRIBUTIONS
 0.0  0.0  0.0                   EULER ANGLES [OMEGA,THETA,PHI](deg) FOR BOX ROTATION Rz(PHI).Ry(THETA).Rz(OMEGA).r
 0.0  0.0  0.0                   TRANSLATION [DX,DY,DZ](cm) OF BOX CENTER POSITION
 0                               SOURCE MATERIAL (0=DON'T CARE, >0 FOR LOCAL SOURCE, <0 FOR IN-FIELD BEAM)
  SUBSECTION FOR PARTICLE DIRECTION:
 0.0  0.0  1.0                   DIRECTION VECTOR; NO NEED TO NORMALIZE
 0.0 180.0                       DIRECTION POLAR ANGLE INTERVAL [THETA0,THETA1], BOTH VALUES IN [0,180]deg
 0.0 360.0                       DIRECTION AZIMUTHAL ANGLE INTERVAL PHI0 IN [0,360)deg AND DeltaPHI IN [0,360]deg
 0                               APPLY ALSO TO DIRECTION THE ROTATION USED FOR BOX POSITION (0=NO, 1=YES)
[END OF BIGS SECTION]
```

Figure 4.1: Example of the BIGS section in a penEasy input file, making use of the PenNuc package.

4.1.2. DECDATA Software

The decay input file can be provided by the software DECDATA, developed by K. F. Eckerman and A. Endo [86]. This software creates files with decay information based on ICRP Publication 107 [60]. When using DECDATA, the files are divided according to the type of particle emitted, *e.g.*, for a beta emitter with emission of AE and γ rays, there will be three different files to use as input: one for the beta spectrum, one for the energies emitted by electrons, and one for the energies emitted by photons.

In more detail, if a radionuclide only produces beta particles, the software only generates a file with the energies emitted by those particles and their respective yield; if the radionuclide also emits electrons and photons, the software provides a file with all the energies and yields, along with a numerical code to distinguish the type of particle or radiation associated with each energy.

Therefore, the software output produces a .RAD file (radiation file) that lists discrete or mean energies (MeV) and the absolute yields of the radiations emitted in nuclear transformations, sorted by increasing energies. The .BET file samples the beta spectra for the nuclide, by deriving the energies and intensities of the emitted radiations, *i.e.*, this file presents the electron energy E (MeV) and the number of electrons emitted per nuclear transformation with energy between E and $E + dE$. In this case, the .RAD file only contains the mean energies of beta transition. The AE and CK spectra is described in the .ACK file, which contains electron energy E (eV) and the yield. Since the .RAD file does not present information for more than fifteen discrete emissions, the .ACK file is essential for accessing comprehensive data regarding this type of fluorescent radiation. γ and x-emission data are only provided in the .RAD file.

The files downloaded from the software were not conceived to be used in PENELOPE simulations. For that reason, they are not available in the appropriate format for direct use. To address this, Fortran codes were developed to transform these files into the required format by applying Equation 3.9 (section 3.2.2). Moreover, for nuclides with AE and CK emissions, the code must ensure that there are no repeated data by combining them. The Fortran codes also create two output files: one for monoenergetic electrons and one for photons. Since this software cannot be used in the same manner as PenNuc, the only method to utilize this database is to develop different spectrum files for PENELOPE and define the particle type in the input file (Figure 4.2).

```
[SECTION SOURCE BOX ISOTROPIC GAUSS SPECTRUM v.2014-12-21]
 ON                              STATUS (ON or OFF)
 1                               PARTICLE TYPE (1=ELECTRON, 2=PHOTON, 3=POSITRON) OR RADIONUCLIDE FILENAME

  SUBSECTION FOR PARTICLE ENERGY:  (REMOVE THIS SUBSECTION IF RADIONUCLIDE IS USED AS PARTICLE TYPE)
 I-131_electrons.spc             ENERGY SPECTRUM FILE NAME; ENTER '-' TO ENTER SPECTRUM IN NEXT LINES
 0.0                             FWHM(eV) OF GAUSSIAN ENERGY DISTRIB. [NOTE FWHM=SIGMA*sqrt(8*ln(2))]
[END OF BIGS SECTION]
```

Figure 4.2: Application of DECDATA data in the input file for PENELOPE program.

When using the DECDATA software, it is necessary to perform three different simulations when the nuclide emits beta particles. Specifically, a simulation must be conducted using the beta spectrum (defining the particle type as electrons), a simulation for the monoenergetic electron energy spectrum (particle type: 1), and a simulation for the photon spectrum (particle type: 2). Hence, to accurately assess the absorbed dose due to the decay of a nuclide, when using this software, there is a necessity to weight the contribution of each spectrum. To facilitate this process, a Python code was developed to calculate the values by combining all the simulations and considering the yields of each contribution.

4.1.3. ICRU Report 56

The decay data can also be given by ICRU Report 56 [20], which includes information regarding beta rays for radiation protection. Moreover, this report focuses on dosimetry considerations, such as relevant quantities to beta rays dosimetry, the anatomical and radiobiological basis of skin dosimetry, beta-rays spectra, the physics of the interaction of electrons and matter, calculations of dose distributions, *etc*. For this dissertation, ICRU Report 56 [20] allows access to a database that contains a small number of beta-emitting radionuclides. Similarly to the previous database, the beta spectra in this one are not available in the appropriate PENELOPE format. To use this data, a Python code was developed to convert the energy and yield values into the required format. This code takes into consideration Equation 3.9 (section 3.2.2) to perform the integrals needed to accomplish the PENELOPE format (Figure 4.3). Although this is an extensive and complex reference in literature, in this study, this database was only used for a few nuclides to assess the impact of the decay data of the nuclide in the calculations of S-values. As an older report (1997), it does not contribute to the primary aim of this dissertation, which is to update the currently available values.

```
[SECTION SOURCE BOX ISOTROPIC GAUSS SPECTRUM v.2014-12-21]
 ON                              STATUS (ON or OFF)
 1                               PARTICLE TYPE (1=ELECTRON, 2=PHOTON, 3=POSITRON) OR RADIONUCLIDE FILENAME

  SUBSECTION FOR PARTICLE ENERGY:  (REMOVE THIS SUBSECTION IF RADIONUCLIDE IS USED AS PARTICLE TYPE)
 P-32_ICRU56_Penelope.spc        ENERGY SPECTRUM FILE NAME; ENTER '-' TO ENTER SPECTRUM IN NEXT LINES
 0.0                             FWHM(eV) OF GAUSSIAN ENERGY DISTRIB. [NOTE FWHM=SIGMA*sqrt(8*ln(2))]
[END OF BIGS SECTION]
```

Figure 4.3: Application of ICRU data in the input file for PENELOPE program.

4.2. Voxel-level S-values

MIRD Pamphlet 17 [50] was used as a reference for S-values at the voxel level. This pamphlet tabulated S-values for five radionuclides (^{131}I, ^{32}P, ^{89}Sr, ^{99m}Tc, ^{90}Y) and for two voxel dimensions. However, it dates from 1998 and there have been some developments in nuclear and atomic physics since then. This reference used the PRESTA algorithm of EGS version 4, while all the results presented in Chapter 5 were obtained using the PENELOPE program (2018 version) for MC simulations. In an initial approach, all the simulations were made with similar methods of MIRD Pamphlet 17 [50] to compare and analyse the differences of using two different MC codes.

MC simulations require considerable computational effort, thus, the geometry used was simplified, allowing to achieve the targeted values without compromising the results. For instance, using the Spatial Dose Distribution Tally, described in section 3.2.2, there is no need to create individual voxels for the geometry. For that reason, a geometry was defined with just a sphere large enough to be considered approximately infinite for the studied voxel sizes. Consequently, there were no boundaries for the emitted particles and the voxels are fictitiously constructed by the tally for dose scoring. The non-boundary feature allows to compute a faster simulation since, in a detail-by-detail simulation, the presence of a boundary means the generation of a new path for the particle. After defining the geometry, the material must be defined in the input file, along with the transport parameters, explained in detail in section 4.2.2. Firstly, the infinite geometry was defined as composed by liquid water. This material was selected based on the fact that water is the major component of the human body and could give a good estimate of the absorbed dose. However, attending to the available literature, the results presented in

Chapter 5 were scored in a medium made with a specific composition of soft tissue. Hence, the materials were selected from the list of compounds available in PENELOPE. Regarding soft tissue, this list includes information for two compositions, one based on the ICRP Publication 89 (2003) [57] recommendations (with 13 elements and unit mass density) and the other one based on the guidelines of ICRU Report 44 (1989) [87] (with 4 elements and also unit density). Considering the aim of this dissertation, the soft tissue composition from ICRP Publication 89 (2003) [60] was used due to its more recent publication date and updated information.

According to MIRD Pamphlet 17 [50], the radionuclide (radiation source) is uniformly distributed within the central voxel, and it is calculated the radioactivity that passes through the adjacent voxels. In the initial stages of this dissertation simulations, the source was either distributed uniformly in the central voxel or on a central point. However, for comparison to the values of MIRD Pamphlet 17 [50], the simulations were performed with the radionuclide uniformly distributed in the central voxel. As mentioned in section 3.2.2, the input file for PENELOPE simulations has a section to characterize the radioactive source, which allows the user to indicate the type of particle emitted, where it is located and the dimensions (Figure 4.1). Therefore, when the source is a point placed in the central box, the user must set to zero the sides of the box created to allocate the source. In the case of a uniformly distributed source, the sizes of the box created must be the dimensions of the centre voxel. In both cases, the coordinates of the box centre were placed in the centre of the geometry.

For the present dissertation, the package PenNuc was used to provide information regarding the radioactive source. Initially, it was considered the radionuclides from MIRD Pamphlet 17 [50]: ^{131}I, ^{32}P, ^{89}Sr, ^{99m}Tc, and ^{90}Y. However, as mentioned in section 2.2, the isotopes ^{177}Lu and ^{153}Sm have become relevant for therapies in nuclear medicine, so they were added to the list of radionuclides used in our simulations. To assess the impact of the decay data in the simulated values and to comprehend the differences from the MIRD Pamphlet 17 [50] values, other nuclear decay databases were selected. For some isotopes, the Fermi energy spectrum was taken from ICRU Report 56 [20] and from the software, DECDATA. Regarding the voxel dimensions, initially, as described in the literature, it was selected 3 mm and 6 mm and, posteriorly, S-values were calculated for the dimensions required for a SPECT/CT device (Table 2.3).

4.2.1. Monoenergetic sources

MIRD Pamphlet 17 [50] reported simulation results for monoenergetic sources (electrons and photons) of energies of 0.01 MeV, 0.1 MeV and 1 MeV, presenting the results in two graphs. In this study, simulations were conducted for monoenergetic sources (electrons and photons) with energies of 0.1 MeV and 1.0 MeV, and for voxel dimensions of 3 mm and 6 mm using PENELOPE (version 2018).

This dissertation evaluated the impact of updated versions of MC programs in comparison with the values available in the literature. As described in previous sections, the influence of different decay data was assessed. When performing simulations with different decay databases, two factors distinguish these simulations from those performed in MIRD Pamphlet 17 [50]: the MC code and the radioactive source. In this study, one of these factors was eliminated by using the same source characteristics and placing it in the same positions. Therefore, this approach allowed validation of the results, as the simulations were carried out using the same source with the same energies, changing only the MC code used.

4.2.2. Simulation parameters

For direct comparison to MIRD Pamphlet 17 [50], the simulations were done for 3 mm and 6 mm voxel size, running 5×10^7 histories. This number of histories was chosen to balance between achieving low uncertainty and reasonable computational time. The simulation is controlled by seven user-defined parameters: the absorption energy for electrons, photons and positrons, *i.e*., the cutoff energy below which the simulation of particle tracks is discontinued and the residual energy of the particle deposited locally. These parameters must be defined for each material in the geometry. Table 4.1 shows the parameters applied for the simulation results presented.

Table 4.1: User-defined parameters for the input files.

PARAMETERS	VALUES
$\boldsymbol{E_{abs}(e^-)}$	10 keV
$\boldsymbol{E_{abs}(ph)}$	
$\boldsymbol{E_{abs}(e^+)}$	
$\boldsymbol{C_1}$	0.05
$\boldsymbol{C_2}$	0.05
$\boldsymbol{W_{CC}}$	1 keV
$\boldsymbol{W_{CR}}$	10 keV

The first three parameters of Table 4.1 are the cutoff energies (or absorption energies), *i.e.*, when the energy of a particle is below the E_{abs}, the particle is considered stopped and the remaining energy is deposited locally. This approach prevents the simulation of low-energy particle interactions that do not significantly affect the result, thereby reducing computation time. The C_1 and C_2, known as transport steps, are values that determine the accuracy and speed of the simulation. They must be low to ensure good accuracy. C_1 represents the average angular deflection, $C_1 \simeq 1 - \langle cos\theta \rangle$, caused by elastic scattering, and C_2 the maximum average fractional energy loss between consecutive hard elastic events. Note that these parameters, C_1 and C_2 only apply to electrons. W_{CC} and W_{CR} are the cutoff energy losses for hard inelastic collisions and hard bremsstrahlung emission, respectively [76].

4.2.3. Tally and data output

The output provided by the PENELOPE program penEasy was tallied by the Spatial Dose Distribution Tally, which gives the absorbed dose distribution per history. This tally is specified in a section of the input file, and it was the only tally with ‘on’ status. Depending on the size chosen for the bins, it is required to define the number of bins for each axis and the dimensions where they will take place (Figure 4.4). In addition, the user is asked to state the requested relative uncertainty, which is a parameter to stop the simulation.

As described in section 3.2.3, this tally divides the geometry into cubical voxels. In this study, we worked with an infinite geometry divided into a cube of 11×11×11 small cubes, resulting in 1331 individual voxels (bins). Figure 4.5 demonstrates an example output of a penEasy simulation, using the referred tally. The first lines are comments to facilitate the user to understand the data, indicating the number of bins considered along each axis, the dimensions of the geometry and the widths of the bins.

The absorbed dose values are complemented with the two values per bin coordinate: the low and the middle point coordinates in the x, y and z axes, respectively, for each bin. Each absorbed dose value is presented for each bin in eV/g, and complemented with the uncertainty of two σ.

```
[SECTION TALLY SPATIAL DOSE DISTRIB v.2009-06-15]
 ON                                STATUS (ON or OFF)
 -1.65   1.65   11                XMIN,XMAX(cm),NXBIN (0 FOR DX=infty)
 -1.65   1.65   11                YMIN,YMAX(cm),NYBIN (0 FOR DY=infty)
 -1.65   1.65   11                ZMIN,ZMAX(cm),NZBIN (0 FOR DZ=infty)
 1                                 PRINT COORDINATES IN REPORT (1=YES,0=NO,-1=NO&BINARYFORMAT)
 0.0                               RELATIVE UNCERTAINTY (%) REQUESTED
[END OF SDD SECTION]
```

Figure 4.4: Input file, section of Spatial Dose Distribution Tally.

The cubical arrangement of the voxels allows cubical symmetry. Thus, the voxels placed at the same distances from the radiation source should absorb, apart from the inherent statistical fluctuations, the same amount of absorbed dose. A Python script was developed to aggregate the voxels into different groups according to their distance from the central voxel, which contains the radioactive source (Figure 4.6). The voxels were grouped into 45 different groups, corresponding to 45 different distances from the central voxel. All distance calculations were performed in three dimensions by equations for Cartesian coordinates (Equation 4.1). In the output, the central voxel containing the radioactive source is assumed to be placed at (0,0,0).

$$d = \sqrt{x^2 + y^2 + z^2} \tag{4.1}$$

MIRD Pamphlet 17 [50] tabulates S-values for voxels within an octant of 6×6×6, and coordinates ranging from 0 to 5. That means that the entry (0,0,0) is the central voxel irradiating itself and the (5,5,5) entry is the farthest voxel. The remaining octants have negative coordinates and were ignored in the results because they can be obtained by symmetry operations. As illustrated in Figure 4.5, the output delivered also associates Cartesian coordinates to each bin. However, those coordinates range from 1 to 11, meaning that the central voxel corresponds to the bin (6,6,6). To compare both values, a transformation for the output coordinates was applied in the Python script, to convert them into MIRD methodology. Figure 4.7 illustrates, in two dimensions, how this conversion was made.

```
#>>>>>>>>>>>>>>>>>>>>>>>>>>>>>>>>>>>>>>>>>>>>>>>>>>>>>>>>>>>>>>>>>>>>>>>>>>>>>>>
# [SECTION REPORT SPATIAL DOSE DISTRIB]
# Dose units are: eV/g per history
#
# No. of bins in x,y,z directions and total:
#  11 11 11 1331
# Min values for x,y,z(cm):
#  -1.65000E+00 -1.65000E+00 -1.65000E+00
# Bin widths for x,y,z(cm):
#   3.00000E-01  3.00000E-01  3.00000E-01
#
# For plotting purposes, two values per bin coordinate are given, namely, the low end and the middle point of each bin.
#
# xBinIndex : xLow(cm) : xMiddle(cm) : yBinIndex : yLow(cm) : yMiddle(cm) : zBinIndex : zLow(cm) : zMiddle(cm) : dose : +-2sigma
     1 -1.65000E+00 -1.50000E+00     1 -1.65000E+00 -1.50000E+00     1 -1.65000E+00 -1.50000E+00  1.52242E+02 8.0E+00
     2 -1.35000E+00 -1.20000E+00     1 -1.65000E+00 -1.50000E+00     1 -1.65000E+00 -1.50000E+00  1.67609E+02 8.4E+00
     3 -1.05000E+00 -9.00000E-01     1 -1.65000E+00 -1.50000E+00     1 -1.65000E+00 -1.50000E+00  1.84980E+02 8.9E+00
     4 -7.50000E-01 -6.00000E-01     1 -1.65000E+00 -1.50000E+00     1 -1.65000E+00 -1.50000E+00  2.06423E+02 9.6E+00
     5 -4.50000E-01 -3.00000E-01     1 -1.65000E+00 -1.50000E+00     1 -1.65000E+00 -1.50000E+00  2.19635E+02 9.9E+00
     6 -1.50000E-01  8.32667E-17     1 -1.65000E+00 -1.50000E+00     1 -1.65000E+00 -1.50000E+00  2.23401E+02 9.8E+00
     7  1.50000E-01  3.00000E-01     1 -1.65000E+00 -1.50000E+00     1 -1.65000E+00 -1.50000E+00  2.26219E+02 1.0E+01
     8  4.50000E-01  6.00000E-01     1 -1.65000E+00 -1.50000E+00     1 -1.65000E+00 -1.50000E+00  2.10236E+02 9.6E+00
     9  7.50000E-01  9.00000E-01     1 -1.65000E+00 -1.50000E+00     1 -1.65000E+00 -1.50000E+00  1.84917E+02 8.9E+00
    10  1.05000E+00  1.20000E+00     1 -1.65000E+00 -1.50000E+00     1 -1.65000E+00 -1.50000E+00  1.75240E+02 8.7E+00
    11  1.35000E+00  1.50000E+00     1 -1.65000E+00 -1.50000E+00     1 -1.65000E+00 -1.50000E+00  1.41718E+02 7.6E+00

     1 -1.65000E+00 -1.50000E+00     2 -1.35000E+00 -1.20000E+00     1 -1.65000E+00 -1.50000E+00  1.66645E+02 8.4E+00
     2 -1.35000E+00 -1.20000E+00     2 -1.35000E+00 -1.20000E+00     1 -1.65000E+00 -1.50000E+00  1.93805E+02 9.2E+00
     3 -1.05000E+00 -9.00000E-01     2 -1.35000E+00 -1.20000E+00     1 -1.65000E+00 -1.50000E+00  2.23319E+02 9.8E+00
     4 -7.50000E-01 -6.00000E-01     2 -1.35000E+00 -1.20000E+00     1 -1.65000E+00 -1.50000E+00  2.49091E+02 1.1E+01
     5 -4.50000E-01 -3.00000E-01     2 -1.35000E+00 -1.20000E+00     1 -1.65000E+00 -1.50000E+00  2.77102E+02 1.1E+01
     6 -1.50000E-01  8.32667E-17     2 -1.35000E+00 -1.20000E+00     1 -1.65000E+00 -1.50000E+00  2.83820E+02 1.1E+01
     7  1.50000E-01  3.00000E-01     2 -1.35000E+00 -1.20000E+00     1 -1.65000E+00 -1.50000E+00  2.73389E+02 1.1E+01
     8  4.50000E-01  6.00000E-01     2 -1.35000E+00 -1.20000E+00     1 -1.65000E+00 -1.50000E+00  2.51196E+02 1.0E+01
     9  7.50000E-01  9.00000E-01     2 -1.35000E+00 -1.20000E+00     1 -1.65000E+00 -1.50000E+00  2.35497E+02 1.0E+01
    10  1.05000E+00  1.20000E+00     2 -1.35000E+00 -1.20000E+00     1 -1.65000E+00 -1.50000E+00  1.95326E+02 9.1E+00
    11  1.35000E+00  1.50000E+00     2 -1.35000E+00 -1.20000E+00     1 -1.65000E+00 -1.50000E+00  1.72510E+02 8.5E+00
```

Figure 4.5: Output file of the Spatial Dose Distribution Tally.

With those modifications, the distances are associated with coordinates, *i.e.*, each distance value has the corresponding voxel coordinates listed. The voxels placed at the same distance from the source voxel are identified by the coordinates. As made in MIRD Pamphlet 17 [50] methodology, the voxel coordinates with negative values were ignored, since the absorbed dose in those voxels could be determined due to the symmetric properties. At this point, the Python script to calculate the S-values only recognizes the absorbed dose values for one octant. As mentioned previously, the S-values of the voxels at the same distance must be equal, being calculated on the basis of this proposition:

1. Firstly, the absorbed doses for the voxels placed at equal distances were identified;
2. The mean dose was calculated;
3. The values were converted into the appropriate units which are $\mathrm{mGy} \cdot \mathrm{MBq}^{-1} \cdot \mathrm{s}^{-1}$.

Additionally, the Python script also was written to calculate the absolute uncertainties related to each S-value (Equation 4.2).

$$\mu = \frac{1}{N}\sqrt{\sum_{i=1}^{N} \mu_i^2} \tag{4.2}$$

This methodology required the computation of 137 MC simulations and allowed to tabulate S-values for different radionuclides, voxel dimensions and decay databases.

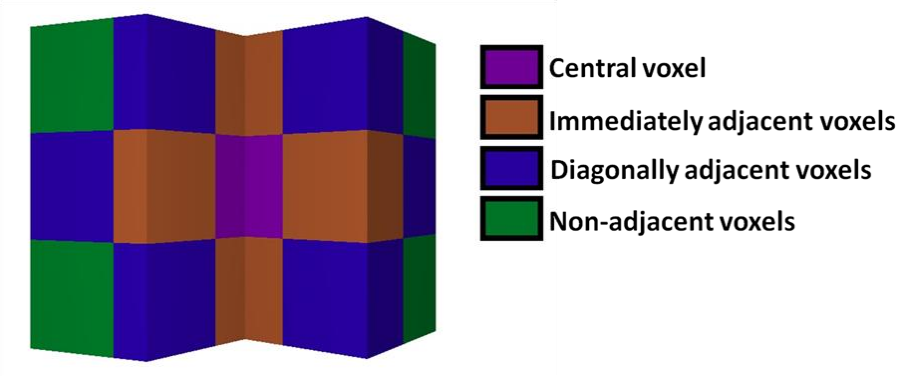

Figure 4.6: Simplified geometry. In this case, it is represented a small cube of 3×3×3 voxels, where each coloured group of voxels represents a different distance from the central voxel that contains the source. (from [88]).

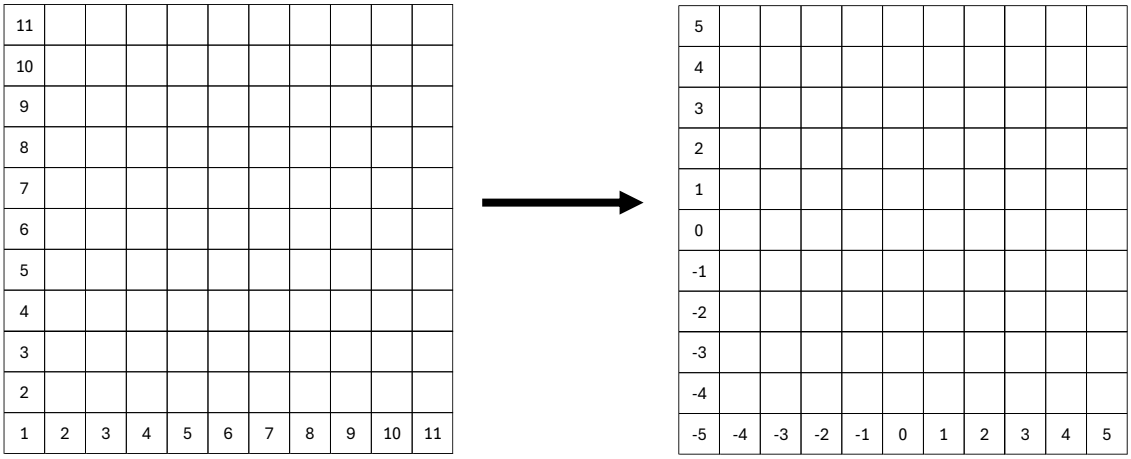

Figure 4.7: Coordinates conversion in 2D.

4.3. Cellular-level S-values

Regarding S-values at the cellular level, the methods employed were similar to the ones described in the previous section. All the simulations were done by PENELOPE MC code, version 2018, and the penEasy main program.

First, the selection of the radionuclides was driven by the range that the radiation runs within the cells (in this situation, about few μm). For that reason, the radionuclides present a decay scheme that includes AE and CK electrons. Therefore, those emissions will affect predominantly the areas around the cells due to their penetration power within tissues. Similar to the methodology implemented for S-values at the voxel level, one of the objectives for cellular S-values was also the comparison between different decay databases. In this case, the simulations were carried out for the PenNuc and DECDATA databases (explained in detail in sections 4.1.1 and 4.1.2, respectively).

Cellular-level S-values, as indicated by the name, quantify the absorbed dose within cell compartments. Consequently, the geometry created is a reproduction of a cell, formed by two concentric spheres based on the article by Falzone *et al.* [75], and the combinations of the radii of the cell and the nucleus for each geometry were replicated from this reference. In total, there were 39 geometries considered, where 3 μm < R_C < 12 μm and 1 μm < R_N < 11 μm. Cellular S-values were calculated for source-target combinations: N ← N and N ← Cy. In the geometry file, the two spheres were defined as being made up of different materials, as well as the infinite medium in which they were defined. The nucleus of the cell is composed of material 1, the cytoplasm of material 2 and the infinite medium of material 3. Although all these compartments are formed by different materials, in the input file, the three materials have been defined as liquid water, since this is the compound with the greatest quantity in the cells. The defined geometry was the simplest cellular model. Despite the existence of more realistic geometries such as ellipsoidal and/or eccentric cell-nucleus arrangements, as well as rotated nuclei, these were not considered due to the use of DPK which cannot be applied to non-concentric geometries.

Section 2.6.2 reviewed the current methodology for those calculations and the results presented in this dissertation were obtained by applying direct MC simulations and DPK methods.

4.3.1. Simulation parameters

Similarly to voxel level simulations, simulation parameters were selected based on the current bibliography to allow a complete comparison with the databases available (Table 4.2). Following the considerations of Falzone *et al.* [75], the cutoff energy parameters for electrons, photons and positrons were set to 50 eV. As the values were being analysed at small sub-micrometer distances, these parameters must be reduced considerably, compared to those defined for the voxel level simulations.

The remaining parameters were defined as zero. They define the simulation for transport of electrons and positrons and, when set to zero, force detailed simulation.

For cell-level S-values, the simulations were done by running 1×10^7 primary histories. This number was defined to provide a reasonable balance between the simulation time and the desired uncertainty. These parameters were used for both cellular S-values methodologies.

Table 4.2: User-defined parameters for the input files.

PARAMETERS	VALUES
$\boldsymbol{E_{abs}(e^-)}$	50 eV
$\boldsymbol{E_{abs}(ph)}$	
$\boldsymbol{E_{abs}(e^+)}$	
$\boldsymbol{C_1}$	0.0
$\boldsymbol{C_2}$	
$\boldsymbol{W_{CC}}$	
$\boldsymbol{W_{CR}}$	

4.3.2. Direct MC simulations

The S-values, calculated by means of direct MC simulations, followed a similar methodology to the one previously described. An input file was created for each geometry file (39 combinations of nucleus and cell radii), source-target combinations and radionuclides. The selected combinations have in common the target region, which is the cell nucleus for both situations. This resulted in the need of performing 936 MC simulations.

The input file allows the user to define two conditions for the placement of the source: a spherical region, which sides could be specified, and the source material for that region. For the source-target combination N ← N, the source must be placed in the centre of the smaller sphere (centre of the geometry) and must have the dimensions of the nucleus. Therefore, as demonstrated in Figure 4.8, for N ← N simulations, the box sides must be equal to the nucleus diameter. To implement the rejection method, the acceptable source material must be 1, which is the material that composes the nucleus.

```
 SUBSECTION FOR PARTICLE POSITION:
0.0  0.0  0.0                  COORDINATES (cm) OF BOX CENTER
8.0E-4 8.0E-4 8.0E-4           BOX SIDES (cm)
0.0  0.0                       FWHMs (cm) OF GAUSSIAN X,Y DISTRIBUTIONS
0.0  0.0  0.0                  EULER ANGLES [OMEGA,THETA,PHI](deg) FOR BOX ROTATION Rz(PHI).Ry(THETA).Rz(OMEGA).r
0.0  0.0  0.0                  TRANSLATION [DX,DY,DZ](cm) OF BOX CENTER POSITION
1                              SOURCE MATERIAL (0=DON'T CARE, >0 FOR LOCAL SOURCE, <0 FOR IN-FIELD BEAM)
```

Figure 4.8: Input file for N ← N combination and $(R_C, R_N) = (6\ \mu m, 4\ \mu m)$.

In the case that the source is located in the cell's cytoplasm, the box sides must have the dimensions of the cell's diameter, and the material must be the same as the one defined for the composition of the cytoplasm (Figure 4.9). This ensures that the source is defined as the cytoplasm.

```
 SUBSECTION FOR PARTICLE POSITION:
0.0  0.0  0.0                  COORDINATES (cm) OF BOX CENTER
12.0E-4 12.0E-4 12.0E-4        BOX SIDES (cm)
0.0  0.0                       FWHMs (cm) OF GAUSSIAN X,Y DISTRIBUTIONS
0.0  0.0  0.0                  EULER ANGLES [OMEGA,THETA,PHI](deg) FOR BOX ROTATION Rz(PHI).Ry(THETA).Rz(OMEGA).r
0.0  0.0  0.0                  TRANSLATION [DX,DY,DZ](cm) OF BOX CENTER POSITION
2                              SOURCE MATERIAL (0=DON'T CARE, >0 FOR LOCAL SOURCE, <0 FOR IN-FIELD BEAM)
```

Figure 4.9: Input file for N ← Cy combination and $(R_C, R_N) = (6\ \mu m, 4\ \mu m)$.

Once the source has been defined, the required tallies must be configured in the input file. The absorbed dose values were obtained by turning on the Energy Deposition Tally. This tally scores the energy deposited in each material, reported in eV per history. Figure 4.10 shows the parameters to define it: the detection material and the relative uncertainty desired. The first one allows the selection of the target. Since the cell compartments are composed of different materials, the target can be defined by the material in which the deposited dose is scored.

```
[SECTION TALLY ENERGY DEPOSITION v.2012-06-01]
 ON                            STATUS (ON or OFF)
 1                             DETECTION MATERIAL
 0.0                           RELATIVE UNCERTAINTY (%) REQUESTED
[END OF EDP SECTION]
```

Figure 4.10: Input file, section of Energy Deposition Tally.

Despite this definition in the input file, the deposited energy is tallied for each material defined for the simulation (Figure 4.11). Additionally, those values were also complemented with the relative uncertainties. To assess the absorbed dose in each material, a Python script was developed. The energy deposited was converted into the appropriate units. When using the DECDATA database, the S-values were calculated taking into consideration the contributions of each spectrum, as previously explained.

```
#>>>>>>>>>>>>>>>>>>>>>>>>>>>>>>>>>>>>>>>>>>>>>>>>>>>>>>>>>>>>>>>>>>>>>>>>>>>>
# [SECTION REPORT ENERGY DEPOSITION]
# Units are eV per history
#
# Material : Energy (eV/hist) : +-2sigma
   1  4.26107E+03  4.2E+00
   2  1.03764E+03  2.1E+00
   3  1.24372E+05  1.1E+02
```

Figure 4.11: Output file of the Energy Deposition Tally.

4.3.3. Dose Point Kernel

The background theory behind this methodology was explained in detail in section 2.6.2. When using a method based on DPK, a single simulation per radionuclide is needed to determine S-values for cell geometries with different cell and nucleus radii values and any source-target combinations.

The input files were prepared by Dr. J.M. Fernández-Varea and the geometry employed was an infinite medium. For DPK methods, the Spherical Dose Distribution Tally was selected, which scores the absorbed dose in a specific interval using radial bins (spherical shells). The user has the responsibility to ensure that the bins are homogeneous. This tally gives two values for the radii, the low and the average radius of the spherical shell, and the dose value are complemented with the respective uncertainty (Figure 4.12).

The absorbed dose values are presented in eV/g per history and it was defined 50000 as the number of bins with a width of 1 nm. Similarly to the prior methods, the values provided by the simulations must be processed by a Python script. The equations exhibited in section 2.6.2 were useful to determine the geometrical factor (GRF), essential to calculate the final S-values. The Python code was written to analyse the output of this specific tally, applying the theory explained previously.

```
#>>>>>>>>>>>>>>>>>>>>>>>>>>>>>>>>>>>>>>>>>>>>>>>>>>>>>>>>>>>>>>>>>>>>>>>>>>>>
# [SECTION REPORT SPHERICAL DOSE DISTRIB]
# Dose units are eV/g per history
#
# No. of radial (r) bins:
#  50000
# Min r and bin width (cm):
#   0.00000E+00  1.00000E-07
#
# For plotting purposes, two radii r for each bin are given, namely, the low end and an average radius;
#
# rBinIndex : rLow(cm) : rAve(cm) : dose : +-2sigma
     1  0.00000E+00  7.50000E-08  6.22156E+21  4.4E+18
     2  1.00000E-07  1.60714E-07  3.14870E+20  5.0E+17
     3  2.00000E-07  2.56579E-07  7.43959E+19  1.6E+17
     4  3.00000E-07  3.54730E-07  3.42397E+19  7.9E+16
     5  4.00000E-07  4.53689E-07  2.08657E+19  4.9E+16
     6  5.00000E-07  5.53022E-07  1.45920E+19  3.5E+16
     7  6.00000E-07  6.52559E-07  1.09595E+19  2.6E+16
     8  7.00000E-07  7.52219E-07  8.70032E+18  2.1E+16
     9  8.00000E-07  8.51959E-07  7.11780E+18  1.7E+16
    10  9.00000E-07  9.51753E-07  5.97353E+18  1.4E+16
```

Figure 4.12: Output file of the Spherical Dose Distribution Tally.

CHAPTER 5

Results and Discussion

In this chapter, the results and findings of this dissertation, along with the discussion of them, will be presented. Firstly, the results of the simulations at the voxel level are graphically represented to allow better visualisation and comparison of the data. The second subsection of this chapter includes the results from cellular level simulations. The tables with all S-values calculated and the respective uncertainties are available in Appendix B and Appendix C (note that when the uncertainty is presented as 0.00E+00, it indicates that the uncertainty is negligible to the extent that it does not affect the last decimal place of the value).

5.1. Voxel-level S-values

When considering S-values at the voxel level, the absorbed dose is evaluated in a homogeneous medium divided into identical cubical voxels. In subsection 2.6.1, there is a brief description of the studied geometry. Figure 4.6 illustrates a fraction of the geometry that aids in understanding the methodology employed: the cubes painted in the same colour are equidistant from the central cube. Although this figure depicts only a 3×3×3 voxels cube, it is possible to make an analogy to a larger geometry. The simulations were conducted for a 11×11×11 voxels cube and the data analysis was done only for an octant of this cube (6×6×6 voxels). A geometry of these dimensions implies 45 different distances to the central voxel.

Figure 5.1 and Figure 5.2 show the S-values calculated for the investigated radioactive sources as a function of distance from the central voxel. This means that each point marked on the graph does not correspond to a voxel, but to a distance, and thus can represent more than one voxel. As mentioned in the previous chapter, the S-values are computed as the mean absorbed dose scored in voxels at the same distance. This procedure takes advantage of the symmetry of the arrangement of cubic voxels to reduce the statistical uncertainties. Consequently, each point on the plot represents the S-value of a large number of voxels, depending on the distance. All graphs presented in this subsection follow these criteria for the x-axis.

Initial simulations were carried out for monoenergetic sources. Although there is no application of this type of sources in clinical practices, these simulations served to verify the differences in the MC code used, in comparison with the one used in MIRD Pamphlet 17 [50]. Figure 5.1 and Figure 5.2 display data for monoenergetic sources (electrons and photons) for 3 mm and 6 mm voxel sizes, respectively. When compared to the corresponding graphs in the referenced literature, the behaviour of the curves is similar for both electrons and photons. While a point-by-point comparison is not feasible (the MIRD Committee did not provide numerical values for those situations), it is possible to verify that they are approximately equal. From these graphs, it is also possible to conclude that electrons have a greater contribution to the absorbed dose values at distances closer to the centre of the source. At larger distances, photons are the particles with a stronger influence on these S-values. This observation is consistent for both voxel sizes (3 mm and 6 mm) and for the energies (0.1 and 1 MeV) analysed.

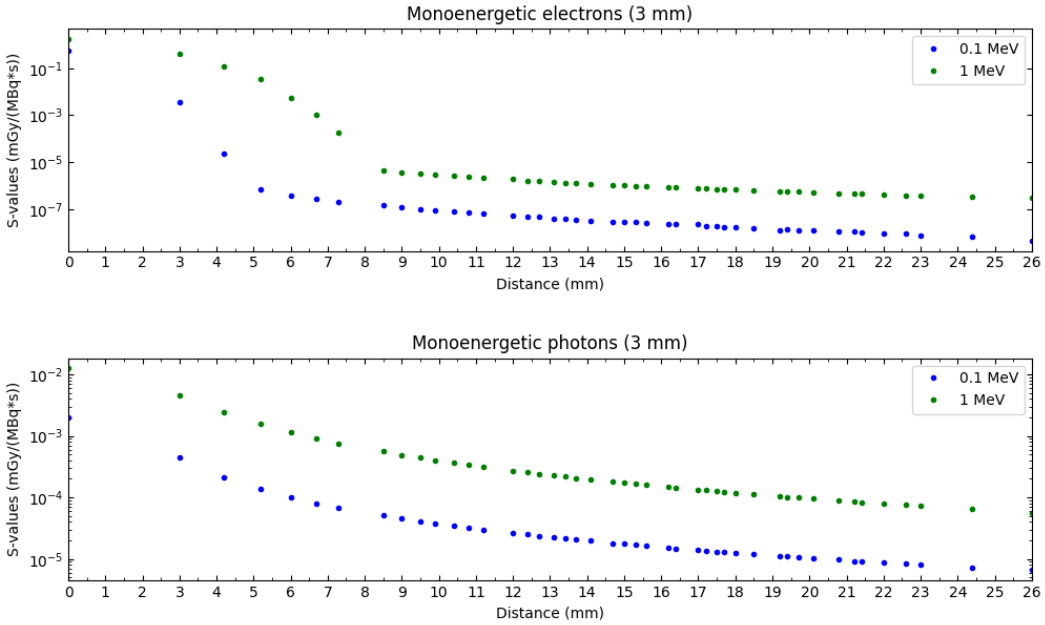

Figure 5.1: S-values for monoenergetic sources (electrons in the top graph and photons in the bottom graph) within 3 mm voxels.

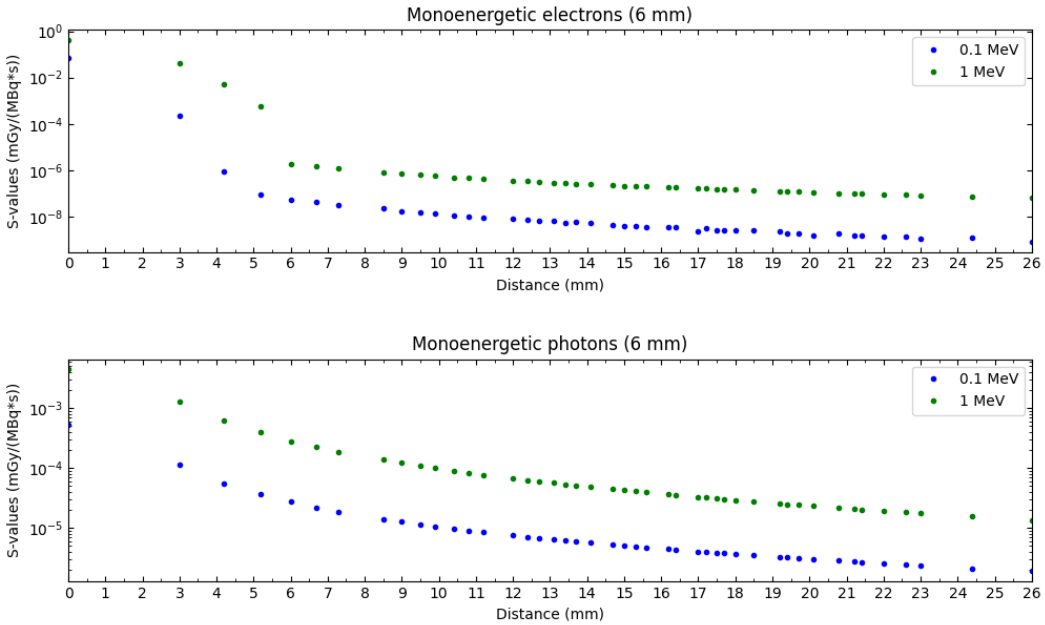

Figure 5.2: S-values for monoenergetic sources (electrons in the top graph and photons in the bottom graph) within 6 mm voxels.

In this dissertation, different databases for nuclear decay data were compared. The analysis of the following graphs allows to quantify the impact of each database on the calculated S-values. The graphs created are result of the methodology previously explained. Two graphs are presented for each radionuclide: for 3 mm and 6 mm voxel sizes. The first five radionuclides have bibliographic reference values.

Figure 5.3 to Figure 5.12 illustrate the variation of the S-values as a function of the distance to the central voxel for ^{32}P, ^{89}Sr, ^{99m}Tc, ^{131}I and ^{90}Y sources. These figures display, in common, curves for MIRD, DECDATA database and PenNuc database, as well as the corresponding ratios for comparison. The ratios are calculated relative to the values calculated by the MIRD Committee. As expected, all graphs show that the absorbed dose decreases with increasing distance from the source voxel for the PenNuc, DECDATA and ICRU curves. It is important to note that the plotted ratios show prominent oscillations due to the large uncertainties of the S-values published by the MIRD Committee. This pamphlet does not provide any information regarding this, which difficult the analysis of the ratios.

Table 5.1 presents the maximum percentage deviation observed in the analysis conducted for each radionuclide and voxel size. This analysis corroborates the conclusions by the observation of the graphs and also quantifies the discrepancies between the S-values calculated with any of the nuclear decay databases and the S-values published by the MIRD Committee. The analysis of this table denotes that these discrepancies are generally more pronounced for voxels with a size of 3 mm.

The observation of the graphs for ^{99m}Tc and ^{131}I (Figure 5.3 – Figure 5.6) indicates that there is excellent agreement between all calculated values, regardless of the adopted decay database, when compared with the remaining graphs for other radionuclides. The curves representing the ratios for both sources and all voxel sizes are close to one, showing consistency in the values and maximum percentage differences ranging between 15.1% - 22.2% for 3 mm voxels and 8.5% - 11.4% for 6 mm voxels.

For the ^{32}P and ^{89}Sr sources (Figure 5.7 - Figure 5.9), a similar behaviour is observed for both radionuclides: S-values calculated with DECDATA and PenNuc are in strong accordance. However, the ratios comparing those values with the ones published by the MIRD Committee exhibit more oscillations than the previous radionuclides, meaning that these differences may result from updates in the decay data or the version of the PENELOPE program. For these sources, the maximum percentage differences are considerably higher, ranging from 72.9% up to 89.6% for 3 mm voxels and from 55.8% up to 81.1% for 6 mm voxels (Table 5.1).

Table 5.1: Maximum percentage deviation per radionuclide and per voxel size with respect to MIRD for voxel S-values.

Radionuclide	**Maximum Percentage Difference**			
	PenNuc database		DECDATA database	
	3 mm	6 mm	3 mm	6 mm
^{99m}Tc	15.6%	9.3%	15.1%	8.5%
^{131}I	22.2%	11.4%	19.7%	11.4%
^{32}P	79.4%	55.8%	72.9%	59.7%
^{89}Sr	84.4%	81.1%	89.6%	76.1%
^{90}Y	91.8%	86.6%	91.7%	86.6%

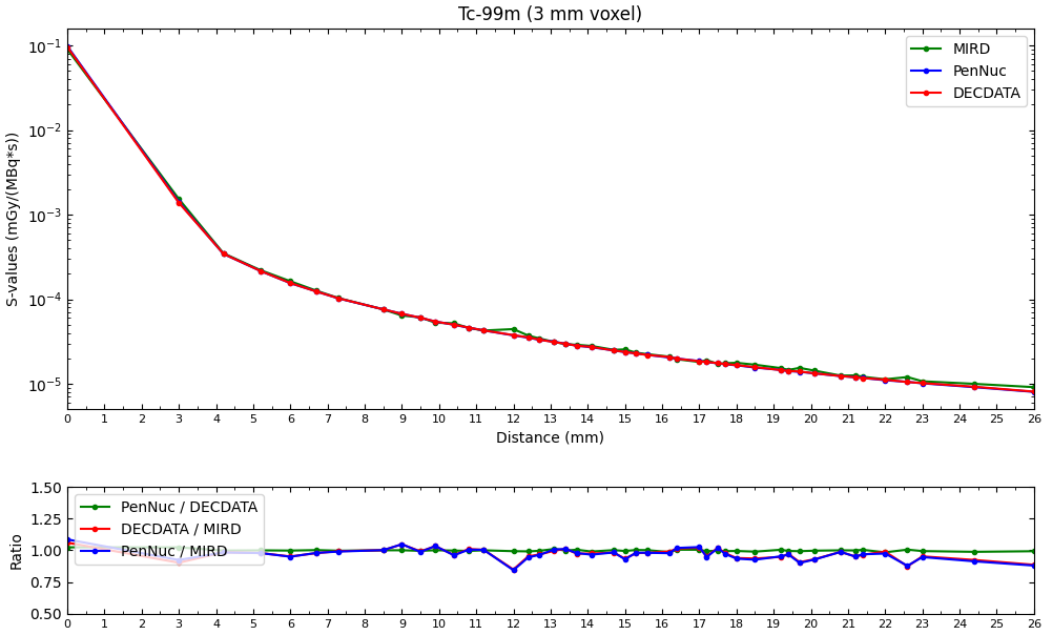

Figure 5.3: Representation of S-values due to ^{99m}Tc decay within 3 mm voxels for different decay databases.

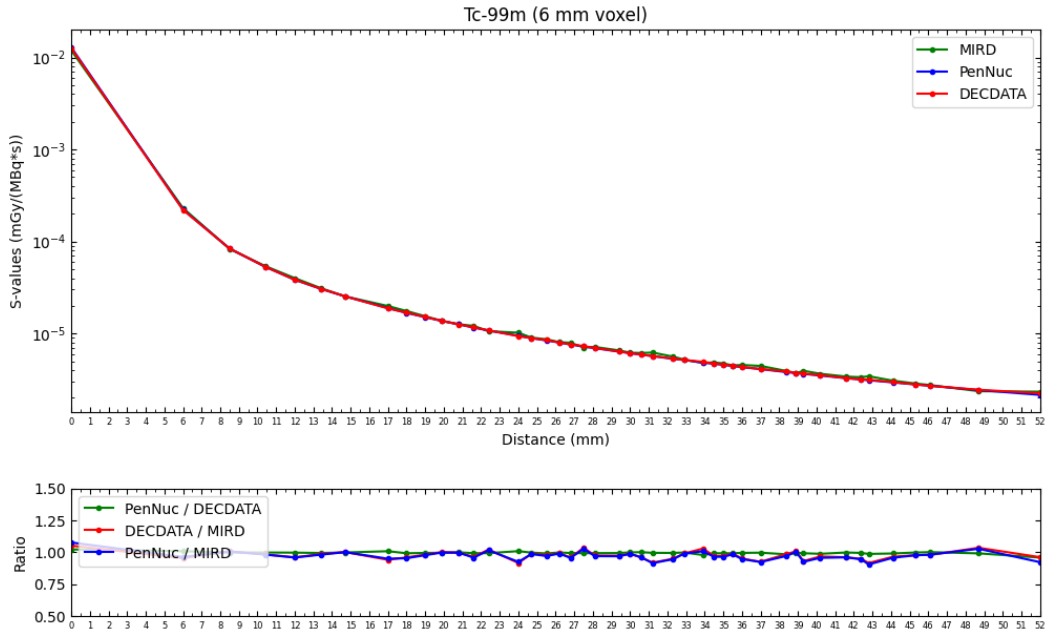

Figure 5.4: Representation of S-values due to ^{99m}Tc decay within 6 mm voxels for different decay databases.

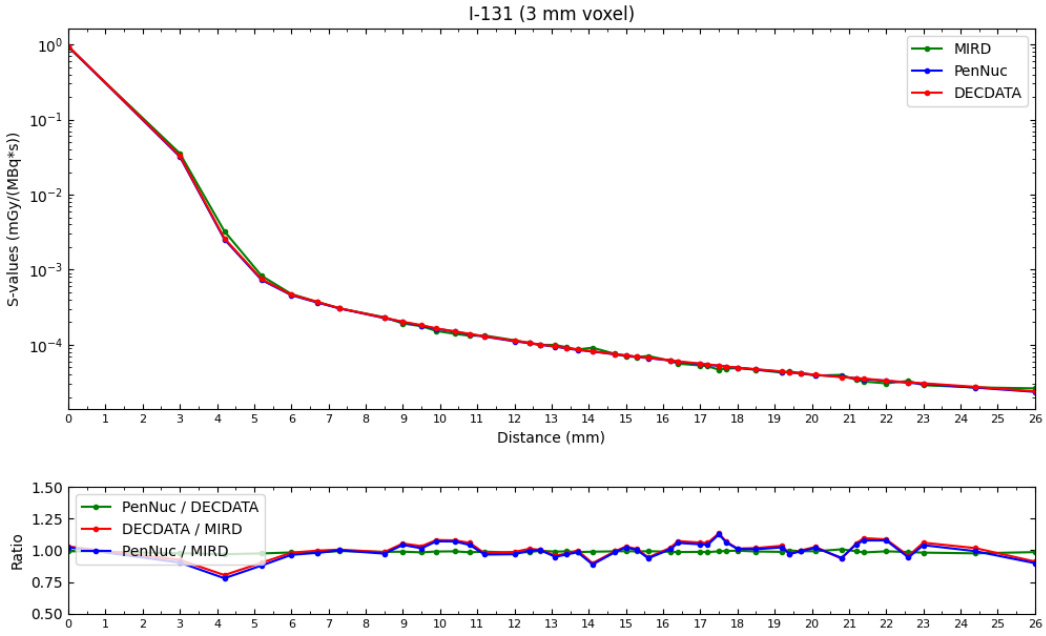

Figure 5.5: Representation of S-values due to ^{131}I decay within 3 mm voxels for different decay databases.

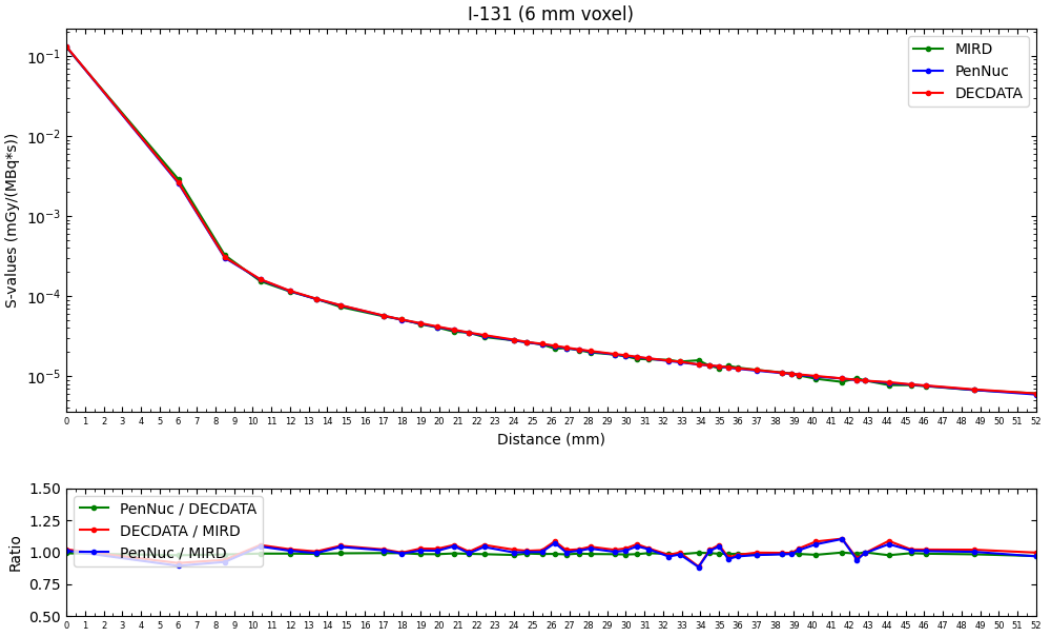

Figure 5.6: Representation of S-values due to ^{131}I decay within 6 mm voxels for different decay databases.

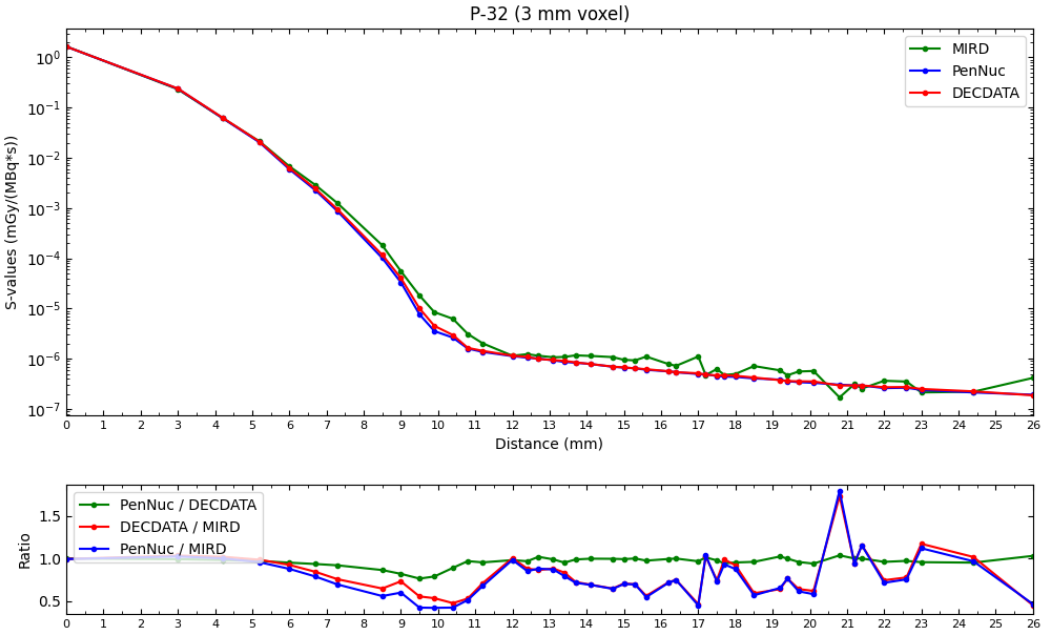

Figure 5.7: Representation of S-values due to ^{32}P decay within 3 mm voxels for different decay databases.

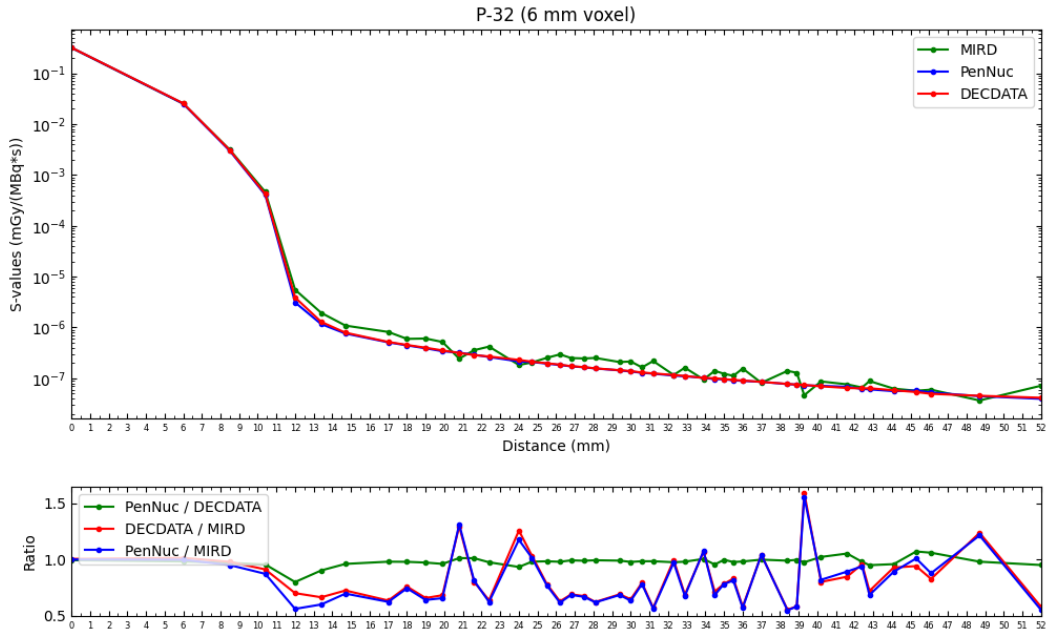

Figure 5.8: Representation of S-values due to ^{32}P decay within 6 mm voxels for different decay databases.

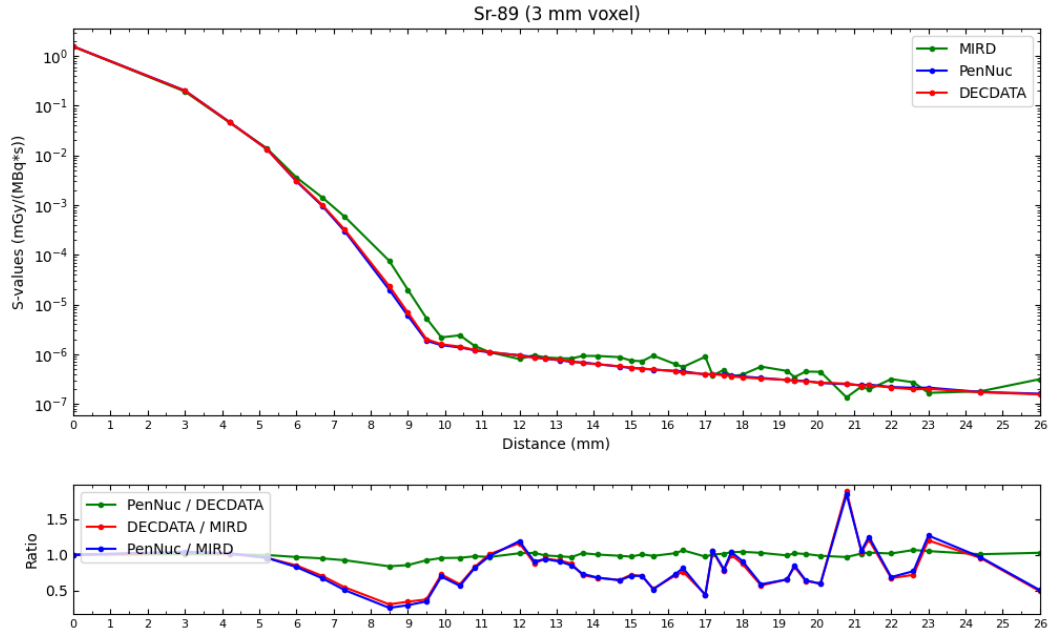

Figure 5.9: Representation of S-values due to ^{89}Sr decay within 3 mm voxels for different decay databases.

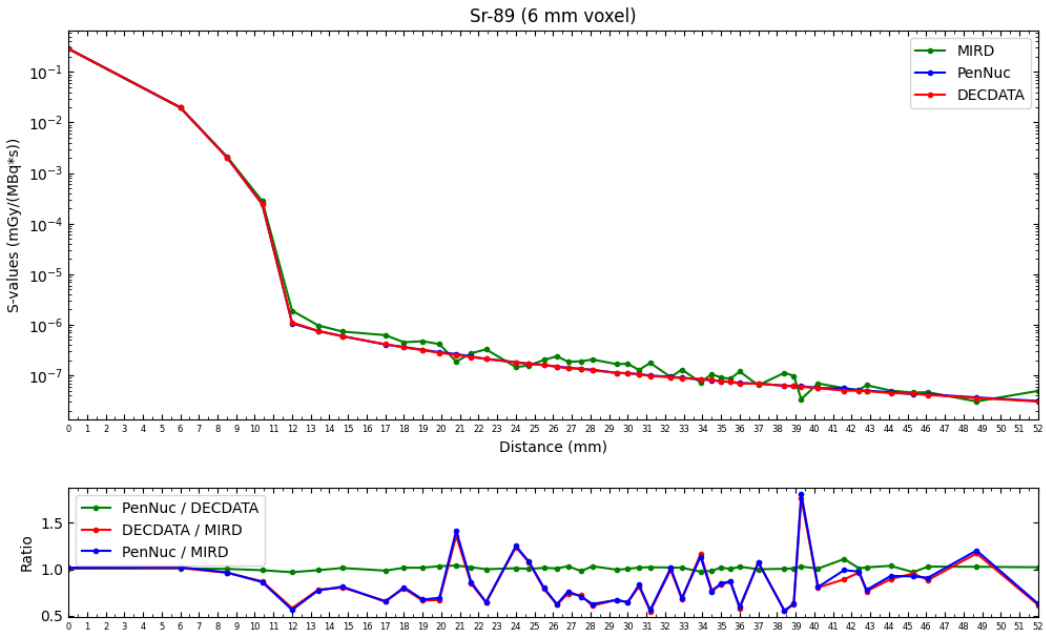

Figure 5.10: Representation of S-values due to ^{89}Sr decay within 6 mm voxels for different decay databases.

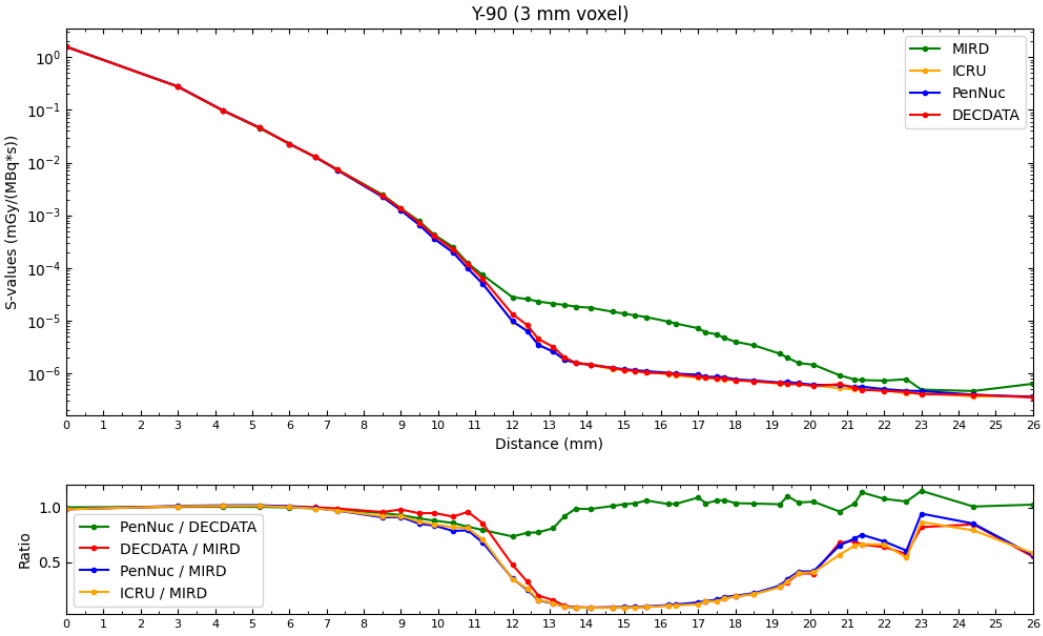

Figure 5.11: Representation of S-values due to ^{90}Y decay within 3 mm voxels for different decay databases.

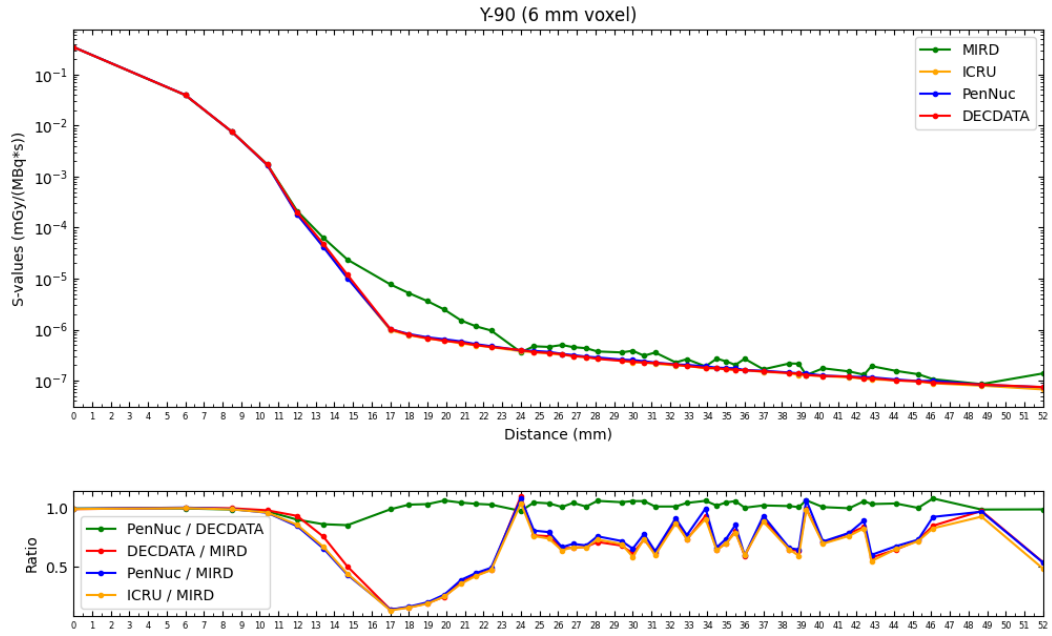

Figure 5.12: Representation of S-values due to ^{90}Y decay within 6 mm voxels for different decay databases.

An analysis was conducted for the radionuclide ^{32}P and for a voxel size of 3 mm by applying the MIRD Committee's methodology, to discard the possibility that the differences indicated by the ratios might be due to the implementation of a simplified methodology (which calculates only one S-value for each different distance to the radioactive source). S-values were calculated for all voxels in the octant individually, regardless of their distance from the radioactive source, which resulted in 216 S-values, displayed in Figure 5.13 where it is presented the ratios between the S-values calculated using PenNuc and DECDATA databases and compared to the ones provided by the MIRD Committee. The x-axis values do not represent the distance from the central voxel, but the indexes of the voxels, since the analysis does not need to be done as a function of the distance. This graph emphasizes that, even without averaging the absorbed dose calculations, these ratios do not approximate the unity. It can be concluded that the discrepancies persisted when not considering the simplification and thus these differences are not due to variations in the methodology, but to differences in decay schemes or the version used for the MC simulations.

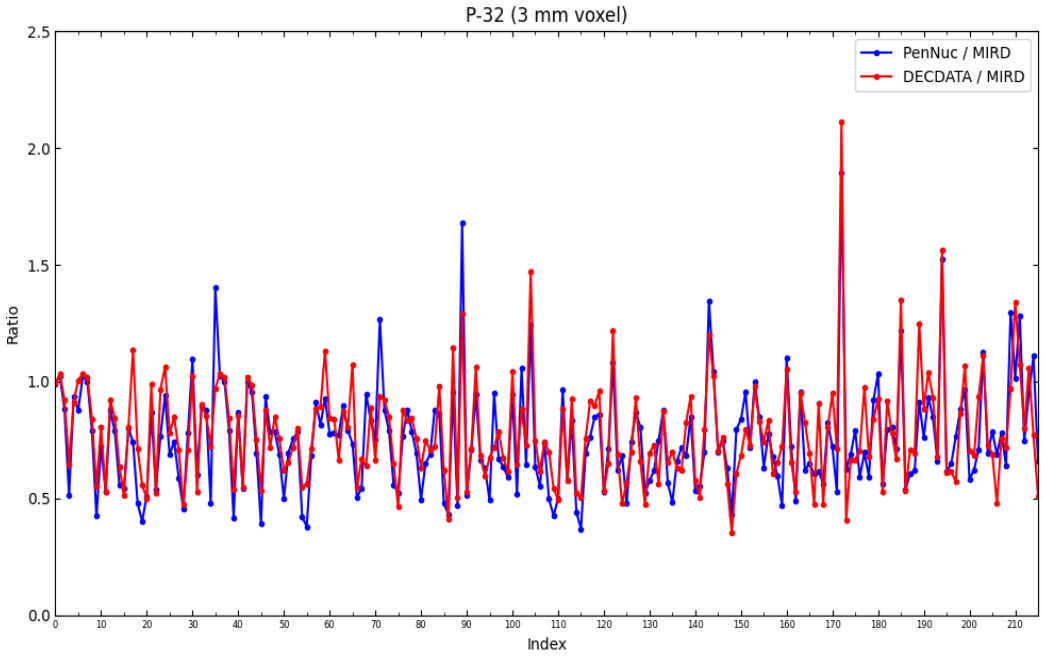

Figure 5.13: Ratios between S-values calculated using both the DECDATA and PenNuc databases, compared to the MIRD values, ^{32}P decay within 3 mm voxels.

The ^{90}Y graphs (Figure 5.11 - Figure 5.12) reveal concordance between all the databases for the closest voxels to the radioactive source; however, for distances between 11 and 24 mm approximately, there is a significant deviation of the S-values calculated by the MIRD Committee. Regardless of the decay database used, the maximum percentage differences registered are about 91.8% for 3 mm voxels and 86.6% for 6 mm voxels. The ICRU database was included to analyse these substantial differences by assuring that these differences are not caused by the nuclear decay data. As observed in Figure 5.12, the ICRU curve lines up with the remaining ones, rejecting the previous hypothesis.

The decay scheme of this radionuclide indicates that ^{90}Y is predominantly obtained from the decay of ^{90}Sr and, due to its long half-time of 28.8 years, they are in secular equilibrium and should be studied together. However, their contributions to the S-values must be carefully analysed.

As described in Equation 2.4 (section 2.4), the S-value is the mean absorbed dose to a target volume per unit of cumulated activity. Although ^{90}Sr and ^{90}Y are in secular equilibrium, the energy released per decay is significantly different for the two radionuclides, *i.e.*, ^{90}Y emits much more energetic beta particles compared to ^{90}Sr. This difference in energy release is already considered in the individual S-values of each radionuclide, as the absorbed dose depends not only on the number of decays but also on the energy deposited in the tissue. In secular equilibrium, the activities of both radionuclides are equal, which means they undergo the same number of decays per second; however, the cumulated activities of ^{90}Sr and ^{90}Y depend on their respective half-lives and the initial activity. Therefore, in the total S-value, the contribution of ^{90}Y will be significantly larger due to its higher energy release per decay, despite the activities being equal at a specific moment. Consequently, no additional scaling factors are needed, as the difference in energy is inherently included in the individual S-values. Figure 5.14 demonstrates the S-values curve by summing both contributions of ^{90}Y and ^{90}Sr, where the discrepancy of the S-values calculated by the MIRD Committee continues considerable. After this careful study, it can be inferred that the differences are not related to the data in the decay databases, but to the calculations of S-values by the MIRD Committee.

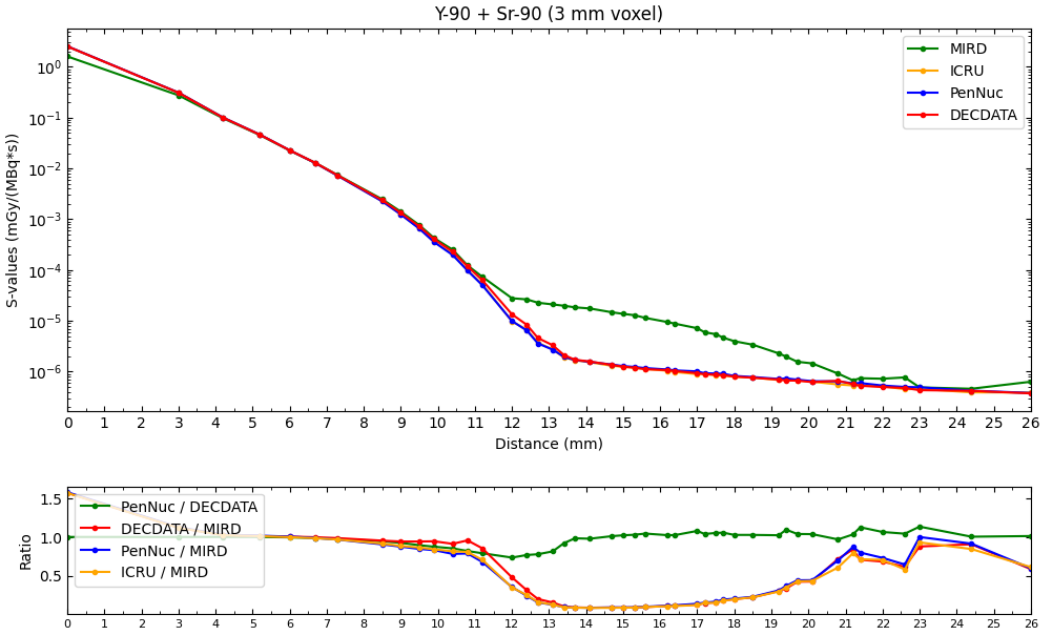

Figure 5.14: Representation of S-values due to ^{90}Y + ^{90}Sr decay within 3 mm voxels for different decay databases.

The reference considered for the comparison of the S-values calculated in this dissertation, the MIRD Pamphlet 17 [50], provides results for only five radionuclides. One of the aims of this study is to expand this list by calculating the S-values for two additional isotopes. The graphs of Figure 5.15 - Figure 5.18 illustrate the behaviour of the S-values for ^{177}Lu and ^{153}Sm, where it is noticed the decrease of S-values with the increasing of the distance from the radioactive source. Two curves are represented for both databases and they are in great agreement, as expected.

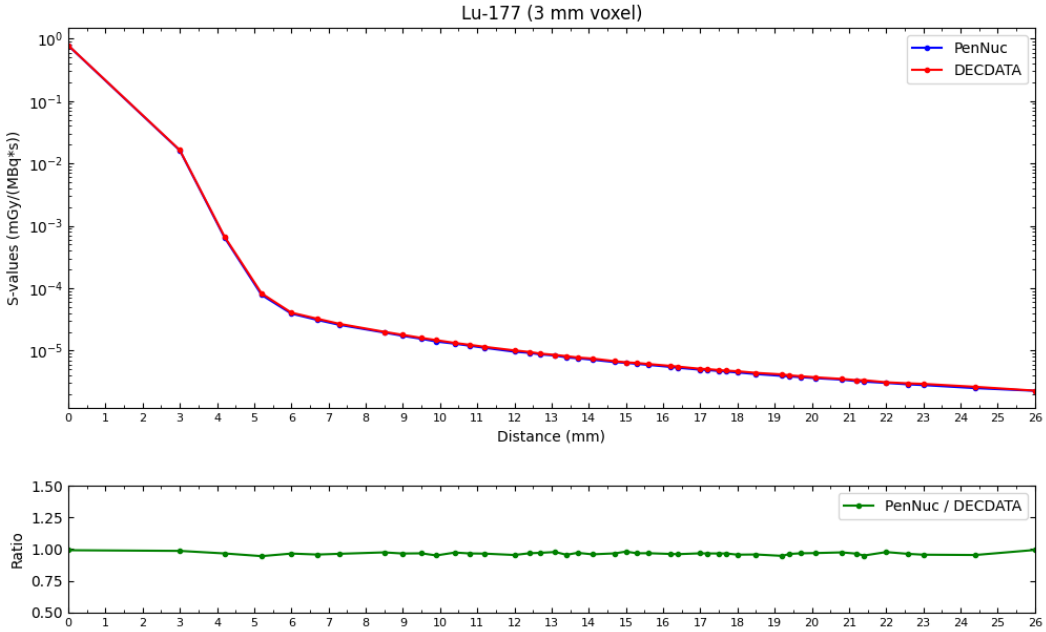

Figure 5.15: Representation of S-values due to ^{177}Lu decay within 3 mm voxels for different decay databases.

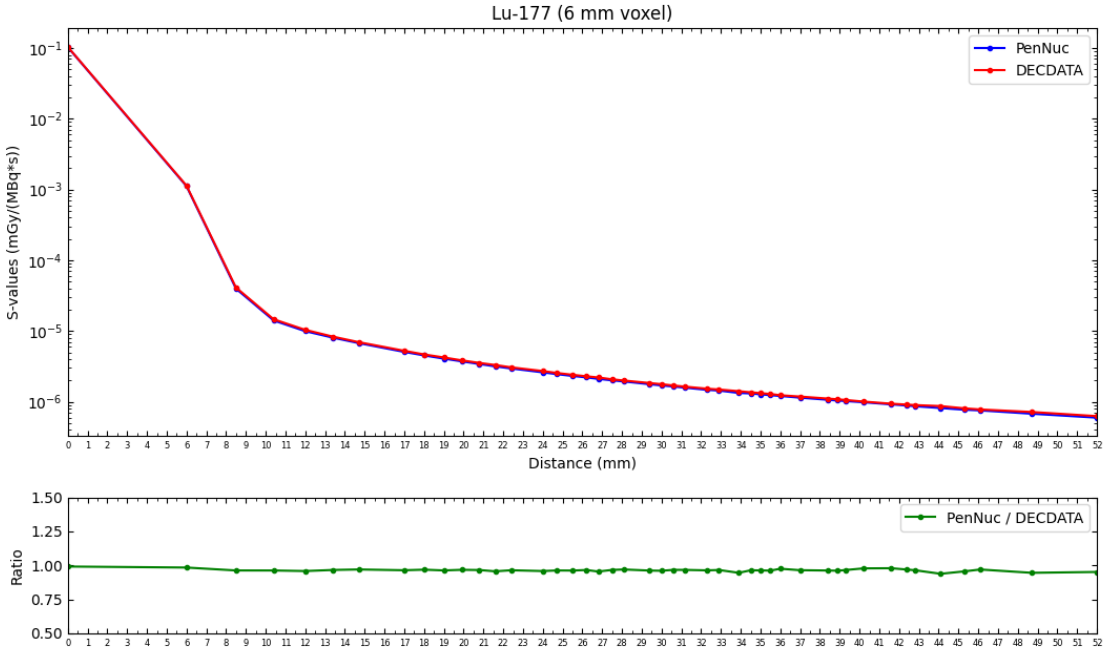

Figure 5.16: Representation of S-values due to ^{177}Lu decay within 6 mm voxels for different decay databases.

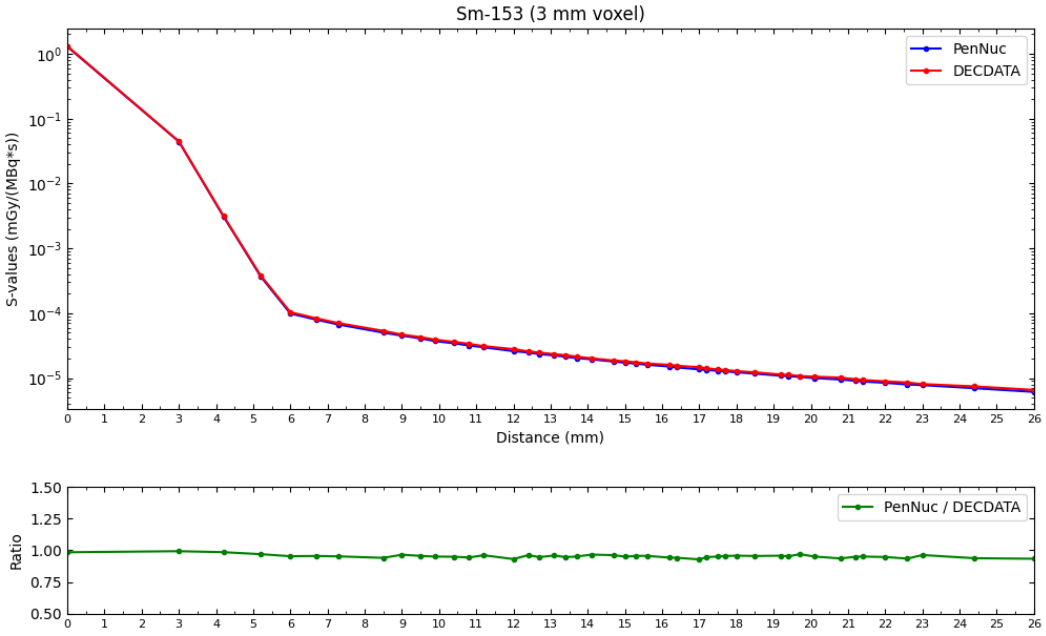

Figure 5.17: Representation of S-values due to ^{153}Sm decay within 3 mm voxels for different decay databases.

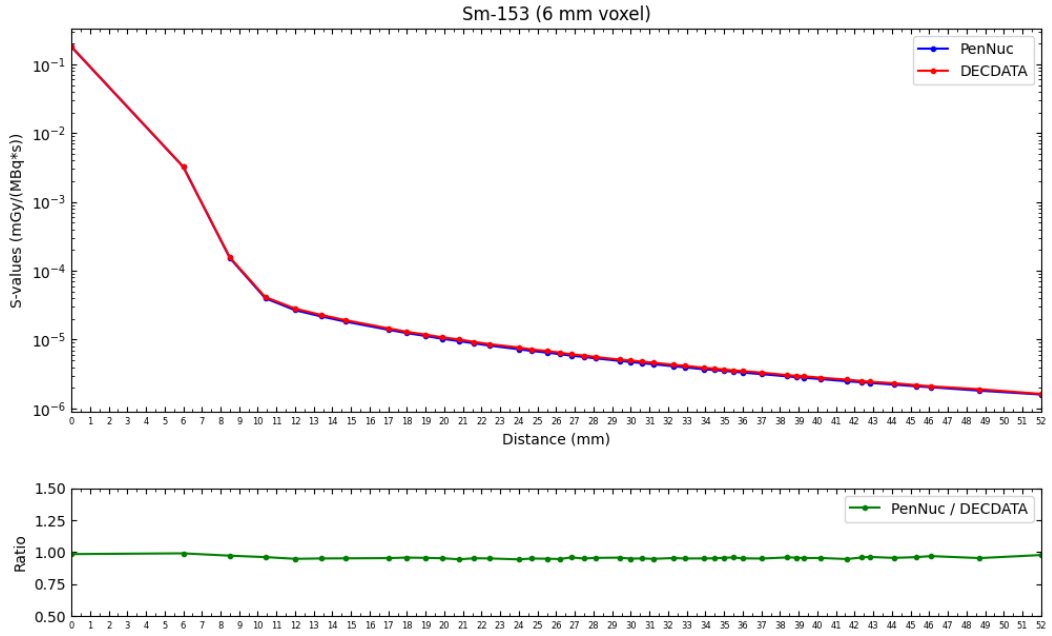

Figure 5.18: Representation of S-values due to ^{153}Sm decay within 6 mm voxels for different decay databases.

Appendix B includes the tables with the results for all the simulations carried out at the voxel level. For each radionuclide two tables were constructed, one for 3 mm and one for 6 mm voxel size, and they are composed of several columns with information to help the reader better understand them: the distances in millimetres from the central voxel, the coordinates corresponding to these distances, the S-values ($mGy \cdot MBq^{-1} \cdot s^{-1}$) and the respective uncertainties. Note that the coordinates are given in a simplified form, *i.e.*, each set of three coordinates represents a combination of them (*e.g.*, (0,0,2) can also represent (2,0,0) and (0,2,0)). The uncertainties presented in the tables were calculated for each S-value individually and were useful for accurate assessments. The simulations were performed until all primary histories were simulated and therefore the uncertainties can be considered as extremely high in reliability.

To fulfil another aim of this dissertation, Appendix B also includes tables with S-values calculated for three other voxel sizes: 2.26 mm, 4.52 mm and 9.04 mm. DECDATA database is based on an internationally referenced report for nuclear data; therefore, these additional S-values were calculated using only this database. These tables include the distances in millimetres, the corresponding coordinates, the S-values as well as their uncertainties, for each radionuclide defined at the top of the column.

5.2. Cellular-level S-values

The results of the simulations conducted at the cellular level will be presented in this subsection. The S-values at the cellular level were calculated by applying two different methodologies: direct MC simulations and DPK. The S-values were assessed for four radionuclides (^{67}Ga, ^{123}I, ^{111}In and ^{201}Tl) and for two source-target combination (N ← N and N ← Cy). The geometry applied for the calculation of these S-values requires 39 possible combinations of cell and nucleus radii and it is based on the representation of Figure 2.6 (section 2.6.2). Similar to the voxel-level simulations, both decay databases, DECDATA and PenNuc, were evaluated.

5.2.1. Direct MC simulations

Figure 5.19 displays the results of the MC simulations performed by showing the ratios between the S-values calculated with each decay database and the ones used as reference, calculated by Falzone *et al.* [75]. To facilitate the interpretation of the graphs, the curves in the graphs were plotted as a function of an index, which represents a combination of cell and nucleus radii (*e.g.* when the index is 8, the radii of the cell and its nucleus are 6 µm and 3 µm, respectively). Table 5.2 makes the association between the index and (R_C, R_N).

Table 5.2: Correlation between cell and nucleus radii and respective index.

Index	Cell radii (µm)	Nucleus radii (µm)		Index	Cell radii (µm)	Nucleus radii (µm)
1	3	1		**23**	10	5
2		2		**24**		6
3	4	2		**25**		7
4		3		**26**		8
5	5	2		**27**		9
6		3		**28**	11	5
7		4		**29**		6
8	6	3		**30**		7
9		4		**31**		8
10		5		**32**		9
11	7	3		**33**		10
12		4		**34**	12	6
13		5		**35**		7
14		6		**36**		8
15	8	4		**37**		9
16		5		**38**		10
17		6		**39**		11
18		7				
19	9	5				
20		6				
21		7				
22		8				

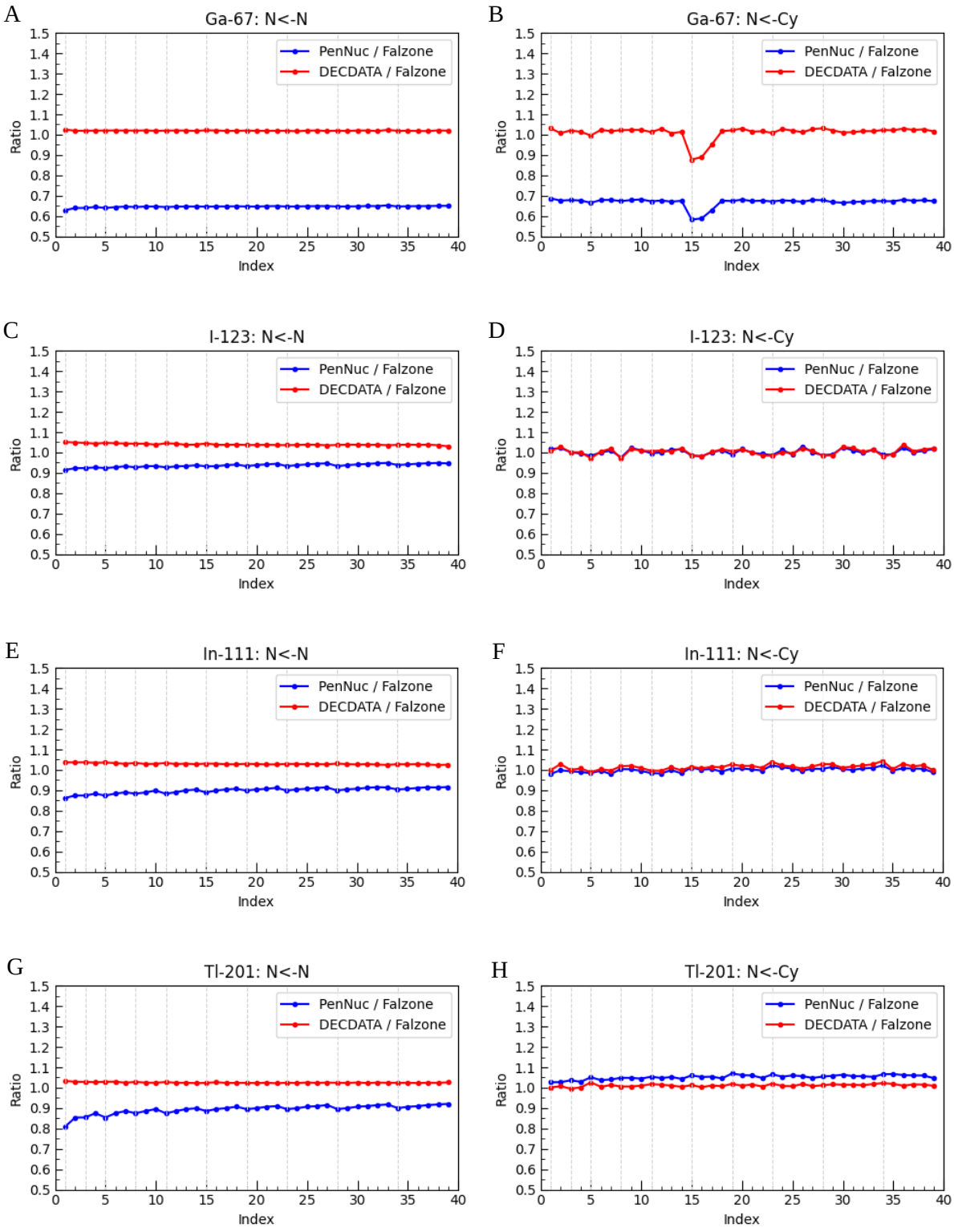

Figure 5.19: Ratios between S-values calculated using the DECDATA and PenNuc decay database and the reference bibliography for the ^{67}Ga, ^{123}I, ^{111}In and ^{201}Tl radionuclides. The graphs on the left side represent the results when the source and the target are the nucleus of the cell; the graphs on the right side represent the results when the source is the cytoplasm and the target is the cell nucleus.

The graphs in Figure 5.19 show approximately a straight line near the unit except for some slight differences. Table 5.3 presents the maximum percentage differences between the S-values calculated and the referenced ones, indicating the radionuclide, the database and the source-target combination. These percentages are generally higher for N←N compared to N←Cy combination, which corroborates with the analysis that can be done by the observation of Figure 5.19.

The graphs for ^{67}Ga, for both source-target combinations (Figure 5.19 A, B), reveal a significant discrepancy between the PenNuc/Falzone and DECDATA/Falzone ratios that is not observed in the graphs for the remaining radionuclides. An in-depth observation indicates that the ratios for the S-values calculated with the DECDATA database are generally close to one whereas the ratios for PenNuc are around 0.6 up to 0.7. According to Table 5.3, the maximum percentage differences for this radionuclide are superior when the PenNuc database is used. This might allow to conclude that these discrepancies occur due to differences in the decay scheme of the radionuclide because this is only observed for this radionuclide. Therefore, the results for ^{67}Ga are an exception compared to the other radionuclides.

The graphs for the radionuclides ^{123}I, ^{111}In and ^{201}Tl (Figure 5.19 C-H) show curves with approximately the same behaviour when considering the same source-target combinations. When the nucleus is both the source and the target (Figure 5.19 C, E, G), the ratios DECDATA/Falzone are approximately one. The maximum percentage differences between the S-values calculated with this database and the reference S-values range from 3.5% up to 5.2%, which indicates great concordance (Table 5.3). The largest discrepancies are observed in the values calculated with PenNuc, with maximum percentage differences around 8.4%-19.1%. These differences are more pronounced for smaller indexes, as can be seen in the graphs. Recall that Falzone *et al.* [75] used an earlier version of PENELOPE/penEasy. When the source is the cytoplasm and the target is placed in the nucleus (Figure 5.19 D, F, H), the results calculated with DECDATA and PenNuc are similar and both ratios are close to one, with maximum percentage differences ranging from 2.0% to 7.0%.

Since the S-values calculated at the cellular level followed the same methodology as the one implemented by Falzone *et al.* [75], the results should indicate great accordance. The mentioned article, as described in section 2.6.2, uses a software called RADTABS as the nuclear decay database, which is an earlier version of the DECDATA database. Therefore, the ratios for the S-values calculated with this database have less difference from the S-values used as reference, as expected. In this situation, the differences between the DECDATA and RADTABS databases are less significant than the differences between the PenNuc and RADTABS databases. Important to note that the divergences also result from the use of different versions of PENELOPE MC code.

Appendix C includes tables with the S-values calculated at the cellular level by using direct MC simulations. Two tables for each radionuclide were published: one for each source-target combination. The tables present columns that list the values of the cell radii and nucleus radii, the S-values from the article of Falzone *et al.* [75], the S-values calculated using the DECDATA and PenNuc databases, and their respective uncertainties and ratios.

Table 5.3: Maximum percentage deviation per radionuclide and per source-target combination with respect to Falzone for cellular S-values.

Radionuclide	**Maximum Percentage Difference**			
	PenNuc database		DECDATA database	
	N ← N	N ← Cy	N ← N	N ← Cy
^{67}Ga	37.1%	41.8%	2.6%	12.2%
^{123}I	8.4%	2.0%	5.2%	3.0%
^{111}I	13.6%	2.2%	3.6%	4.4%
^{201}Tl	19.1%	7.0%	3.5%	2.4%

5.2.2. Dose Point Kernel

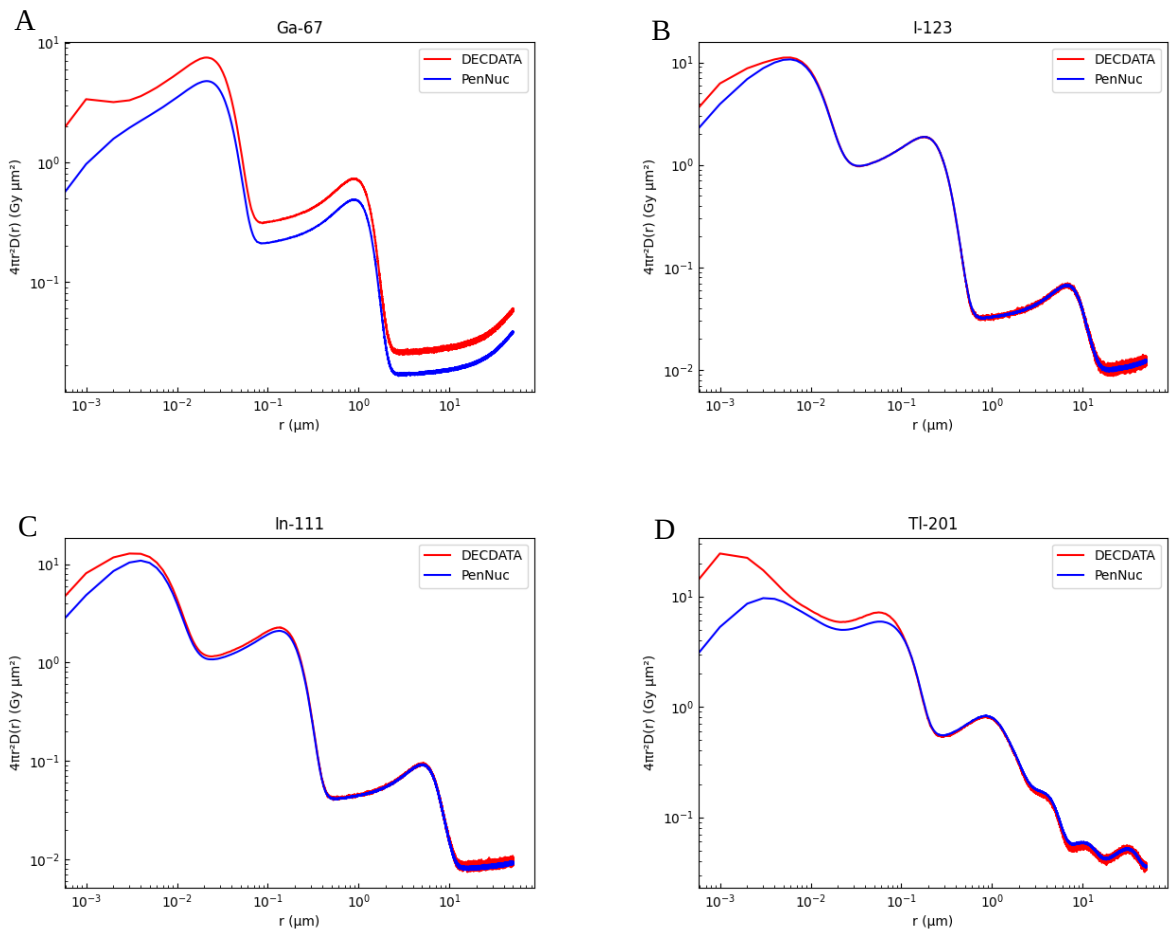

Figure 5.20: DPKs calculated by using the DECDATA and PenNuc decay database for the AE, CK and IE electrons emitted in the decay of ^{67}Ga, ^{123}I, ^{111}In and ^{201}Tl.

S-values at the cellular level were also obtained by applying the DPK approach. Only a single simulation per radionuclide was required to obtain the S-values, regardless of the source-target combinations or the dimensions of the cell and nucleus and both decay databases were evaluated.

Figure 5.20 illustrates the radial dose distribution times $4\pi r^2$ as a function of the distance from the radioactive source for each radionuclide (^{67}Ga, ^{123}I, ^{111}In and ^{201}Tl). All graphs follow a similar pattern, with increased dose at small distances followed by a gradual decreasing trend that results from the attenuation of radiation. The oscillations are due to the various groups of AE and CK electrons emitted during the atomic relaxation that follows electron capture or internal conversion. In the ^{123}I, ^{111}In and ^{201}Tl graphs (Figure 5.20 B-D), the DECDATA and PenNuc curves show a close agreement in the dose distribution, by remaining closely aligned throughout approximately the entire distance (r) spectrum. This reinforces the consistency of the DPK methodology regardless of the decay database used. Although the graph for ^{67}Ga exhibits similar dose distribution behaviour, the curves for DECDATA and PenNuc databases are not as quite close as the curves for the remaining radionuclides, which indicates divergencies in the decay databases (as denoted in the direct MC simulations analysis).

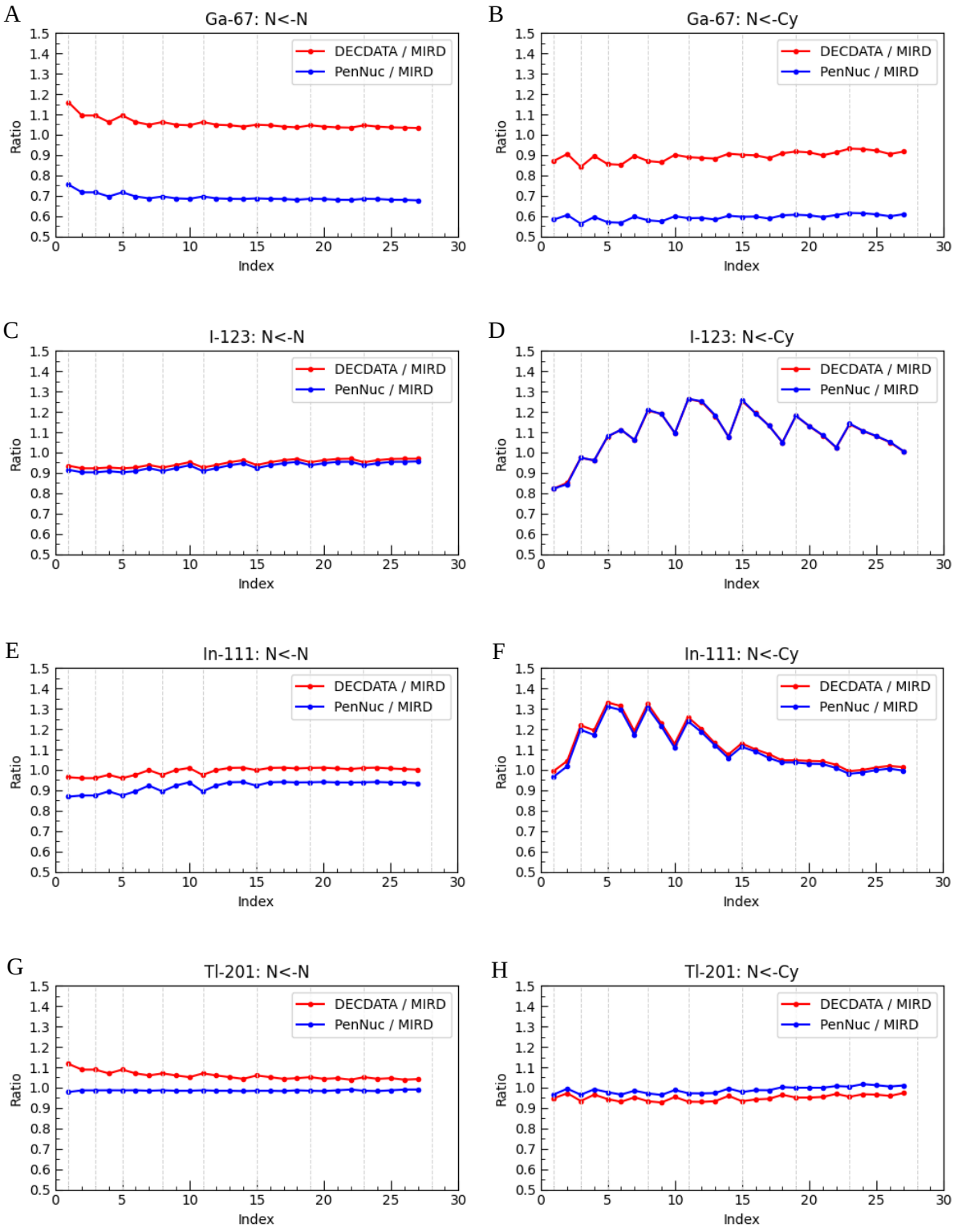

Figure 5.21: Ratios of S-values, calculated by applying the DPK methodology, between values calculated with DECDATA and PenNuc decay database and the reference bibliography for ^{67}Ga, ^{123}I, ^{111}In and ^{201}Tl radionuclides. The graphs on the left side represent the results when the source and the target are the nucleus of the cell; the graphs on the right side represent the results when the source is the cytoplasm and the target is the cell nucleus.

The S-values that result from the application of DPK were compared to those published by the MIRD Committee since they employed a similar methodology. However, the MIRD Committee only provides S-values for cells with a maximum radii dimension of 10 μm. For this reason, only the first 27 values were plotted in the graphs; the S-values for the remaining radii dimensions were only presented in the published tables, in Appendix C.

The graphs of Figure 5.21 show the ratios between the S-values calculated using the DECDATA and PenNuc databases and the S-values published by the MIRD Committee, as a function of an index. Table 5.4 presents the maximum percentage difference between the S-values computed for the aim of this dissertation and the S-values considered as a reference (calculated by the MIRD Committee), and they are listed for both databases and both source-target combinations.

The radionuclide ^{67}Ga can be considered an exception when comparing its graphs to the curves of other radionuclides. As detected in Figure 5.20, when it is plotted the distribution of the radial dose before the application of the geometric reduction factor (GRF), there are differences between the curves of the DECDATA and PenNuc databases. For ^{67}Ga graphs (Figure 5.21 A, B), the ratios that compare the S-values calculated with the PenNuc database and the S-values calculated by the MIRD Committee are more distant from the unit than the ratios for S-values calculated with the DECDATA database. For this radionuclide, the maximum percentage differences are 32.3% and 43.8% when using the PenNuc database, and around 15.8% - 15.9% when using the DECDATA database.

When the source-target combination is N←Cy, for ^{123}I and ^{111}In radionuclides, the graphs (Figure 5.21 D, F) show that, despite the results for both decay databases being aligned, there are strong discrepancies between the calculated S-values and the reference S-values. The maximum percentage differences are around 26.5% for ^{123}I and between 31.1% and 33.1% for ^{111}In. The vertical lines displayed in the graphs are placed in the indexes where there is a change in the R_C. Thus, the accentuated differences are placed in these lines, indicating that the S-values are closer to the ones calculated by the MIRD Committee when the geometry of the cell has a nucleus with bigger dimensions. This conclusion was previously reached by Falzone *et al.* [75], indicating that larger discrepancies occur when the source and target volumes are farther apart.

For the remaining cases - when the source-target combination is N←N for ^{123}I and ^{111}In (Figure 5.21 C, E) and both combinations for ^{201}Tl (Figure 5.21 G, H) - the curves displayed in the graphs have a similar behaviour, which can be considered as expected. They are approximately straight, indicating that the calculated S-values are essentially in agreement with the referenced ones.

Table 5.4: Maximum percentage deviation per radionuclide and per source-target combination with respect to MIRD for cellular S-values.

Radionuclide	**Maximum Percentage Difference**			
	PenNuc database		DECDATA database	
	N ← N	N ← Cy	N ← N	N ← Cy
^{67}Ga	32.3%	43.8%	15.8%	15.9%
^{123}I	9.8%	26.5%	7.9%	26.5%
^{111}I	13.1%	31.1%	4.2%	33.1%
^{201}Tl	1.4%	3.5%	26.1%	7.2%

When analysing this comparison, it is important to note that the S-values calculated by the MIRD Committee are based on the DPK methodology but with significant differences in the underlying physics employed. The MIRD DPKs assume that the electron trajectories are straight lines, which neglects elastic scattering. Also, the energy loss is calculated within the CSDA, thus ignoring

fluctuations in the energy loss. On the other hand, the S-values presented in this dissertation were calculated with the PENELOPE MC code, where these physical effects are considered so that the electron tracks are more realistic and the stochastic nature of inelastic collisions is preserved. Therefore, there is a notable impact on the final S-values and the differences observed in this comparison (Table 5.4) are attributed to the physics models, with the approach used by the MIRD Committee being less accurate.

Similarly to the previous methodology, the S-values calculated by DPK are given in Appendix C. The tables contain the cell and nucleus radii, the S-values calculated by the MIRD Committee, the S-values calculated using the DECDATA and PenNuc databases, and their respective uncertainties and ratios, for both source-target combinations.

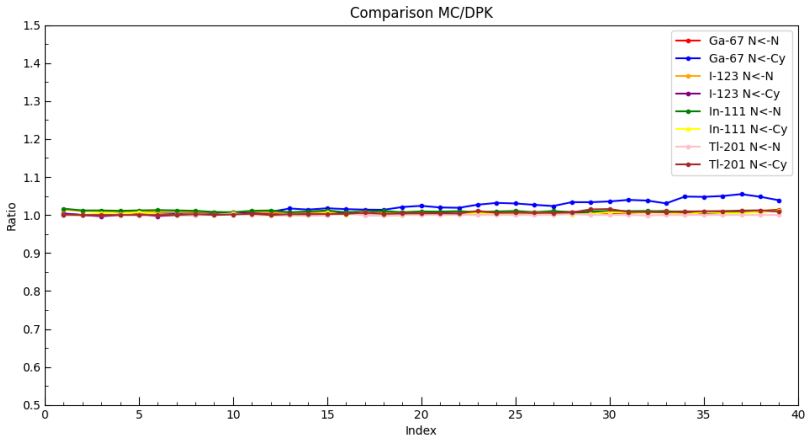

Figure 5.22: Comparison between the two methodologies: direct MC simulations and DPK.

Cellular S-values were calculated for two distinct methodologies and compared to S-values calculated with similar approaches. Despite that, the S-values, tabulated in Appendix C, are related to the same conditions (radionuclide, source-target combination and (R_C, R_N)), regardless of the methodology applied. Thus, Figure 5.22 provides a comparison between the S-values calculated for both methodologies, by plotting the ratio between S-values calculated with direct MC simulations and DPK as a function of an index. The behaviour of the ratios for each radionuclide and source-target combination shows excellent agreement of the values. This analysis corroborates that the cellular S-values were correctly calculated.

CHAPTER 6

Conclusion

In this dissertation, various methodologies were evaluated to verify their effect on dosimetry calculations for nuclear medicine, which required numerous MC simulations. The results were expected to indicate divergencies since different MC codes and databases for radioactive decay data were used.

At the voxel level, the simulations produced results that can be assumed as expected. A simplified methodology was implemented, allowing to reduce the dimensions of the current tables for S-values. The results showed differences between the S-values calculated in this study and the S-values considered as reference. The simplification of the methodology was proven not to increase the deviations, which allowed to conclude that they are produced by other factors, such as the decay database and the version of the PENELOPE MC code used. When calculating the S-values, these are the only two differences in the employed methodology, as clarified in section 2.6.1 where it is assessed and compared all the details regarding these approaches. Therefore, we can observe that the percentage deviations of the S-values for ^{99m}Tc and ^{131}I are smaller when compared with the deviations for ^{32}P, ^{89}Sr and ^{90}Y S-values. Although the difference may vary, the results strongly suggest that the calculation of the S-values using updated decay databases and the most recent version of PENELOPE introduces significant changes for the S-values, which are useful for absorbed dose calculations in nuclear medicine. To complete the update of the tables, S-values have been calculated for two previously unreported radionuclides and three additional voxel sizes. These updated tables will be useful as they list values for voxel sizes currently used in nuclear medicine practices.

The S-values at the cellular level were calculated by applying two different methodologies. The first approach, direct MC simulations, confirmed that the S-values calculated with the PenNuc database are in less conformity with the reference S-values, particularly for the N ← N combination. When using the DECDATA database, the S-values are in great concordance with the reference ones, as the nuclear decay database are similar. When the DPK approach was applied, contrarily to the previous findings, the S-values calculated with both decay databases were proven to be in more agreement with the S-values calculated by the MIRD Committee for the N ← N combination than for the N ← Cy combination. The differences found in this comparison between the S-values calculated with DPK methodology and those calculated by the MIRD Committee are due to variations in the physics models applied for the calculation of S-values. Besides not as pronounced as the deviations for S-values at the voxel level, at the cellular level significant percentage differences were also obtained, which indicates that, when using updated resources, notable changes in the calculations of S-values may be introduced.

In conclusion, this dissertation presents updated tables of S-values at the voxel and cellular level. The methodologies explained above introduced considerable differences; the causes of which were attributed to variations in the decay databases used and the MC code version. The atomic and nuclear models of radionuclides are continually being studied, which makes it reasonable to assume that these are the reasons behind the differences obtained in the S-values. Unfortunately, no experimental or external validation can be made that would allow to conclude that the S-values published in this dissertation are more correct than the reference ones.

Some limitations of this study must be referred and analysed. The computational time for some of the simulations took several days to complete, making the analysis of the output and the detection of possible errors difficult. For each set of simulations, the number of primary histories as well as the simulation parameters were evaluated taking into consideration the computational time.

In summary, all the objectives for this dissertation have been successfully achieved. This report summarizes the work carried out in 6 months; the published tables are the results of the computation of 1069 simulations in total; however, this number only includes successful simulations and simulations with contributions for the publication of results.

6.1. Future work

In the dosimetry field, there are still significant improvements required to facilitate calculations performed by medical physicists. Ideally, S-values should be calculated from patient-specific images (*e.g.*, CT images) and considering the individual composition and morphology of each patient. In the future, the development of deep learning and machine learning algorithms might help in organ segmentation on CT images and, hence, estimate the absorbed dose for each individual organ [89].

At the cellular level, the simplest cellular model - a pair of concentric spheres - was employed for calculating the S-values. Future work should consider more complex and realistic geometries, such as ellipsoidal or eccentric cell-nucleus arrangements as well as rotated nuclei. These geometries can only be dealt with using direct MC simulations, and not DPK approaches. In summary, these suggestions represent areas for future research with the aim at developing more accurate dosimetry calculations.

The decay databases evaluated in this dissertation have distinct functioning: PenNuc takes consideration of all transitions allowing to have only one input file, while when using DECDATA it is necessary to have one input file per type of particle emitted. DECDATA implies the computation of one simulation for each input file and posteriorly combines the outputs by manually applying the contributions of each emitted particle (yield). Thus, it may be useful to convert the DECDATA database in the same configuration as PenNuc to facilitate its use and allow to perform only one simulation for each radionuclide.

Additionally, this study already provides tables with updated calculated values. Therefore, it would be appropriate in the future to create a user-friendly online platform to make this data more easily accessible.

All these tasks were beyond the scope of the present thesis and also beyond the time available and, therefore, were not addressed in this study.

References

[1] M. M. Graham and D. F. Metter, "Evolution of Nuclear Medicine Training: Past, Present, and Future," *Journal of Nuclear Medicine*, vol. 48, no. 2, pp. 257–268, 2007.

[2] B. Gutfilen and G. Valentini, "Radiopharmaceuticals in nuclear medicine: Recent developments for SPECT and PET studies," *Biomed Res Int*, vol. 2014, 2014, doi: 10.1155/2014/426892.

[3] M. Desrosiers *et al.*, "The Importance of Dosimetry Standardization in Radiobiology," *J Res Natl Inst Stand Technol*, vol. 118, pp. 403–418, Dec. 2013, doi: 10.6028/jres.118.021.

[4] H. M. Thierens, M. A. Monsieurs, and K. Bacher, "Patient dosimetry in radionuclide therapy: the whys and the wherefores," *Nucl Med Commun*, vol. 26, no. 7, pp. 593–599, 2005, doi: 10.1097/01.mnm.0000167910.76718.ad.

[5] A. Meghzifene, D. R. Dance, D. McLean, and H. M. Kramer, "Dosimetry in diagnostic radiology," *Eur J Radiol*, vol. 76, no. 1, pp. 11–14, Oct. 2010, doi: 10.1016/j.ejrad.2010.06.032.

[6] A. Rahmim and H. Zaidi, "PET versus SPECT: strengths, limitations and challenges," *Nucl Med Commun*, vol. 29, no. 3, pp. 193–207, 2008, doi: 10.1097/MNM.0b013e3282f3a515.

[7] M. N. Wernick and J. N. Aarsvold, *Emission tomography: the fundamentals of PET and SPECT*. Elsevier Academic Press, 2004. Accessed: Sep. 18, 2024. [Online]. Available: https://books.google.pt/books?id=x-F2lAEACAAJ

[8] S. St. James *et al.*, "Current Status of Radiopharmaceutical Therapy," *Int J Radiat Oncol Biol Phys*, vol. 109, no. 4, pp. 891–901, Mar. 2021, doi: 10.1016/j.ijrobp.2020.08.035.

[9] F. Constantin and F. Turcu, "Whole body PET based on an RPC system," *IEEE Nuclear Science Symposium Conference Record*, vol. 6, pp. 3826–3830, 2004, doi: 10.1109/nssmic.2004.1466714.

[10] C. Xu *et al.*, "Nanoparticle-based monitoring of cell therapy," *Nanotechnology*, vol. 22, no. 49, Dec. 2011, doi: 10.1088/0957-4484/22/49/494001.

[11] A. K. Buck *et al.*, "SPECT/CT," *Journal of Nuclear Medicine*, vol. 49, no. 8, pp. 1305–1319, Aug. 2008, doi: 10.2967/jnumed.107.050195.

[12] S. Alsharef, M. Alanazi, F. Alharthi, D. Qandil, and M. Qushawy, "Review about radiopharmaceuticals: Preparation, radioactivity, and applications," *International Journal of Applied Pharmaceutics*, vol. 12, no. 3, pp. 8–15, 2020, doi: 10.22159/ijap.2020v12i3.37150.

[13] K. Vermeulen, M. Vandamme, G. Bormans, and F. Cleeren, "Design and Challenges of Radiopharmaceuticals," *Semin Nucl Med*, vol. 49, no. 5, pp. 339–356, Sep. 2019, doi: 10.1053/j.semnuclmed.2019.07.001.

[14] F. B. Payolla, A. C. Massabni, and C. Orvig, "Radiopharmaceuticals for diagnosis in nuclear medicine: A short review," *Ecletica Quimica*, vol. 44, no. 3, pp. 11–19, 2019, doi: 10.26850/1678-4618eqj.

[15] R. J. Callahan, H. M. Chilton, J. A. Ponto, D. P. Swanson, H. D. Royal, and A. D. Bruce, "Procedure Guideline for the Use of Radiopharmaceuticals 4.0," *Journal of Nuclear Medicine Tecnology*, vol. 35, no. 4, pp. 272–275, Dec. 2007, doi: 10.2967/jnmt.107.044156.

[16] J. E. Turner, "Interaction fo Ionizing Radiation with Matter," *Health Phys*, vol. 86, no. 3, pp. 228–252, Mar. 2004, doi: 10.1097/00004032-200403000-00002.

[17] B. Nilsson and A. Brahme, "Interaction of Ionizing Radiation with Matter," in *Comprehensive Biomedical Physics*, vol. 9, Elsevier, 2014, pp. 1–36. doi: 10.1016/B978-0-444-53632-7.00920-5.

[18] L. Hayen, N. Severijns, K. Bodek, D. Rozpedzik, and X. Mougeot, "High precision analytical description of the allowed β spectrum shape," *Rev Mod Phys*, vol. 90, no. 1, p. 015008, Mar. 2018, doi: 10.1103/RevModPhys.90.015008.

[19] X. Mougeot, "Reliability of usual assumptions in the calculation of β and ν spectra," *Phys Rev C Nucl Phys*, vol. 91, no. 5, p. 055504, May 2015, doi: 10.1103/PhysRevC.91.055504.

[20] W. G. Cross, J. Böhm, M. Charles, E. Piesch, and S. M. Seltzer, "Dosimetry of External Beta Rays for Radiatio Protrection. ICRU Report 56," vol. 29, no. 1, pp. 8–11, Jan. 1997.

[21] E. García-Toraño, V. Peyres, M. M. Bé, C. Dulieu, M. C. Lépy, and F. Salvat, "Simulation of decay processes and radiation transport times in radioactivity measurements," *Nucl Instrum Methods Phys Res B*, vol. 396, pp. 43–49, Apr. 2017, doi: 10.1016/j.nimb.2017.02.002.

[22] J. M. Fernández-Varea, "Pedagogical material: Interacción de las radiaciones ionizantes con la materia," Universitat de Barcelona.

[23] J. F. Eary and Winfried. Brenner, *Nuclear medicine therapy*. CRC Press, 2007, doi: 10.3109/9781420016642.

[24] R. Gonzàlez Vegas, "Master's Thesis in Medical Physics: Calculation of single-cell S-values for monoenergetic electrons and radionuclides," Universitat de València, 2022.

[25] E. Pirayesh *et al.*, "Technical Considerations of Phosphorous-32 Bremsstrahlung SPECT Imaging after Radioembolization of Hepatic Tumors: A Clinical Assessment with a Review of Imaging Parameters," *Radiol Res Pract*, vol. 2014, pp. 1–7, 2014, doi: 10.1155/2014/407158.

[26] S. M. Qaim, "Nuclear data for production and medical application of radionuclides: Present status and future needs," *Nucl Med Biol*, vol. 44, pp. 31–49, Jan. 2017, doi: 10.1016/j.nucmedbio.2016.08.016.

[27] P. Hogg, V. Veloso, and C. Pestean, "Radionuclide Metabolic Therapy," 2013. [Online]. Available: https://www.researchgate.net/publication/259465482

[28] B. Meng, J. Song, L. Liu, L. Chen, and X. Chen, "Added value of hybrid SPECT with CT imaging for predicting poor therapeutic efficacy of 89Sr in patients with bone metastasis," *Sci Rep*, vol. 10, no. 1, p. 21207, Dec. 2020, doi: 10.1038/s41598-020-78372-5.

[29] A. S. Pasciak, A. C. Bourgeois, and Y. C. Bradley, "A comparison of techniques for 90Y PET/CT image-based dosimetry following radioembolization with resin microspheres," *Front Oncol*, vol. 4, no. 121, Mar. 2014, doi: 10.3389/fonc.2014.00121.

[30] T. Carlier, K. P. Willowson, E. Fourkal, D. L. Bailey, M. Doss, and M. Conti, "90Y-PET imaging: Exploring limitations and accuracy under conditions of low counts and high random fraction," *Med Phys*, vol. 42, no. 7, pp. 4295–4309, Jul. 2015, doi: 10.1118/1.4922685.

[31] S. L. Pimlott, "Radioisotopes for medical imaging," *International Journal of Modern Physics A*, vol. 29, no. 14, p. 1441003, Jun. 2014, doi: 10.1142/S0217751X14410036.

[32] Y. K. Dewaraja *et al.*, "Accurate Dosimetry in I-131 Radionuclide Therapy Using Patient-Specific, 3-Dimensional Methods for SPECT Reconstruction and Absorbed Dose Calculation," *Journal of Nuclear Medicine*, vol. 46, no. 5, pp. 840–849, 2005.

[33] M. Fallahpoor, M. Abbasi, A. Sen, and F. Kalantari, "SU-C-201-06: Utility of Quantitative 3D SPECT/CT Imaging in Patient Specific Internal Dosimetry of 153- Samarium with GATE Monte Carlo Package," *Med Phys*, vol. 42, pp. 3203–3203, 2015, doi: 10.1118/1.4923844.

[34] J. Tran-Gia *et al.*, "A multicentre and multi-national evaluation of the accuracy of quantitative Lu-177 SPECT/CT imaging performed within the MRTDosimetry project," *EJNMMI Phys*, vol. 8, no. 55, Dec. 2021, doi: 10.1186/s40658-021-00397-0.

[35] P. Jackson, M. Hofman, L. McIntosh, J. P. Buteau, and A. Ravi Kumar, "Radiation Dosimetry in 177Lu-PSMA-617 Therapy," Mar. 01, 2022, *Elsevier*. doi: 10.1053/j.semnuclmed.2021.11.003.

[36] K. Sjögreen Gleisner *et al.*, "EANM dosimetry committee recommendations for dosimetry of 177Lu-labelled somatostatin-receptor- and PSMA-targeting ligands," *Eur J Nucl Med Mol Imaging*, vol. 49, no. 6, pp. 1778–1809, May 2022, doi: 10.1007/s00259-022-05727-7.

[37] M. F. bin Othman, N. R. Mitry, V. J. Lewington, P. J. Blower, and S. Y. A. Terry, "Re-assessing gallium-67 as a therapeutic radionuclide," *Nucl Med Biol*, vol. 46, pp. 12–18, Oct. 2016, doi: 10.1016/j.nucmedbio.2016.10.008.

[38] D. J. O. Dittrich RP, "Gallium Scan," Treasure Island (FL): StatPearls Publishing. Accessed: Aug. 05, 2024. [Online]. Available: https://www.ncbi.nlm.nih.gov/books/NBK567748/

[39] E. K. J. Pauwels, V. R. Mccready, J. H. M. B. Stoot, and D. F. P. Van Deurzen, "The mechanism of accumulation of tumour-localising radiopharmaceuticals," *Journal of Nuclear Medicine*, vol. 25, no. 3, pp. 277–305, Mar. 1998, doi: 10.1007/s002590050229.

[40] N. Lanconelli *et al.*, "A free database of radionuclide voxel S values for the dosimetry of nonuniform activity distributions," *Phys Med Biol*, vol. 57, no. 2, pp. 517–533, Jan. 2012, doi: 10.1088/0031-9155/57/2/517.

[41] S. M. Goddu, R. W. Howell, and D. V. Rao, "Cellular Dosimetry: Absorbed Fractions for Monoenergetic Electron and Alpha Particle Sources and S-values for Radionuclides Uniformly Distributed in Different Cell Compartments," *Journal of Nuclear Medicine*, vol. 35, no. 2, pp. 303–316, 1993.

[42] M. S. Lee *et al.*, "Whole-body voxel-based personalized dosimetry: The multiple voxel s-value approach for heterogeneous media with nonuniform activity distributions," *Journal of Nuclear Medicine*, vol. 59, no. 7, pp. 1133–1139, Jul. 2018, doi: 10.2967/jnumed.117.201095.

[43] M. Stabin, "Nuclear medicine dosimetry," *Phys Med Biol*, vol. 51, no. 13, pp. R187–R202, Jul. 2006, doi: 10.1088/0031-9155/51/13/R12.

[44] M. G. Stabin and J. A. Siegel, "RADAR dose estimate report: A compendium of radiopharmaceutical dose estimates based on OLINDA/EXM version 2.0," *Journal of Nuclear Medicine*, vol. 59, no. 1, pp. 154–160, Jan. 2018, doi: 10.2967/jnumed.117.196261.

[45] G. Sgouros, "Dosimetry of Internal Emitters," *Journal of Nuclear Medicine*, vol. 46, no. 1, pp. 18S-27S, Jan. 2005.

[46] M. Bardiès and J. I. Gear, "Scientific Developments in Imaging and Dosimetry for Molecular Radiotherapy," *Clin Oncol*, vol. 33, no. 2, pp. 117–124, Feb. 2021, doi: 10.1016/j.clon.2020.11.005.

[47] J. O'Donoghue, P. Zanzonico, J. Humm, and A. Kesner, "Dosimetry in Radiopharmaceutical Therapy," *Journal of Nuclear Medicine*, vol. 63, no. 10, pp. 1467–1474, Oct. 2022, doi: 10.2967/jnumed.121.262305.

[48] D. Pistone, L. Auditore, A. Italiano, S. Baldari, and E. Amato, "An analytic model to calculate Voxel S-Values for 177-Lu," *Biomed Phys Eng Express*, vol. 8, no. 6, Nov. 2022, doi: 10.1088/2057-1976/ac997e.

[49] G. Pirovano, T. C. Wilson, and T. Reiner, "Auger: The future of precision medicine," May 01, 2021, *Elsevier Inc.* doi: 10.1016/j.nucmedbio.2021.03.002.

[50] W. E. Bolch *et al.*, "MIRD Pamphlet No.17: The Dosimetry of Nonuniform Activity Distributions - "Radionuclide S Values at the Voxel Level," *Journal of Nuclear Medicine*, vol. 40, no. 1, pp. 11S-36S, Jan. 1999.

[51] M. Cristy and K. F. Eckerman, "Specific Absorbed Fractions of Energy at Various Ages from Internal Photon Sources: 1, Methods," *Oak Ridge National Laboratory*, Apr. 2002, doi: 10.2172/6233735.

[52] K. F. Eckerman, R. J. Westfall, J. C. Ryman, and M. Cristy, "Nuclear Decay Data Files of the Dosimetry Research Group," *Oak Ridge National Laboratory*, 1993, doi: 10.2172/10116928.

[53] M. G. Stabin and L. C. Q. P. Da Luz, "Decay Data for Internal and External Dose Assessment," *Health Phys*, vol. 83, no. 4, pp. 471–475, Oct. 2002, doi: 10.1097/00004032-200210000-00004.

[54] ICRU, "Physical Aspects of Irradiation: Recommendations of the International Commission on Radiological Units and Measurements Report 10b," May 1964.

[55] M. G. Stabin, R. B. Sparks, and E. Crowe, "OLINDA/EXM: The Second-Generation Personal Computer Software for Internal Dose Assessment in Nuclear Medicine," *Journal of Nuclear Medicine*, vol. 46, no. 6, pp. 1023–1027, 2005.

[56] W. P. Segars, B. M. W. Tsui, D. Lalush, E. Frey, D. Manocha, and M. King, "Development and Application of the New Dynamic Nurbs-based Cardiac-torso (NCAT) Phantom," *Journal of Nuclear Medicine*, vol. 42, no. 5, p. 23, May 2001.

[57] R. Alexaklrin Obninsk *et al.*, "Basic Anatomical and Physiological Data for Use in Radiological Protection: Reference Values," *ICRP Publication 89*, vol. 32, 2003.

[58] M. Andersson, L. Johansson, K. Eckerman, and S. Mattsson, "IDAC-Dose 2.1, an internal dosimetry program for diagnostic nuclear medicine based on the ICRP adult reference voxel phantoms," *EJNMMI Res*, vol. 7, no. 88, Nov. 2017, doi: 10.1186/s13550-017-0339-3.

[59] W. E. Bolch, C. H. Clement, H. Ogino, and International Commission on Radiological Protection, "The ICRP Computational framework for internal dose assessment for reference adults: specific absorbed fractions," *ICRP Publication 133*, vol. 45, no. 2, pp. 1–74, 2016.

[60] ICRP, "Nuclear Decay Data for Dosimetric Calculations," *ICRP Publication 107*, vol. 38, no. 3, 2007.

[61] M. Chauvin *et al.*, "OpenDose: Open-access resource for nuclear medicine dosimetry," *Journal of Nuclear Medicine*, vol. 61, no. 10, pp. 1514–1519, Oct. 2020, doi: 10.2967/jnumed.119.240366.

[62] ICRP and ICRU, "Adult reference computational phantoms," *ICRP Publication 110*, vol. 39, no. 2, p. 165, 2009.

[63] D. Villoing, T. A. Cuthbert, C. M. Kitahara, and C. Lee, "NCINM: Organ Dose Calculator for Patients Undergoing Nuclear Medicine Procedures," *Biomed. Phys. Eng. Express*, vol. 6, no. 5, p. 055010, Jul. 2020, doi: 10.1088/2057-1976/aba41e.

[64] E. Seeram, *Computed Tomography: Physical Principles, Clinical Applications, and Quality Control*, 4th ed. Elsevier Health Sciences, 2015.

[65] J. L. Humm, R. W. Howell, and D. V. Rao, "Dosimetry of Auger-electron-emitting radionuclides: Report No.3 of AAPM Nuclear Medicine Task Group No.6a)," *Med Phys*, vol. 21, no. 12, pp. 1901–1915, Dec. 1994, doi: 10.1118/1.597227.

[66] J. Stepanek, B. Larsson, and R. Weinreich, "Auger-electron spectra of radionuclides for theraphy and diagnostics," *Acta Oncol (Madr)*, vol. 35, no. 7, pp. 863–868, 1996, doi: 10.3109/02841869609104038.

[67] M. Bardiès and M. J. Myers, "Computational methods in radionuclide dosimetry," *Phys Med Biol*, vol. 41, no. 10, pp. 1941–1955, Oct. 1996, doi: 10.1088/0031-9155/41/10/007.

[68] J. Bolcaen *et al.*, "Marshalling the Potential of Auger Electron Radiopharmaceutical Therapy," *Journal of Nuclear Medicine*, vol. 64, no. 9, pp. 1344–1351, 2023, doi: 10.2967/jnumed.122.265039.

[69] S. Goddu, R. Howell, L. Bouchet, W. Bolch, and D. Rao, "MIRD Cellular S Values: Self-absorbed Dose Per Unit Cumulated Activity for Selected Radionuclides and Monoenergetic Electron and Alpha Particle Emitters Incorporated into Different Cell Compartments," *Society of Nuclear Medicine and Molecular Imaging*, 1997.

[70] S. Hubert, "Master's Thesis: Tools for the Monte Carlo calculation of cellular S-values," KTH School of Technology and Health, Stockholm, 2009.

[71] D. A. Weber, K. F. Eckerman, L. T. Dillman, and J. C. Ryman, *MIRD radionuclide data and decay schemes*. Society of Nuclear Medicine, 1989. Accessed: Sep. 18, 2024. [Online]. Available: https://books.google.pt/books?id=vIstAAAACAAJ

[72] R. W. Howell, "Radiation Spectra for Auger-electron emitting radionuclides: Report No.2 of AAPM Nuclear Medicine Task Group No.6," *Med Phys*, vol. 19, no. 6, pp. 1371–1383, Nov. 1992, doi: 10.1118/1.596927.

[73] H. Uusijärvi, N. Chouin, M. Bardiès, and J. M. Fernández-Varea, "Cellular S-values generated with the Monte Carlo codes PENELOPE, MCNPX and GEANT4", 27th ESTRO Conference (ESTRO 27), Göteborg (Sweden), 14-18 September 2008.

[74] H. Uusijärvi, N. Chouin, P. Bernhardt, L. Ferrer, M. Bardiès, and E. Forssell-Aronsson, "Comparison of Electron Dose-Point Kernels in Water Generated by the Monte Carlo Codes, PENELOPE, GEANT4, MCNPX, and ETRAN," *Cancer Biother Radiopharm*, vol. 24, no. 4, pp. 461–467, 2009, doi: 10.1089/cbr.2008.0573.

[75] N. Falzone, J. M. Fernández-Varea, G. Flux, and K. A. Vallis, "Monte Carlo evaluation of Auger electron-emitting theranostic radionuclides," *Journal of Nuclear Medicine*, vol. 56, no. 9, pp. 1441–1446, Sep. 2015, doi: 10.2967/jnumed.114.153502.

[76] F. Salvat, "PENELOPE-2018 A Code System for Monte Carlo Simulation of Electron and Photon Transport", *Workshop Proceedings*, 2019. doi: doi.org/10.1787/32da5043-en.

[77] F. Salvat, J. M. Fernández-Varea, and R. Mayol, "Monte Carlo Simulation of Electron Transport," in *Electron Microscopy in Materials Science*, 1991, pp. 603–619. doi: 10.1016/B978-0-12-780584-9.X5001-6.

[78] D. J. Earl and M. W. Deem, "Monte Carlo Simulations," in *Methods in Molecular Biology*, vol. 443, A. Kukol, Ed., Humana Press, 2008, ch. 2, pp. 25–35. doi: 10.1007/978-1-59745-177-2_2.

[79] J. M. Fernández-Varea, "Monte Carlo Simulation of Photon and Electron Transport in Matter", *Handbook of Nuclear Medicine and Molecular Imaging for Physicists: Modelling, Dosimetry and Radiation Protection, Volume II*, vol. 2, CRC Press, 2022, ch. 8, pp. 123–140. doi: 10.1201/9780429489549-8.

[80] R. L. Harrison, "Introduction to Monte Carlo simulation," *AIP Conf Proc*, vol. 1204, pp. 17–21, Jan. 2010, doi: 10.1063/1.3295638.

[81] J. H. Hubbell, H. A. Gimm, and I. O/verbo, "Pair, Triplet, and Total Atomic Cross Sections (and Mass Attenuation Coefficients) for 1 MeV-100 GeV Photons in Elements Z=1 to 100," *J Phys Chem Ref Data*, vol. 9, no. 4, pp. 1023–1148, 1980, doi: 10.1063/1.555629.

[82] J. Sempau, "PENELOPE/penEasy User Manual," 2019.

[83] J. Sempau, "Pedagogical material: PENELOPE MC code", Universitat Politècnica de Catalunya, 2024.

[84] E. García-Toraño, V. Peyres, and F. Salvat, "PenNuc: Monte Carlo simulation of the decay of radionuclides", *Comput Phys Commun*, vol. 245, p. 106849, Aug. 2019, doi: 10.17632/dy28h8xmkv.1.

[85] M.-M. Bé *et al.*, "Table of Radionuclides," Bureau International des Poids et Mesures, Sèvres. Accessed: Feb. 06, 2024. [Online]. Available: http://www.nucleide.org/

[86] K. F. Eckerman and A. Endo, "User Guide to MIRD CD and RADTABS software.", Annals of the ICRP. 38. 10.1016/j.icrp.2008.10.001.

[87] ICRU, "Tissue substitutes in radiation dosimetry and measurement," *ICRU Report 44*, May 1989.

[88] M. E. Seren Takahashi, J. M. Fernández-Varea, A. O. Santos, S. Q. Brunetto and C. D. Ramos, "Influência da Geometria da Fonte na Dosimetria por Voxel em Radiosinovectoma", XXXI Congresso Brasileiro de Medicina Nuclear, Costão do Santinho (Brasil), 2-4 November 2017.

[89] Y. K. Dewaraja *et al.*, "A Pipeline for Automated Voxel Dosimetry: Application in Patients with Multi-SPECT/CT Imaging After 177Lu-Peptide Receptor Radionuclide Therapy," *J Nucl Med*, vol. 63, no. 11, pp. 1665–1672, Nov. 2022, doi: 10.2967/jnumed.121.263738.

Appendix A

A.1 Phosphorus-32

Figure A.1: Decay scheme of ^{32}P (from [85]).

A.2 Strontium-89

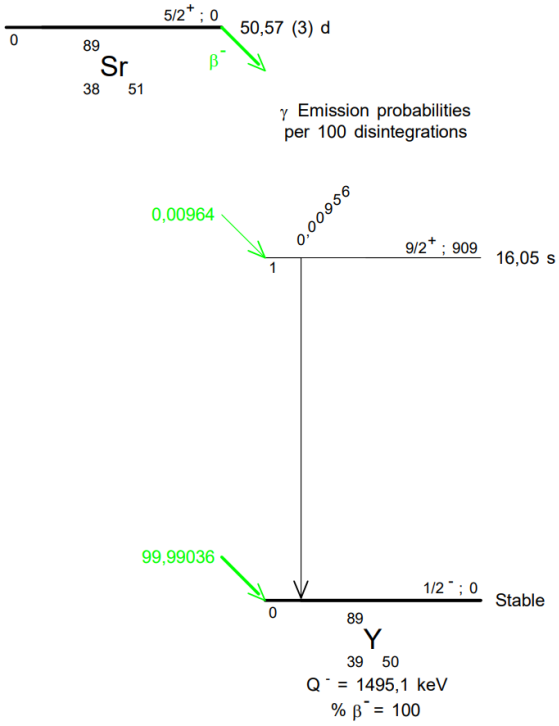

Figure A.2: Decay scheme of ^{89}Sr (from [85]).

A.3 Yttrium-90

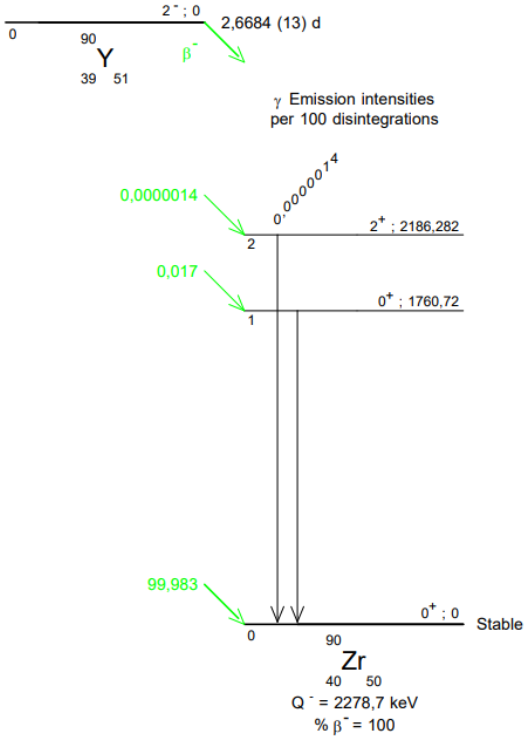

Figure A.3: Decay scheme of ^{90}Y (from [85]).

A.4 Iodine-131

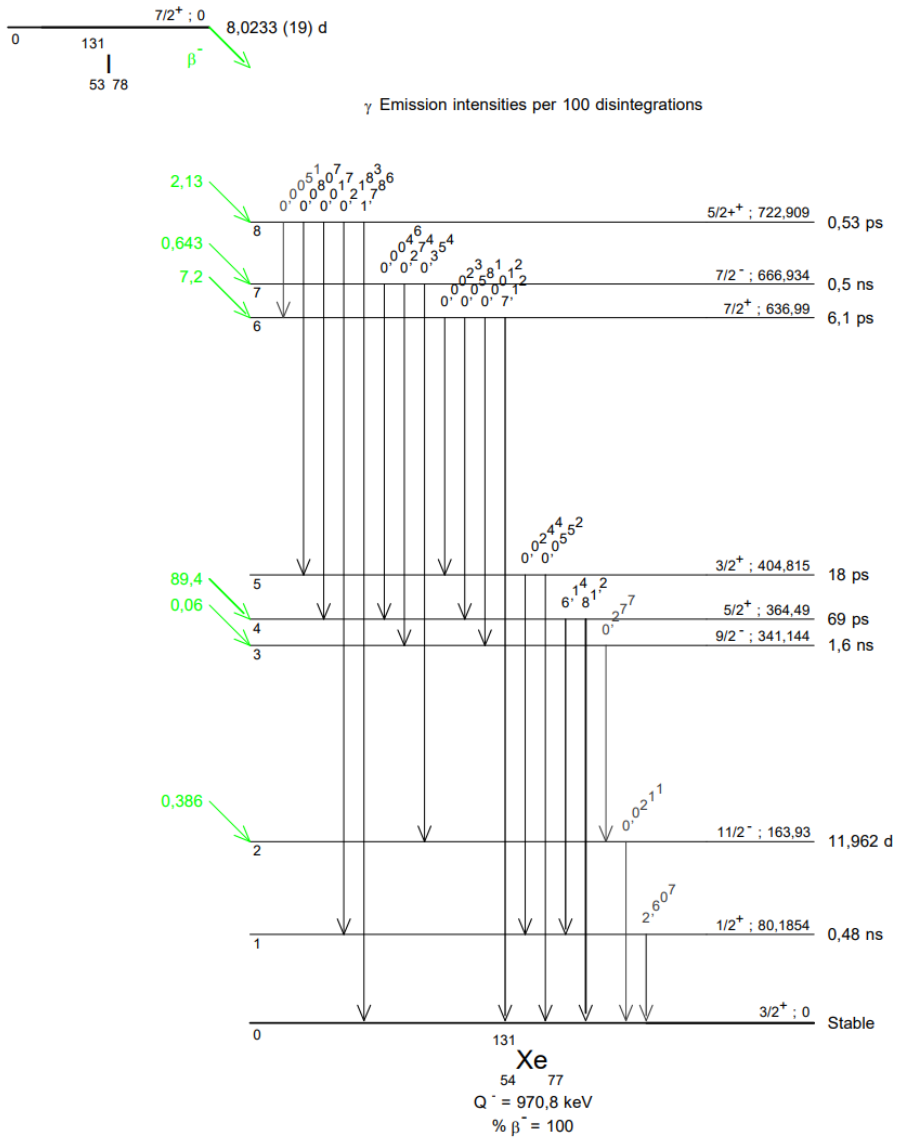

Figure A.4: Decay scheme of ^{131}I (from [85]).

A.5 Samarium-153

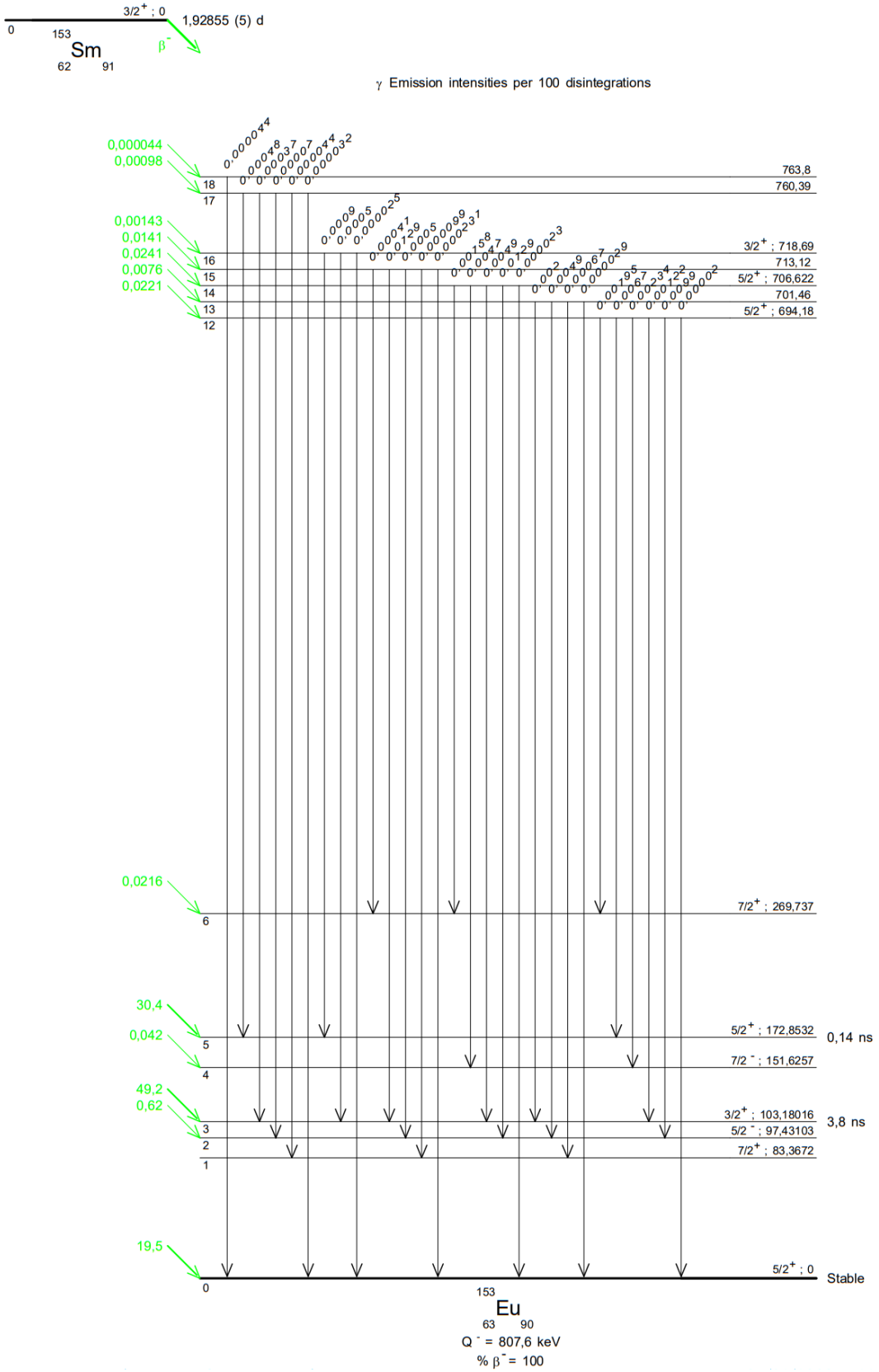

Figure A.5: Decay scheme of ^{153}Sm (from [85]).

A.6 Lutetium-177

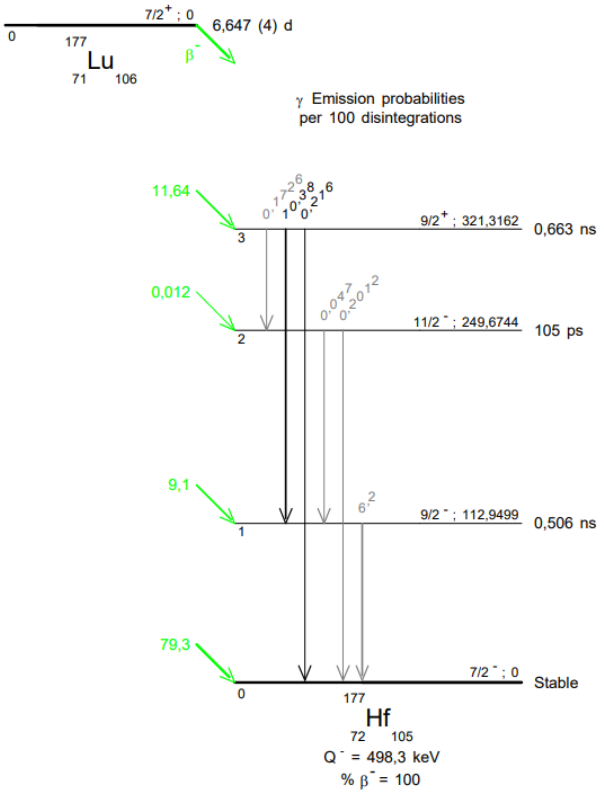

Figure A.6: Decay scheme of ^{177}Lu (from [85]).

A.7 Technetium-99m

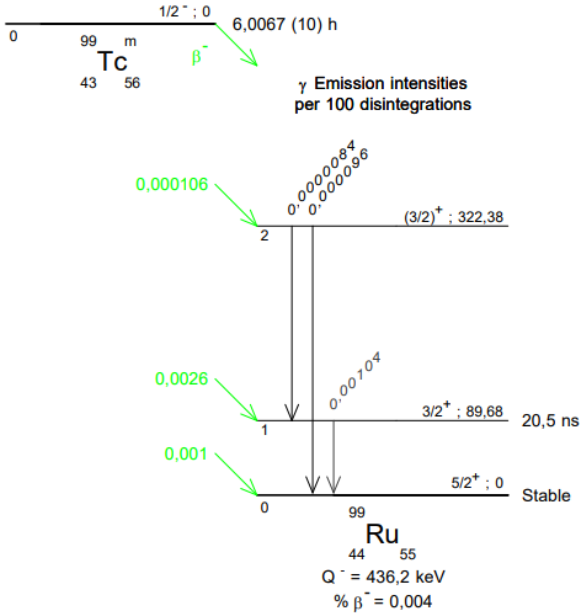

Figure A.7: Decay scheme of ^{99m}Tc (from [85]).

A.8 Gallium-67

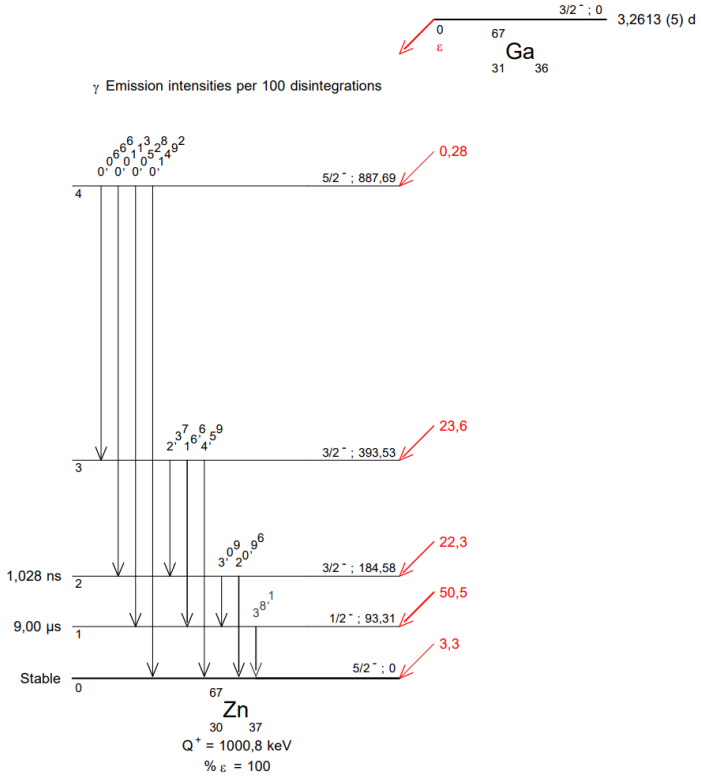

Figure A.8: Decay scheme of ^{67}Ga (from [85]).

A.9 Indium-111

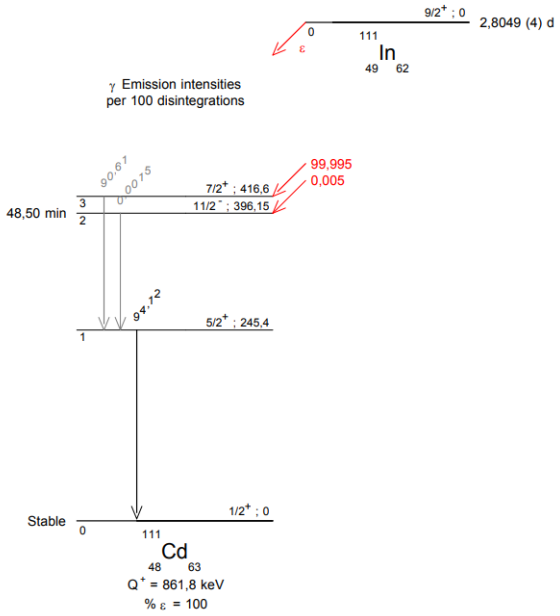

Figure A.9: Decay scheme of ^{111}In (from [85]).

A.10 Iodine-123

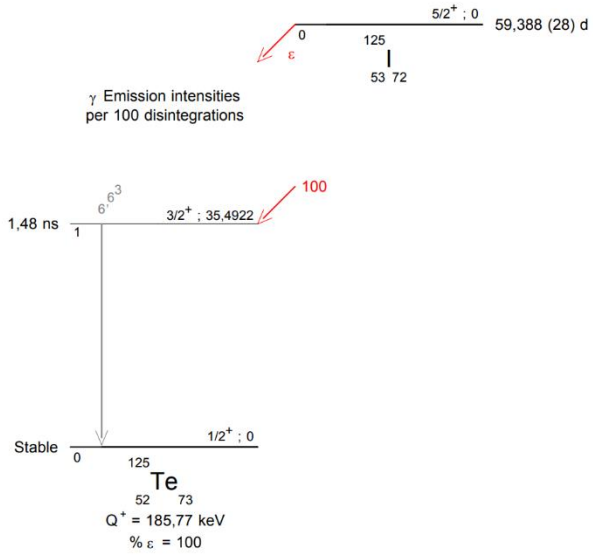

Figure A.10: Decay scheme of ^{123}I (from [85]).

A.11 Tallium-201

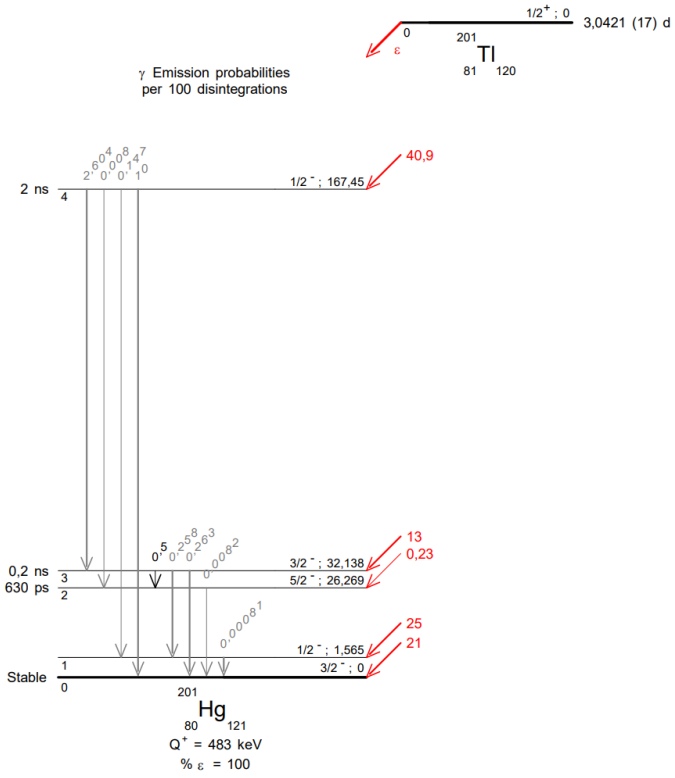

Figure A.11: Decay scheme of ^{201}Tl (from [85]).

Appendix B

Table B.1: S-values (mGy·MBq^{-1}·s^{-1}) for ^{99m}Tc within cubical voxels of 3 mm and respective uncertainties.

Distance (mm)	Coordinates	MIRD	PenNuc	PenNuc Uncertainty	PenNuc / MIRD	DECDATA	DECDATA Uncertainty	DECDATA / MIRD
0.0	[0, 0, 0]	9.02E-02	9.80E-02	0.01E-02	1.09	9.57E-02	0.02E-02	1.06
3.0	[0, 0, 1]	1.53E-03	1.41E-03	0.00E-03	0.92	1.38E-03	0.01E-03	0.90
4.2	[0, 1, 1]	3.49E-04	3.43E-04	0.01E-04	0.98	3.44E-04	0.02E-04	0.98
5.2	[1, 1, 1]	2.20E-04	2.15E-04	0.01E-04	0.98	2.15E-04	0.02E-04	0.98
6.0	[0, 0, 2]	1.63E-04	1.55E-04	0.01E-04	0.95	1.55E-04	0.02E-04	0.95
6.7	[0, 1, 2]	1.26E-04	1.23E-04	0.00E-04	0.98	1.23E-04	0.01E-04	0.98
7.3	[1, 1, 2]	1.03E-04	1.02E-04	0.00E-04	0.99	1.02E-04	0.01E-04	0.99
8.5	[0, 2, 2]	7.57E-05	7.58E-05	0.03E-05	1.00	7.58E-05	0.08E-05	1.00
9.0	[1, 2, 2]; [0, 0, 3]	6.41E-05	6.72E-05	0.02E-05	1.05	6.71E-05	0.05E-05	1.05
9.5	[0, 1, 3]	6.09E-05	6.02E-05	0.02E-05	0.99	6.04E-05	0.05E-05	0.99
9.9	[1, 1, 3]	5.27E-05	5.45E-05	0.02E-05	1.03	5.44E-05	0.05E-05	1.03
10.4	[2, 2, 2]	5.19E-05	4.99E-05	0.03E-05	0.96	5.00E-05	0.08E-05	0.96
10.8	[0, 2, 3]	4.57E-05	4.59E-05	0.02E-05	1.01	4.62E-05	0.05E-05	1.01
11.2	[1, 2, 3]	4.26E-05	4.28E-05	0.01E-05	1.00	4.28E-05	0.03E-05	1.00
12.0	[0, 0, 4]	4.43E-05	3.74E-05	0.03E-05	0.84	3.76E-05	0.08E-05	0.85
12.4	[2, 2, 3]; [0, 1, 4]	3.71E-05	3.50E-05	0.01E-05	0.94	3.53E-05	0.03E-05	0.95
12.7	[1, 1, 4]; [0, 3, 3]	3.44E-05	3.31E-05	0.01E-05	0.96	3.32E-05	0.03E-05	0.97
13.1	[1, 3, 3]	3.12E-05	3.14E-05	0.01E-05	1.01	3.11E-05	0.04E-05	1.00
13.4	[0, 2, 4]	2.94E-05	2.97E-05	0.01E-05	1.01	2.98E-05	0.04E-05	1.01
13.7	[1, 2, 4]	2.89E-05	2.83E-05	0.01E-05	0.98	2.81E-05	0.03E-05	0.97
14.1	[2, 3, 3]	2.80E-05	2.70E-05	0.01E-05	0.97	2.73E-05	0.04E-05	0.97
14.7	[2, 2, 4]	2.52E-05	2.48E-05	0.01E-05	0.98	2.47E-05	0.03E-05	0.98
15.0	[0, 3, 4]; [0, 0, 5]	2.55E-05	2.37E-05	0.01E-05	0.93	2.38E-05	0.03E-05	0.93
15.3	[0, 1, 5]; [1, 3, 4]	2.33E-05	2.29E-05	0.01E-05	0.98	2.28E-05	0.02E-05	0.98
15.6	[1, 1, 5]; [3, 3, 3]	2.24E-05	2.20E-05	0.01E-05	0.98	2.19E-05	0.03E-05	0.98
16.2	[2, 3, 4]; [0, 2, 5]	2.09E-05	2.04E-05	0.01E-05	0.98	2.07E-05	0.02E-05	0.99
16.4	[1, 2, 5]	1.95E-05	1.99E-05	0.01E-05	1.02	1.98E-05	0.02E-05	1.01
17.0	[0, 4, 4]	1.81E-05	1.86E-05	0.02E-05	1.03	1.85E-05	0.04E-05	1.02
17.2	[1, 4, 4]; [2, 2, 5]	1.90E-05	1.80E-05	0.01E-05	0.95	1.81E-05	0.02E-05	0.95
17.5	[0, 3, 5]; [3, 3, 4]	1.72E-05	1.75E-05	0.01E-05	1.02	1.75E-05	0.02E-05	1.02
17.7	[1, 3, 5]	1.75E-05	1.70E-05	0.01E-05	0.97	1.71E-05	0.02E-05	0.98
18.0	[2, 4, 4]	1.77E-05	1.65E-05	0.01E-05	0.93	1.66E-05	0.03E-05	0.94
18.5	[2, 3, 5]	1.68E-05	1.56E-05	0.01E-05	0.93	1.57E-05	0.02E-05	0.94
19.2	[3, 4, 4]; [0, 4, 5]	1.53E-05	1.46E-05	0.01E-05	0.95	1.45E-05	0.02E-05	0.95
19.4	[1, 4, 5]	1.46E-05	1.41E-05	0.01E-05	0.97	1.42E-05	0.02E-05	0.97
19.7	[3, 3, 5]	1.54E-05	1.39E-05	0.01E-05	0.90	1.40E-05	0.02E-05	0.91
20.1	[2, 4, 5]	1.43E-05	1.33E-05	0.01E-05	0.93	1.33E-05	0.02E-05	0.93
20.8	[4, 4, 4]	1.25E-05	1.23E-05	0.02E-05	0.99	1.23E-05	0.04E-05	0.99
21.2	[0, 5, 5]; [3, 4, 5]	1.25E-05	1.19E-05	0.01E-05	0.95	1.19E-05	0.01E-05	0.95
21.4	[1, 5, 5]	1.21E-05	1.17E-05	0.01E-05	0.97	1.17E-05	0.02E-05	0.97
22.0	[2, 5, 5]	1.13E-05	1.10E-05	0.01E-05	0.97	1.12E-05	0.02E-05	0.99
22.6	[4, 4, 5]	1.20E-05	1.05E-05	0.01E-05	0.88	1.05E-05	0.02E-05	0.87
23.0	[3, 5, 5]	1.07E-05	1.01E-05	0.01E-05	0.95	1.02E-05	0.02E-05	0.95
24.4	[4, 5, 5]	9.98E-06	9.11E-06	0.08E-06	0.91	9.22E-06	0.20E-06	0.92
26.0	[5, 5, 5]	9.12E-06	8.02E-06	0.13E-06	0.88	8.08E-06	0.33E-06	0.89

Table B.2: S-values (mGy·MBq^{-1}·s^{-1}) for ^{99m}Tc within cubical voxels of 6 mm and respective uncertainties.

Distance (mm)	Coordinates	MIRD	PenNuc	PenNuc Uncertainty	PenNuc / MIRD	DECDATA	DECDATA Uncertainty	DECDATA / MIRD
0.0	[0, 0, 0]	1.20E-02	1.29E-02	0.00E-02	1.08	1.26E-02	0.00E-02	1.05
6.0	[0, 0, 1]	2.31E-04	2.23E-04	0.00E-04	0.96	2.21E-04	0.01E-04	0.95
8.5	[0, 1, 1]	8.32E-05	8.38E-05	0.01E-05	1.01	8.39E-05	0.03E-05	1.01
10.4	[1, 1, 1]	5.42E-05	5.33E-05	0.01E-05	0.98	5.33E-05	0.03E-05	0.98
12.0	[0, 0, 2]	4.00E-05	3.84E-05	0.01E-05	0.96	3.85E-05	0.03E-05	0.96
13.4	[0, 1, 2]	3.11E-05	3.05E-05	0.01E-05	0.98	3.07E-05	0.01E-05	0.99
14.7	[1, 1, 2]	2.53E-05	2.53E-05	0.00E-05	1.00	2.54E-05	0.01E-05	1.00
17.0	[0, 2, 2]	1.99E-05	1.89E-05	0.01E-05	0.95	1.87E-05	0.01E-05	0.94
18.0	[1, 2, 2]; [0, 0, 3]	1.75E-05	1.67E-05	0.00E-05	0.95	1.69E-05	0.01E-05	0.96
19.0	[0, 1, 3]	1.54E-05	1.51E-05	0.00E-05	0.98	1.51E-05	0.01E-05	0.98
19.9	[1, 1, 3]	1.37E-05	1.37E-05	0.00E-05	1.00	1.37E-05	0.01E-05	1.00
20.8	[2, 2, 2]	1.26E-05	1.26E-05	0.01E-05	1.00	1.26E-05	0.01E-05	1.00
21.6	[0, 2, 3]	1.21E-05	1.16E-05	0.00E-05	0.96	1.17E-05	0.01E-05	0.96
22.4	[1, 2, 3]	1.06E-05	1.08E-05	0.00E-05	1.02	1.08E-05	0.01E-05	1.02
24.0	[0, 0, 4]	1.02E-05	9.44E-06	0.06E-06	0.93	9.35E-06	0.15E-06	0.92
24.7	[2, 2, 3]; [0, 1, 4]	9.02E-06	8.90E-06	0.02E-06	0.99	8.92E-06	0.05E-06	0.99
25.5	[1, 1, 4]; [0, 3, 3]	8.65E-06	8.41E-06	0.02E-06	0.97	8.48E-06	0.06E-06	0.98
26.2	[1, 3, 3]	8.05E-06	7.98E-06	0.03E-06	0.99	7.98E-06	0.07E-06	0.99
26.8	[0, 2, 4]	7.93E-06	7.58E-06	0.03E-06	0.96	7.62E-06	0.07E-06	0.96
27.5	[1, 2, 4]	7.04E-06	7.24E-06	0.02E-06	1.03	7.29E-06	0.05E-06	1.04
28.1	[2, 3, 3]	7.14E-06	6.93E-06	0.02E-06	0.97	6.97E-06	0.06E-06	0.98
29.4	[2, 2, 4]	6.55E-06	6.35E-06	0.02E-06	0.97	6.38E-06	0.06E-06	0.97
30.0	[0, 3, 4]; [0, 0, 5]	6.19E-06	6.12E-06	0.02E-06	0.99	6.12E-06	0.05E-06	0.99
30.6	[0, 1, 5]; [1, 3, 4]	6.13E-06	5.89E-06	0.01E-06	0.96	5.88E-06	0.03E-06	0.96
31.2	[1, 1, 5]; [3, 3, 3]	6.21E-06	5.68E-06	0.02E-06	0.92	5.70E-06	0.05E-06	0.92
32.3	[2, 3, 4]; [0, 2, 5]	5.60E-06	5.30E-06	0.01E-06	0.95	5.33E-06	0.03E-06	0.95
32.9	[1, 2, 5]	5.20E-06	5.15E-06	0.01E-06	0.99	5.16E-06	0.04E-06	0.99
33.9	[0, 4, 4]	4.78E-06	4.82E-06	0.03E-06	1.01	4.92E-06	0.07E-06	1.03
34.5	[1, 4, 4]; [2, 2, 5]	4.86E-06	4.69E-06	0.01E-06	0.97	4.72E-06	0.04E-06	0.97
35.0	[0, 3, 5]; [3, 3, 4]	4.72E-06	4.56E-06	0.01E-06	0.97	4.59E-06	0.04E-06	0.97
35.5	[1, 3, 5]	4.50E-06	4.43E-06	0.01E-06	0.98	4.46E-06	0.04E-06	0.99
36.0	[2, 4, 4]	4.55E-06	4.31E-06	0.02E-06	0.95	4.33E-06	0.05E-06	0.95
37.0	[2, 3, 5]	4.44E-06	4.10E-06	0.01E-06	0.92	4.11E-06	0.03E-06	0.93
38.4	[3, 4, 4]; [0, 4, 5]	3.91E-06	3.80E-06	0.01E-06	0.97	3.86E-06	0.03E-06	0.99
38.9	[1, 4, 5]	3.70E-06	3.72E-06	0.01E-06	1.00	3.73E-06	0.03E-06	1.01
39.3	[3, 3, 5]	3.93E-06	3.64E-06	0.02E-06	0.93	3.66E-06	0.04E-06	0.93
40.2	[2, 4, 5]	3.65E-06	3.49E-06	0.01E-06	0.96	3.53E-06	0.03E-06	0.97
41.6	[4, 4, 4]	3.40E-06	3.27E-06	0.03E-06	0.96	3.27E-06	0.07E-06	0.96
42.4	[0, 5, 5]; [3, 4, 5]	3.35E-06	3.16E-06	0.01E-06	0.95	3.18E-06	0.03E-06	0.95
42.8	[1, 5, 5]	3.43E-06	3.11E-06	0.02E-06	0.91	3.14E-06	0.04E-06	0.92
44.1	[2, 5, 5]	3.07E-06	2.94E-06	0.02E-06	0.96	2.97E-06	0.04E-06	0.97
45.3	[4, 4, 5]	2.86E-06	2.79E-06	0.02E-06	0.98	2.80E-06	0.04E-06	0.98
46.1	[3, 5, 5]	2.75E-06	2.70E-06	0.02E-06	0.98	2.70E-06	0.04E-06	0.98
48.7	[4, 5, 5]	2.36E-06	2.43E-06	0.01E-06	1.03	2.45E-06	0.04E-06	1.04
52.0	[5, 5, 5]	2.33E-06	2.15E-06	0.02E-06	0.92	2.24E-06	0.06E-06	0.96

Table B.3: S-values (mGy·MBq^{-1}·s^{-1}) for ^{131}I within cubical voxels of 3 mm and respective uncertainties.

Distance (mm)	Coordinates	MIRD	PenNuc	PenNuc Uncertainty	PenNuc / MIRD	DECDATA	DECDATA Uncertainty	DECDATA / MIRD
0.0	[0, 0, 0]	9.20E-01	9.41E-01	0.00E-01	1.02	9.48E-01	0.00E-01	1.03
3.0	[0, 0, 1]	3.54E-02	3.20E-02	0.00E-02	0.90	3.27E-02	0.00E-02	0.92
4.2	[0, 1, 1]	3.25E-03	2.53E-03	0.00E-03	0.78	2.61E-03	0.01E-03	0.80
5.2	[1, 1, 1]	8.29E-04	7.30E-04	0.03E-04	0.88	7.48E-04	0.05E-04	0.90
6.0	[0, 0, 2]	4.75E-04	4.58E-04	0.02E-04	0.96	4.66E-04	0.03E-04	0.98
6.7	[0, 1, 2]	3.73E-04	3.66E-04	0.01E-04	0.98	3.72E-04	0.01E-04	1.00
7.3	[1, 1, 2]	3.05E-04	3.05E-04	0.01E-04	1.00	3.07E-04	0.01E-04	1.01
8.5	[0, 2, 2]	2.33E-04	2.27E-04	0.01E-04	0.97	2.30E-04	0.02E-04	0.99
9.0	[1, 2, 2]; [0, 0, 3]	1.92E-04	2.01E-04	0.01E-04	1.04	2.03E-04	0.01E-04	1.05
9.5	[0, 1, 3]	1.77E-04	1.80E-04	0.01E-04	1.02	1.83E-04	0.01E-04	1.03
9.9	[1, 1, 3]	1.53E-04	1.64E-04	0.01E-04	1.07	1.65E-04	0.01E-04	1.08
10.4	[2, 2, 2]	1.40E-04	1.50E-04	0.01E-04	1.07	1.51E-04	0.02E-04	1.08
10.8	[0, 2, 3]	1.32E-04	1.38E-04	0.01E-04	1.04	1.40E-04	0.01E-04	1.06
11.2	[1, 2, 3]	1.33E-04	1.29E-04	0.00E-04	0.97	1.30E-04	0.01E-04	0.98
12.0	[0, 0, 4]	1.15E-04	1.11E-04	0.01E-04	0.97	1.14E-04	0.02E-04	0.99
12.4	[2, 2, 3]; [0, 1, 4]	1.05E-04	1.05E-04	0.00E-04	1.00	1.07E-04	0.01E-04	1.01
12.7	[1, 1, 4]; [0, 3, 3]	1.00E-04	1.00E-04	0.00E-04	1.00	1.00E-04	0.01E-04	1.00
13.1	[1, 3, 3]	9.96E-05	9.45E-05	0.05E-05	0.95	9.54E-05	0.07E-05	0.96
13.4	[0, 2, 4]	9.28E-05	8.97E-05	0.05E-05	0.97	9.05E-05	0.07E-05	0.97
13.7	[1, 2, 4]	8.66E-05	8.53E-05	0.04E-05	0.99	8.65E-05	0.05E-05	1.00
14.1	[2, 3, 3]	9.16E-05	8.14E-05	0.05E-05	0.89	8.23E-05	0.07E-05	0.90
14.7	[2, 2, 4]	7.59E-05	7.47E-05	0.05E-05	0.98	7.53E-05	0.07E-05	0.99
15.0	[0, 3, 4]; [0, 0, 5]	7.02E-05	7.19E-05	0.04E-05	1.02	7.24E-05	0.06E-05	1.03
15.3	[0, 1, 5]; [1, 3, 4]	6.88E-05	6.89E-05	0.03E-05	1.00	6.95E-05	0.04E-05	1.01
15.6	[1, 1, 5]; [3, 3, 3]	7.11E-05	6.66E-05	0.04E-05	0.94	6.71E-05	0.05E-05	0.94
16.2	[2, 3, 4]; [0, 2, 5]	6.12E-05	6.18E-05	0.02E-05	1.01	6.25E-05	0.03E-05	1.02
16.4	[1, 2, 5]	5.61E-05	5.94E-05	0.03E-05	1.06	6.02E-05	0.04E-05	1.07
17.0	[0, 4, 4]	5.31E-05	5.56E-05	0.06E-05	1.05	5.63E-05	0.08E-05	1.06
17.2	[1, 4, 4]; [2, 2, 5]	5.18E-05	5.41E-05	0.03E-05	1.04	5.48E-05	0.04E-05	1.06
17.5	[0, 3, 5]; [3, 3, 4]	4.67E-05	5.26E-05	0.03E-05	1.13	5.30E-05	0.04E-05	1.13
17.7	[1, 3, 5]	4.82E-05	5.12E-05	0.03E-05	1.06	5.15E-05	0.04E-05	1.07
18.0	[2, 4, 4]	4.90E-05	4.95E-05	0.04E-05	1.01	4.97E-05	0.05E-05	1.01
18.5	[2, 3, 5]	4.65E-05	4.69E-05	0.03E-05	1.01	4.73E-05	0.04E-05	1.02
19.2	[3, 4, 4]; [0, 4, 5]	4.26E-05	4.36E-05	0.03E-05	1.02	4.42E-05	0.03E-05	1.04
19.4	[1, 4, 5]	4.42E-05	4.29E-05	0.03E-05	0.97	4.29E-05	0.03E-05	0.97
19.7	[3, 3, 5]	4.19E-05	4.16E-05	0.04E-05	0.99	4.19E-05	0.05E-05	1.00
20.1	[2, 4, 5]	3.89E-05	3.97E-05	0.02E-05	1.02	4.00E-05	0.03E-05	1.03
20.8	[4, 4, 4]	3.98E-05	3.74E-05	0.06E-05	0.94	3.72E-05	0.08E-05	0.93
21.2	[0, 5, 5]; [3, 4, 5]	3.40E-05	3.57E-05	0.02E-05	1.05	3.60E-05	0.03E-05	1.06
21.4	[1, 5, 5]	3.24E-05	3.49E-05	0.03E-05	1.08	3.55E-05	0.04E-05	1.10
22.0	[2, 5, 5]	3.07E-05	3.31E-05	0.03E-05	1.08	3.34E-05	0.04E-05	1.09
22.6	[4, 4, 5]	3.31E-05	3.12E-05	0.03E-05	0.94	3.17E-05	0.04E-05	0.96
23.0	[3, 5, 5]	2.90E-05	3.02E-05	0.03E-05	1.04	3.07E-05	0.04E-05	1.06
24.4	[4, 5, 5]	2.71E-05	2.69E-05	0.03E-05	0.99	2.76E-05	0.04E-05	1.02
26.0	[5, 5, 5]	2.63E-05	2.36E-05	0.04E-05	0.90	2.40E-05	0.06E-05	0.91

Table B.4: S-values (mGy·MBq^{-1}·s^{-1}) for ^{131}I within cubical voxels of 6 mm and respective uncertainties.

Distance (mm)	Coordinates	MIRD	PenNuc	PenNuc Uncertainty	PenNuc / MIRD	DECDATA	DECDATA Uncertainty	DECDATA / MIRD
0.0	[0, 0, 0]	1.29E-01	1.31E-01	0.00E-01	1.01	1.32E-01	0.00E-01	1.02
6.0	[0, 0, 1]	2.90E-03	2.59E-03	0.00E-03	0.89	2.66E-03	0.00E-03	0.92
8.5	[0, 1, 1]	3.25E-04	3.00E-04	0.01E-04	0.92	3.06E-04	0.01E-04	0.94
10.4	[1, 1, 1]	1.54E-04	1.61E-04	0.00E-04	1.05	1.63E-04	0.01E-04	1.06
12.0	[0, 0, 2]	1.14E-04	1.15E-04	0.00E-04	1.01	1.17E-04	0.01E-04	1.02
13.4	[0, 1, 2]	9.24E-05	9.18E-05	0.02E-05	0.99	9.29E-05	0.03E-05	1.01
14.7	[1, 1, 2]	7.34E-05	7.65E-05	0.02E-05	1.04	7.71E-05	0.02E-05	1.05
17.0	[0, 2, 2]	5.61E-05	5.70E-05	0.02E-05	1.02	5.73E-05	0.03E-05	1.02
18.0	[1, 2, 2]; [0, 0, 3]	5.10E-05	5.05E-05	0.01E-05	0.99	5.08E-05	0.02E-05	1.00
19.0	[0, 1, 3]	4.46E-05	4.52E-05	0.01E-05	1.01	4.59E-05	0.02E-05	1.03
19.9	[1, 1, 3]	4.06E-05	4.11E-05	0.01E-05	1.01	4.17E-05	0.02E-05	1.03
20.8	[2, 2, 2]	3.60E-05	3.77E-05	0.02E-05	1.05	3.81E-05	0.03E-05	1.06
21.6	[0, 2, 3]	3.49E-05	3.46E-05	0.01E-05	0.99	3.51E-05	0.02E-05	1.00
22.4	[1, 2, 3]	3.09E-05	3.22E-05	0.01E-05	1.04	3.27E-05	0.01E-05	1.06
24.0	[0, 0, 4]	2.80E-05	2.80E-05	0.02E-05	1.00	2.86E-05	0.03E-05	1.02
24.7	[2, 2, 3]; [0, 1, 4]	2.64E-05	2.65E-05	0.01E-05	1.00	2.67E-05	0.01E-05	1.01
25.5	[1, 1, 4]; [0, 3, 3]	2.49E-05	2.50E-05	0.01E-05	1.00	2.54E-05	0.01E-05	1.02
26.2	[1, 3, 3]	2.21E-05	2.37E-05	0.01E-05	1.07	2.40E-05	0.01E-05	1.09
26.8	[0, 2, 4]	2.24E-05	2.24E-05	0.01E-05	1.00	2.28E-05	0.01E-05	1.02
27.5	[1, 2, 4]	2.11E-05	2.14E-05	0.01E-05	1.01	2.16E-05	0.01E-05	1.02
28.1	[2, 3, 3]	1.98E-05	2.04E-05	0.01E-05	1.03	2.07E-05	0.01E-05	1.04
29.4	[2, 2, 4]	1.86E-05	1.87E-05	0.01E-05	1.00	1.90E-05	0.01E-05	1.02
30.0	[0, 3, 4]; [0, 0, 5]	1.77E-05	1.79E-05	0.01E-05	1.01	1.82E-05	0.01E-05	1.03
30.6	[0, 1, 5]; [1, 3, 4]	1.64E-05	1.72E-05	0.00E-05	1.05	1.75E-05	0.01E-05	1.06
31.2	[1, 1, 5]; [3, 3, 3]	1.62E-05	1.66E-05	0.01E-05	1.02	1.68E-05	0.01E-05	1.03
32.3	[2, 3, 4]; [0, 2, 5]	1.60E-05	1.55E-05	0.00E-05	0.97	1.57E-05	0.01E-05	0.98
32.9	[1, 2, 5]	1.52E-05	1.49E-05	0.01E-05	0.98	1.52E-05	0.01E-05	1.00
33.9	[0, 4, 4]	1.58E-05	1.40E-05	0.01E-05	0.88	1.40E-05	0.01E-05	0.89
34.5	[1, 4, 4]; [2, 2, 5]	1.34E-05	1.36E-05	0.00E-05	1.01	1.37E-05	0.01E-05	1.02
35.0	[0, 3, 5]; [3, 3, 4]	1.26E-05	1.32E-05	0.00E-05	1.04	1.33E-05	0.01E-05	1.06
35.5	[1, 3, 5]	1.35E-05	1.28E-05	0.00E-05	0.95	1.30E-05	0.01E-05	0.96
36.0	[2, 4, 4]	1.28E-05	1.24E-05	0.01E-05	0.97	1.25E-05	0.01E-05	0.98
37.0	[2, 3, 5]	1.20E-05	1.17E-05	0.00E-05	0.98	1.20E-05	0.01E-05	1.00
38.4	[3, 4, 4]; [0, 4, 5]	1.11E-05	1.09E-05	0.00E-05	0.98	1.10E-05	0.01E-05	1.00
38.9	[1, 4, 5]	1.08E-05	1.07E-05	0.00E-05	0.99	1.07E-05	0.01E-05	0.99
39.3	[3, 3, 5]	1.02E-05	1.04E-05	0.01E-05	1.02	1.05E-05	0.01E-05	1.03
40.2	[2, 4, 5]	9.29E-06	9.87E-06	0.04E-06	1.06	1.01E-05	0.01E-05	1.08
41.6	[4, 4, 4]	8.48E-06	9.36E-06	0.10E-06	1.10	9.38E-06	0.14E-06	1.11
42.4	[0, 5, 5]; [3, 4, 5]	9.46E-06	8.90E-06	0.04E-06	0.94	9.00E-06	0.05E-06	0.95
42.8	[1, 5, 5]	8.86E-06	8.79E-06	0.06E-06	0.99	8.79E-06	0.07E-06	0.99
44.1	[2, 5, 5]	7.74E-06	8.23E-06	0.05E-06	1.06	8.43E-06	0.07E-06	1.09
45.3	[4, 4, 5]	7.73E-06	7.84E-06	0.05E-06	1.01	7.90E-06	0.07E-06	1.02
46.1	[3, 5, 5]	7.50E-06	7.57E-06	0.05E-06	1.01	7.65E-06	0.07E-06	1.02
48.7	[4, 5, 5]	6.70E-06	6.72E-06	0.05E-06	1.00	6.83E-06	0.07E-06	1.02
52.0	[5, 5, 5]	6.10E-06	5.90E-06	0.08E-06	0.97	6.08E-06	0.11E-06	1.00

Table B.5: S-values (mGy·MBq^{-1}·s^{-1}) for ^{32}P within cubical voxels of 3 mm and respective uncertainties.

Distance (mm)	Coordinates	MIRD	PenNuc	PenNuc Uncertainty	PenNuc / MIRD	DECDATA	DECDATA Uncertainty	DECDATA / MIRD
0.0	[0, 0, 0]	1.65E+00	1.64E+00	0.00E+00	0.99	1.64E+00	0.00E+00	0.99
3.0	[0, 0, 1]	2.32E-01	2.37E-01	0.00E-01	1.02	2.40E-01	0.00E-01	1.03
4.2	[0, 1, 1]	6.20E-02	6.20E-02	0.00E-02	1.00	6.32E-02	0.00E-02	1.02
5.2	[1, 1, 1]	2.12E-02	2.02E-02	0.00E-02	0.95	2.09E-02	0.00E-02	0.98
6.0	[0, 0, 2]	6.78E-03	5.95E-03	0.01E-03	0.88	6.26E-03	0.01E-03	0.92
6.7	[0, 1, 2]	2.88E-03	2.27E-03	0.00E-03	0.79	2.43E-03	0.00E-03	0.84
7.3	[1, 1, 2]	1.24E-03	8.60E-04	0.03E-04	0.69	9.36E-04	0.03E-04	0.75
8.5	[0, 2, 2]	1.81E-04	1.01E-04	0.01E-04	0.56	1.17E-04	0.01E-04	0.65
9.0	[1, 2, 2]; [0, 0, 3]	5.54E-05	3.32E-05	0.04E-05	0.60	4.05E-05	0.04E-05	0.73
9.5	[0, 1, 3]	1.82E-05	7.68E-06	0.18E-06	0.42	1.01E-05	0.02E-05	0.55
9.9	[1, 1, 3]	8.49E-06	3.56E-06	0.10E-06	0.42	4.52E-06	0.13E-06	0.53
10.4	[2, 2, 2]	6.25E-06	2.64E-06	0.14E-06	0.42	2.97E-06	0.16E-06	0.47
10.8	[0, 2, 3]	3.12E-06	1.60E-06	0.04E-06	0.51	1.65E-06	0.05E-06	0.53
11.2	[1, 2, 3]	2.03E-06	1.37E-06	0.03E-06	0.68	1.44E-06	0.03E-06	0.71
12.0	[0, 0, 4]	1.15E-06	1.13E-06	0.06E-06	0.98	1.15E-06	0.06E-06	1.00
12.4	[2, 2, 3]; [0, 1, 4]	1.24E-06	1.05E-06	0.02E-06	0.85	1.09E-06	0.02E-06	0.88
12.7	[1, 1, 4]; [0, 3, 3]	1.15E-06	1.01E-06	0.03E-06	0.88	9.92E-07	0.27E-07	0.86
13.1	[1, 3, 3]	1.07E-06	9.31E-07	0.31E-07	0.87	9.42E-07	0.31E-07	0.88
13.4	[0, 2, 4]	1.09E-06	8.63E-07	0.31E-07	0.79	9.08E-07	0.33E-07	0.83
13.7	[1, 2, 4]	1.17E-06	8.35E-07	0.21E-07	0.71	8.46E-07	0.22E-07	0.72
14.1	[2, 3, 3]	1.14E-06	7.85E-07	0.30E-07	0.69	7.88E-07	0.29E-07	0.69
14.7	[2, 2, 4]	1.08E-06	6.94E-07	0.27E-07	0.64	6.97E-07	0.27E-07	0.65
15.0	[0, 3, 4]; [0, 0, 5]	9.53E-07	6.66E-07	0.25E-07	0.70	6.72E-07	0.24E-07	0.71
15.3	[0, 1, 5]; [1, 3, 4]	9.29E-07	6.46E-07	0.15E-07	0.69	6.46E-07	0.15E-07	0.70
15.6	[1, 1, 5]; [3, 3, 3]	1.11E-06	6.03E-07	0.22E-07	0.55	6.19E-07	0.23E-07	0.56
16.2	[2, 3, 4]; [0, 2, 5]	7.85E-07	5.61E-07	0.14E-07	0.71	5.65E-07	0.14E-07	0.72
16.4	[1, 2, 5]	7.23E-07	5.40E-07	0.17E-07	0.75	5.41E-07	0.17E-07	0.75
17.0	[0, 4, 4]	1.11E-06	4.97E-07	0.31E-07	0.45	5.14E-07	0.34E-07	0.46
17.2	[1, 4, 4]; [2, 2, 5]	4.74E-07	4.90E-07	0.16E-07	1.04	4.85E-07	0.17E-07	1.02
17.5	[0, 3, 5]; [3, 3, 4]	6.26E-07	4.55E-07	0.15E-07	0.73	4.67E-07	0.16E-07	0.74
17.7	[1, 3, 5]	4.76E-07	4.43E-07	0.16E-07	0.93	4.70E-07	0.17E-07	0.99
18.0	[2, 4, 4]	4.99E-07	4.37E-07	0.22E-07	0.87	4.58E-07	0.23E-07	0.92
18.5	[2, 3, 5]	7.16E-07	4.06E-07	0.16E-07	0.57	4.23E-07	0.15E-07	0.59
19.2	[3, 4, 4]; [0, 4, 5]	5.88E-07	3.84E-07	0.15E-07	0.65	3.76E-07	0.15E-07	0.64
19.4	[1, 4, 5]	4.70E-07	3.58E-07	0.14E-07	0.76	3.59E-07	0.14E-07	0.76
19.7	[3, 3, 5]	5.58E-07	3.42E-07	0.19E-07	0.61	3.57E-07	0.20E-07	0.64
20.1	[2, 4, 5]	5.72E-07	3.32E-07	0.14E-07	0.58	3.53E-07	0.15E-07	0.62
20.8	[4, 4, 4]	1.70E-07	3.05E-07	0.31E-07	1.79	2.94E-07	0.31E-07	1.73
21.2	[0, 5, 5]; [3, 4, 5]	3.14E-07	2.95E-07	0.11E-07	0.94	2.95E-07	0.11E-07	0.94
21.4	[1, 5, 5]	2.55E-07	2.94E-07	0.19E-07	1.15	2.94E-07	0.18E-07	1.15
22.0	[2, 5, 5]	3.65E-07	2.60E-07	0.18E-07	0.71	2.71E-07	0.19E-07	0.74
22.6	[4, 4, 5]	3.52E-07	2.65E-07	0.18E-07	0.75	2.73E-07	0.18E-07	0.78
23.0	[3, 5, 5]	2.14E-07	2.39E-07	0.16E-07	1.12	2.51E-07	0.17E-07	1.17
24.4	[4, 5, 5]	2.21E-07	2.14E-07	0.16E-07	0.97	2.25E-07	0.17E-07	1.02
26.0	[5, 5, 5]	4.16E-07	1.93E-07	0.29E-07	0.46	1.87E-07	0.23E-07	0.45

Table B.6: S-values (mGy·MBq^{-1}·s^{-1}) for ^{32}P within cubical voxels of 6 mm and respective uncertainties.

Distance (mm)	Coordinates	MIRD	PenNuc	PenNuc Uncertainty	PenNuc / MIRD	DECDATA	DECDATA Uncertainty	DECDATA / MIRD
0.0	[0, 0, 0]	3.19E-01	3.19E-01	0.00E-01	1.00	3.21E-01	0.00E-01	1.01
6.0	[0, 0, 1]	2.53E-02	2.53E-02	0.00E-02	1.00	2.57E-02	0.00E-02	1.02
8.5	[0, 1, 1]	3.13E-03	2.98E-03	0.00E-03	0.95	3.07E-03	0.00E-03	0.98
10.4	[1, 1, 1]	4.64E-04	4.05E-04	0.01E-04	0.87	4.24E-04	0.01E-04	0.91
12.0	[0, 0, 2]	5.54E-06	3.11E-06	0.08E-06	0.56	3.89E-06	0.09E-06	0.70
13.4	[0, 1, 2]	1.94E-06	1.17E-06	0.02E-06	0.60	1.29E-06	0.02E-06	0.67
14.7	[1, 1, 2]	1.09E-06	7.60E-07	0.11E-07	0.70	7.91E-07	0.12E-07	0.73
17.0	[0, 2, 2]	8.17E-07	5.10E-07	0.12E-07	0.62	5.20E-07	0.12E-07	0.64
18.0	[1, 2, 2]; [0, 0, 3]	5.97E-07	4.45E-07	0.07E-07	0.74	4.54E-07	0.07E-07	0.76
19.0	[0, 1, 3]	6.07E-07	3.89E-07	0.08E-07	0.64	4.00E-07	0.08E-07	0.66
19.9	[1, 1, 3]	5.19E-07	3.41E-07	0.07E-07	0.66	3.55E-07	0.07E-07	0.68
20.8	[2, 2, 2]	2.44E-07	3.20E-07	0.12E-07	1.31	3.16E-07	0.12E-07	1.30
21.6	[0, 2, 3]	3.58E-07	2.91E-07	0.07E-07	0.81	2.87E-07	0.07E-07	0.80
22.4	[1, 2, 3]	4.21E-07	2.63E-07	0.04E-07	0.62	2.69E-07	0.05E-07	0.64
24.0	[0, 0, 4]	1.83E-07	2.15E-07	0.11E-07	1.18	2.30E-07	0.12E-07	1.26
24.7	[2, 2, 3]; [0, 1, 4]	2.06E-07	2.09E-07	0.04E-07	1.02	2.13E-07	0.04E-07	1.03
25.5	[1, 1, 4]; [0, 3, 3]	2.53E-07	1.95E-07	0.04E-07	0.77	1.98E-07	0.04E-07	0.78
26.2	[1, 3, 3]	2.96E-07	1.83E-07	0.05E-07	0.62	1.86E-07	0.05E-07	0.63
26.8	[0, 2, 4]	2.51E-07	1.72E-07	0.05E-07	0.69	1.73E-07	0.05E-07	0.69
27.5	[1, 2, 4]	2.46E-07	1.65E-07	0.04E-07	0.67	1.66E-07	0.04E-07	0.68
28.1	[2, 3, 3]	2.52E-07	1.56E-07	0.05E-07	0.62	1.57E-07	0.05E-07	0.62
29.4	[2, 2, 4]	2.09E-07	1.43E-07	0.05E-07	0.69	1.45E-07	0.05E-07	0.69
30.0	[0, 3, 4]; [0, 0, 5]	2.15E-07	1.36E-07	0.04E-07	0.63	1.39E-07	0.04E-07	0.65
30.6	[0, 1, 5]; [1, 3, 4]	1.64E-07	1.28E-07	0.03E-07	0.78	1.30E-07	0.03E-07	0.79
31.2	[1, 1, 5]; [3, 3, 3]	2.19E-07	1.23E-07	0.04E-07	0.56	1.25E-07	0.04E-07	0.57
32.3	[2, 3, 4]; [0, 2, 5]	1.17E-07	1.13E-07	0.02E-07	0.97	1.16E-07	0.02E-07	1.00
32.9	[1, 2, 5]	1.62E-07	1.10E-07	0.03E-07	0.68	1.12E-07	0.03E-07	0.69
33.9	[0, 4, 4]	9.51E-08	1.02E-07	0.06E-07	1.08	1.02E-07	0.06E-07	1.07
34.5	[1, 4, 4]; [2, 2, 5]	1.41E-07	9.63E-08	0.27E-08	0.69	1.01E-07	0.03E-07	0.72
35.0	[0, 3, 5]; [3, 3, 4]	1.23E-07	9.63E-08	0.28E-08	0.78	9.65E-08	0.29E-08	0.78
35.5	[1, 3, 5]	1.12E-07	9.12E-08	0.26E-08	0.81	9.32E-08	0.27E-08	0.83
36.0	[2, 4, 4]	1.56E-07	8.91E-08	0.38E-08	0.57	9.06E-08	0.38E-08	0.58
37.0	[2, 3, 5]	8.17E-08	8.52E-08	0.26E-08	1.04	8.52E-08	0.26E-08	1.04
38.4	[3, 4, 4]; [0, 4, 5]	1.40E-07	7.70E-08	0.24E-08	0.55	7.77E-08	0.24E-08	0.56
38.9	[1, 4, 5]	1.29E-07	7.51E-08	0.25E-08	0.58	7.53E-08	0.24E-08	0.58
39.3	[3, 3, 5]	4.66E-08	7.26E-08	0.34E-08	1.56	7.44E-08	0.37E-08	1.60
40.2	[2, 4, 5]	8.68E-08	7.12E-08	0.25E-08	0.82	6.96E-08	0.24E-08	0.80
41.6	[4, 4, 4]	7.62E-08	6.81E-08	0.59E-08	0.89	6.46E-08	0.50E-08	0.85
42.4	[0, 5, 5]; [3, 4, 5]	6.60E-08	6.21E-08	0.20E-08	0.94	6.34E-08	0.20E-08	0.96
42.8	[1, 5, 5]	8.84E-08	6.06E-08	0.30E-08	0.69	6.38E-08	0.34E-08	0.72
44.1	[2, 5, 5]	6.27E-08	5.59E-08	0.32E-08	0.89	5.83E-08	0.32E-08	0.93
45.3	[4, 4, 5]	5.70E-08	5.76E-08	0.35E-08	1.01	5.37E-08	0.29E-08	0.94
46.1	[3, 5, 5]	5.99E-08	5.26E-08	0.30E-08	0.88	4.96E-08	0.27E-08	0.83
48.7	[4, 5, 5]	3.67E-08	4.46E-08	0.28E-08	1.21	4.54E-08	0.26E-08	1.24
52.0	[5, 5, 5]	7.16E-08	3.95E-08	0.40E-08	0.55	4.15E-08	0.49E-08	0.58

Table B.7: S-values (mGy·MBq^{-1}·s^{-1}) for ^{89}Sr within cubical voxels of 3 mm and respective uncertainties.

Distance (mm)	Coordinates	MIRD	PenNuc	PenNuc Uncertainty	PenNuc / MIRD	DECDATA	DECDATA Uncertainty	DECDATA / MIRD
0.0	[0, 0, 0]	1.55E+00	1.56E+00	0.00E+00	1.00	1.55E+00	0.00E+00	1.00
3.0	[0, 0, 1]	1.93E-01	2.02E-01	0.00E-01	1.05	2.00E-01	0.00E-01	1.04
4.2	[0, 1, 1]	4.60E-02	4.72E-02	0.00E-02	1.03	4.67E-02	0.00E-02	1.02
5.2	[1, 1, 1]	1.40E-02	1.35E-02	0.00E-02	0.96	1.35E-02	0.00E-02	0.96
6.0	[0, 0, 2]	3.62E-03	3.02E-03	0.01E-03	0.83	3.10E-03	0.01E-03	0.86
6.7	[0, 1, 2]	1.42E-03	9.58E-04	0.03E-04	0.67	1.00E-03	0.00E-03	0.71
7.3	[1, 1, 2]	5.85E-04	2.98E-04	0.01E-04	0.51	3.22E-04	0.01E-04	0.55
8.5	[0, 2, 2]	7.55E-05	1.98E-05	0.04E-05	0.26	2.34E-05	0.05E-05	0.31
9.0	[1, 2, 2]; [0, 0, 3]	1.98E-05	5.92E-06	0.13E-06	0.30	6.89E-06	0.15E-06	0.35
9.5	[0, 1, 3]	5.28E-06	1.86E-06	0.05E-06	0.35	2.01E-06	0.05E-06	0.38
9.9	[1, 1, 3]	2.18E-06	1.52E-06	0.04E-06	0.70	1.59E-06	0.04E-06	0.73
10.4	[2, 2, 2]	2.40E-06	1.37E-06	0.06E-06	0.57	1.42E-06	0.07E-06	0.59
10.8	[0, 2, 3]	1.46E-06	1.20E-06	0.03E-06	0.82	1.22E-06	0.03E-06	0.83
11.2	[1, 2, 3]	1.10E-06	1.09E-06	0.02E-06	0.99	1.12E-06	0.02E-06	1.01
12.0	[0, 0, 4]	7.99E-07	9.56E-07	0.65E-07	1.20	9.32E-07	0.59E-07	1.17
12.4	[2, 2, 3]; [0, 1, 4]	9.60E-07	8.75E-07	0.22E-07	0.91	8.49E-07	0.19E-07	0.88
12.7	[1, 1, 4]; [0, 3, 3]	8.59E-07	8.10E-07	0.24E-07	0.94	8.15E-07	0.23E-07	0.95
13.1	[1, 3, 3]	8.30E-07	7.53E-07	0.29E-07	0.91	7.66E-07	0.28E-07	0.92
13.4	[0, 2, 4]	8.20E-07	7.01E-07	0.30E-07	0.86	7.22E-07	0.26E-07	0.88
13.7	[1, 2, 4]	9.24E-07	6.82E-07	0.19E-07	0.74	6.64E-07	0.18E-07	0.72
14.1	[2, 3, 3]	9.22E-07	6.32E-07	0.26E-07	0.69	6.27E-07	0.24E-07	0.68
14.7	[2, 2, 4]	8.73E-07	5.64E-07	0.23E-07	0.65	5.70E-07	0.23E-07	0.65
15.0	[0, 3, 4]; [0, 0, 5]	7.43E-07	5.27E-07	0.21E-07	0.71	5.38E-07	0.21E-07	0.72
15.3	[0, 1, 5]; [1, 3, 4]	7.23E-07	5.14E-07	0.14E-07	0.71	5.09E-07	0.13E-07	0.70
15.6	[1, 1, 5]; [3, 3, 3]	9.38E-07	4.89E-07	0.21E-07	0.52	4.95E-07	0.19E-07	0.53
16.2	[2, 3, 4]; [0, 2, 5]	6.29E-07	4.63E-07	0.13E-07	0.74	4.50E-07	0.12E-07	0.72
16.4	[1, 2, 5]	5.53E-07	4.53E-07	0.17E-07	0.82	4.24E-07	0.15E-07	0.77
17.0	[0, 4, 4]	8.90E-07	3.90E-07	0.31E-07	0.44	3.99E-07	0.28E-07	0.45
17.2	[1, 4, 4]; [2, 2, 5]	3.75E-07	3.99E-07	0.15E-07	1.06	3.96E-07	0.15E-07	1.06
17.5	[0, 3, 5]; [3, 3, 4]	4.83E-07	3.87E-07	0.15E-07	0.80	3.79E-07	0.14E-07	0.79
17.7	[1, 3, 5]	3.59E-07	3.74E-07	0.15E-07	1.04	3.60E-07	0.13E-07	1.00
18.0	[2, 4, 4]	3.89E-07	3.56E-07	0.21E-07	0.92	3.40E-07	0.18E-07	0.88
18.5	[2, 3, 5]	5.63E-07	3.33E-07	0.14E-07	0.59	3.23E-07	0.13E-07	0.57
19.2	[3, 4, 4]; [0, 4, 5]	4.60E-07	3.03E-07	0.13E-07	0.66	3.04E-07	0.12E-07	0.66
19.4	[1, 4, 5]	3.47E-07	2.97E-07	0.13E-07	0.86	2.90E-07	0.12E-07	0.83
19.7	[3, 3, 5]	4.47E-07	2.89E-07	0.17E-07	0.65	2.85E-07	0.18E-07	0.64
20.1	[2, 4, 5]	4.42E-07	2.64E-07	0.13E-07	0.60	2.67E-07	0.11E-07	0.60
20.8	[4, 4, 4]	1.35E-07	2.49E-07	0.31E-07	1.85	2.56E-07	0.26E-07	1.90
21.2	[0, 5, 5]; [3, 4, 5]	2.24E-07	2.38E-07	0.10E-07	1.06	2.33E-07	0.09E-07	1.04
21.4	[1, 5, 5]	1.95E-07	2.45E-07	0.17E-07	1.26	2.37E-07	0.16E-07	1.22
22.0	[2, 5, 5]	3.16E-07	2.19E-07	0.17E-07	0.69	2.14E-07	0.14E-07	0.68
22.6	[4, 4, 5]	2.72E-07	2.11E-07	0.16E-07	0.77	1.97E-07	0.14E-07	0.72
23.0	[3, 5, 5]	1.67E-07	2.13E-07	0.17E-07	1.27	2.01E-07	0.15E-07	1.21
24.4	[4, 5, 5]	1.79E-07	1.74E-07	0.15E-07	0.97	1.72E-07	0.14E-07	0.96
26.0	[5, 5, 5]	3.15E-07	1.61E-07	0.27E-07	0.51	1.56E-07	0.22E-07	0.49

Table B.8: S-values (mGy·MBq^{-1}·s^{-1}) for ^{89}Sr within cubical voxels of 6 mm and respective uncertainties.

Distance (mm)	Coordinates	MIRD	PenNuc	PenNuc Uncertainty	PenNuc / MIRD	DECDATA	DECDATA Uncertainty	DECDATA / MIRD
0.0	[0, 0, 0]	2.85E-01	2.90E-01	0.00E-01	1.02	2.88E-01	0.00E-01	1.01
6.0	[0, 0, 1]	1.96E-02	2.00E-02	0.00E-02	1.02	1.99E-02	0.00E-02	1.01
8.5	[0, 1, 1]	2.13E-03	2.06E-03	0.00E-03	0.97	2.05E-03	0.00E-03	0.96
10.4	[1, 1, 1]	2.79E-04	2.41E-04	0.01E-04	0.86	2.43E-04	0.01E-04	0.87
12.0	[0, 0, 2]	1.90E-06	1.07E-06	0.03E-06	0.56	1.11E-06	0.03E-06	0.58
13.4	[0, 1, 2]	9.72E-07	7.52E-07	0.11E-07	0.77	7.59E-07	0.10E-07	0.78
14.7	[1, 1, 2]	7.35E-07	5.98E-07	0.09E-07	0.81	5.90E-07	0.08E-07	0.80
17.0	[0, 2, 2]	6.25E-07	4.07E-07	0.11E-07	0.65	4.13E-07	0.11E-07	0.66
18.0	[1, 2, 2]; [0, 0, 3]	4.51E-07	3.64E-07	0.07E-07	0.81	3.58E-07	0.06E-07	0.79
19.0	[0, 1, 3]	4.74E-07	3.20E-07	0.07E-07	0.68	3.15E-07	0.06E-07	0.66
19.9	[1, 1, 3]	4.15E-07	2.88E-07	0.07E-07	0.69	2.79E-07	0.06E-07	0.67
20.8	[2, 2, 2]	1.87E-07	2.64E-07	0.12E-07	1.41	2.54E-07	0.10E-07	1.36
21.6	[0, 2, 3]	2.73E-07	2.36E-07	0.06E-07	0.86	2.31E-07	0.06E-07	0.84
22.4	[1, 2, 3]	3.27E-07	2.11E-07	0.04E-07	0.65	2.11E-07	0.04E-07	0.65
24.0	[0, 0, 4]	1.46E-07	1.83E-07	0.10E-07	1.25	1.81E-07	0.09E-07	1.24
24.7	[2, 2, 3]; [0, 1, 4]	1.57E-07	1.70E-07	0.04E-07	1.08	1.69E-07	0.03E-07	1.08
25.5	[1, 1, 4]; [0, 3, 3]	2.02E-07	1.62E-07	0.04E-07	0.80	1.59E-07	0.04E-07	0.79
26.2	[1, 3, 3]	2.39E-07	1.49E-07	0.05E-07	0.63	1.48E-07	0.04E-07	0.62
26.8	[0, 2, 4]	1.86E-07	1.42E-07	0.05E-07	0.76	1.37E-07	0.04E-07	0.74
27.5	[1, 2, 4]	1.90E-07	1.34E-07	0.03E-07	0.71	1.37E-07	0.03E-07	0.72
28.1	[2, 3, 3]	2.06E-07	1.29E-07	0.05E-07	0.63	1.25E-07	0.04E-07	0.61
29.4	[2, 2, 4]	1.67E-07	1.12E-07	0.04E-07	0.67	1.12E-07	0.04E-07	0.67
30.0	[0, 3, 4]; [0, 0, 5]	1.70E-07	1.10E-07	0.04E-07	0.65	1.09E-07	0.03E-07	0.64
30.6	[0, 1, 5]; [1, 3, 4]	1.28E-07	1.06E-07	0.02E-07	0.83	1.04E-07	0.02E-07	0.82
31.2	[1, 1, 5]; [3, 3, 3]	1.77E-07	9.94E-08	0.35E-08	0.56	9.72E-08	0.30E-08	0.55
32.3	[2, 3, 4]; [0, 2, 5]	9.24E-08	9.36E-08	0.24E-08	1.01	9.19E-08	0.21E-08	0.99
32.9	[1, 2, 5]	1.30E-07	8.98E-08	0.28E-08	0.69	8.83E-08	0.24E-08	0.68
33.9	[0, 4, 4]	7.29E-08	8.27E-08	0.58E-08	1.14	8.49E-08	0.51E-08	1.16
34.5	[1, 4, 4]; [2, 2, 5]	1.05E-07	8.03E-08	0.26E-08	0.76	8.17E-08	0.25E-08	0.78
35.0	[0, 3, 5]; [3, 3, 4]	9.07E-08	7.71E-08	0.25E-08	0.85	7.57E-08	0.23E-08	0.83
35.5	[1, 3, 5]	8.59E-08	7.47E-08	0.25E-08	0.87	7.44E-08	0.23E-08	0.87
36.0	[2, 4, 4]	1.19E-07	7.09E-08	0.35E-08	0.60	6.90E-08	0.29E-08	0.58
37.0	[2, 3, 5]	6.39E-08	6.86E-08	0.25E-08	1.07	6.86E-08	0.23E-08	1.07
38.4	[3, 4, 4]; [0, 4, 5]	1.12E-07	6.26E-08	0.23E-08	0.56	6.22E-08	0.21E-08	0.55
38.9	[1, 4, 5]	9.76E-08	6.15E-08	0.23E-08	0.63	6.09E-08	0.21E-08	0.62
39.3	[3, 3, 5]	3.39E-08	6.14E-08	0.31E-08	1.81	5.97E-08	0.29E-08	1.76
40.2	[2, 4, 5]	6.94E-08	5.62E-08	0.21E-08	0.81	5.58E-08	0.20E-08	0.80
41.6	[4, 4, 4]	5.59E-08	5.54E-08	0.61E-08	0.99	4.99E-08	0.42E-08	0.89
42.4	[0, 5, 5]; [3, 4, 5]	5.16E-08	5.03E-08	0.18E-08	0.97	4.97E-08	0.17E-08	0.96
42.8	[1, 5, 5]	6.41E-08	4.99E-08	0.31E-08	0.78	4.89E-08	0.25E-08	0.76
44.1	[2, 5, 5]	4.99E-08	4.63E-08	0.28E-08	0.93	4.47E-08	0.25E-08	0.90
45.3	[4, 4, 5]	4.58E-08	4.23E-08	0.26E-08	0.92	4.37E-08	0.26E-08	0.95
46.1	[3, 5, 5]	4.64E-08	4.22E-08	0.26E-08	0.91	4.10E-08	0.25E-08	0.88
48.7	[4, 5, 5]	3.05E-08	3.67E-08	0.24E-08	1.20	3.57E-08	0.23E-08	1.17
52.0	[5, 5, 5]	4.94E-08	3.12E-08	0.33E-08	0.63	3.05E-08	0.33E-08	0.62

Table B.9: S-values (mGy·MBq^{-1}·s^{-1}) for ^{90}Y within cubical voxels of 3 mm and respective uncertainties.

Distance (mm)	Coordinates	MIRD	PenNuc	PenNuc Uncertainty	PenNuc / MIRD	DECDATA	DECDATA Uncertainty	DECDATA / MIRD	ICRU	ICRU Uncertainty	ICRU / MIRD
0.0	[0, 0, 0]	1.61E+00	1.58E+00	0.00E+00	0.98	1.58E+00	0.00E+00	0.98	1.58E+00	0.00E+00	0.98
3.0	[0, 0, 1]	2.76E-01	2.80E-01	0.00E-01	1.01	2.78E-01	0.00E-01	1.01	2.79E-01	0.00E-01	1.01
4.2	[0, 1, 1]	9.76E-02	9.95E-02	0.00E-02	1.02	9.89E-02	0.00E-02	1.01	9.90E-02	0.00E-02	1.01
5.2	[1, 1, 1]	4.53E-02	4.62E-02	0.00E-02	1.02	4.60E-02	0.00E-02	1.02	4.59E-02	0.00E-02	1.01
6.0	[0, 0, 2]	2.26E-02	2.28E-02	0.00E-02	1.01	2.28E-02	0.00E-02	1.01	2.27E-02	0.00E-02	1.00
6.7	[0, 1, 2]	1.28E-02	1.27E-02	0.00E-02	0.99	1.28E-02	0.00E-02	1.00	1.27E-02	0.00E-02	0.99
7.3	[1, 1, 2]	7.38E-03	7.17E-03	0.01E-03	0.97	7.31E-03	0.01E-03	0.99	7.17E-03	0.01E-03	0.97
8.5	[0, 2, 2]	2.47E-03	2.25E-03	0.01E-03	0.91	2.37E-03	0.01E-03	0.96	2.27E-03	0.01E-03	0.92
9.0	[1, 2, 2]; [0, 0, 3]	1.36E-03	1.24E-03	0.00E-03	0.91	1.33E-03	0.00E-03	0.98	1.25E-03	0.00E-03	0.92
9.5	[0, 1, 3]	7.65E-04	6.50E-04	0.02E-04	0.85	7.24E-04	0.03E-04	0.95	6.64E-04	0.02E-04	0.87
9.9	[1, 1, 3]	4.25E-04	3.54E-04	0.02E-04	0.83	4.03E-04	0.02E-04	0.95	3.59E-04	0.02E-04	0.84
10.4	[2, 2, 2]	2.51E-04	1.97E-04	0.02E-04	0.79	2.30E-04	0.02E-04	0.92	2.06E-04	0.02E-04	0.82
10.8	[0, 2, 3]	1.23E-04	9.71E-05	0.09E-05	0.79	1.18E-04	0.01E-04	0.96	9.95E-05	0.09E-05	0.81
11.2	[1, 2, 3]	7.35E-05	4.99E-05	0.04E-05	0.68	6.29E-05	0.05E-05	0.86	5.19E-05	0.04E-05	0.71
12.0	[0, 0, 4]	2.78E-05	9.72E-06	0.46E-06	0.35	1.32E-05	0.06E-05	0.48	9.61E-06	0.45E-06	0.35
12.4	[2, 2, 3]; [0, 1, 4]	2.55E-05	6.28E-06	0.13E-06	0.25	8.18E-06	0.15E-06	0.32	6.50E-06	0.13E-06	0.25
12.7	[1, 1, 4]; [0, 3, 3]	2.30E-05	3.43E-06	0.09E-06	0.15	4.44E-06	0.11E-06	0.19	3.54E-06	0.10E-06	0.15
13.1	[1, 3, 3]	2.10E-05	2.56E-06	0.09E-06	0.12	3.16E-06	0.11E-06	0.15	2.59E-06	0.09E-06	0.12
13.4	[0, 2, 4]	1.98E-05	1.83E-06	0.07E-06	0.09	1.99E-06	0.07E-06	0.10	1.77E-06	0.06E-06	0.09
13.7	[1, 2, 4]	1.84E-05	1.57E-06	0.04E-06	0.09	1.59E-06	0.04E-06	0.09	1.55E-06	0.04E-06	0.08
14.1	[2, 3, 3]	1.75E-05	1.44E-06	0.05E-06	0.08	1.46E-06	0.05E-06	0.08	1.42E-06	0.05E-06	0.08
14.7	[2, 2, 4]	1.47E-05	1.27E-06	0.05E-06	0.09	1.25E-06	0.04E-06	0.09	1.20E-06	0.04E-06	0.08
15.0	[0, 3, 4]; [0, 0, 5]	1.35E-05	1.19E-06	0.04E-06	0.09	1.15E-06	0.04E-06	0.09	1.14E-06	0.04E-06	0.08
15.3	[0, 1, 5]; [1, 3, 4]	1.25E-05	1.15E-06	0.03E-06	0.09	1.11E-06	0.02E-06	0.09	1.10E-06	0.02E-06	0.09
15.6	[1, 1, 5]; [3, 3, 3]	1.17E-05	1.09E-06	0.04E-06	0.09	1.03E-06	0.03E-06	0.09	1.04E-06	0.03E-06	0.09
16.2	[2, 3, 4]; [0, 2, 5]	9.51E-06	1.02E-06	0.03E-06	0.11	9.89E-07	0.23E-07	0.10	9.60E-07	0.22E-07	0.10
16.4	[1, 2, 5]	8.77E-06	9.81E-07	0.29E-07	0.11	9.50E-07	0.28E-07	0.11	9.07E-07	0.26E-07	0.10
17.0	[0, 4, 4]	7.14E-06	9.36E-07	0.64E-07	0.13	8.58E-07	0.52E-07	0.12	8.20E-07	0.47E-07	0.11
17.2	[1, 4, 4]; [2, 2, 5]	5.95E-06	8.56E-07	0.28E-07	0.14	8.23E-07	0.25E-07	0.14	8.36E-07	0.26E-07	0.14
17.5	[0, 3, 5]; [3, 3, 4]	5.49E-06	8.53E-07	0.29E-07	0.16	8.03E-07	0.24E-07	0.15	7.79E-07	0.25E-07	0.14
17.7	[1, 3, 5]	4.66E-06	8.40E-07	0.30E-07	0.18	7.87E-07	0.25E-07	0.17	7.71E-07	0.25E-07	0.17
18.0	[2, 4, 4]	3.96E-06	7.63E-07	0.38E-07	0.19	7.34E-07	0.32E-07	0.19	7.33E-07	0.36E-07	0.18
18.5	[2, 3, 5]	3.38E-06	7.27E-07	0.26E-07	0.22	7.02E-07	0.24E-07	0.21	7.02E-07	0.23E-07	0.21
19.2	[3, 4, 4]; [0, 4, 5]	2.34E-06	6.66E-07	0.25E-07	0.28	6.47E-07	0.23E-07	0.28	6.35E-07	0.21E-07	0.27
19.4	[1, 4, 5]	1.97E-06	6.83E-07	0.27E-07	0.35	6.20E-07	0.21E-07	0.31	6.43E-07	0.24E-07	0.33
19.7	[3, 3, 5]	1.56E-06	6.45E-07	0.37E-07	0.41	6.17E-07	0.33E-07	0.40	6.25E-07	0.31E-07	0.40
20.1	[2, 4, 5]	1.45E-06	6.03E-07	0.24E-07	0.42	5.73E-07	0.22E-07	0.39	5.88E-07	0.22E-07	0.41
20.8	[4, 4, 4]	9.13E-07	5.95E-07	0.70E-07	0.65	6.18E-07	0.66E-07	0.68	5.17E-07	0.42E-07	0.57
21.2	[0, 5, 5]; [3, 4, 5]	7.62E-07	5.46E-07	0.21E-07	0.72	5.28E-07	0.19E-07	0.69	4.95E-07	0.17E-07	0.65
21.4	[1, 5, 5]	7.40E-07	5.55E-07	0.37E-07	0.75	4.88E-07	0.28E-07	0.66	4.90E-07	0.27E-07	0.66
22.0	[2, 5, 5]	7.23E-07	4.97E-07	0.32E-07	0.69	4.61E-07	0.27E-07	0.64	4.78E-07	0.27E-07	0.66
22.6	[4, 4, 5]	7.68E-07	4.65E-07	0.30E-07	0.60	4.41E-07	0.26E-07	0.57	4.16E-07	0.25E-07	0.54
23.0	[3, 5, 5]	4.88E-07	4.60E-07	0.31E-07	0.94	4.00E-07	0.24E-07	0.82	4.23E-07	0.27E-07	0.87
24.4	[4, 5, 5]	4.59E-07	3.91E-07	0.28E-07	0.85	3.88E-07	0.27E-07	0.85	3.63E-07	0.25E-07	0.79
26.0	[5, 5, 5]	6.31E-07	3.55E-07	0.48E-07	0.56	3.47E-07	0.43E-07	0.55	3.67E-07	0.47E-07	0.58

Table B.10: S-values (mGy·MBq^{-1}·s^{-1}) for ^{90}Y within cubical voxels of 6 mm and respective uncertainties.

Distance (mm)	Coordinates	MIRD	PenNuc	PenNuc Uncertainty	PenNuc / MIRD	DECDATA	DECDATA Uncertainty	DECDATA / MIRD	ICRU	ICRU Uncertainty	ICRU / MIRD
0.0	[0, 0, 0]	3.46E-01	3.46E-01	0.00E-01	1.00	3.45E-01	0.00E-01	1.00	3.45E-01	0.00E-01	1.00
6.0	[0, 0, 1]	3.95E-02	3.99E-02	0.00E-02	1.01	3.98E-02	0.00E-02	1.01	3.98E-02	0.00E-02	1.01
8.5	[0, 1, 1]	7.57E-03	7.56E-03	0.01E-03	1.00	7.60E-03	0.01E-03	1.00	7.53E-03	0.01E-03	1.00
10.4	[1, 1, 1]	1.74E-03	1.68E-03	0.00E-03	0.97	1.72E-03	0.00E-03	0.99	1.68E-03	0.00E-03	0.97
12.0	[0, 0, 2]	2.13E-04	1.81E-04	0.01E-04	0.85	2.00E-04	0.01E-04	0.94	1.84E-04	0.01E-04	0.86
13.4	[0, 1, 2]	6.36E-05	4.20E-05	0.02E-05	0.66	4.85E-05	0.02E-05	0.76	4.29E-05	0.02E-05	0.67
14.7	[1, 1, 2]	2.36E-05	1.02E-05	0.01E-05	0.43	1.19E-05	0.01E-05	0.50	1.04E-05	0.01E-05	0.44
17.0	[0, 2, 2]	7.71E-06	1.03E-06	0.03E-06	0.13	1.03E-06	0.02E-06	0.13	9.74E-07	0.22E-07	0.13
18.0	[1, 2, 2]; [0, 0, 3]	5.19E-06	8.21E-07	0.14E-07	0.16	7.93E-07	0.12E-07	0.15	7.84E-07	0.12E-07	0.15
19.0	[0, 1, 3]	3.61E-06	7.08E-07	0.14E-07	0.20	6.81E-07	0.12E-07	0.19	6.67E-07	0.12E-07	0.18
19.9	[1, 1, 3]	2.47E-06	6.48E-07	0.14E-07	0.26	6.05E-07	0.11E-07	0.24	6.10E-07	0.11E-07	0.25
20.8	[2, 2, 2]	1.51E-06	5.88E-07	0.24E-07	0.39	5.59E-07	0.19E-07	0.37	5.38E-07	0.18E-07	0.36
21.6	[0, 2, 3]	1.16E-06	5.20E-07	0.12E-07	0.45	4.99E-07	0.11E-07	0.43	4.91E-07	0.10E-07	0.42
22.4	[1, 2, 3]	9.64E-07	4.74E-07	0.08E-07	0.49	4.58E-07	0.07E-07	0.48	4.55E-07	0.07E-07	0.47
24.0	[0, 0, 4]	3.61E-07	3.92E-07	0.20E-07	1.09	4.00E-07	0.19E-07	1.11	3.78E-07	0.17E-07	1.05
24.7	[2, 2, 3]; [0, 1, 4]	4.72E-07	3.84E-07	0.07E-07	0.81	3.64E-07	0.06E-07	0.77	3.61E-07	0.06E-07	0.76
25.5	[1, 1, 4]; [0, 3, 3]	4.60E-07	3.67E-07	0.09E-07	0.80	3.51E-07	0.07E-07	0.76	3.42E-07	0.07E-07	0.74
26.2	[1, 3, 3]	5.01E-07	3.36E-07	0.10E-07	0.67	3.31E-07	0.09E-07	0.66	3.22E-07	0.09E-07	0.64
26.8	[0, 2, 4]	4.55E-07	3.18E-07	0.10E-07	0.70	3.03E-07	0.08E-07	0.66	3.05E-07	0.08E-07	0.67
27.5	[1, 2, 4]	4.33E-07	2.96E-07	0.06E-07	0.68	2.91E-07	0.06E-07	0.67	2.89E-07	0.06E-07	0.67
28.1	[2, 3, 3]	3.74E-07	2.85E-07	0.09E-07	0.76	2.67E-07	0.08E-07	0.71	2.75E-07	0.08E-07	0.74
29.4	[2, 2, 4]	3.58E-07	2.59E-07	0.09E-07	0.72	2.45E-07	0.07E-07	0.68	2.49E-07	0.07E-07	0.70
30.0	[0, 3, 4]; [0, 0, 5]	3.87E-07	2.54E-07	0.08E-07	0.66	2.38E-07	0.07E-07	0.62	2.27E-07	0.06E-07	0.59
30.6	[0, 1, 5]; [1, 3, 4]	3.08E-07	2.42E-07	0.05E-07	0.78	2.27E-07	0.04E-07	0.73	2.28E-07	0.04E-07	0.74
31.2	[1, 1, 5]; [3, 3, 3]	3.56E-07	2.26E-07	0.07E-07	0.64	2.22E-07	0.06E-07	0.62	2.15E-07	0.06E-07	0.60
32.3	[2, 3, 4]; [0, 2, 5]	2.28E-07	2.09E-07	0.05E-07	0.92	2.05E-07	0.04E-07	0.90	1.99E-07	0.04E-07	0.87
32.9	[1, 2, 5]	2.64E-07	2.04E-07	0.06E-07	0.77	1.94E-07	0.05E-07	0.74	1.95E-07	0.05E-07	0.74
33.9	[0, 4, 4]	1.91E-07	1.91E-07	0.10E-07	1.00	1.79E-07	0.09E-07	0.94	1.74E-07	0.09E-07	0.91
34.5	[1, 4, 4]; [2, 2, 5]	2.70E-07	1.80E-07	0.05E-07	0.67	1.76E-07	0.04E-07	0.65	1.74E-07	0.04E-07	0.64
35.0	[0, 3, 5]; [3, 3, 4]	2.40E-07	1.77E-07	0.05E-07	0.74	1.68E-07	0.04E-07	0.70	1.68E-07	0.04E-07	0.70
35.5	[1, 3, 5]	2.04E-07	1.76E-07	0.05E-07	0.86	1.65E-07	0.05E-07	0.81	1.62E-07	0.04E-07	0.80
36.0	[2, 4, 4]	2.69E-07	1.61E-07	0.07E-07	0.60	1.60E-07	0.06E-07	0.59	1.62E-07	0.06E-07	0.60
37.0	[2, 3, 5]	1.67E-07	1.57E-07	0.05E-07	0.94	1.52E-07	0.04E-07	0.91	1.48E-07	0.04E-07	0.89
38.4	[3, 4, 4]; [0, 4, 5]	2.18E-07	1.44E-07	0.05E-07	0.66	1.41E-07	0.04E-07	0.65	1.42E-07	0.04E-07	0.65
38.9	[1, 4, 5]	2.15E-07	1.40E-07	0.05E-07	0.65	1.38E-07	0.04E-07	0.64	1.28E-07	0.04E-07	0.60
39.3	[3, 3, 5]	1.29E-07	1.39E-07	0.07E-07	1.07	1.29E-07	0.05E-07	1.00	1.28E-07	0.05E-07	0.99
40.2	[2, 4, 5]	1.75E-07	1.26E-07	0.04E-07	0.72	1.24E-07	0.04E-07	0.71	1.22E-07	0.04E-07	0.70
41.6	[4, 4, 4]	1.52E-07	1.20E-07	0.10E-07	0.79	1.20E-07	0.09E-07	0.79	1.17E-07	0.09E-07	0.77
42.4	[0, 5, 5]; [3, 4, 5]	1.31E-07	1.18E-07	0.04E-07	0.90	1.11E-07	0.03E-07	0.84	1.09E-07	0.03E-07	0.83
42.8	[1, 5, 5]	1.93E-07	1.17E-07	0.06E-07	0.60	1.12E-07	0.05E-07	0.58	1.06E-07	0.05E-07	0.55
44.1	[2, 5, 5]	1.56E-07	1.06E-07	0.06E-07	0.68	1.01E-07	0.05E-07	0.65	1.02E-07	0.05E-07	0.65
45.3	[4, 4, 5]	1.34E-07	9.84E-08	0.52E-08	0.73	9.77E-08	0.49E-08	0.73	9.67E-08	0.47E-08	0.72
46.1	[3, 5, 5]	1.07E-07	9.95E-08	0.57E-08	0.93	9.14E-08	0.46E-08	0.85	8.90E-08	0.43E-08	0.83
48.7	[4, 5, 5]	8.57E-08	8.35E-08	0.50E-08	0.97	8.41E-08	0.44E-08	0.98	7.99E-08	0.41E-08	0.93
52.0	[5, 5, 5]	1.39E-07	7.46E-08	0.75E-08	0.54	7.50E-08	0.77E-08	0.54	6.75E-08	0.75E-08	0.49

Table B.11: S-values (mGy·MBq^{-1}·s^{-1}) for ^{177}Lu within cubical voxels of 3 mm and respective uncertainties.

Distance (mm)	Coordinates	PenNuc	PenNuc Uncertainty	DECDATA	DECDATA Uncertainty
0.0	[0, 0, 0]	7.73E-01	0.00E-01	7.80E-01	0.00E-01
3.0	[0, 0, 1]	1.61E-02	0.00E-02	1.64E-02	0.00E-02
4.2	[0, 1, 1]	6.52E-04	0.02E-04	6.75E-04	0.03E-04
5.2	[1, 1, 1]	7.79E-05	0.06E-05	8.25E-05	0.11E-05
6.0	[0, 0, 2]	3.92E-05	0.04E-05	4.06E-05	0.06E-05
6.7	[0, 1, 2]	3.10E-05	0.02E-05	3.24E-05	0.02E-05
7.3	[1, 1, 2]	2.58E-05	0.02E-05	2.68E-05	0.02E-05
8.5	[0, 2, 2]	1.95E-05	0.02E-05	2.00E-05	0.03E-05
9.0	[1, 2, 2]; [0, 0, 3]	1.72E-05	0.01E-05	1.79E-05	0.02E-05
9.5	[0, 1, 3]	1.54E-05	0.01E-05	1.60E-05	0.02E-05
9.9	[1, 1, 3]	1.40E-05	0.01E-05	1.47E-05	0.02E-05
10.4	[2, 2, 2]	1.29E-05	0.02E-05	1.33E-05	0.03E-05
10.8	[0, 2, 3]	1.19E-05	0.01E-05	1.24E-05	0.02E-05
11.2	[1, 2, 3]	1.11E-05	0.01E-05	1.15E-05	0.01E-05
12.0	[0, 0, 4]	9.60E-06	0.20E-06	1.01E-05	0.03E-05
12.4	[2, 2, 3]; [0, 1, 4]	9.20E-06	0.07E-06	9.52E-06	0.09E-06
12.7	[1, 1, 4]; [0, 3, 3]	8.68E-06	0.08E-06	8.94E-06	0.10E-06
13.1	[1, 3, 3]	8.33E-06	0.09E-06	8.52E-06	0.12E-06
13.4	[0, 2, 4]	7.78E-06	0.09E-06	8.14E-06	0.12E-06
13.7	[1, 2, 4]	7.53E-06	0.06E-06	7.75E-06	0.08E-06
14.1	[2, 3, 3]	7.14E-06	0.09E-06	7.45E-06	0.12E-06
14.7	[2, 2, 4]	6.53E-06	0.08E-06	6.76E-06	0.11E-06
15.0	[0, 3, 4]; [0, 0, 5]	6.36E-06	0.07E-06	6.49E-06	0.10E-06
15.3	[0, 1, 5]; [1, 3, 4]	6.12E-06	0.05E-06	6.33E-06	0.06E-06
15.6	[1, 1, 5]; [3, 3, 3]	5.90E-06	0.07E-06	6.09E-06	0.09E-06
16.2	[2, 3, 4]; [0, 2, 5]	5.47E-06	0.04E-06	5.69E-06	0.06E-06
16.4	[1, 2, 5]	5.31E-06	0.05E-06	5.53E-06	0.07E-06
17.0	[0, 4, 4]	4.94E-06	0.10E-06	5.11E-06	0.13E-06
17.2	[1, 4, 4]; [2, 2, 5]	4.88E-06	0.05E-06	5.05E-06	0.07E-06
17.5	[0, 3, 5]; [3, 3, 4]	4.71E-06	0.05E-06	4.88E-06	0.07E-06
17.7	[1, 3, 5]	4.61E-06	0.05E-06	4.77E-06	0.07E-06
18.0	[2, 4, 4]	4.46E-06	0.07E-06	4.67E-06	0.09E-06
18.5	[2, 3, 5]	4.21E-06	0.05E-06	4.39E-06	0.06E-06
19.2	[3, 4, 4]; [0, 4, 5]	3.93E-06	0.04E-06	4.15E-06	0.06E-06
19.4	[1, 4, 5]	3.85E-06	0.04E-06	4.00E-06	0.06E-06
19.7	[3, 3, 5]	3.75E-06	0.06E-06	3.88E-06	0.08E-06
20.1	[2, 4, 5]	3.62E-06	0.04E-06	3.73E-06	0.06E-06
20.8	[4, 4, 4]	3.43E-06	0.10E-06	3.52E-06	0.14E-06
21.2	[0, 5, 5]; [3, 4, 5]	3.24E-06	0.04E-06	3.36E-06	0.05E-06
21.4	[1, 5, 5]	3.18E-06	0.06E-06	3.36E-06	0.08E-06
22.0	[2, 5, 5]	3.03E-06	0.05E-06	3.10E-06	0.07E-06
22.6	[4, 4, 5]	2.87E-06	0.05E-06	2.99E-06	0.07E-06
23.0	[3, 5, 5]	2.80E-06	0.05E-06	2.93E-06	0.07E-06
24.4	[4, 5, 5]	2.50E-06	0.05E-06	2.62E-06	0.07E-06
26.0	[5, 5, 5]	2.27E-06	0.08E-06	2.28E-06	0.10E-06

Table B.12: S-values (mGy·MBq^{-1}·s^{-1}) for ^{177}Lu within cubical voxels of 6 mm and respective uncertainties.

Distance (mm)	Coordinates	PenNuc	PenNuc Uncertainty	DECDATA	DECDATA Uncertainty
0.0	[0, 0, 0]	1.03E-01	0.00E-01	1.04E-01	0.00E-01
6.0	[0, 0, 1]	1.11E-03	0.00E-03	1.13E-03	0.00E-03
8.5	[0, 1, 1]	3.97E-05	0.01E-05	4.12E-05	0.02E-05
10.4	[1, 1, 1]	1.41E-05	0.01E-05	1.47E-05	0.01E-05
12.0	[0, 0, 2]	9.95E-06	0.07E-06	1.04E-05	0.01E-05
13.4	[0, 1, 2]	8.05E-06	0.03E-06	8.33E-06	0.04E-06
14.7	[1, 1, 2]	6.75E-06	0.03E-06	6.96E-06	0.04E-06
17.0	[0, 2, 2]	5.07E-06	0.04E-06	5.26E-06	0.05E-06
18.0	[1, 2, 2]; [0, 0, 3]	4.52E-06	0.02E-06	4.67E-06	0.03E-06
19.0	[0, 1, 3]	4.07E-06	0.02E-06	4.23E-06	0.03E-06
19.9	[1, 1, 3]	3.73E-06	0.02E-06	3.85E-06	0.03E-06
20.8	[2, 2, 2]	3.42E-06	0.04E-06	3.54E-06	0.05E-06
21.6	[0, 2, 3]	3.16E-06	0.02E-06	3.31E-06	0.03E-06
22.4	[1, 2, 3]	2.96E-06	0.01E-06	3.07E-06	0.02E-06
24.0	[0, 0, 4]	2.61E-06	0.04E-06	2.72E-06	0.05E-06
24.7	[2, 2, 3]; [0, 1, 4]	2.46E-06	0.01E-06	2.56E-06	0.02E-06
25.5	[1, 1, 4]; [0, 3, 3]	2.32E-06	0.01E-06	2.41E-06	0.02E-06
26.2	[1, 3, 3]	2.21E-06	0.02E-06	2.29E-06	0.02E-06
26.8	[0, 2, 4]	2.11E-06	0.02E-06	2.21E-06	0.02E-06
27.5	[1, 2, 4]	2.01E-06	0.01E-06	2.08E-06	0.01E-06
28.1	[2, 3, 3]	1.94E-06	0.02E-06	2.00E-06	0.02E-06
29.4	[2, 2, 4]	1.77E-06	0.01E-06	1.84E-06	0.02E-06
30.0	[0, 3, 4]; [0, 0, 5]	1.70E-06	0.01E-06	1.77E-06	0.02E-06
30.6	[0, 1, 5]; [1, 3, 4]	1.64E-06	0.01E-06	1.70E-06	0.01E-06
31.2	[1, 1, 5]; [3, 3, 3]	1.58E-06	0.01E-06	1.64E-06	0.02E-06
32.3	[2, 3, 4]; [0, 2, 5]	1.47E-06	0.01E-06	1.53E-06	0.01E-06
32.9	[1, 2, 5]	1.44E-06	0.01E-06	1.49E-06	0.01E-06
33.9	[0, 4, 4]	1.33E-06	0.02E-06	1.41E-06	0.02E-06
34.5	[1, 4, 4]; [2, 2, 5]	1.31E-06	0.01E-06	1.36E-06	0.01E-06
35.0	[0, 3, 5]; [3, 3, 4]	1.27E-06	0.01E-06	1.32E-06	0.01E-06
35.5	[1, 3, 5]	1.24E-06	0.01E-06	1.29E-06	0.01E-06
36.0	[2, 4, 4]	1.21E-06	0.01E-06	1.24E-06	0.02E-06
37.0	[2, 3, 5]	1.14E-06	0.01E-06	1.19E-06	0.01E-06
38.4	[3, 4, 4]; [0, 4, 5]	1.07E-06	0.01E-06	1.11E-06	0.01E-06
38.9	[1, 4, 5]	1.04E-06	0.01E-06	1.08E-06	0.01E-06
39.3	[3, 3, 5]	1.02E-06	0.01E-06	1.06E-06	0.01E-06
40.2	[2, 4, 5]	9.84E-07	0.08E-07	1.01E-06	0.01E-06
41.6	[4, 4, 4]	9.19E-07	0.18E-07	9.39E-07	0.24E-07
42.4	[0, 5, 5]; [3, 4, 5]	8.84E-07	0.06E-07	9.12E-07	0.09E-07
42.8	[1, 5, 5]	8.66E-07	0.10E-07	8.98E-07	0.13E-07
44.1	[2, 5, 5]	8.15E-07	0.10E-07	8.70E-07	0.13E-07
45.3	[4, 4, 5]	7.72E-07	0.09E-07	8.08E-07	0.13E-07
46.1	[3, 5, 5]	7.55E-07	0.09E-07	7.79E-07	0.12E-07
48.7	[4, 5, 5]	6.78E-07	0.09E-07	7.17E-07	0.12E-07
52.0	[5, 5, 5]	5.96E-07	0.14E-07	6.27E-07	0.19E-07

Table B.13: S-values (mGy·MBq^{-1}·s^{-1}) for ^{153}Sm within cubical voxels of 3 mm and respective uncertainties.

Distance (mm)	Coordinates	PenNuc	PenNuc Uncertainty	DECDATA	DECDATA Uncertainty
0.0	[0, 0, 0]	1.29E+00	0.00E+00	1.31E+00	0.00E+00
3.0	[0, 0, 1]	4.44E-02	0.00E-02	4.47E-02	0.00E-02
4.2	[0, 1, 1]	3.12E-03	0.01E-03	3.16E-03	0.01E-03
5.2	[1, 1, 1]	3.70E-04	0.02E-04	3.82E-04	0.04E-04
6.0	[0, 0, 2]	9.89E-05	0.05E-05	1.04E-04	0.02E-04
6.7	[0, 1, 2]	7.96E-05	0.02E-05	8.33E-05	0.07E-05
7.3	[1, 1, 2]	6.69E-05	0.02E-05	7.02E-05	0.07E-05
8.5	[0, 2, 2]	5.03E-05	0.03E-05	5.34E-05	0.08E-05
9.0	[1, 2, 2]; [0, 0, 3]	4.52E-05	0.02E-05	4.68E-05	0.05E-05
9.5	[0, 1, 3]	4.09E-05	0.02E-05	4.28E-05	0.05E-05
9.9	[1, 1, 3]	3.71E-05	0.02E-05	3.91E-05	0.05E-05
10.4	[2, 2, 2]	3.44E-05	0.03E-05	3.62E-05	0.08E-05
10.8	[0, 2, 3]	3.18E-05	0.01E-05	3.38E-05	0.05E-05
11.2	[1, 2, 3]	2.99E-05	0.01E-05	3.11E-05	0.03E-05
12.0	[0, 0, 4]	2.60E-05	0.03E-05	2.80E-05	0.09E-05
12.4	[2, 2, 3]; [0, 1, 4]	2.48E-05	0.01E-05	2.58E-05	0.03E-05
12.7	[1, 1, 4]; [0, 3, 3]	2.34E-05	0.01E-05	2.48E-05	0.03E-05
13.1	[1, 3, 3]	2.24E-05	0.01E-05	2.33E-05	0.04E-05
13.4	[0, 2, 4]	2.13E-05	0.01E-05	2.25E-05	0.04E-05
13.7	[1, 2, 4]	2.04E-05	0.01E-05	2.14E-05	0.03E-05
14.1	[2, 3, 3]	1.95E-05	0.01E-05	2.02E-05	0.03E-05
14.7	[2, 2, 4]	1.79E-05	0.01E-05	1.86E-05	0.03E-05
15.0	[0, 3, 4]; [0, 0, 5]	1.73E-05	0.01E-05	1.82E-05	0.03E-05
15.3	[0, 1, 5]; [1, 3, 4]	1.67E-05	0.01E-05	1.74E-05	0.02E-05
15.6	[1, 1, 5]; [3, 3, 3]	1.60E-05	0.01E-05	1.68E-05	0.03E-05
16.2	[2, 3, 4]; [0, 2, 5]	1.51E-05	0.01E-05	1.60E-05	0.02E-05
16.4	[1, 2, 5]	1.46E-05	0.01E-05	1.55E-05	0.02E-05
17.0	[0, 4, 4]	1.36E-05	0.01E-05	1.47E-05	0.04E-05
17.2	[1, 4, 4]; [2, 2, 5]	1.33E-05	0.01E-05	1.41E-05	0.02E-05
17.5	[0, 3, 5]; [3, 3, 4]	1.30E-05	0.01E-05	1.36E-05	0.02E-05
17.7	[1, 3, 5]	1.27E-05	0.01E-05	1.33E-05	0.02E-05
18.0	[2, 4, 4]	1.23E-05	0.01E-05	1.28E-05	0.03E-05
18.5	[2, 3, 5]	1.17E-05	0.01E-05	1.23E-05	0.02E-05
19.2	[3, 4, 4]; [0, 4, 5]	1.09E-05	0.01E-05	1.13E-05	0.02E-05
19.4	[1, 4, 5]	1.07E-05	0.01E-05	1.13E-05	0.02E-05
19.7	[3, 3, 5]	1.04E-05	0.01E-05	1.08E-05	0.03E-05
20.1	[2, 4, 5]	10.00E-06	0.06E-06	1.05E-05	0.02E-05
20.8	[4, 4, 4]	9.51E-06	0.14E-06	1.02E-05	0.04E-05
21.2	[0, 5, 5]; [3, 4, 5]	9.10E-06	0.05E-06	9.59E-06	0.15E-06
21.4	[1, 5, 5]	8.86E-06	0.08E-06	9.31E-06	0.24E-06
22.0	[2, 5, 5]	8.46E-06	0.07E-06	8.93E-06	0.23E-06
22.6	[4, 4, 5]	7.97E-06	0.07E-06	8.53E-06	0.23E-06
23.0	[3, 5, 5]	7.78E-06	0.07E-06	8.08E-06	0.22E-06
24.4	[4, 5, 5]	6.98E-06	0.07E-06	7.44E-06	0.21E-06
26.0	[5, 5, 5]	6.13E-06	0.11E-06	6.57E-06	0.34E-06

Table B.14: S-values ($mGy \cdot MBq^{-1} \cdot s^{-1}$) for ^{153}Sm within cubical voxels of 6 mm and respective uncertainties.

Distance (mm)	Coordinates	PenNuc	PenNuc Uncertainty	DECDATA	DECDATA Uncertainty
0.0	[0, 0, 0]	1.79E-01	0.00E-01	1.82E-01	0.00E-01
6.0	[0, 0, 1]	3.24E-03	0.00E-03	3.26E-03	0.00E-03
8.5	[0, 1, 1]	1.53E-04	0.00E-04	1.57E-04	0.01E-04
10.4	[1, 1, 1]	4.00E-05	0.01E-05	4.16E-05	0.04E-05
12.0	[0, 0, 2]	2.68E-05	0.01E-05	2.83E-05	0.03E-05
13.4	[0, 1, 2]	2.17E-05	0.00E-05	2.28E-05	0.01E-05
14.7	[1, 1, 2]	1.83E-05	0.00E-05	1.92E-05	0.01E-05
17.0	[0, 2, 2]	1.39E-05	0.00E-05	1.46E-05	0.02E-05
18.0	[1, 2, 2]; [0, 0, 3]	1.24E-05	0.00E-05	1.30E-05	0.01E-05
19.0	[0, 1, 3]	1.13E-05	0.00E-05	1.18E-05	0.01E-05
19.9	[1, 1, 3]	1.03E-05	0.00E-05	1.08E-05	0.01E-05
20.8	[2, 2, 2]	9.51E-06	0.05E-06	1.01E-05	0.02E-05
21.6	[0, 2, 3]	8.82E-06	0.03E-06	9.26E-06	0.08E-06
22.4	[1, 2, 3]	8.21E-06	0.02E-06	8.63E-06	0.06E-06
24.0	[0, 0, 4]	7.25E-06	0.05E-06	7.68E-06	0.15E-06
24.7	[2, 2, 3]; [0, 1, 4]	6.84E-06	0.02E-06	7.20E-06	0.05E-06
25.5	[1, 1, 4]; [0, 3, 3]	6.49E-06	0.02E-06	6.84E-06	0.06E-06
26.2	[1, 3, 3]	6.15E-06	0.02E-06	6.49E-06	0.07E-06
26.8	[0, 2, 4]	5.86E-06	0.02E-06	6.11E-06	0.07E-06
27.5	[1, 2, 4]	5.59E-06	0.02E-06	5.89E-06	0.05E-06
28.1	[2, 3, 3]	5.36E-06	0.02E-06	5.61E-06	0.06E-06
29.4	[2, 2, 4]	4.92E-06	0.02E-06	5.13E-06	0.06E-06
30.0	[0, 3, 4]; [0, 0, 5]	4.73E-06	0.02E-06	4.98E-06	0.06E-06
30.6	[0, 1, 5]; [1, 3, 4]	4.56E-06	0.01E-06	4.79E-06	0.03E-06
31.2	[1, 1, 5]; [3, 3, 3]	4.40E-06	0.02E-06	4.64E-06	0.05E-06
32.3	[2, 3, 4]; [0, 2, 5]	4.11E-06	0.01E-06	4.30E-06	0.03E-06
32.9	[1, 2, 5]	3.97E-06	0.01E-06	4.18E-06	0.04E-06
33.9	[0, 4, 4]	3.71E-06	0.02E-06	3.90E-06	0.08E-06
34.5	[1, 4, 4]; [2, 2, 5]	3.62E-06	0.01E-06	3.80E-06	0.04E-06
35.0	[0, 3, 5]; [3, 3, 4]	3.52E-06	0.01E-06	3.68E-06	0.04E-06
35.5	[1, 3, 5]	3.43E-06	0.01E-06	3.58E-06	0.04E-06
36.0	[2, 4, 4]	3.33E-06	0.02E-06	3.49E-06	0.05E-06
37.0	[2, 3, 5]	3.16E-06	0.01E-06	3.32E-06	0.04E-06
38.4	[3, 4, 4]; [0, 4, 5]	2.93E-06	0.01E-06	3.05E-06	0.03E-06
38.9	[1, 4, 5]	2.85E-06	0.01E-06	2.97E-06	0.03E-06
39.3	[3, 3, 5]	2.80E-06	0.02E-06	2.93E-06	0.05E-06
40.2	[2, 4, 5]	2.67E-06	0.01E-06	2.80E-06	0.03E-06
41.6	[4, 4, 4]	2.48E-06	0.02E-06	2.62E-06	0.08E-06
42.4	[0, 5, 5]; [3, 4, 5]	2.40E-06	0.01E-06	2.50E-06	0.03E-06
42.8	[1, 5, 5]	2.36E-06	0.01E-06	2.45E-06	0.04E-06
44.1	[2, 5, 5]	2.22E-06	0.01E-06	2.33E-06	0.04E-06
45.3	[4, 4, 5]	2.10E-06	0.01E-06	2.19E-06	0.04E-06
46.1	[3, 5, 5]	2.03E-06	0.01E-06	2.10E-06	0.04E-06
48.7	[4, 5, 5]	1.82E-06	0.01E-06	1.91E-06	0.04E-06
52.0	[5, 5, 5]	1.60E-06	0.02E-06	1.63E-06	0.06E-06

Table B.15: S-values (mGy·MBq^{-1}·s^{-1}) for ^{131}I, ^{177}Lu, ^{32}P, ^{153}Sm, ^{89}Sr, ^{99m}Tc and ^{90}Y within cubical voxels of 2.26 mm and respective uncertainties.

Distance (mm)	Coordinates	I-131	Uncertainty	Lu-177	Uncertainty	P-32	Uncertainty	Sm-153	Uncertainty	Sr-89	Uncertainty	Tc-99m	Uncertainty	Y-90	Uncertainty
0.0	[0, 0, 0]	2.08E+00	0.00E+00	1.75E+00	0.00E+00	3.01E+00	0.00E+00	2.87E+00	0.00E+00	2.91E+00	0.00E+00	2.19E-01	0.00E-01	2.85E+00	0.00E+00
2.3	[0, 0, 1]	9.24E-02	0.01E-02	4.82E-02	0.00E-02	5.15E-01	0.00E-01	1.26E-01	0.00E-01	4.46E-01	0.00E-01	3.30E-03	0.02E-03	5.43E-01	0.00E-01
3.2	[0, 1, 1]	1.01E-02	0.00E-02	2.52E-03	0.01E-03	1.70E-01	0.00E-01	1.19E-02	0.00E-02	1.35E-01	0.00E-01	6.20E-04	0.05E-04	2.17E-01	0.00E-01
3.9	[1, 1, 1]	4.24E-03	0.04E-03	2.43E-04	0.03E-04	7.30E-02	0.01E-02	1.56E-03	0.01E-03	5.26E-02	0.01E-02	3.81E-04	0.04E-04	1.16E-01	0.00E-01
4.5	[0, 0, 2]	1.78E-03	0.01E-03	6.99E-05	0.11E-05	3.26E-02	0.00E-02	1.85E-04	0.04E-04	2.06E-02	0.00E-02	2.72E-04	0.03E-04	6.86E-02	0.01E-02
5.1	[0, 1, 2]	1.76E-03	0.01E-03	5.69E-05	0.05E-05	1.69E-02	0.00E-02	1.44E-04	0.02E-04	9.52E-03	0.01E-03	2.18E-04	0.02E-04	4.52E-02	0.00E-02
5.5	[1, 1, 2]	1.77E-03	0.01E-03	4.67E-05	0.05E-05	8.91E-03	0.01E-03	1.20E-04	0.01E-04	4.41E-03	0.01E-03	1.80E-04	0.01E-04	3.08E-02	0.00E-02
6.4	[0, 2, 2]	1.13E-03	0.01E-03	3.51E-05	0.06E-05	2.44E-03	0.01E-03	9.16E-05	0.17E-05	8.72E-04	0.05E-04	1.33E-04	0.02E-04	1.49E-02	0.00E-02
6.8	[1, 2, 2]; [0, 0, 3]	1.13E-03	0.01E-03	3.13E-05	0.03E-05	1.27E-03	0.00E-03	8.03E-05	0.10E-05	3.75E-04	0.02E-04	1.18E-04	0.01E-04	1.05E-02	0.00E-02
7.1	[0, 1, 3]	8.26E-04	0.16E-04	2.79E-05	0.04E-05	6.17E-04	0.03E-04	7.25E-05	0.10E-05	1.36E-04	0.01E-04	1.06E-04	0.01E-04	7.43E-03	0.01E-03
7.5	[1, 1, 3]	8.20E-04	0.08E-04	2.54E-05	0.03E-05	3.20E-04	0.02E-04	6.66E-05	0.10E-05	5.81E-05	0.08E-05	9.75E-05	0.10E-05	5.30E-03	0.01E-03
7.8	[2, 2, 2]	8.07E-04	0.16E-04	2.33E-05	0.06E-05	1.76E-04	0.03E-04	5.99E-05	0.16E-05	3.16E-05	0.11E-05	8.82E-05	0.17E-05	3.77E-03	0.01E-03
8.1	[0, 2, 3]	6.52E-04	0.07E-04	2.16E-05	0.03E-05	8.05E-05	0.11E-05	5.69E-05	0.09E-05	1.05E-05	0.03E-05	8.12E-05	0.09E-05	2.66E-03	0.01E-03
8.5	[1, 2, 3]	6.47E-04	0.07E-04	2.00E-05	0.02E-05	4.00E-05	0.05E-05	5.27E-05	0.06E-05	5.27E-06	0.14E-06	7.56E-05	0.06E-05	1.88E-03	0.00E-03
9.0	[0, 0, 4]	6.53E-04	0.05E-04	1.74E-05	0.06E-05	7.63E-06	0.53E-06	4.55E-05	0.16E-05	1.92E-06	0.13E-06	6.46E-05	0.16E-05	9.00E-04	0.08E-04
9.3	[2, 2, 3]; [0, 1, 4]	6.50E-04	0.07E-04	1.65E-05	0.02E-05	5.27E-06	0.15E-06	4.36E-05	0.06E-05	1.81E-06	0.05E-06	6.21E-05	0.06E-05	6.32E-04	0.02E-04
9.6	[1, 1, 4]; [0, 3, 3]	6.55E-04	0.07E-04	1.57E-05	0.02E-05	3.17E-06	0.11E-06	4.21E-05	0.07E-05	1.66E-06	0.05E-06	5.84E-05	0.06E-05	4.32E-04	0.02E-04
9.9	[1, 3, 3]	5.36E-04	0.06E-04	1.47E-05	0.03E-05	2.52E-06	0.11E-06	4.01E-05	0.08E-05	1.52E-06	0.06E-06	5.50E-05	0.08E-05	2.97E-04	0.02E-04
10.1	[0, 2, 4]	5.39E-04	0.05E-04	1.41E-05	0.02E-05	1.96E-06	0.08E-06	3.83E-05	0.08E-05	1.37E-06	0.05E-06	5.25E-05	0.07E-05	1.99E-04	0.02E-04
10.4	[1, 2, 4]	5.39E-04	0.05E-04	1.33E-05	0.02E-05	1.72E-06	0.05E-06	3.61E-05	0.05E-05	1.32E-06	0.04E-06	4.96E-05	0.05E-05	1.35E-04	0.01E-04
10.6	[2, 3, 3]	5.41E-04	0.06E-04	1.25E-05	0.02E-05	1.61E-06	0.06E-06	3.44E-05	0.07E-05	1.20E-06	0.05E-06	4.80E-05	0.07E-05	9.03E-05	0.12E-05
11.1	[2, 2, 4]	4.04E-04	0.06E-04	1.17E-05	0.02E-05	1.42E-06	0.06E-06	3.11E-05	0.07E-05	1.14E-06	0.05E-06	4.37E-05	0.07E-05	3.88E-05	0.08E-05
11.3	[0, 3, 4]; [0, 0, 5]	3.99E-04	0.06E-04	1.14E-05	0.02E-05	1.38E-06	0.05E-06	3.11E-05	0.06E-05	1.05E-06	0.04E-06	4.20E-05	0.06E-05	2.49E-05	0.05E-05
11.5	[0, 1, 5]; [1, 3, 4]	4.04E-04	0.06E-04	1.09E-05	0.01E-05	1.29E-06	0.03E-06	2.95E-05	0.04E-05	1.02E-06	0.03E-06	4.03E-05	0.04E-05	1.62E-05	0.03E-05
11.7	[1, 1, 5]; [3, 3, 3]	3.48E-04	0.10E-04	1.05E-05	0.02E-05	1.24E-06	0.05E-06	2.85E-05	0.06E-05	9.82E-07	0.39E-07	3.87E-05	0.05E-05	1.03E-05	0.03E-05
12.2	[2, 3, 4]; [0, 2, 5]	3.57E-04	0.04E-04	9.73E-06	0.12E-06	1.13E-06	0.03E-06	2.69E-05	0.04E-05	9.05E-07	0.25E-07	3.65E-05	0.04E-05	5.04E-06	0.13E-06
12.4	[1, 2, 5]	3.55E-04	0.05E-04	9.43E-06	0.14E-06	1.05E-06	0.04E-06	2.57E-05	0.04E-05	8.61E-07	0.30E-07	3.51E-05	0.04E-05	3.45E-06	0.12E-06
12.8	[0, 4, 4]	3.59E-04	0.05E-04	8.94E-06	0.28E-06	9.72E-07	0.62E-07	2.47E-05	0.09E-05	7.84E-07	0.64E-07	3.32E-05	0.08E-05	2.48E-06	0.18E-06
13.0	[1, 4, 4]; [2, 2, 5]	3.62E-04	0.05E-04	8.53E-06	0.13E-06	9.70E-07	0.34E-07	2.36E-05	0.04E-05	7.67E-07	0.29E-07	3.16E-05	0.04E-05	1.90E-06	0.07E-06
13.2	[0, 3, 5]; [3, 3, 4]	3.58E-04	0.04E-04	8.40E-06	0.13E-06	9.17E-07	0.33E-07	2.28E-05	0.04E-05	7.23E-07	0.27E-07	3.07E-05	0.04E-05	1.73E-06	0.06E-06
13.4	[1, 3, 5]	3.59E-04	0.11E-04	8.13E-06	0.13E-06	8.77E-07	0.31E-07	2.25E-05	0.04E-05	6.99E-07	0.26E-07	2.99E-05	0.04E-05	1.61E-06	0.05E-06
13.6	[2, 4, 4]	3.23E-04	0.05E-04	7.91E-06	0.18E-06	8.99E-07	0.47E-07	2.17E-05	0.06E-05	7.03E-07	0.40E-07	2.89E-05	0.06E-05	1.52E-06	0.08E-06
13.9	[2, 3, 5]	3.21E-04	0.05E-04	7.41E-06	0.12E-06	8.09E-07	0.32E-07	2.07E-05	0.04E-05	6.65E-07	0.28E-07	2.73E-05	0.04E-05	1.37E-06	0.05E-06
14.5	[3, 4, 4]; [0, 4, 5]	3.19E-04	0.04E-04	7.05E-06	0.12E-06	7.64E-07	0.32E-07	1.92E-05	0.04E-05	5.76E-07	0.24E-07	2.54E-05	0.04E-05	1.30E-06	0.05E-06
14.6	[1, 4, 5]	3.21E-04	0.05E-04	6.88E-06	0.12E-06	7.14E-07	0.30E-07	1.88E-05	0.04E-05	5.59E-07	0.24E-07	2.47E-05	0.04E-05	1.24E-06	0.04E-06
14.8	[3, 3, 5]	3.23E-04	0.05E-04	6.63E-06	0.17E-06	6.66E-07	0.40E-07	1.86E-05	0.05E-05	5.65E-07	0.35E-07	2.41E-05	0.05E-05	1.17E-06	0.06E-06
15.2	[2, 4, 5]	2.94E-04	0.05E-04	6.37E-06	0.11E-06	6.74E-07	0.30E-07	1.76E-05	0.04E-05	5.50E-07	0.27E-07	2.31E-05	0.03E-05	1.14E-06	0.05E-06
15.7	[4, 4, 4]	2.93E-04	0.03E-04	6.09E-06	0.28E-06	6.73E-07	0.77E-07	1.57E-05	0.08E-05	4.85E-07	0.50E-07	2.19E-05	0.08E-05	1.06E-06	0.12E-06
16.0	[0, 5, 5]; [3, 4, 5]	2.92E-04	0.03E-04	5.82E-06	0.10E-06	5.65E-07	0.24E-07	1.62E-05	0.03E-05	4.46E-07	0.19E-07	2.09E-05	0.03E-05	9.50E-07	0.35E-07
16.1	[1, 5, 5]	2.91E-04	0.05E-04	5.84E-06	0.16E-06	5.53E-07	0.36E-07	1.56E-05	0.05E-05	4.77E-07	0.42E-07	2.06E-05	0.05E-05	9.49E-07	0.55E-07
16.6	[2, 5, 5]	2.64E-04	0.04E-04	5.50E-06	0.15E-06	5.15E-07	0.36E-07	1.46E-05	0.05E-05	3.98E-07	0.27E-07	1.90E-05	0.04E-05	8.78E-07	0.50E-07
17.1	[4, 4, 5]	2.65E-04	0.05E-04	5.09E-06	0.14E-06	5.04E-07	0.39E-07	1.46E-05	0.05E-05	3.70E-07	0.25E-07	1.83E-05	0.04E-05	8.27E-07	0.50E-07
17.4	[3, 5, 5]	2.49E-04	0.04E-04	4.96E-06	0.14E-06	4.65E-07	0.31E-07	1.37E-05	0.04E-05	3.80E-07	0.28E-07	1.80E-05	0.04E-05	7.86E-07	0.49E-07
18.4	[4, 5, 5]	2.43E-04	0.04E-04	4.38E-06	0.13E-06	4.47E-07	0.33E-07	1.24E-05	0.04E-05	3.33E-07	0.26E-07	1.59E-05	0.04E-05	7.11E-07	0.48E-07
19.6	[5, 5, 5]	2.46E-04	0.03E-04	3.99E-06	0.22E-06	3.72E-07	0.52E-07	1.08E-05	0.07E-05	3.15E-07	0.45E-07	1.39E-05	0.07E-05	6.02E-07	0.74E-07

Table B.16: S-values (mGy·MBq^{-1}·s^{-1}) for ^{131}I, ^{177}Lu, ^{32}P, ^{153}Sm, ^{89}Sr, ^{99m}Tc and ^{90}Y within cubical voxels of 4.52 mm and respective uncertainties.

Distance (mm)	Coordinates	I-131	Uncertainty	Lu-177	Uncertainty	P-32	Uncertainty	Sm-153	Uncertainty	Sr-89	Uncertainty	Tc-99m	Uncertainty	Y-90	Uncertainty
0.0	[0, 0, 0]	3.23E-01	0.00E-01	2.53E-01	0.00E-01	7.12E-01	0.00E-01	4.11E-01	0.00E-01	5.89E-01	0.00E-01	2.89E-02	0.01E-02	6.56E-01	0.00E-01
4.5	[0, 0, 1]	3.48E-03	0.01E-03	9.45E-04	0.02E-04	6.04E-02	0.00E-02	9.57E-03	0.01E-03	5.36E-02	0.00E-02	4.45E-04	0.03E-04	9.40E-02	0.00E-02
6.4	[0, 1, 1]	4.87E-04	0.02E-04	4.80E-05	0.03E-05	9.57E-03	0.01E-03	4.99E-04	0.02E-04	7.77E-03	0.01E-03	1.48E-04	0.01E-04	2.45E-02	0.00E-02
7.8	[1, 1, 1]	2.82E-04	0.01E-04	2.48E-05	0.02E-05	1.78E-03	0.00E-03	8.48E-05	0.09E-05	1.32E-03	0.00E-03	9.41E-05	0.06E-05	7.90E-03	0.01E-03
9.0	[0, 0, 2]	2.05E-04	0.01E-04	1.80E-05	0.02E-05	1.30E-04	0.01E-04	4.75E-05	0.06E-05	4.13E-05	0.05E-05	6.74E-05	0.06E-05	2.24E-03	0.01E-03
10.1	[0, 1, 2]	1.64E-04	0.01E-04	1.44E-05	0.01E-05	2.60E-05	0.02E-05	3.86E-05	0.03E-05	8.11E-06	0.11E-06	5.42E-05	0.03E-05	8.17E-04	0.02E-04
11.1	[1, 1, 2]	1.35E-04	0.00E-04	1.19E-05	0.01E-05	5.86E-06	0.09E-06	3.23E-05	0.02E-05	2.24E-06	0.05E-06	4.47E-05	0.02E-05	2.92E-04	0.01E-04
12.8	[0, 2, 2]	1.01E-04	0.01E-04	9.01E-06	0.10E-06	1.07E-06	0.03E-06	2.49E-05	0.03E-05	8.00E-07	0.21E-07	3.34E-05	0.03E-05	2.92E-05	0.04E-05
13.6	[1, 2, 2]; [0, 0, 3]	8.97E-05	0.03E-05	8.03E-06	0.06E-06	8.96E-07	0.15E-07	2.21E-05	0.02E-05	7.00E-07	0.13E-07	2.95E-05	0.02E-05	9.23E-06	0.12E-06
14.3	[0, 1, 3]	8.05E-05	0.04E-05	7.25E-06	0.06E-06	7.67E-07	0.16E-07	2.01E-05	0.02E-05	6.22E-07	0.13E-07	2.66E-05	0.02E-05	2.30E-06	0.05E-06
15.0	[1, 1, 3]	7.30E-05	0.03E-05	6.57E-06	0.06E-06	6.77E-07	0.15E-07	1.82E-05	0.02E-05	5.56E-07	0.13E-07	2.40E-05	0.02E-05	1.41E-06	0.03E-06
15.7	[2, 2, 2]	6.69E-05	0.06E-05	6.03E-06	0.10E-06	6.22E-07	0.26E-07	1.67E-05	0.03E-05	4.86E-07	0.19E-07	2.19E-05	0.03E-05	1.24E-06	0.05E-06
16.3	[0, 2, 3]	6.19E-05	0.03E-05	5.63E-06	0.05E-06	5.57E-07	0.13E-07	1.56E-05	0.02E-05	4.53E-07	0.12E-07	2.04E-05	0.02E-05	9.76E-07	0.22E-07
16.9	[1, 2, 3]	5.72E-05	0.02E-05	5.25E-06	0.04E-06	5.06E-07	0.09E-07	1.46E-05	0.01E-05	4.20E-07	0.08E-07	1.89E-05	0.01E-05	8.81E-07	0.14E-07
18.1	[0, 0, 4]	5.01E-05	0.06E-05	4.53E-06	0.10E-06	4.44E-07	0.26E-07	1.29E-05	0.03E-05	3.43E-07	0.19E-07	1.67E-05	0.03E-05	7.46E-07	0.38E-07
18.6	[2, 2, 3]; [0, 1, 4]	4.71E-05	0.02E-05	4.34E-06	0.03E-06	4.07E-07	0.08E-07	1.22E-05	0.01E-05	3.26E-07	0.07E-07	1.55E-05	0.01E-05	6.99E-07	0.13E-07
19.2	[1, 1, 4]; [0, 3, 3]	4.45E-05	0.02E-05	4.12E-06	0.04E-06	3.87E-07	0.10E-07	1.15E-05	0.01E-05	3.02E-07	0.08E-07	1.45E-05	0.01E-05	6.63E-07	0.14E-07
19.7	[1, 3, 3]	4.19E-05	0.03E-05	3.91E-06	0.04E-06	3.59E-07	0.11E-07	1.11E-05	0.01E-05	2.76E-07	0.09E-07	1.40E-05	0.01E-05	6.27E-07	0.18E-07
20.2	[0, 2, 4]	4.01E-05	0.03E-05	3.71E-06	0.04E-06	3.34E-07	0.11E-07	1.04E-05	0.01E-05	2.72E-07	0.09E-07	1.34E-05	0.01E-05	5.70E-07	0.17E-07
20.7	[1, 2, 4]	3.81E-05	0.02E-05	3.55E-06	0.03E-06	3.20E-07	0.07E-07	1.00E-05	0.01E-05	2.56E-07	0.06E-07	1.26E-05	0.01E-05	5.56E-07	0.12E-07
21.2	[2, 3, 3]	3.65E-05	0.02E-05	3.40E-06	0.04E-06	3.09E-07	0.10E-07	9.57E-06	0.13E-06	2.41E-07	0.08E-07	1.19E-05	0.01E-05	5.06E-07	0.15E-07
22.1	[2, 2, 4]	3.36E-05	0.02E-05	3.12E-06	0.04E-06	2.70E-07	0.10E-07	8.81E-06	0.13E-06	2.20E-07	0.08E-07	1.12E-05	0.01E-05	4.70E-07	0.15E-07
22.6	[0, 3, 4]; [0, 0, 5]	3.20E-05	0.02E-05	3.01E-06	0.04E-06	2.57E-07	0.09E-07	8.60E-06	0.11E-06	2.06E-07	0.07E-07	1.06E-05	0.01E-05	4.42E-07	0.13E-07
23.0	[0, 1, 5]; [1, 3, 4]	3.09E-05	0.01E-05	2.89E-06	0.02E-06	2.48E-07	0.05E-07	8.20E-06	0.07E-06	1.99E-07	0.05E-07	1.02E-05	0.01E-05	4.23E-07	0.08E-07
23.5	[1, 1, 5]; [3, 3, 3]	2.97E-05	0.02E-05	2.78E-06	0.03E-06	2.31E-07	0.08E-07	7.95E-06	0.10E-06	1.91E-07	0.07E-07	9.83E-06	0.10E-06	4.16E-07	0.13E-07
24.3	[2, 3, 4]; [0, 2, 5]	2.75E-05	0.01E-05	2.62E-06	0.02E-06	2.19E-07	0.05E-07	7.37E-06	0.07E-06	1.77E-07	0.04E-07	9.14E-06	0.06E-06	3.84E-07	0.08E-07
24.8	[1, 2, 5]	2.66E-05	0.01E-05	2.53E-06	0.03E-06	2.07E-07	0.06E-07	7.15E-06	0.08E-06	1.64E-07	0.05E-07	8.88E-06	0.08E-06	3.68E-07	0.10E-07
25.6	[0, 4, 4]	2.50E-05	0.03E-05	2.41E-06	0.05E-06	1.86E-07	0.11E-07	6.81E-06	0.16E-06	1.58E-07	0.10E-07	8.41E-06	0.15E-06	3.44E-07	0.18E-07
26.0	[1, 4, 4]; [2, 2, 5]	2.41E-05	0.01E-05	2.32E-06	0.02E-06	1.87E-07	0.06E-07	6.55E-06	0.08E-06	1.51E-07	0.05E-07	8.09E-06	0.07E-06	3.26E-07	0.09E-07
26.4	[0, 3, 5]; [3, 3, 4]	2.36E-05	0.01E-05	2.26E-06	0.02E-06	1.80E-07	0.06E-07	6.35E-06	0.08E-06	1.47E-07	0.05E-07	7.88E-06	0.07E-06	3.14E-07	0.09E-07
26.7	[1, 3, 5]	2.27E-05	0.01E-05	2.17E-06	0.02E-06	1.77E-07	0.06E-07	6.25E-06	0.07E-06	1.43E-07	0.05E-07	7.66E-06	0.07E-06	3.03E-07	0.08E-07
27.1	[2, 4, 4]	2.22E-05	0.02E-05	2.11E-06	0.03E-06	1.63E-07	0.07E-07	5.97E-06	0.10E-06	1.29E-07	0.06E-07	7.37E-06	0.10E-06	3.03E-07	0.13E-07
27.9	[2, 3, 5]	2.10E-05	0.01E-05	2.02E-06	0.02E-06	1.61E-07	0.05E-07	5.70E-06	0.07E-06	1.29E-07	0.04E-07	7.02E-06	0.07E-06	2.81E-07	0.08E-07
28.9	[3, 4, 4]; [0, 4, 5]	1.95E-05	0.01E-05	1.88E-06	0.02E-06	1.52E-07	0.05E-07	5.26E-06	0.07E-06	1.19E-07	0.04E-07	6.55E-06	0.07E-06	2.51E-07	0.08E-07
29.3	[1, 4, 5]	1.90E-05	0.01E-05	1.86E-06	0.02E-06	1.38E-07	0.05E-07	5.21E-06	0.07E-06	1.15E-07	0.04E-07	6.40E-06	0.06E-06	2.45E-07	0.08E-07
29.6	[3, 3, 5]	1.86E-05	0.02E-05	1.81E-06	0.03E-06	1.44E-07	0.08E-07	5.05E-06	0.10E-06	1.11E-07	0.06E-07	6.40E-06	0.09E-06	2.40E-07	0.11E-07
30.3	[2, 4, 5]	1.78E-05	0.01E-05	1.74E-06	0.02E-06	1.37E-07	0.05E-07	4.90E-06	0.07E-06	1.03E-07	0.04E-07	5.93E-06	0.06E-06	2.27E-07	0.08E-07
31.3	[4, 4, 4]	1.63E-05	0.03E-05	1.60E-06	0.05E-06	1.15E-07	0.10E-07	4.59E-06	0.16E-06	9.44E-08	0.92E-08	5.73E-06	0.15E-06	2.06E-07	0.18E-07
32.0	[0, 5, 5]; [3, 4, 5]	1.59E-05	0.01E-05	1.58E-06	0.02E-06	1.20E-07	0.04E-07	4.38E-06	0.06E-06	9.60E-08	0.36E-08	5.43E-06	0.05E-06	2.04E-07	0.07E-07
32.3	[1, 5, 5]	1.57E-05	0.02E-05	1.53E-06	0.03E-06	1.14E-07	0.06E-07	4.36E-06	0.09E-06	9.54E-08	0.55E-08	5.33E-06	0.08E-06	1.92E-07	0.09E-07
33.2	[2, 5, 5]	1.48E-05	0.02E-05	1.44E-06	0.03E-06	1.08E-07	0.07E-07	4.03E-06	0.08E-06	8.76E-08	0.57E-08	5.02E-06	0.08E-06	1.94E-07	0.10E-07
34.1	[4, 4, 5]	1.39E-05	0.01E-05	1.38E-06	0.03E-06	1.00E-07	0.06E-07	3.88E-06	0.08E-06	7.99E-08	0.48E-08	4.78E-06	0.08E-06	1.79E-07	0.10E-07
34.7	[3, 5, 5]	1.36E-05	0.01E-05	1.32E-06	0.02E-06	1.01E-07	0.07E-07	3.73E-06	0.08E-06	7.48E-08	0.46E-08	4.59E-06	0.08E-06	1.62E-07	0.09E-07
36.7	[4, 5, 5]	1.20E-05	0.01E-05	1.21E-06	0.02E-06	8.81E-08	0.60E-08	3.33E-06	0.07E-06	7.09E-08	0.47E-08	4.15E-06	0.07E-06	1.57E-07	0.09E-07
39.1	[5, 5, 5]	1.06E-05	0.02E-05	1.09E-06	0.04E-06	8.28E-08	1.07E-08	2.93E-06	0.13E-06	6.01E-08	0.69E-08	3.67E-06	0.12E-06	1.32E-07	0.14E-07

Table B.17: S-values (mGy·MBq^{-1}·s^{-1}) for ^{131}I, ^{177}Lu, ^{32}P, ^{153}Sm, ^{89}Sr, ^{99m}Tc and ^{90}Y within cubical voxels of 9.04 mm and respective uncertainties.

Distance (mm)	Coordinates	I-131	Uncertainty	Lu-177	Uncertainty	P-32	Uncertainty	Sm-153	Uncertainty	Sr-89	Uncertainty	Tc-99m	Uncertainty	Y-90	Uncertainty
0.0	[0, 0, 0]	4.02E-02	0.00E-02	3.11E-02	0.00E-02	1.10E-01	0.00E-01	5.51E-02	0.00E-02	9.67E-02	0.00E-02	3.84E-03	0.01E-03	1.27E-01	0.00E-01
9.0	[0, 0, 1]	6.62E-04	0.01E-04	2.37E-04	0.00E-04	5.82E-03	0.00E-03	6.91E-04	0.01E-04	4.41E-03	0.00E-03	8.63E-05	0.03E-05	9.95E-03	0.00E-03
12.8	[0, 1, 1]	1.18E-04	0.00E-04	1.24E-05	0.01E-05	4.32E-04	0.01E-04	3.98E-05	0.02E-05	2.86E-04	0.00E-04	3.68E-05	0.01E-05	1.16E-03	0.00E-03
15.7	[1, 1, 1]	7.12E-05	0.02E-05	6.47E-06	0.04E-06	3.68E-05	0.02E-05	1.80E-05	0.01E-05	2.12E-05	0.01E-05	2.35E-05	0.01E-05	1.53E-04	0.00E-04
18.1	[0, 0, 2]	5.15E-05	0.02E-05	4.68E-06	0.04E-06	4.66E-07	0.09E-07	1.32E-05	0.01E-05	3.66E-07	0.07E-07	1.70E-05	0.01E-05	1.13E-06	0.02E-06
20.2	[0, 1, 2]	4.11E-05	0.01E-05	3.82E-06	0.02E-06	3.52E-07	0.04E-07	1.07E-05	0.00E-05	2.81E-07	0.03E-07	1.36E-05	0.00E-05	6.41E-07	0.07E-07
22.1	[1, 1, 2]	3.41E-05	0.01E-05	3.20E-06	0.01E-06	2.87E-07	0.04E-07	8.99E-06	0.05E-06	2.27E-07	0.03E-07	1.13E-05	0.00E-05	4.96E-07	0.06E-07
25.6	[0, 2, 2]	2.55E-05	0.01E-05	2.42E-06	0.02E-06	1.99E-07	0.04E-07	6.86E-06	0.06E-06	1.59E-07	0.03E-07	8.50E-06	0.05E-06	3.46E-07	0.07E-07
27.1	[1, 2, 2]; [0, 0, 3]	2.25E-05	0.01E-05	2.16E-06	0.01E-06	1.75E-07	0.03E-07	6.10E-06	0.03E-06	1.37E-07	0.02E-07	7.53E-06	0.03E-06	3.03E-07	0.04E-07
28.6	[0, 1, 3]	2.02E-05	0.01E-05	1.95E-06	0.01E-06	1.55E-07	0.03E-07	5.48E-06	0.04E-06	1.23E-07	0.02E-07	6.79E-06	0.03E-06	2.67E-07	0.04E-07
30.0	[1, 1, 3]	1.83E-05	0.01E-05	1.78E-06	0.01E-06	1.37E-07	0.03E-07	4.99E-06	0.03E-06	1.11E-07	0.02E-07	6.19E-06	0.03E-06	2.42E-07	0.04E-07
31.3	[2, 2, 2]	1.69E-05	0.01E-05	1.65E-06	0.02E-06	1.23E-07	0.04E-07	4.58E-06	0.06E-06	9.43E-08	0.32E-08	5.75E-06	0.05E-06	2.17E-07	0.07E-07
32.6	[0, 2, 3]	1.55E-05	0.01E-05	1.53E-06	0.01E-06	1.15E-07	0.02E-07	4.27E-06	0.03E-06	9.01E-08	0.19E-08	5.27E-06	0.03E-06	2.01E-07	0.04E-07
33.8	[1, 2, 3]	1.44E-05	0.00E-05	1.41E-06	0.01E-06	1.05E-07	0.02E-07	3.97E-06	0.02E-06	8.47E-08	0.14E-08	4.92E-06	0.02E-06	1.85E-07	0.03E-07
36.2	[0, 0, 4]	1.26E-05	0.01E-05	1.25E-06	0.02E-06	8.97E-08	0.42E-08	3.50E-06	0.06E-06	7.22E-08	0.35E-08	4.30E-06	0.05E-06	1.56E-07	0.06E-07
37.3	[2, 2, 3]; [0, 1, 4]	1.18E-05	0.00E-05	1.18E-06	0.01E-06	8.37E-08	0.14E-08	3.27E-06	0.02E-06	6.79E-08	0.12E-08	4.06E-06	0.02E-06	1.50E-07	0.02E-07
38.4	[1, 1, 4]; [0, 3, 3]	1.11E-05	0.00E-05	1.12E-06	0.01E-06	7.90E-08	0.16E-08	3.09E-06	0.02E-06	6.32E-08	0.13E-08	3.88E-06	0.02E-06	1.39E-07	0.02E-07
39.4	[1, 3, 3]	1.05E-05	0.00E-05	1.06E-06	0.01E-06	7.50E-08	0.19E-08	2.93E-06	0.03E-06	5.92E-08	0.16E-08	3.69E-06	0.03E-06	1.34E-07	0.03E-07
40.4	[0, 2, 4]	9.95E-06	0.04E-06	10.00E-07	0.08E-07	7.11E-08	0.19E-08	2.79E-06	0.02E-06	5.51E-08	0.15E-08	3.50E-06	0.02E-06	1.25E-07	0.03E-07
41.4	[1, 2, 4]	9.52E-06	0.03E-06	9.63E-07	0.05E-07	6.66E-08	0.13E-08	2.66E-06	0.02E-06	5.32E-08	0.11E-08	3.34E-06	0.02E-06	1.17E-07	0.02E-07
42.4	[2, 3, 3]	9.08E-06	0.04E-06	9.21E-07	0.07E-07	6.23E-08	0.17E-08	2.51E-06	0.02E-06	4.89E-08	0.14E-08	3.20E-06	0.02E-06	1.11E-07	0.03E-07
44.3	[2, 2, 4]	8.28E-06	0.04E-06	8.56E-07	0.07E-07	5.66E-08	0.16E-08	2.32E-06	0.02E-06	4.44E-08	0.13E-08	2.92E-06	0.02E-06	9.98E-08	0.26E-08
45.2	[0, 3, 4]; [0, 0, 5]	7.97E-06	0.03E-06	8.16E-07	0.06E-07	5.50E-08	0.15E-08	2.22E-06	0.02E-06	4.31E-08	0.12E-08	2.83E-06	0.02E-06	9.68E-08	0.23E-08
46.1	[0, 1, 5]; [1, 3, 4]	7.68E-06	0.02E-06	7.86E-07	0.04E-07	5.22E-08	0.09E-08	2.14E-06	0.01E-06	4.14E-08	0.08E-08	2.74E-06	0.01E-06	9.28E-08	0.14E-08
47.0	[1, 1, 5]; [3, 3, 3]	7.36E-06	0.03E-06	7.52E-07	0.06E-07	4.96E-08	0.13E-08	2.07E-06	0.02E-06	3.94E-08	0.11E-08	2.62E-06	0.02E-06	8.92E-08	0.21E-08
48.7	[2, 3, 4]; [0, 2, 5]	6.84E-06	0.02E-06	7.11E-07	0.04E-07	4.66E-08	0.09E-08	1.91E-06	0.01E-06	3.66E-08	0.07E-08	2.46E-06	0.01E-06	8.30E-08	0.14E-08
49.5	[1, 2, 5]	6.62E-06	0.02E-06	6.80E-07	0.04E-07	4.43E-08	0.10E-08	1.83E-06	0.01E-06	3.42E-08	0.08E-08	2.38E-06	0.01E-06	7.97E-08	0.16E-08
51.1	[0, 4, 4]	6.17E-06	0.05E-06	6.44E-07	0.09E-07	4.23E-08	0.21E-08	1.70E-06	0.03E-06	3.28E-08	0.16E-08	2.25E-06	0.03E-06	7.54E-08	0.33E-08
51.9	[1, 4, 4]; [2, 2, 5]	6.00E-06	0.02E-06	6.23E-07	0.04E-07	4.02E-08	0.10E-08	1.67E-06	0.01E-06	3.12E-08	0.08E-08	2.19E-06	0.01E-06	7.19E-08	0.16E-08
52.7	[0, 3, 5]; [3, 3, 4]	5.84E-06	0.02E-06	6.11E-07	0.04E-07	3.93E-08	0.10E-08	1.61E-06	0.01E-06	3.10E-08	0.08E-08	2.12E-06	0.01E-06	7.13E-08	0.16E-08
53.5	[1, 3, 5]	5.65E-06	0.02E-06	5.91E-07	0.04E-07	3.78E-08	0.09E-08	1.55E-06	0.01E-06	2.97E-08	0.08E-08	2.07E-06	0.01E-06	6.76E-08	0.16E-08
54.2	[2, 4, 4]	5.49E-06	0.03E-06	5.76E-07	0.06E-07	3.64E-08	0.13E-08	1.51E-06	0.02E-06	2.88E-08	0.11E-08	2.01E-06	0.02E-06	6.45E-08	0.21E-08
55.7	[2, 3, 5]	5.20E-06	0.02E-06	5.45E-07	0.04E-07	3.36E-08	0.09E-08	1.43E-06	0.01E-06	2.77E-08	0.08E-08	1.91E-06	0.01E-06	6.15E-08	0.15E-08
57.9	[3, 4, 4]; [0, 4, 5]	4.81E-06	0.02E-06	5.08E-07	0.04E-07	3.16E-08	0.09E-08	1.31E-06	0.01E-06	2.46E-08	0.07E-08	1.78E-06	0.01E-06	5.73E-08	0.14E-08
58.6	[1, 4, 5]	4.68E-06	0.02E-06	4.92E-07	0.04E-07	2.95E-08	0.08E-08	1.30E-06	0.01E-06	2.43E-08	0.07E-08	1.73E-06	0.01E-06	5.57E-08	0.14E-08
59.3	[3, 3, 5]	4.60E-06	0.03E-06	4.84E-07	0.05E-07	2.86E-08	0.11E-08	1.25E-06	0.02E-06	2.36E-08	0.10E-08	1.69E-06	0.02E-06	5.44E-08	0.19E-08
60.6	[2, 4, 5]	4.36E-06	0.02E-06	4.61E-07	0.04E-07	2.78E-08	0.08E-08	1.19E-06	0.01E-06	2.19E-08	0.07E-08	1.63E-06	0.01E-06	5.21E-08	0.14E-08
62.6	[4, 4, 4]	4.09E-06	0.05E-06	4.40E-07	0.09E-07	2.65E-08	0.18E-08	1.10E-06	0.03E-06	1.98E-08	0.15E-08	1.50E-06	0.03E-06	5.00E-08	0.34E-08
63.9	[0, 5, 5]; [3, 4, 5]	3.92E-06	0.02E-06	4.15E-07	0.03E-07	2.46E-08	0.07E-08	1.06E-06	0.01E-06	1.98E-08	0.06E-08	1.47E-06	0.01E-06	4.60E-08	0.11E-08
64.6	[1, 5, 5]	3.83E-06	0.03E-06	4.06E-07	0.05E-07	2.44E-08	0.11E-08	1.03E-06	0.01E-06	1.99E-08	0.09E-08	1.44E-06	0.02E-06	4.46E-08	0.17E-08
66.4	[2, 5, 5]	3.61E-06	0.03E-06	3.83E-07	0.05E-07	2.36E-08	0.11E-08	9.63E-07	0.15E-07	1.75E-08	0.08E-08	1.36E-06	0.01E-06	4.17E-08	0.17E-08
68.3	[4, 4, 5]	3.42E-06	0.02E-06	3.68E-07	0.04E-07	2.11E-08	0.10E-08	9.13E-07	0.14E-07	1.70E-08	0.08E-08	1.29E-06	0.01E-06	3.87E-08	0.16E-08
69.4	[3, 5, 5]	3.29E-06	0.02E-06	3.50E-07	0.04E-07	2.07E-08	0.10E-08	8.77E-07	0.14E-07	1.61E-08	0.08E-08	1.26E-06	0.01E-06	3.85E-08	0.17E-08
73.4	[4, 5, 5]	2.94E-06	0.02E-06	3.14E-07	0.04E-07	1.84E-08	0.09E-08	7.65E-07	0.13E-07	1.44E-08	0.08E-08	1.13E-06	0.01E-06	3.31E-08	0.15E-08
78.3	[5, 5, 5]	2.57E-06	0.04E-06	2.80E-07	0.07E-07	1.54E-08	0.14E-08	6.63E-07	0.21E-07	1.16E-08	0.11E-08	9.92E-07	0.22E-07	2.94E-08	0.24E-08

Appendix C

Table C.1: Cellular S-values (mGy·MBq^{-1}·s^{-1}) for ^{67}Ga when the source and the target are the nucleus of the cell.

S (N<-N)								
Cell radii (µm)	Nucleus radii (µm)	Falzone	DECDATA	DECDATA Uncertainty	DECDATA / Falzone	PenNuc	PenNuc Uncertainty	PenNuc / Falzone
3.00	1.00	1.53E-01	1.57E-01	0.00E-01	1.03	9.62E-02	0.01E-02	0.63
3.00	2.00	2.57E-02	2.62E-02	0.00E-02	1.02	1.64E-02	0.00E-02	0.64
4.00	2.00	2.57E-02	2.62E-02	0.00E-02	1.02	1.64E-02	0.00E-02	0.64
4.00	3.00	8.45E-03	8.62E-03	0.01E-03	1.02	5.44E-03	0.00E-03	0.64
5.00	2.00	2.57E-02	2.62E-02	0.00E-02	1.02	1.64E-02	0.00E-02	0.64
5.00	3.00	8.45E-03	8.62E-03	0.01E-03	1.02	5.44E-03	0.00E-03	0.64
5.00	4.00	3.78E-03	3.86E-03	0.00E-03	1.02	2.44E-03	0.00E-03	0.65
6.00	3.00	8.45E-03	8.62E-03	0.01E-03	1.02	5.44E-03	0.00E-03	0.64
6.00	4.00	3.78E-03	3.86E-03	0.00E-03	1.02	2.44E-03	0.00E-03	0.65
6.00	5.00	2.02E-03	2.06E-03	0.00E-03	1.02	1.31E-03	0.00E-03	0.65
7.00	3.00	8.45E-03	8.62E-03	0.01E-03	1.02	5.44E-03	0.00E-03	0.64
7.00	4.00	3.78E-03	3.86E-03	0.00E-03	1.02	2.44E-03	0.00E-03	0.65
7.00	5.00	2.02E-03	2.06E-03	0.00E-03	1.02	1.31E-03	0.00E-03	0.65
7.00	6.00	1.21E-03	1.23E-03	0.00E-03	1.02	7.82E-04	0.01E-04	0.65
8.00	4.00	3.78E-03	3.86E-03	0.00E-03	1.02	2.44E-03	0.00E-03	0.65
8.00	5.00	2.02E-03	2.06E-03	0.00E-03	1.02	1.31E-03	0.00E-03	0.65
8.00	6.00	1.21E-03	1.23E-03	0.00E-03	1.02	7.83E-04	0.01E-04	0.65
8.00	7.00	7.83E-04	7.98E-04	0.01E-04	1.02	5.07E-04	0.00E-04	0.65
9.00	5.00	2.02E-03	2.06E-03	0.00E-03	1.02	1.31E-03	0.00E-03	0.65
9.00	6.00	1.21E-03	1.23E-03	0.00E-03	1.02	7.82E-04	0.01E-04	0.65
9.00	7.00	7.83E-04	7.98E-04	0.01E-04	1.02	5.07E-04	0.00E-04	0.65
9.00	8.00	5.38E-04	5.48E-04	0.01E-04	1.02	3.49E-04	0.00E-04	0.65
10.00	5.00	2.02E-03	2.06E-03	0.00E-03	1.02	1.31E-03	0.00E-03	0.65
10.00	6.00	1.21E-03	1.23E-03	0.00E-03	1.02	7.83E-04	0.01E-04	0.65
10.00	7.00	7.83E-04	7.99E-04	0.01E-04	1.02	5.07E-04	0.00E-04	0.65
10.00	8.00	5.38E-04	5.49E-04	0.01E-04	1.02	3.49E-04	0.00E-04	0.65
10.00	9.00	3.87E-04	3.94E-04	0.00E-04	1.02	2.51E-04	0.00E-04	0.65
11.00	5.00	2.02E-03	2.06E-03	0.00E-03	1.02	1.31E-03	0.00E-03	0.65
11.00	6.00	1.21E-03	1.23E-03	0.00E-03	1.02	7.83E-04	0.01E-04	0.65
11.00	7.00	7.83E-04	7.99E-04	0.01E-04	1.02	5.07E-04	0.00E-04	0.65
11.00	8.00	5.38E-04	5.49E-04	0.01E-04	1.02	3.49E-04	0.00E-04	0.65
11.00	9.00	3.87E-04	3.94E-04	0.00E-04	1.02	2.51E-04	0.00E-04	0.65
11.00	10.00	2.87E-04	2.94E-04	0.00E-04	1.02	1.87E-04	0.00E-04	0.65
12.00	6.00	1.21E-03	1.23E-03	0.00E-03	1.02	7.82E-04	0.01E-04	0.65
12.00	7.00	7.83E-04	7.98E-04	0.01E-04	1.02	5.07E-04	0.00E-04	0.65
12.00	8.00	5.38E-04	5.48E-04	0.01E-04	1.02	3.49E-04	0.00E-04	0.65
12.00	9.00	3.87E-04	3.94E-04	0.00E-04	1.02	2.51E-04	0.00E-04	0.65
12.00	10.00	2.88E-04	2.94E-04	0.00E-04	1.02	1.87E-04	0.00E-04	0.65
12.00	11.00	2.21E-04	2.25E-04	0.00E-04	1.02	1.44E-04	0.00E-04	0.65

Table C.2: Cellular S-values (mGy·MBq^{-1}·s^{-1}) for ^{67}Ga when the source is the cytoplasm and the target is the cell nucleus.

S (N<-Cy)								
Cell radii (µm)	**Nucleus radii (µm)**	**Falzone**	**DECDATA**	**DECDATA Uncertainty**	**DECDATA / Falzone**	**PenNuc**	**PenNuc Uncertainty**	**PenNuc / Falzone**
3.00	1.00	4.45E-03	4.59E-03	0.05E-03	1.03	3.06E-03	0.01E-03	0.69
3.00	2.00	3.21E-03	3.23E-03	0.01E-03	1.01	2.17E-03	0.00E-03	0.68
4.00	2.00	1.25E-03	1.28E-03	0.01E-03	1.02	8.48E-04	0.03E-04	0.68
4.00	3.00	1.19E-03	1.21E-03	0.00E-03	1.01	8.05E-04	0.02E-04	0.68
5.00	2.00	6.64E-04	6.62E-04	0.06E-04	1.00	4.41E-04	0.02E-04	0.66
5.00	3.00	5.33E-04	5.45E-04	0.03E-04	1.02	3.62E-04	0.01E-04	0.68
5.00	4.00	5.77E-04	5.87E-04	0.02E-04	1.02	3.92E-04	0.01E-04	0.68
6.00	3.00	3.13E-04	3.20E-04	0.02E-04	1.02	2.11E-04	0.01E-04	0.67
6.00	4.00	2.85E-04	2.92E-04	0.02E-04	1.02	1.93E-04	0.00E-04	0.68
6.00	5.00	3.28E-04	3.36E-04	0.01E-04	1.02	2.23E-04	0.00E-04	0.68
7.00	3.00	2.08E-04	2.11E-04	0.02E-04	1.01	1.40E-04	0.01E-04	0.67
7.00	4.00	1.80E-04	1.85E-04	0.01E-04	1.03	1.22E-04	0.00E-04	0.68
7.00	5.00	1.77E-04	1.78E-04	0.01E-04	1.01	1.19E-04	0.00E-04	0.67
7.00	6.00	2.10E-04	2.13E-04	0.01E-04	1.01	1.42E-04	0.00E-04	0.67
8.00	4.00	1.48E-04	1.30E-04	0.01E-04	0.88	8.61E-05	0.03E-05	0.58
8.00	5.00	1.34E-04	1.19E-04	0.01E-04	0.89	7.88E-05	0.02E-05	0.59
8.00	6.00	1.26E-04	1.20E-04	0.01E-04	0.95	7.92E-05	0.02E-05	0.63
8.00	7.00	1.43E-04	1.45E-04	0.00E-04	1.02	9.66E-05	0.02E-05	0.68
9.00	5.00	8.63E-05	8.82E-05	0.06E-05	1.02	5.81E-05	0.02E-05	0.67
9.00	6.00	8.11E-05	8.36E-05	0.05E-05	1.03	5.52E-05	0.02E-05	0.68
9.00	7.00	8.40E-05	8.52E-05	0.04E-05	1.01	5.65E-05	0.01E-05	0.67
9.00	8.00	1.03E-04	1.05E-04	0.00E-04	1.02	6.96E-05	0.01E-05	0.68
10.00	5.00	6.76E-05	6.82E-05	0.06E-05	1.01	4.54E-05	0.02E-05	0.67
10.00	6.00	6.23E-05	6.40E-05	0.04E-05	1.03	4.22E-05	0.01E-05	0.68
10.00	7.00	6.04E-05	6.16E-05	0.03E-05	1.02	4.07E-05	0.01E-05	0.67
10.00	8.00	6.30E-05	6.37E-05	0.03E-05	1.01	4.22E-05	0.01E-05	0.67
10.00	9.00	7.67E-05	7.88E-05	0.03E-05	1.03	5.21E-05	0.01E-05	0.68
11.00	5.00	5.42E-05	5.59E-05	0.05E-05	1.03	3.67E-05	0.02E-05	0.68
11.00	6.00	5.05E-05	5.16E-05	0.04E-05	1.02	3.37E-05	0.01E-05	0.67
11.00	7.00	4.80E-05	4.85E-05	0.03E-05	1.01	3.19E-05	0.01E-05	0.66
11.00	8.00	4.70E-05	4.76E-05	0.03E-05	1.01	3.14E-05	0.01E-05	0.67
11.00	9.00	4.89E-05	4.98E-05	0.02E-05	1.02	3.28E-05	0.01E-05	0.67
11.00	10.00	6.00E-05	6.10E-05	0.02E-05	1.02	4.04E-05	0.01E-05	0.67
12.00	6.00	4.18E-05	4.28E-05	0.04E-05	1.02	2.81E-05	0.01E-05	0.67
12.00	7.00	3.91E-05	3.99E-05	0.03E-05	1.02	2.63E-05	0.01E-05	0.67
12.00	8.00	3.71E-05	3.82E-05	0.02E-05	1.03	2.52E-05	0.01E-05	0.68
12.00	9.00	3.70E-05	3.79E-05	0.02E-05	1.02	2.50E-05	0.01E-05	0.67
12.00	10.00	3.87E-05	3.97E-05	0.02E-05	1.03	2.62E-05	0.01E-05	0.68
12.00	11.00	4.79E-05	4.87E-05	0.02E-05	1.02	3.22E-05	0.01E-05	0.67

Table C.3: Cellular S-values (mGy·MBq^{-1}·s^{-1}) for ^{123}I when the source and the target are the nucleus of the cell.

S (N<-N)								
Cell radii (µm)	**Nucleus radii (µm)**	**Falzone**	**DECDATA**	**DECDATA Uncertainty**	**DECDATA / Falzone**	**PenNuc**	**PenNuc Uncertainty**	**PenNuc / Falzone**
3.00	1.00	1.55E-01	1.63E-01	0.00E-01	1.05	1.42E-01	0.00E-01	0.91
3.00	2.00	2.12E-02	2.22E-02	0.00E-02	1.05	1.96E-02	0.00E-02	0.92
4.00	2.00	2.12E-02	2.22E-02	0.00E-02	1.05	1.96E-02	0.00E-02	0.92
4.00	3.00	6.67E-03	6.96E-03	0.01E-03	1.04	6.18E-03	0.00E-03	0.93
5.00	2.00	2.12E-02	2.22E-02	0.00E-02	1.05	1.96E-02	0.00E-02	0.92
5.00	3.00	6.67E-03	6.97E-03	0.01E-03	1.05	6.18E-03	0.00E-03	0.93
5.00	4.00	2.97E-03	3.10E-03	0.01E-03	1.04	2.77E-03	0.00E-03	0.93
6.00	3.00	6.67E-03	6.96E-03	0.01E-03	1.04	6.18E-03	0.00E-03	0.93
6.00	4.00	2.97E-03	3.10E-03	0.01E-03	1.04	2.77E-03	0.00E-03	0.93
6.00	5.00	1.61E-03	1.67E-03	0.00E-03	1.04	1.50E-03	0.00E-03	0.93
7.00	3.00	6.67E-03	6.97E-03	0.01E-03	1.05	6.18E-03	0.00E-03	0.93
7.00	4.00	2.97E-03	3.10E-03	0.01E-03	1.04	2.77E-03	0.00E-03	0.93
7.00	5.00	1.61E-03	1.67E-03	0.00E-03	1.04	1.50E-03	0.00E-03	0.93
7.00	6.00	9.77E-04	1.01E-03	0.00E-03	1.04	9.16E-04	0.01E-04	0.94
8.00	4.00	2.97E-03	3.10E-03	0.01E-03	1.04	2.77E-03	0.00E-03	0.93
8.00	5.00	1.61E-03	1.67E-03	0.00E-03	1.04	1.50E-03	0.00E-03	0.93
8.00	6.00	9.77E-04	1.01E-03	0.00E-03	1.04	9.16E-04	0.01E-04	0.94
8.00	7.00	6.42E-04	6.67E-04	0.02E-04	1.04	6.04E-04	0.00E-04	0.94
9.00	5.00	1.61E-03	1.67E-03	0.00E-03	1.04	1.50E-03	0.00E-03	0.93
9.00	6.00	9.77E-04	1.01E-03	0.00E-03	1.04	9.17E-04	0.01E-04	0.94
9.00	7.00	6.42E-04	6.66E-04	0.01E-04	1.04	6.04E-04	0.00E-04	0.94
9.00	8.00	4.46E-04	4.62E-04	0.01E-04	1.04	4.21E-04	0.00E-04	0.94
10.00	5.00	1.61E-03	1.67E-03	0.00E-03	1.04	1.50E-03	0.00E-03	0.93
10.00	6.00	9.77E-04	1.01E-03	0.00E-03	1.04	9.16E-04	0.01E-04	0.94
10.00	7.00	6.42E-04	6.67E-04	0.02E-04	1.04	6.04E-04	0.00E-04	0.94
10.00	8.00	4.46E-04	4.63E-04	0.01E-04	1.04	4.21E-04	0.00E-04	0.94
10.00	9.00	3.23E-04	3.34E-04	0.01E-04	1.04	3.06E-04	0.00E-04	0.95
11.00	5.00	1.61E-03	1.67E-03	0.00E-03	1.04	1.50E-03	0.00E-03	0.93
11.00	6.00	9.77E-04	1.01E-03	0.00E-03	1.04	9.16E-04	0.01E-04	0.94
11.00	7.00	6.42E-04	6.66E-04	0.02E-04	1.04	6.04E-04	0.00E-04	0.94
11.00	8.00	4.46E-04	4.63E-04	0.01E-04	1.04	4.21E-04	0.00E-04	0.94
11.00	9.00	3.23E-04	3.35E-04	0.01E-04	1.04	3.06E-04	0.00E-04	0.95
11.00	10.00	2.42E-04	2.51E-04	0.01E-04	1.04	2.30E-04	0.00E-04	0.95
12.00	6.00	9.77E-04	1.01E-03	0.00E-03	1.04	9.16E-04	0.01E-04	0.94
12.00	7.00	6.42E-04	6.67E-04	0.02E-04	1.04	6.04E-04	0.00E-04	0.94
12.00	8.00	4.46E-04	4.63E-04	0.01E-04	1.04	4.21E-04	0.00E-04	0.94
12.00	9.00	3.23E-04	3.35E-04	0.01E-04	1.04	3.06E-04	0.00E-04	0.95
12.00	10.00	2.42E-04	2.51E-04	0.01E-04	1.04	2.30E-04	0.00E-04	0.95
12.00	11.00	1.87E-04	1.93E-04	0.00E-04	1.03	1.77E-04	0.00E-04	0.95

Table C.4: Cellular S-values (mGy·MBq^{-1}·s^{-1}) for ^{123}I when the source is the cytoplasm and the target is the cell nucleus.

S (N<-Cy)								
Cell radii (µm)	**Nucleus radii (µm)**	**Falzone**	**DECDATA**	**DECDATA Uncertainty**	**DECDATA / Falzone**	**PenNuc**	**PenNuc Uncertainty**	**PenNuc / Falzone**
3.00	1.00	1.37E-03	1.38E-03	0.03E-03	1.01	1.39E-03	0.01E-03	1.02
3.00	2.00	1.01E-03	1.04E-03	0.01E-03	1.03	1.03E-03	0.00E-03	1.02
4.00	2.00	5.57E-04	5.58E-04	0.09E-04	1.00	5.58E-04	0.02E-04	1.00
4.00	3.00	5.06E-04	5.06E-04	0.05E-04	1.00	5.03E-04	0.01E-04	0.99
5.00	2.00	3.88E-04	3.77E-04	0.08E-04	0.97	3.82E-04	0.02E-04	0.98
5.00	3.00	3.27E-04	3.29E-04	0.05E-04	1.01	3.27E-04	0.01E-04	1.00
5.00	4.00	3.05E-04	3.11E-04	0.03E-04	1.02	3.08E-04	0.01E-04	1.01
6.00	3.00	2.54E-04	2.47E-04	0.04E-04	0.97	2.48E-04	0.01E-04	0.98
6.00	4.00	2.16E-04	2.20E-04	0.03E-04	1.02	2.21E-04	0.01E-04	1.02
6.00	5.00	2.05E-04	2.07E-04	0.02E-04	1.01	2.07E-04	0.01E-04	1.01
7.00	3.00	1.98E-04	1.99E-04	0.04E-04	1.01	1.97E-04	0.01E-04	1.00
7.00	4.00	1.74E-04	1.76E-04	0.03E-04	1.01	1.74E-04	0.01E-04	1.00
7.00	5.00	1.53E-04	1.54E-04	0.02E-04	1.00	1.55E-04	0.00E-04	1.01
7.00	6.00	1.42E-04	1.45E-04	0.01E-04	1.02	1.44E-04	0.00E-04	1.02
8.00	4.00	1.43E-04	1.41E-04	0.02E-04	0.99	1.41E-04	0.01E-04	0.98
8.00	5.00	1.27E-04	1.25E-04	0.02E-04	0.98	1.25E-04	0.00E-04	0.98
8.00	6.00	1.11E-04	1.11E-04	0.01E-04	1.00	1.11E-04	0.00E-04	1.00
8.00	7.00	1.03E-04	1.05E-04	0.01E-04	1.02	1.04E-04	0.00E-04	1.01
9.00	5.00	1.03E-04	1.04E-04	0.02E-04	1.01	1.02E-04	0.00E-04	0.99
9.00	6.00	8.91E-05	9.05E-05	0.12E-05	1.02	9.06E-05	0.03E-05	1.02
9.00	7.00	8.18E-05	8.17E-05	0.09E-05	1.00	8.17E-05	0.02E-05	1.00
9.00	8.00	7.79E-05	7.68E-05	0.07E-05	0.99	7.73E-05	0.02E-05	0.99
10.00	5.00	8.52E-05	8.38E-05	0.14E-05	0.98	8.41E-05	0.04E-05	0.99
10.00	6.00	7.41E-05	7.43E-05	0.11E-05	1.00	7.50E-05	0.03E-05	1.01
10.00	7.00	6.78E-05	6.75E-05	0.08E-05	1.00	6.71E-05	0.02E-05	0.99
10.00	8.00	5.95E-05	6.07E-05	0.07E-05	1.02	6.13E-05	0.02E-05	1.03
10.00	9.00	5.88E-05	5.93E-05	0.05E-05	1.01	5.88E-05	0.01E-05	1.00
11.00	5.00	7.02E-05	6.91E-05	0.13E-05	0.98	6.93E-05	0.03E-05	0.99
11.00	6.00	6.29E-05	6.21E-05	0.10E-05	0.99	6.23E-05	0.02E-05	0.99
11.00	7.00	5.47E-05	5.62E-05	0.08E-05	1.03	5.61E-05	0.02E-05	1.03
11.00	8.00	5.04E-05	5.15E-05	0.06E-05	1.02	5.09E-05	0.01E-05	1.01
11.00	9.00	4.73E-05	4.74E-05	0.05E-05	1.00	4.72E-05	0.01E-05	1.00
11.00	10.00	4.52E-05	4.59E-05	0.04E-05	1.01	4.58E-05	0.01E-05	1.01
12.00	6.00	5.23E-05	5.13E-05	0.09E-05	0.98	5.17E-05	0.02E-05	0.99
12.00	7.00	4.72E-05	4.68E-05	0.07E-05	0.99	4.68E-05	0.02E-05	0.99
12.00	8.00	4.17E-05	4.33E-05	0.05E-05	1.04	4.27E-05	0.01E-05	1.02
12.00	9.00	3.94E-05	3.96E-05	0.04E-05	1.01	3.94E-05	0.01E-05	1.00
12.00	10.00	3.66E-05	3.72E-05	0.04E-05	1.02	3.69E-05	0.01E-05	1.01
12.00	11.00	3.57E-05	3.64E-05	0.03E-05	1.02	3.63E-05	0.01E-05	1.02

Table C.5: Cellular S-values (mGy·MBq^{-1}·s^{-1}) for ^{111}In when the source and the target are the nucleus of the cell.

S (N<-N)								
Cell radii (µm)	**Nucleus radii (µm)**	**Falzone**	**DECDATA**	**DECDATA Uncertainty**	**DECDATA/ Falzone**	**PenNuc**	**PenNuc Uncertainty**	**PenNuc/ Falzone**
3.00	1.00	1.40E-01	1.45E-01	0.00E-01	1.04	1.21E-01	0.00E-01	0.86
3.00	2.00	1.93E-02	2.00E-02	0.00E-02	1.04	1.69E-02	0.00E-02	0.87
4.00	2.00	1.93E-02	2.00E-02	0.00E-02	1.04	1.69E-02	0.00E-02	0.87
4.00	3.00	6.22E-03	6.44E-03	0.01E-03	1.03	5.49E-03	0.00E-03	0.88
5.00	2.00	1.93E-02	2.00E-02	0.00E-02	1.04	1.69E-02	0.00E-02	0.87
5.00	3.00	6.22E-03	6.43E-03	0.01E-03	1.03	5.50E-03	0.00E-03	0.88
5.00	4.00	2.85E-03	2.93E-03	0.00E-03	1.03	2.54E-03	0.00E-03	0.89
6.00	3.00	6.22E-03	6.44E-03	0.01E-03	1.03	5.49E-03	0.00E-03	0.88
6.00	4.00	2.85E-03	2.93E-03	0.00E-03	1.03	2.53E-03	0.00E-03	0.89
6.00	5.00	1.56E-03	1.61E-03	0.00E-03	1.03	1.40E-03	0.00E-03	0.90
7.00	3.00	6.22E-03	6.43E-03	0.01E-03	1.03	5.49E-03	0.00E-03	0.88
7.00	4.00	2.85E-03	2.93E-03	0.00E-03	1.03	2.54E-03	0.00E-03	0.89
7.00	5.00	1.56E-03	1.61E-03	0.00E-03	1.03	1.40E-03	0.00E-03	0.90
7.00	6.00	9.55E-04	9.82E-04	0.02E-04	1.03	8.63E-04	0.01E-04	0.90
8.00	4.00	2.85E-03	2.94E-03	0.00E-03	1.03	2.54E-03	0.00E-03	0.89
8.00	5.00	1.56E-03	1.61E-03	0.00E-03	1.03	1.40E-03	0.00E-03	0.90
8.00	6.00	9.55E-04	9.82E-04	0.02E-04	1.03	8.63E-04	0.01E-04	0.90
8.00	7.00	6.29E-04	6.46E-04	0.01E-04	1.03	5.71E-04	0.00E-04	0.91
9.00	5.00	1.56E-03	1.61E-03	0.00E-03	1.03	1.40E-03	0.00E-03	0.90
9.00	6.00	9.55E-04	9.82E-04	0.02E-04	1.03	8.63E-04	0.01E-04	0.90
9.00	7.00	6.29E-04	6.46E-04	0.01E-04	1.03	5.70E-04	0.00E-04	0.91
9.00	8.00	4.36E-04	4.48E-04	0.01E-04	1.03	3.98E-04	0.00E-04	0.91
10.00	5.00	1.56E-03	1.61E-03	0.00E-03	1.03	1.40E-03	0.00E-03	0.90
10.00	6.00	9.55E-04	9.83E-04	0.02E-04	1.03	8.63E-04	0.01E-04	0.90
10.00	7.00	6.29E-04	6.47E-04	0.01E-04	1.03	5.71E-04	0.00E-04	0.91
10.00	8.00	4.36E-04	4.48E-04	0.01E-04	1.03	3.97E-04	0.00E-04	0.91
10.00	9.00	3.15E-04	3.24E-04	0.01E-04	1.03	2.88E-04	0.00E-04	0.91
11.00	5.00	1.56E-03	1.61E-03	0.00E-03	1.03	1.40E-03	0.00E-03	0.90
11.00	6.00	9.55E-04	9.82E-04	0.02E-04	1.03	8.63E-04	0.01E-04	0.90
11.00	7.00	6.29E-04	6.46E-04	0.01E-04	1.03	5.71E-04	0.00E-04	0.91
11.00	8.00	4.36E-04	4.48E-04	0.01E-04	1.03	3.98E-04	0.00E-04	0.91
11.00	9.00	3.15E-04	3.23E-04	0.01E-04	1.03	2.88E-04	0.00E-04	0.92
11.00	10.00	2.36E-04	2.42E-04	0.00E-04	1.02	2.16E-04	0.00E-04	0.91
12.00	6.00	9.55E-04	9.82E-04	0.02E-04	1.03	8.63E-04	0.01E-04	0.90
12.00	7.00	6.29E-04	6.46E-04	0.01E-04	1.03	5.70E-04	0.00E-04	0.91
12.00	8.00	4.36E-04	4.48E-04	0.01E-04	1.03	3.97E-04	0.00E-04	0.91
12.00	9.00	3.15E-04	3.23E-04	0.01E-04	1.03	2.88E-04	0.00E-04	0.91
12.00	10.00	2.36E-04	2.42E-04	0.00E-04	1.02	2.16E-04	0.00E-04	0.91
12.00	11.00	1.81E-04	1.86E-04	0.00E-04	1.03	1.66E-04	0.00E-04	0.92

Table C.6: Cellular S-values (mGy·MBq^{-1}·s^{-1}) for ^{111}In when the source is the cytoplasm and the target is the cell nucleus.

S(N<-Cy)								
Cell radii (µm)	**Nucleus radii (µm)**	**Falzone**	**DECDATA**	**DECDATA Uncertainty**	**DECDATA/ Falzone**	**PenNuc**	**PenNuc Uncertainty**	**PenNuc/ Falzone**
3.00	1.00	1.50E-03	1.50E-03	0.02E-03	1.00	1.47E-03	0.01E-03	0.98
3.00	2.00	1.14E-03	1.17E-03	0.01E-03	1.03	1.14E-03	0.00E-03	1.00
4.00	2.00	7.26E-04	7.26E-04	0.09E-04	1.00	7.21E-04	0.03E-04	0.99
4.00	3.00	6.28E-04	6.32E-04	0.05E-04	1.01	6.22E-04	0.02E-04	0.99
5.00	2.00	5.31E-04	5.25E-04	0.08E-04	0.99	5.23E-04	0.03E-04	0.98
5.00	3.00	4.43E-04	4.44E-04	0.05E-04	1.00	4.41E-04	0.02E-04	1.00
5.00	4.00	3.89E-04	3.88E-04	0.03E-04	1.00	3.81E-04	0.01E-04	0.98
6.00	3.00	3.33E-04	3.39E-04	0.04E-04	1.02	3.34E-04	0.01E-04	1.00
6.00	4.00	2.81E-04	2.87E-04	0.03E-04	1.02	2.82E-04	0.01E-04	1.00
6.00	5.00	2.46E-04	2.48E-04	0.02E-04	1.01	2.45E-04	0.01E-04	1.00
7.00	3.00	2.58E-04	2.57E-04	0.04E-04	1.00	2.54E-04	0.01E-04	0.98
7.00	4.00	2.21E-04	2.20E-04	0.02E-04	1.00	2.17E-04	0.01E-04	0.98
7.00	5.00	1.85E-04	1.87E-04	0.02E-04	1.01	1.85E-04	0.01E-04	1.00
7.00	6.00	1.66E-04	1.66E-04	0.01E-04	1.00	1.63E-04	0.00E-04	0.98
8.00	4.00	1.66E-04	1.69E-04	0.02E-04	1.02	1.68E-04	0.01E-04	1.01
8.00	5.00	1.44E-04	1.45E-04	0.01E-04	1.01	1.44E-04	0.00E-04	1.00
8.00	6.00	1.25E-04	1.27E-04	0.01E-04	1.02	1.26E-04	0.00E-04	1.00
8.00	7.00	1.15E-04	1.16E-04	0.01E-04	1.01	1.14E-04	0.00E-04	0.99
9.00	5.00	1.12E-04	1.15E-04	0.01E-04	1.03	1.13E-04	0.00E-04	1.01
9.00	6.00	9.85E-05	1.00E-04	0.01E-04	1.02	9.92E-05	0.03E-05	1.01
9.00	7.00	8.84E-05	9.02E-05	0.07E-05	1.02	8.86E-05	0.02E-05	1.00
9.00	8.00	8.27E-05	8.35E-05	0.05E-05	1.01	8.24E-05	0.02E-05	1.00
10.00	5.00	8.64E-05	8.99E-05	0.11E-05	1.04	8.83E-05	0.04E-05	1.02
10.00	6.00	7.74E-05	7.91E-05	0.08E-05	1.02	7.84E-05	0.03E-05	1.01
10.00	7.00	7.02E-05	7.14E-05	0.06E-05	1.02	7.07E-05	0.02E-05	1.01
10.00	8.00	6.52E-05	6.56E-05	0.05E-05	1.01	6.49E-05	0.02E-05	1.00
10.00	9.00	6.12E-05	6.22E-05	0.04E-05	1.02	6.15E-05	0.01E-05	1.01
11.00	5.00	6.87E-05	7.07E-05	0.10E-05	1.03	6.90E-05	0.03E-05	1.00
11.00	6.00	6.12E-05	6.29E-05	0.07E-05	1.03	6.21E-05	0.02E-05	1.01
11.00	7.00	5.65E-05	5.71E-05	0.05E-05	1.01	5.67E-05	0.02E-05	1.00
11.00	8.00	5.21E-05	5.30E-05	0.04E-05	1.02	5.21E-05	0.01E-05	1.00
11.00	9.00	4.85E-05	4.96E-05	0.04E-05	1.02	4.88E-05	0.01E-05	1.01
11.00	10.00	4.67E-05	4.80E-05	0.03E-05	1.03	4.72E-05	0.01E-05	1.01
12.00	6.00	4.82E-05	5.03E-05	0.06E-05	1.04	4.92E-05	0.02E-05	1.02
12.00	7.00	4.55E-05	4.57E-05	0.05E-05	1.00	4.54E-05	0.02E-05	1.00
12.00	8.00	4.17E-05	4.29E-05	0.04E-05	1.03	4.20E-05	0.01E-05	1.01
12.00	9.00	3.92E-05	3.99E-05	0.03E-05	1.02	3.95E-05	0.01E-05	1.01
12.00	10.00	3.75E-05	3.84E-05	0.03E-05	1.02	3.77E-05	0.01E-05	1.01
12.00	11.00	3.75E-05	3.75E-05	0.02E-05	1.00	3.71E-05	0.01E-05	0.99

Table C.7: Cellular S-values (mGy·MBq^{-1}·s^{-1}) for ^{201}Tl when the source and the target are the nucleus of the cell.

S (N<-N)								
Cell radii (µm)	**Nucleus radii (µm)**	**Falzone**	**DECDATA**	**DECDATA Uncertainty**	**DECDATA / Falzone**	**PenNuc**	**PenNuc Uncertainty**	**PenNuc / Falzone**
3.00	1.00	3.46E-01	3.58E-01	0.01E-01	1.03	2.80E-01	0.00E-01	0.81
3.00	2.00	5.44E-02	5.60E-02	0.01E-02	1.03	4.65E-02	0.00E-02	0.85
4.00	2.00	5.44E-02	5.60E-02	0.01E-02	1.03	4.65E-02	0.00E-02	0.85
4.00	3.00	1.81E-02	1.86E-02	0.00E-02	1.03	1.58E-02	0.00E-02	0.87
5.00	2.00	5.44E-02	5.60E-02	0.01E-02	1.03	4.65E-02	0.00E-02	0.85
5.00	3.00	1.81E-02	1.86E-02	0.00E-02	1.03	1.58E-02	0.00E-02	0.88
5.00	4.00	8.24E-03	8.44E-03	0.01E-03	1.02	7.30E-03	0.00E-03	0.89
6.00	3.00	1.81E-02	1.86E-02	0.00E-02	1.03	1.58E-02	0.00E-02	0.87
6.00	4.00	8.24E-03	8.44E-03	0.01E-03	1.02	7.30E-03	0.00E-03	0.89
6.00	5.00	4.44E-03	4.55E-03	0.01E-03	1.02	3.98E-03	0.00E-03	0.90
7.00	3.00	1.81E-02	1.86E-02	0.00E-02	1.03	1.58E-02	0.00E-02	0.87
7.00	4.00	8.24E-03	8.44E-03	0.01E-03	1.02	7.30E-03	0.00E-03	0.89
7.00	5.00	4.44E-03	4.55E-03	0.01E-03	1.02	3.97E-03	0.00E-03	0.89
7.00	6.00	2.68E-03	2.74E-03	0.00E-03	1.02	2.41E-03	0.00E-03	0.90
8.00	4.00	8.24E-03	8.44E-03	0.01E-03	1.02	7.30E-03	0.00E-03	0.89
8.00	5.00	4.44E-03	4.56E-03	0.01E-03	1.03	3.98E-03	0.00E-03	0.90
8.00	6.00	2.68E-03	2.74E-03	0.00E-03	1.02	2.41E-03	0.00E-03	0.90
8.00	7.00	1.74E-03	1.78E-03	0.00E-03	1.02	1.58E-03	0.00E-03	0.91
9.00	5.00	4.44E-03	4.55E-03	0.01E-03	1.02	3.97E-03	0.00E-03	0.89
9.00	6.00	2.68E-03	2.74E-03	0.00E-03	1.02	2.41E-03	0.00E-03	0.90
9.00	7.00	1.74E-03	1.78E-03	0.00E-03	1.02	1.58E-03	0.00E-03	0.91
9.00	8.00	1.20E-03	1.23E-03	0.00E-03	1.02	1.09E-03	0.00E-03	0.91
10.00	5.00	4.44E-03	4.55E-03	0.01E-03	1.02	3.97E-03	0.00E-03	0.90
10.00	6.00	2.68E-03	2.74E-03	0.00E-03	1.02	2.41E-03	0.00E-03	0.90
10.00	7.00	1.74E-03	1.78E-03	0.00E-03	1.03	1.58E-03	0.00E-03	0.91
10.00	8.00	1.20E-03	1.23E-03	0.00E-03	1.02	1.09E-03	0.00E-03	0.91
10.00	9.00	8.62E-04	8.84E-04	0.02E-04	1.03	7.89E-04	0.00E-04	0.91
11.00	5.00	4.44E-03	4.55E-03	0.01E-03	1.02	3.98E-03	0.00E-03	0.90
11.00	6.00	2.68E-03	2.74E-03	0.00E-03	1.02	2.41E-03	0.00E-03	0.90
11.00	7.00	1.74E-03	1.78E-03	0.00E-03	1.03	1.58E-03	0.00E-03	0.91
11.00	8.00	1.20E-03	1.23E-03	0.00E-03	1.02	1.09E-03	0.00E-03	0.91
11.00	9.00	8.62E-04	8.84E-04	0.02E-04	1.03	7.88E-04	0.00E-04	0.91
11.00	10.00	6.42E-04	6.58E-04	0.01E-04	1.02	5.89E-04	0.00E-04	0.92
12.00	6.00	2.68E-03	2.74E-03	0.00E-03	1.02	2.41E-03	0.00E-03	0.90
12.00	7.00	1.74E-03	1.78E-03	0.00E-03	1.02	1.58E-03	0.00E-03	0.91
12.00	8.00	1.20E-03	1.23E-03	0.00E-03	1.02	1.09E-03	0.00E-03	0.91
12.00	9.00	8.62E-04	8.83E-04	0.02E-04	1.02	7.89E-04	0.00E-04	0.91
12.00	10.00	6.42E-04	6.57E-04	0.01E-04	1.02	5.89E-04	0.00E-04	0.92
12.00	11.00	4.92E-04	5.05E-04	0.01E-04	1.03	4.53E-04	0.00E-04	0.92

Table C.8: Cellular S-values (mGy·MBq^{-1}·s^{-1}) for ^{201}Tl when the source is the cytoplasm and the target is the cell nucleus.

S (N<-Cy)								
Cell radii (µm)	**Nucleus radii (µm)**	**Falzone**	**DECDATA**	**DECDATA Uncertainty**	**DECDATA / Falzone**	**PenNuc**	**PenNuc Uncertainty**	**PenNuc / Falzone**
3.00	1.00	8.64E-03	8.65E-03	0.12E-03	1.00	8.87E-03	0.03E-03	1.03
3.00	2.00	6.15E-03	6.20E-03	0.04E-03	1.01	6.32E-03	0.01E-03	1.03
4.00	2.00	2.97E-03	2.96E-03	0.03E-03	1.00	3.08E-03	0.01E-03	1.04
4.00	3.00	2.55E-03	2.55E-03	0.02E-03	1.00	2.62E-03	0.00E-03	1.03
5.00	2.00	1.69E-03	1.73E-03	0.02E-03	1.03	1.78E-03	0.00E-03	1.05
5.00	3.00	1.39E-03	1.40E-03	0.01E-03	1.00	1.44E-03	0.00E-03	1.04
5.00	4.00	1.29E-03	1.31E-03	0.01E-03	1.01	1.34E-03	0.00E-03	1.04
6.00	3.00	8.65E-04	8.70E-04	0.10E-04	1.01	9.07E-04	0.02E-04	1.05
6.00	4.00	7.54E-04	7.59E-04	0.06E-04	1.01	7.90E-04	0.01E-04	1.05
6.00	5.00	7.51E-04	7.58E-04	0.04E-04	1.01	7.84E-04	0.01E-04	1.04
7.00	3.00	5.81E-04	5.91E-04	0.08E-04	1.02	6.13E-04	0.02E-04	1.05
7.00	4.00	5.00E-04	5.07E-04	0.05E-04	1.01	5.24E-04	0.01E-04	1.05
7.00	5.00	4.61E-04	4.66E-04	0.04E-04	1.01	4.85E-04	0.01E-04	1.05
7.00	6.00	4.81E-04	4.83E-04	0.03E-04	1.00	5.02E-04	0.01E-04	1.04
8.00	4.00	3.51E-04	3.55E-04	0.04E-04	1.01	3.72E-04	0.01E-04	1.06
8.00	5.00	3.19E-04	3.20E-04	0.03E-04	1.00	3.36E-04	0.01E-04	1.05
8.00	6.00	3.06E-04	3.09E-04	0.02E-04	1.01	3.23E-04	0.00E-04	1.05
8.00	7.00	3.28E-04	3.30E-04	0.02E-04	1.01	3.43E-04	0.00E-04	1.05
9.00	5.00	2.31E-04	2.35E-04	0.03E-04	1.02	2.47E-04	0.01E-04	1.07
9.00	6.00	2.17E-04	2.19E-04	0.02E-04	1.01	2.30E-04	0.00E-04	1.06
9.00	7.00	2.14E-04	2.17E-04	0.02E-04	1.02	2.27E-04	0.00E-04	1.06
9.00	8.00	2.35E-04	2.36E-04	0.01E-04	1.01	2.46E-04	0.00E-04	1.05
10.00	5.00	1.77E-04	1.81E-04	0.02E-04	1.02	1.89E-04	0.00E-04	1.07
10.00	6.00	1.65E-04	1.66E-04	0.02E-04	1.01	1.74E-04	0.00E-04	1.05
10.00	7.00	1.57E-04	1.58E-04	0.01E-04	1.01	1.66E-04	0.00E-04	1.06
10.00	8.00	1.58E-04	1.61E-04	0.01E-04	1.02	1.67E-04	0.00E-04	1.06
10.00	9.00	1.75E-04	1.76E-04	0.01E-04	1.01	1.83E-04	0.00E-04	1.05
11.00	5.00	1.41E-04	1.43E-04	0.02E-04	1.01	1.49E-04	0.00E-04	1.05
11.00	6.00	1.29E-04	1.31E-04	0.02E-04	1.02	1.37E-04	0.00E-04	1.06
11.00	7.00	1.21E-04	1.23E-04	0.01E-04	1.01	1.29E-04	0.00E-04	1.06
11.00	8.00	1.18E-04	1.20E-04	0.01E-04	1.01	1.25E-04	0.00E-04	1.06
11.00	9.00	1.20E-04	1.21E-04	0.01E-04	1.01	1.27E-04	0.00E-04	1.06
11.00	10.00	1.34E-04	1.36E-04	0.01E-04	1.02	1.41E-04	0.00E-04	1.05
12.00	6.00	1.03E-04	1.05E-04	0.01E-04	1.02	1.10E-04	0.00E-04	1.07
12.00	7.00	9.63E-05	9.81E-05	0.11E-05	1.02	1.03E-04	0.00E-04	1.07
12.00	8.00	9.23E-05	9.32E-05	0.09E-05	1.01	9.80E-05	0.02E-05	1.06
12.00	9.00	9.10E-05	9.25E-05	0.07E-05	1.02	9.65E-05	0.02E-05	1.06
12.00	10.00	9.36E-05	9.50E-05	0.07E-05	1.02	9.92E-05	0.01E-05	1.06
12.00	11.00	1.06E-04	1.07E-04	0.01E-04	1.01	1.11E-04	0.00E-04	1.05

Table C.9: Cellular S-values (mGy·MBq^{-1}·s^{-1}) for ^{67}Ga using DPK.

Cell radii (µm)	Nucleus radii (µm)	S (N<-N)					S (N<-Cy)				
		MIRD	DECDATA	DECDATA / MIRD	PenNuc	PenNuc / MIRD	MIRD	DECDATA	DECDATA / MIRD	PenNuc	PenNuc / MIRD
3.00	1.00	1.27E-01	1.47E-01	1.16	9.58E-02	0.75	5.24E-03	4.56E-03	0.87	3.05E-03	0.58
3.00	2.00	2.29E-02	2.51E-02	1.09	1.64E-02	0.72	3.59E-03	3.25E-03	0.90	2.17E-03	0.60
4.00	2.00	2.29E-02	2.51E-02	1.09	1.64E-02	0.72	1.51E-03	1.27E-03	0.84	8.48E-04	0.56
4.00	3.00	7.79E-03	8.27E-03	1.06	5.42E-03	0.70	1.35E-03	1.21E-03	0.90	8.03E-04	0.59
5.00	2.00	2.29E-02	2.51E-02	1.09	1.64E-02	0.72	7.75E-04	6.63E-04	0.86	4.41E-04	0.57
5.00	3.00	7.79E-03	8.27E-03	1.06	5.42E-03	0.70	6.37E-04	5.43E-04	0.85	3.61E-04	0.57
5.00	4.00	3.54E-03	3.71E-03	1.05	2.43E-03	0.69	6.54E-04	5.86E-04	0.90	3.90E-04	0.60
6.00	3.00	7.79E-03	8.27E-03	1.06	5.42E-03	0.70	3.63E-04	3.16E-04	0.87	2.10E-04	0.58
6.00	4.00	3.54E-03	3.71E-03	1.05	2.43E-03	0.69	3.35E-04	2.89E-04	0.86	1.92E-04	0.57
6.00	5.00	1.90E-03	1.99E-03	1.05	1.30E-03	0.68	3.71E-04	3.34E-04	0.90	2.22E-04	0.60
7.00	3.00	7.79E-03	8.27E-03	1.06	5.42E-03	0.70	2.36E-04	2.10E-04	0.89	1.39E-04	0.59
7.00	4.00	3.54E-03	3.71E-03	1.05	2.43E-03	0.69	2.05E-04	1.82E-04	0.89	1.21E-04	0.59
7.00	5.00	1.90E-03	1.99E-03	1.05	1.30E-03	0.68	2.01E-04	1.77E-04	0.88	1.17E-04	0.58
7.00	6.00	1.14E-03	1.19E-03	1.04	7.79E-04	0.68	2.33E-04	2.11E-04	0.91	1.40E-04	0.60
8.00	4.00	3.54E-03	3.71E-03	1.05	2.43E-03	0.69	1.42E-04	1.28E-04	0.90	8.46E-05	0.60
8.00	5.00	1.90E-03	1.99E-03	1.05	1.30E-03	0.68	1.30E-04	1.17E-04	0.90	7.76E-05	0.60
8.00	6.00	1.14E-03	1.19E-03	1.04	7.79E-04	0.68	1.33E-04	1.18E-04	0.88	7.81E-05	0.59
8.00	7.00	7.43E-04	7.70E-04	1.04	5.05E-04	0.68	1.58E-04	1.44E-04	0.91	9.53E-05	0.60
9.00	5.00	1.90E-03	1.99E-03	1.05	1.30E-03	0.68	9.39E-05	8.61E-05	0.92	5.69E-05	0.61
9.00	6.00	1.14E-03	1.19E-03	1.04	7.79E-04	0.68	8.94E-05	8.16E-05	0.91	5.39E-05	0.60
9.00	7.00	7.43E-04	7.70E-04	1.04	5.05E-04	0.68	9.32E-05	8.37E-05	0.90	5.54E-05	0.59
9.00	8.00	5.11E-04	5.29E-04	1.03	3.47E-04	0.68	1.13E-04	1.03E-04	0.91	6.83E-05	0.60
10.00	5.00	1.90E-03	1.99E-03	1.05	1.30E-03	0.68	7.19E-05	6.70E-05	0.93	4.42E-05	0.61
10.00	6.00	1.14E-03	1.19E-03	1.04	7.79E-04	0.68	6.67E-05	6.20E-05	0.93	4.09E-05	0.61
10.00	7.00	7.43E-04	7.70E-04	1.04	5.05E-04	0.68	6.50E-05	5.99E-05	0.92	3.95E-05	0.61
10.00	8.00	5.11E-04	5.29E-04	1.03	3.47E-04	0.68	6.87E-05	6.21E-05	0.90	4.11E-05	0.60
10.00	9.00	3.68E-04	3.80E-04	1.03	2.49E-04	0.68	8.37E-05	7.67E-05	0.92	5.09E-05	0.61
11.00	5.00	-	1.99E-03	-	1.30E-03	-	-	5.39E-05	-	3.55E-05	-
11.00	6.00	-	1.19E-03	-	7.79E-04	-	-	4.95E-05	-	3.26E-05	-
11.00	7.00	-	7.70E-04	-	5.05E-04	-	-	4.66E-05	-	3.08E-05	-
11.00	8.00	-	5.29E-04	-	3.47E-04	-	-	4.57E-05	-	3.02E-05	-
11.00	9.00	-	3.80E-04	-	2.49E-04	-	-	4.78E-05	-	3.16E-05	-
11.00	10.00	-	2.83E-04	-	1.85E-04	-	-	5.91E-05	-	3.92E-05	-
12.00	6.00	-	1.19E-03	-	7.79E-04	-	-	4.08E-05	-	2.68E-05	-
12.00	7.00	-	7.70E-04	-	5.05E-04	-	-	3.81E-05	-	2.51E-05	-
12.00	8.00	-	5.29E-04	-	3.47E-04	-	-	3.64E-05	-	2.40E-05	-
12.00	9.00	-	3.80E-04	-	2.49E-04	-	-	3.60E-05	-	2.37E-05	-
12.00	10.00	-	2.83E-04	-	1.85E-04	-	-	3.79E-05	-	2.50E-05	-
12.00	11.00	-	2.16E-04	-	1.42E-04	-	-	4.68E-05	-	3.10E-05	-

Table C.10: Cellular S-values (mGy·MBq^{-1}·s^{-1}) for ^{123}I using DPK.

Cell radii (µm)	Nucleus radii (µm)	S (N<-N)					S (N<-Cy)				
		MIRD	DECDATA	DECDATA / MIRD	PenNuc	PenNuc / MIRD	MIRD	DECDATA	DECDATA / MIRD	PenNuc	PenNuc / MIRD
3.00	1.00	1.53E-01	1.43E-01	0.94	1.40E-01	0.92	1.69E-03	1.39E-03	0.82	1.39E-03	0.82
3.00	2.00	2.15E-02	1.98E-02	0.92	1.94E-02	0.90	1.22E-03	1.04E-03	0.85	1.03E-03	0.84
4.00	2.00	2.15E-02	1.98E-02	0.92	1.94E-02	0.90	5.75E-04	5.60E-04	0.97	5.60E-04	0.97
4.00	3.00	6.75E-03	6.25E-03	0.93	6.13E-03	0.91	5.23E-04	5.02E-04	0.96	5.03E-04	0.96
5.00	2.00	2.15E-02	1.98E-02	0.92	1.94E-02	0.90	3.53E-04	3.81E-04	1.08	3.81E-04	1.08
5.00	3.00	6.75E-03	6.25E-03	0.93	6.13E-03	0.91	2.95E-04	3.28E-04	1.11	3.28E-04	1.11
5.00	4.00	2.98E-03	2.80E-03	0.94	2.75E-03	0.92	2.90E-04	3.08E-04	1.06	3.08E-04	1.06
6.00	3.00	6.75E-03	6.25E-03	0.93	6.13E-03	0.91	2.05E-04	2.47E-04	1.21	2.48E-04	1.21
6.00	4.00	2.98E-03	2.80E-03	0.94	2.75E-03	0.92	1.85E-04	2.20E-04	1.19	2.20E-04	1.19
6.00	5.00	1.59E-03	1.51E-03	0.95	1.49E-03	0.94	1.88E-04	2.06E-04	1.09	2.06E-04	1.10
7.00	3.00	6.75E-03	6.25E-03	0.93	6.13E-03	0.91	1.55E-04	1.96E-04	1.26	1.96E-04	1.26
7.00	4.00	2.98E-03	2.80E-03	0.94	2.75E-03	0.92	1.39E-04	1.74E-04	1.25	1.74E-04	1.25
7.00	5.00	1.59E-03	1.51E-03	0.95	1.49E-03	0.94	1.31E-04	1.54E-04	1.18	1.55E-04	1.18
7.00	6.00	9.60E-04	9.24E-04	0.96	9.09E-04	0.95	1.34E-04	1.44E-04	1.08	1.44E-04	1.07
8.00	4.00	2.98E-03	2.80E-03	0.94	2.75E-03	0.92	1.12E-04	1.40E-04	1.25	1.41E-04	1.26
8.00	5.00	1.59E-03	1.51E-03	0.95	1.49E-03	0.94	1.04E-04	1.24E-04	1.19	1.24E-04	1.19
8.00	6.00	9.60E-04	9.24E-04	0.96	9.09E-04	0.95	9.81E-05	1.11E-04	1.13	1.11E-04	1.13
8.00	7.00	6.29E-04	6.09E-04	0.97	6.00E-04	0.95	9.91E-05	1.04E-04	1.05	1.04E-04	1.05
9.00	5.00	1.59E-03	1.51E-03	0.95	1.49E-03	0.94	8.64E-05	1.02E-04	1.18	1.02E-04	1.18
9.00	6.00	9.60E-04	9.24E-04	0.96	9.09E-04	0.95	7.99E-05	9.02E-05	1.13	9.03E-05	1.13
9.00	7.00	6.29E-04	6.09E-04	0.97	6.00E-04	0.95	7.49E-05	8.11E-05	1.08	8.13E-05	1.09
9.00	8.00	4.38E-04	4.24E-04	0.97	4.18E-04	0.95	7.51E-05	7.69E-05	1.02	7.70E-05	1.03
10.00	5.00	1.59E-03	1.51E-03	0.95	1.49E-03	0.94	7.34E-05	8.36E-05	1.14	8.38E-05	1.14
10.00	6.00	9.60E-04	9.24E-04	0.96	9.09E-04	0.95	6.74E-05	7.45E-05	1.11	7.46E-05	1.11
10.00	7.00	6.29E-04	6.09E-04	0.97	6.00E-04	0.95	6.19E-05	6.68E-05	1.08	6.69E-05	1.08
10.00	8.00	4.38E-04	4.24E-04	0.97	4.18E-04	0.95	5.80E-05	6.09E-05	1.05	6.10E-05	1.05
10.00	9.00	3.18E-04	3.08E-04	0.97	3.04E-04	0.96	5.80E-05	5.83E-05	1.01	5.84E-05	1.01
11.00	5.00	-	1.51E-03	-	1.49E-03	-	-	6.89E-05	-	6.90E-05	-
11.00	6.00	-	9.24E-04	-	9.09E-04	-	-	6.19E-05	-	6.19E-05	-
11.00	7.00	-	6.09E-04	-	6.00E-04	-	-	5.56E-05	-	5.57E-05	-
11.00	8.00	-	4.24E-04	-	4.18E-04	-	-	5.05E-05	-	5.06E-05	-
11.00	9.00	-	3.08E-04	-	3.04E-04	-	-	4.68E-05	-	4.68E-05	-
11.00	10.00	-	2.31E-04	-	2.28E-04	-	-	4.53E-05	-	4.54E-05	-
12.00	6.00	-	9.24E-04	-	9.09E-04	-	-	5.14E-05	-	5.14E-05	-
12.00	7.00	-	6.09E-04	-	6.00E-04	-	-	4.65E-05	-	4.66E-05	-
12.00	8.00	-	4.24E-04	-	4.18E-04	-	-	4.24E-05	-	4.25E-05	-
12.00	9.00	-	3.08E-04	-	3.04E-04	-	-	3.91E-05	-	3.91E-05	-
12.00	10.00	-	2.31E-04	-	2.28E-04	-	-	3.66E-05	-	3.66E-05	-
12.00	11.00	-	1.78E-04	-	1.75E-04	-	-	3.59E-05	-	3.59E-05	-

Table C.11: Cellular S-values (mGy·MBq^{-1}·s^{-1}) for ^{111}In using DPK.

Cell radii (µm)	Nucleus radii (µm)	S (N<-N)					S (N<-Cy)				
		MIRD	DECDATA	DECDATA / MIRD	PenNuc	PenNuc / MIRD	MIRD	DECDATA	DECDATA / MIRD	PenNuc	PenNuc / MIRD
3.00	1.00	1.37E-01	1.32E-01	0.96	1.19E-01	0.87	1.52E-03	1.51E-03	0.99	1.47E-03	0.97
3.00	2.00	1.91E-02	1.83E-02	0.96	1.67E-02	0.87	1.12E-03	1.17E-03	1.04	1.14E-03	1.02
4.00	2.00	1.91E-02	1.83E-02	0.96	1.67E-02	0.87	5.99E-04	7.30E-04	1.22	7.17E-04	1.20
4.00	3.00	6.07E-03	5.92E-03	0.98	5.43E-03	0.89	5.30E-04	6.33E-04	1.19	6.21E-04	1.17
5.00	2.00	1.91E-02	1.83E-02	0.96	1.67E-02	0.87	3.96E-04	5.27E-04	1.33	5.19E-04	1.31
5.00	3.00	6.07E-03	5.92E-03	0.98	5.43E-03	0.89	3.40E-04	4.47E-04	1.31	4.40E-04	1.29
5.00	4.00	2.72E-03	2.72E-03	1.00	2.51E-03	0.92	3.25E-04	3.87E-04	1.19	3.81E-04	1.17
6.00	3.00	6.07E-03	5.92E-03	0.98	5.43E-03	0.89	2.55E-04	3.38E-04	1.32	3.33E-04	1.31
6.00	4.00	2.72E-03	2.72E-03	1.00	2.51E-03	0.92	2.32E-04	2.85E-04	1.23	2.82E-04	1.22
6.00	5.00	1.48E-03	1.49E-03	1.01	1.39E-03	0.94	2.20E-04	2.48E-04	1.13	2.44E-04	1.11
7.00	3.00	6.07E-03	5.92E-03	0.98	5.43E-03	0.89	2.05E-04	2.58E-04	1.26	2.54E-04	1.24
7.00	4.00	2.72E-03	2.72E-03	1.00	2.51E-03	0.92	1.83E-04	2.20E-04	1.20	2.17E-04	1.19
7.00	5.00	1.48E-03	1.49E-03	1.01	1.39E-03	0.94	1.65E-04	1.87E-04	1.13	1.85E-04	1.12
7.00	6.00	9.09E-04	9.19E-04	1.01	8.55E-04	0.94	1.54E-04	1.66E-04	1.07	1.63E-04	1.06
8.00	4.00	2.72E-03	2.72E-03	1.00	2.51E-03	0.92	1.50E-04	1.70E-04	1.13	1.67E-04	1.11
8.00	5.00	1.48E-03	1.49E-03	1.01	1.39E-03	0.94	1.32E-04	1.45E-04	1.10	1.44E-04	1.09
8.00	6.00	9.09E-04	9.19E-04	1.01	8.55E-04	0.94	1.18E-04	1.27E-04	1.08	1.25E-04	1.06
8.00	7.00	6.02E-04	6.06E-04	1.01	5.65E-04	0.94	1.10E-04	1.15E-04	1.05	1.14E-04	1.04
9.00	5.00	1.48E-03	1.49E-03	1.01	1.39E-03	0.94	1.09E-04	1.14E-04	1.05	1.13E-04	1.04
9.00	6.00	9.09E-04	9.19E-04	1.01	8.55E-04	0.94	9.59E-05	1.00E-04	1.04	9.88E-05	1.03
9.00	7.00	6.02E-04	6.06E-04	1.01	5.65E-04	0.94	8.59E-05	8.96E-05	1.04	8.84E-05	1.03
9.00	8.00	4.20E-04	4.22E-04	1.00	3.94E-04	0.94	8.13E-05	8.34E-05	1.03	8.21E-05	1.01
10.00	5.00	1.48E-03	1.49E-03	1.01	1.39E-03	0.94	8.96E-05	8.91E-05	0.99	8.79E-05	0.98
10.00	6.00	9.09E-04	9.19E-04	1.01	8.55E-04	0.94	7.92E-05	7.92E-05	1.00	7.82E-05	0.99
10.00	7.00	6.02E-04	6.06E-04	1.01	5.65E-04	0.94	7.05E-05	7.13E-05	1.01	7.04E-05	1.00
10.00	8.00	4.20E-04	4.22E-04	1.00	3.94E-04	0.94	6.41E-05	6.54E-05	1.02	6.45E-05	1.01
10.00	9.00	3.05E-04	3.05E-04	1.00	2.85E-04	0.93	6.14E-05	6.22E-05	1.01	6.12E-05	1.00
11.00	5.00	-	1.49E-03	-	1.39E-03	-	-	6.97E-05	-	6.89E-05	-
11.00	6.00	-	9.19E-04	-	8.55E-04	-	-	6.27E-05	-	6.19E-05	-
11.00	7.00	-	6.06E-04	-	5.65E-04	-	-	5.70E-05	-	5.63E-05	-
11.00	8.00	-	4.22E-04	-	3.94E-04	-	-	5.26E-05	-	5.18E-05	-
11.00	9.00	-	3.05E-04	-	2.85E-04	-	-	4.92E-05	-	4.85E-05	-
11.00	10.00	-	2.28E-04	-	2.14E-04	-	-	4.77E-05	-	4.69E-05	-
12.00	6.00	-	9.19E-04	-	8.55E-04	-	-	4.98E-05	-	4.91E-05	-
12.00	7.00	-	6.06E-04	-	5.65E-04	-	-	4.57E-05	-	4.51E-05	-
12.00	8.00	-	4.22E-04	-	3.94E-04	-	-	4.24E-05	-	4.18E-05	-
12.00	9.00	-	3.05E-04	-	2.85E-04	-	-	3.98E-05	-	3.93E-05	-
12.00	10.00	-	2.28E-04	-	2.14E-04	-	-	3.79E-05	-	3.74E-05	-
12.00	11.00	-	1.75E-04	-	1.64E-04	-	-	3.73E-05	-	3.67E-05	-

Table C.12: Cellular S-values (mGy·MBq^{-1}·s^{-1}) for ^{201}Tl using DPK.

Cell radii (µm)	Nucleus radii (µm)	S (N<-N)					S (N<-Cy)				
		MIRD	DECDATA	DECDATA / MIRD	PenNuc	PenNuc / MIRD	MIRD	DECDATA	DECDATA / MIRD	PenNuc	PenNuc / MIRD
3.00	1.00	2.84E-01	3.58E-01	1.26	2.80E-01	0.98	9.16E-03	8.69E-03	0.95	8.86E-03	0.97
3.00	2.00	4.68E-02	5.60E-02	1.20	4.65E-02	0.99	6.35E-03	6.18E-03	0.97	6.32E-03	1.00
4.00	2.00	4.68E-02	5.60E-02	1.20	4.65E-02	0.99	3.19E-03	2.98E-03	0.93	3.08E-03	0.97
4.00	3.00	1.60E-02	1.86E-02	1.16	1.58E-02	0.99	2.64E-03	2.55E-03	0.97	2.62E-03	0.99
5.00	2.00	4.68E-02	5.60E-02	1.20	4.65E-02	0.99	1.82E-03	1.72E-03	0.94	1.78E-03	0.98
5.00	3.00	1.60E-02	1.86E-02	1.16	1.58E-02	0.99	1.49E-03	1.39E-03	0.93	1.44E-03	0.97
5.00	4.00	7.37E-03	8.44E-03	1.15	7.30E-03	0.99	1.36E-03	1.30E-03	0.95	1.34E-03	0.99
6.00	3.00	1.60E-02	1.86E-02	1.16	1.58E-02	0.99	9.31E-04	8.69E-04	0.93	9.05E-04	0.97
6.00	4.00	7.37E-03	8.44E-03	1.15	7.30E-03	0.99	8.19E-04	7.60E-04	0.93	7.90E-04	0.96
6.00	5.00	4.02E-03	4.55E-03	1.13	3.97E-03	0.99	7.92E-04	7.56E-04	0.95	7.83E-04	0.99
7.00	3.00	1.60E-02	1.86E-02	1.16	1.58E-02	0.99	6.28E-04	5.85E-04	0.93	6.11E-04	0.97
7.00	4.00	7.37E-03	8.44E-03	1.15	7.30E-03	0.99	5.39E-04	5.02E-04	0.93	5.24E-04	0.97
7.00	5.00	4.02E-03	4.55E-03	1.13	3.97E-03	0.99	4.97E-04	4.64E-04	0.93	4.84E-04	0.97
7.00	6.00	2.44E-03	2.74E-03	1.12	2.41E-03	0.99	5.03E-04	4.83E-04	0.96	5.01E-04	1.00
8.00	4.00	7.37E-03	8.44E-03	1.15	7.30E-03	0.99	3.79E-04	3.54E-04	0.93	3.71E-04	0.98
8.00	5.00	4.02E-03	4.55E-03	1.13	3.97E-03	0.99	3.39E-04	3.20E-04	0.94	3.35E-04	0.99
8.00	6.00	2.44E-03	2.74E-03	1.12	2.41E-03	0.99	3.25E-04	3.07E-04	0.95	3.21E-04	0.99
8.00	7.00	1.59E-03	1.78E-03	1.12	1.58E-03	0.99	3.41E-04	3.29E-04	0.97	3.42E-04	1.00
9.00	5.00	4.02E-03	4.55E-03	1.13	3.97E-03	0.99	2.46E-04	2.34E-04	0.95	2.46E-04	1.00
9.00	6.00	2.44E-03	2.74E-03	1.12	2.41E-03	0.99	2.29E-04	2.18E-04	0.95	2.29E-04	1.00
9.00	7.00	1.59E-03	1.78E-03	1.12	1.58E-03	0.99	2.26E-04	2.16E-04	0.95	2.26E-04	1.00
9.00	8.00	1.10E-03	1.23E-03	1.11	1.09E-03	0.99	2.43E-04	2.36E-04	0.97	2.45E-04	1.01
10.00	5.00	4.02E-03	4.55E-03	1.13	3.97E-03	0.99	1.86E-04	1.78E-04	0.96	1.87E-04	1.01
10.00	6.00	2.44E-03	2.74E-03	1.12	2.41E-03	0.99	1.70E-04	1.65E-04	0.97	1.73E-04	1.02
10.00	7.00	1.59E-03	1.78E-03	1.12	1.58E-03	0.99	1.63E-04	1.57E-04	0.97	1.65E-04	1.01
10.00	8.00	1.10E-03	1.23E-03	1.11	1.09E-03	0.99	1.65E-04	1.58E-04	0.96	1.66E-04	1.01
10.00	9.00	7.92E-04	8.82E-04	1.11	7.89E-04	1.00	1.80E-04	1.75E-04	0.97	1.82E-04	1.01
11.00	5.00	-	4.55E-03	-	3.97E-03	-	-	1.39E-04	-	1.48E-04	-
11.00	6.00	-	2.74E-03	-	2.41E-03	-	-	1.28E-04	-	1.35E-04	-
11.00	7.00	-	1.78E-03	-	1.58E-03	-	-	1.21E-04	-	1.27E-04	-
11.00	8.00	-	1.23E-03	-	1.09E-03	-	-	1.17E-04	-	1.24E-04	-
11.00	9.00	-	8.82E-04	-	7.89E-04	-	-	1.20E-04	-	1.26E-04	-
11.00	10.00	-	6.57E-04	-	5.89E-04	-	-	1.34E-04	-	1.40E-04	-
12.00	6.00	-	2.74E-03	-	2.41E-03	-	-	1.03E-04	-	1.09E-04	-
12.00	7.00	-	1.78E-03	-	1.58E-03	-	-	9.62E-05	-	1.02E-04	-
12.00	8.00	-	1.23E-03	-	1.09E-03	-	-	9.20E-05	-	9.70E-05	-
12.00	9.00	-	8.82E-04	-	7.89E-04	-	-	9.06E-05	-	9.54E-05	-
12.00	10.00	-	6.57E-04	-	5.89E-04	-	-	9.35E-05	-	9.80E-05	-
12.00	11.00	-	5.03E-04	-	4.53E-04	-	-	1.06E-04	-	1.10E-04	-